Precise Registration Methods in the Manufacture of Printed Circuit Boards

by

Daniel J. Braunstein

B.S., University of California, Berkeley (1992)
S.M.M.E., Massachusetts Institute of Technology (1994)

Submitted to the Department of Mechanical Engineering
in partial fulfillment of the requirements for the degree of

Doctor of Philosophy

at the

MASSACHUSETTS INSTITUTE OF TECHNOLOGY

~~September 1997~~ [JUNE 1998]

©Daniel J. Braunstein, 1997. All rights reserved.

The author hereby grants to MIT permissions to reproduce
and to distribute publicly paper and electronic
copies of this thesis document in whole or in part.

Author ....
Department of Mechanical Engineering
August 25, 1997

Certified by ....
Alexander H. Slocum
Alex and Brit d'Arbeloff Associate Professor of Mechanical Engineering
Thesis Supervisor

Accepted by ....
Ain A. Sonin
Professor of Mechanical Engineering
Chairman, Departmental Graduate Committee

JAN 06 1998

LIBRARIES

ARCHIVES

Precise Registration Methods in the Manufacture of Printed Circuit Boards

by

Daniel J. Braunstein

Submitted to the Department of Mechanical Engineering
on August 25, 1997, in partial fulfillment of the
requirements for the degree of
Doctor of Philosophy

Abstract

Methods for registration of artwork, inner-layer cores, and laminated panels in the manufacture of rigid, multi-layer printed circuit boards are developed. A tolerance study and sensitivity analysis of a high-volume circuit board production facility reveals that pin pitches and via pad diameters are most sensitive to inner-layer imaging processes. Within inner-layer imaging, registration errors are dominated by errors in film and exposure frame alignment. Furthermore, precise registration of artwork and panels is limited by indeterminate tooling schemes.

Optical measurement techniques for film alignment based on moiré interferometry and Fraunhofer diffraction patterns are presented. These methods improve film alignment accuracy by an order of magnitude, significantly reducing position variations of tooling features relative to circuit artwork. Additionally, kinematic tooling features are proposed that demonstrate an order of magnitude improvement in film placement precision. An exposure frame design is also presented.

Implications of the techniques are discussed as they relate to interconnectivity. Inner and outer-layer pad diameters may be reduced by 30%, device pitches may be increased by a factor of three, and photo-defined vias may be placed onto pads with 50% smaller diameters. Additional concepts may reduce these metrics further. Using methods presented in this thesis, printed circuit boards for μBGA, direct chip attach, and other fine pitch devices may be produced readily.

Thesis Supervisor: Alexander H. Slocum
Title: Alex and Brit d'Arbeloff Associate Professor of Mechanical Engineering

Precise Registration Methods in the Manufacture of Printed Circuit Boards

by

Daniel J. Braunstein

Submitted to the Department of Mechanical Engineering
on August 25, 1997, in partial fulfillment of the
requirements for the degree of
Doctor of Philosophy

Abstract

Methods for registration of artwork, inner-layer cores, and laminated panels in the manufacture of rigid, multi-layer printed circuit boards are developed. A tolerance study and sensitivity analysis of a high-volume circuit board production facility reveals that pin pitches and via pad diameters are most sensitive to inner-layer imaging processes. Within inner-layer imaging, registration errors are dominated by errors in film and exposure frame alignment. Furthermore, precise registration of artwork and panels is limited by indeterminate tooling schemes.

Optical measurement techniques for film alignment based on moiré interferometry and Fraunhofer diffraction patterns are presented. These methods improve film alignment accuracy by an order of magnitude, significantly reducing position variations of tooling features relative to circuit artwork. Additionally, kinematic tooling features are proposed that demonstrate an order of magnitude improvement in film placement precision. An exposure frame design is also presented.

Implications of the techniques are discussed as they relate to interconnectivity. Inner and outer-layer pad diameters may be reduced by 30%, device pitches may be increased by a factor of three, and photo-defined vias may be placed onto pads with 50% smaller diameters. Additional concepts may reduce these metrics further. Using methods presented in this thesis, printed circuit boards for μBGA, direct chip attach, and other fine pitch devices may be produced readily.

Thesis Supervisor: Alexander H. Slocum
Title: Alex and Brit d'Arbeloff Associate Professor of Mechanical Engineering

Acknowledgments

Without the advice, encouragement, and inspiration of many people involved with my work, this research would not be complete; it certainly would not have been as much fun.

My advisor, Alex Slocum, provided the intellectual adrenelin. His unremitting technical barages kept the project on a rapid and *focused* course. Unbeknownst to people who have not had the luxury of working with Alex, there is a method to his madness. His patience, drive, and raw horsepower gave this journey significance.

My committee members each deserve credit. Stephen Fantone's willingness to spend many hours on this specific project was invaluable. Even while running Optikos, Steve always made himself available. His contributions are most noted in those sections related to optical metrology. Fellow Berkeley-ite, Sanjay Sarma, helped emphasize the relation of particular advances to their impact on circuit manufacture as a whole. I particularly enjoyed his Strunk and White approach to writing. Warren Seering's encouragement helped drive this thesis home.

My wife, Diane, deserves mountains of credit for being patient and supportive while completing this work. I could not have done any of this without her.

I would like to acknowledge my parents for their support through the years.

MIT friends Samir Nayfeh, Mark West, Sheng Liu, Xiang-dong He, Boo-ho Yang, Sep Kiani, Ryan Vallence, Steve Ludwick, and all the other lab rats of building 35, have helped make this an enjoyable experience.

I would also like to acknowledge Bruce Raaberg for his unparalleled support, enthusiasm and his time spent with me during the production line aspect of this thesis. Also, this thesis would not have been realized, without the support and enthusiasm of Bruce Sorenson and George Strout.

I would also like to thank the following individuals for their assistance: Pete Magnon, Binh Vernet, Mike Fancher, Marcia Millard, Larry Dube, Juan Kamacho, Carlos Gutierrez, Dave Hu, Greg Blake, Steve Gildey, Bok Kim, Dave Angwin, Tim Blair from Morton, Jack O'Brian and Howard Elliott from Polyclad, Michael An-

gelo, Jim Saffery, Don Alzmann, and Ron Ferina from Multiline Technology, and Jack Countryman and Gene Green from Kodak, and Tom Pursch and Dave Anderson from Teradyne.

This thesis was typeset using LaTeX running under Linux.

Contents

1 History and Thesis Overview **19**

1.1 Thesis Outline 22

2 Interconnectivity and Manufacturing Processes **24**

2.1 Connectivity 26

2.2 Printed Circuit Board Processes 31

2.2.1 Laminate Preparation 31

2.2.2 Artwork 31

2.2.3 Inner-Layer Processes 35

2.2.4 Outer-Layer Processes 38

2.3 Chapter Conclusions 44

3 Production Facility Registration Errors **47**

3.1 Artwork Material Considerations 47

3.2 Photo-Plotting 52

3.2.1 Sources of Error 56

3.3 Artwork Tooling 60

3.3.1 Film Placement Simulation 61

3.3.2 Sources of Error 64

3.3.3 Artwork Tooling Summary 70

3.4 Registration Measurement 71

3.5 Exposure Frames 72

3.6 Laminate Material Considerations 77

3.7 Inner-Layer Expose 83

3.8 Post-Etch Punch 85

3.9 Lay-Up 91

3.10 Lamination 95

3.11 Drill 96

3.12 Outer-Layer Imaging Processes 101

3.12.1 Outer-Layer Image 101

3.12.2 Solder Mask and Photo-Defined Vias 102

3.12.3 Outer-Layer Summary 104

3.13 Route 105

3.14 Electrical Test 105

3.15 Sensitivity Analysis 107

4 Artwork and Laminate Metrology 113

4.1 Moiré Interferometry 115

4.1.1 Theoretical Treatment 115

4.1.2 System Overview 119

4.1.3 Resolving Phase 122

4.1.4 Testing 139

4.1.5 Proposed Implementation 142

4.2 Diffraction Method 145

4.2.1 Theoretical Background 145

4.2.2 System Considerations 148

4.2.3 Implementation 156

4.3 Discussion 158

5 Kinematic Artwork Tooling and Expose Frame Design 160

5.1 Film Fixturing 161

5.1.1 Repeatability Results 166

5.2 Exposure Frames 173

5.3 Chapter Conclusions 180

6 Conclusions **184**
6.1 Future Work 187

A Additional Concepts **189**
A.1 Pre-Expose Punching 189
A.2 Post-Expose Punching 190
A.3 Post-Etch Punch 191
A.4 Lay-Up 194
A.5 Lamination 196
A.6 Drill 199
A.7 Outer-layer Image 201
A.8 Solder Mask and Photo-Defined Vias 204
A.9 Electrical Test 207

List of Figures

1-1 Strain gauges on monolithic flexures measure hydrodynamic and contact forces for calculating relevant paste properties. 20

2-1 μBGA package type has as many a 500 I/Os on a $200mm^2$ package area. These and other devices, such as flip-chips, require interconnect densities not easily obtained using current manufacturing methods. . . 26

2-2 $25in/in^2$ could be accomplished with a single layer of 0.020" lines and spaces or two layers of 0.040" lines and spaces. 27

2-3 A road-map for μBGA. Forthcoming array packages exceed the board production capability. 28

2-4 BGA populated board illustrating connectivity. 30

2-5 Distribution of panel size formats. 32

2-6 Saw for rough cutting laminates to size. 32

2-7 Laminates are captured by belts while being in-fed to the edging blades (not shown). 33

2-8 Drum Plotter for producing inner and outer-layer artwork. 34

2-9 Cameras are aligned to targets on the edge of the artwork to verify correct scaling. 34

2-10 Artwork is aligned to reference targets and punched with tooling features for fixturing during laminate exposure. 35

2-11 Multiline Technology artwork punch. 36

2-12 Following edging and cleaning, dry-film photo-resist is applied to both sides of the laminates with hot rollers. 37

2-13 Inner-layer expose process. Top and bottom film must be registered precisely to align top and bottom features on laminates. 38
2-14 Frame to frame repeatability is as important as initial film registration. A proposed method for maintaining frame registration will be presented in Chapter 5. 39
2-15 Core profile after inner-layer expose and DES. 39
2-16 Post-etch punching after material movement has occurred from DES. 40
2-17 One of four punched slots in the laminate. These are used for fixturing the cores during lamination. 40
2-18 Punch and Die used in the post-etch punch. A CCD camera is attached to the punch which measures the position of a target on the laminate for registration. 41
2-19 Four slots punched in cores by post-etch punching are located onto four tooling pins of a lamination plate. 41
2-20 Stacking the various layers before lamination. 42
2-21 Profile of an inner-layer panel ready for drilling and outer-later expose. 42
2-22 Multiple spindle CNC drills may drill approximately twenty panels simultaneously. 43
2-23 A panel with sacrificial top plate is shown. Note the drill holder in foreground. 44
2-24 Panels being loaded from outer-layer dry-film and prepared for outer-layer expose. Dry-film tents drilled holes, although tooling slots on the perimeter are not covered, since they are used to fixture the panels in the expose frames. 45
2-25 After resist is stripped, the electroless plate is etched, leaving the board profile as shown. 45
2-26 A final exposure process exposes only the pads of the devices, which are then hot-air leveled. 46

3-1 Creep and recovery for a typical film, under 6000 psi tension. 49

3-2 Dimensional variations of unprocessed Kodak film. Measurements taken at 21°C 53
3-3 Accuracy and precision of plotted features. 55
3-4 Radial, yaw, and pitch errors of plotter drum. 57
3-5 Sensitive error motions of plotter drum. 58
3-6 Laser carriage error motions. 58
3-7 Current artwork tooling scheme (dimensions in inches). 60
3-8 Distance distribution of an "ideal" point on a film from nominal (zero) position after being fixtured to four pins. 62
3-9 Distance distribution of an "ideal" point for different film sets placed onto the same "perfect" frame, illustrating the contribution from punch variations alone. 63
3-10 Distance distribution of an "ideal" for the same "perfect" film set placed onto different frames, illustrating frame variance contribution tc placement errors. 63
3-11 "Splitting the difference" based upon two plotted features. 65
3-12 Punch removed from guide. Nicked edges can cause film tear and degraded punch repeatability. 67
3-13 Punch in upper guide block. Removal and refitting can cause punch damage due to insertion. 68
3-14 Carlson pins used to verify front-to-back artwork registration. 71
3-15 Three (of four) unconstrained Carlson pins. Since the pins are not constrained relative to each other, the registration measurement does not account for pin positional errors. 71
3-16 Fixturing a film set to the glass of an exposure frame. 73
3-17 Ball in hole constrains x and y frame position. 73
3-18 Peg in hole constrains frame rotation. 74
3-19 Over-constrained glass along its perimeter causes glass warp, requiring large vacuum pressure and draw time to achieve contact printing. . . 75

3-20 Kinematically constrained glass may reduce glass warp. The coupling may be a 6-point contact type to ensure lateral and transverse stiffness. 76
3-21 Ball and post frame repeatability. 77
3-22 Dependence of modulus on weave orientation. 80
3-23 Shear modulus as a function of load direction. 80
3-24 Modulus of laminates is significantly enhanced by copper cladding. . . 81
3-25 Series and parallel combination of stiffnesses after artwork is etched into the laminates. 82
3-26 Block locating mechanism limits punch repeatability. 87
3-27 Sensitive punch/die block locating direction. 87
3-28 Slot width as a function of core thickness. 89
3-29 Extension of cores during punching causes slot size variations as a function of core thickness. 89
3-30 Suspended stage may cause punch errors due to vibrations. 90
3-31 Pin/slot clearances at lay-up. 92
3-32 Distance distribution of an ideal etched feature from its nominal position. 93
3-33 Lamination pins tilt by hammering. 94
3-34 Translation and rotation of cores due to skewed lamination pins. . . . 94
3-35 Pin and slot fit at cure temperature. 96
3-36 Proposed profile ground tooling features for primary drill and route. . 98
3-37 Measuring tilt of drill tooling pins with a machinists square. 98
3-38 Registration error, specified hole diameter, and annular ring determines the required pad size. 100
3-39 Outer-layer frame tooling. 101
3-40 Determination of minimum device pitch from solder mask. 104
3-41 Process deviations and their impact on inner-layer pad diameter. . . . 109
3-42 Process deviations and their impact on outer-layer pad diameter. . . . 109
3-43 Process deviations and their impact on pad pitch. Solder mask over drilled outer-layer vias was used as the criteria. 110

3-44 Process deviations and their impact on pad pitch. Solder mask over undrilled vias was used as the criteria. 110
3-45 Process deviations and their impact on photo-defined via pitch. 111

4-1 Rectangular grid of printed features for obtaining an average measure of artwork position and rotation. 114
4-2 Two binary gratings at relative angle θ creates a fringe effect. 118
4-3 A $1'' \times 2''$ grating is bonded to a $2'' \times 2''$ grating to create the reference fringe pattern against which all measurements will be made. 120
4-4 The $250lp/in$ film grating against the reference grating creates a fringe pattern. Fringes are compared to determine relative position and rotation of the film with respect to the reference. 120
4-5 The system used to measure the gauge capability of the optical alignment methods. 121
4-6 Magnitude of the first 5 Fourier coefficients of a triangle wave. Note that the even harmonics are zero. 125
4-7 Moiré interferogram of two crossed binary gratings. 125
4-8 Spectral content of a triangular intensity pattern. 126
4-9 (a) Moiré interferogram from the film grating and the reference pattern. The phase difference between the two fields represents the displacement of the film relative to the reference. (b) The averaged rasters of each field are used for analysis. 127
4-10 Spectral content of the averaged image. The magnitude response yields the fundamental mode of the fringe pattern, which will be used for determining the phase difference of the signals. 129
4-11 Four interferograms illustrating the phase shift for displaced gratings. (a) Displacement = $\pm 50.8\mu m$; (b) displacement = $5.1\mu m$; (c) displacement = $-2.3\mu m$; and, (d) displacement = $12.6\mu m$. 130
4-12 Intensity patterns corresponding to the interferograms in Figure 4-11. 131

4-13 Four correlation signals for different intensity patterns. The displacement can be calculated from the location of the maximum of the correlation. (a) Displacement = $5\mu m$; (b) displacement = $0\mu m$; (c) displacement = -$7\mu m$; and, (d) displacement = $15\mu m$. 133

4-14 The reported displacement of the Fourier and correlation methods, compared to the Abbe displacement caused by rotation about a remote point indicates the relative sensitivity of the algorithms to frequency modulation. (0-correlation, x-Fourier, - - ideal 134

4-15 Rotation about the locus of points normal to the grating axis and at the low frequency maximum causes a pure frequency shift for the case where $N = 0$ For all other N, a phase shift of $2\pi N$ is introduced because of the Abbe displacement. 136

4-16 Any planar motion of a lamina can be represented by pure rotation. . 137

4-17 The intersection of two loci of rotation points for frequency modulation of the heterodyned moiré patterns is the center of rotation for the film. Rotation of the film about this point will register the artwork with respect to the reference grating positions. 138

4-18 Time series data from the capacitance probe and optical measurement illustrates the repeatability of the moiré technique (solid-moiré, dashed-capacitance probe). 139

4-19 Histogram of the moiré time series data from Figure 4-18. $\sigma_{moire} = 0.08\mu m$ 140

4-20 Comparison of the capacitance probe reading and the moiré method. Trial day 1. 140

4-21 Comparison of the capacitance probe reading and the moiré method. Trial day 2. 141

4-22 Comparison of the capacitance probe reading and the moiré method. Trial day 3. 141

4-23 Gratings placed along the perimeter of the film can be used to center the artwork with respect to reference fringes for a thermocentric design. 143

4-24 Gratings placed at opposite angles relative to each other will generate opposing fringe motion as the film is moved. By aligning the fringes on opposite sides of the film, the artwork is centered. Note that centering is achievable in the presence of thermal errors or artwork scaling. . . . 144
4-25 The observation field $\mathbf{U}(x_0, y_0)$ can be described by the superposition of point sources emanating from the pictured aperture. 146
4-26 Diffraction patterns of linear binary gratings for various design parameters. (a)$d/b = 2$, (b)$d/b = 4$, (c)$d/b = 10$, (d)$N = 5$, (e)$N = 7$, (f) N=15. 149
4-27 As the grating slits become infinitesimally small, approaching a Dirac delta function, the modulation approaches unity, hence the ratio of successive diffraction orders is also unity. 150
4-28 When the reference grating is unobstructed, judicious selection of pitch and slit width causes certain diffraction orders to be zero. 151
4-29 Nominal center grating position places the measured diffractive order near the 1/2 the center intensity. 152
4-30 Grating geometry can be designed to satisfy dynamic range requirements. Furthermore, from conditions of Equation 4.45 and Equation 4.46 directional information can be maintained, unlike the moiré alignment method. 154
4-31 Experimental setup for qualifying the diffraction based measurement method. 155
4-32 Diffraction patterns created by a $250 lp/inch$ grating using a He-Ne laser and an OD3 filter. 156
4-33 The intensity profile of the pattern of Figure 4-32 shows the diffraction orders and the $\sin^2 \beta / \beta^2$ modulation. 157
4-34 Diffraction grating placement for measuring three degrees of freedom. 158
4-35 Film alignment using a thermocentric design is invariant to artwork scaling and thermal errors. 159

5-1 Coordinate system definition for artwork. 161
5-2 One proposed kinematic constraining scheme. 162
5-3 Three different kinematic systems. (a) Vee and flat, corner origin; (b) center origin with oblique preload pin; and, (c) center origin, each pin location with opposing force source. 163
5-4 Preloaded coupling stiffness is calculated from the series connection of springs. 164
5-5 Test fixture for measuring repeatability of kinematically fixtured film. 166
5-6 Time series position data of kinematically tooled film. 168
5-7 Histogram of kinematically tooled film, $3\sigma = 2.5\mu m$. 169
5-8 Time series data for second experiment of kinematically tooled film. . 170
5-9 Histogram of second experiment, $\sigma = 3.2\mu m$. 171
5-10 Kinematic coupling using die-set bushings and ball cages for large out of plane travel. 174
5-11 Exposure frame concept based on die-set kinematic couplings. 175
5-12 Force stiffness of die set bushings of different numbers of rows. 176
5-13 Moment stiffness of die set bushings of different numbers of rows. . . 176
5-14 Force stiffness of a six row die set bushings of different numbers of balls per row. 177
5-15 Moment stiffness of die set bushings as a function of number of balls per row and post rotation. 177
5-16 Die set bushings and cages, with crowned post for kinematic coupling. 178
5-17 Set of three die set posts in vee grooves. 179
5-18 Kinematic die set post in vee groove. 180
5-19 Test table for measuring repeatability of kinematic die set coupling. . 181
5-20 Repeatability results of kinematic die set coupling. 182

A-1 Punch repeatability issues are avoided by pre-expose punching kinematic features since the pattern is exposed with respect to the fixture. 190

A-2 Kinematically coupled punch and die sets can be manufactured as matching sets. 191
A-3 Polymer replicated punch guides will increase repeatability performance of punches. Super Alloy^{TM} castable polymers from Philadelphia Resins are designed for this type of application. 191
A-4 Kinematically coupled punch and die blocks. 192
A-5 Moiré fringe alignment of cores. 194
A-6 Conceptual kinematic press plate. 195
A-7 Pins with large radii reduce contact stress from preload. 197
A-8 Resin replicated tooling features remain kinematic for subsequent processes. 198
A-9 Drill bed to accomodate resin replicated kinematic tooling features. . 199
A-10 Soft-tooled pin changes position along the insensitive coupling axis. . 200
A-11 Meta-stable kinematic coupling using drilled features. 202
A-12 Origin of panel coupling for outer-layer imaging. 202
A-13 Rotation constraining pin has only one sensitive direction. 203
A-14 Geometry of errors generated by pin placement error. 204
A-15 Clamps may be used to protect tooling holes from curtain coating. . . 205
A-16 Gasketing plugs may be used to protect tooling holes. 205
A-17 Six point coupling used for fixturing fabricated boards to the test fixture. 207

List of Tables

3.1 Mechanical properties of polyester film base. 48

3.2 Thermal properties of various polyester film bases. 49

3.3 Performance specifications for an Optrotech Golden Plotter. 54

3.4 Current film alignment capability. 65

3.5 Alignment capability based on smaller field of view and "T" targets. . 66

3.6 Tooling features to circuit board artwork deviation. 67

3.7 Achievable front-to-back artwork registration capability, including simulation data for the indeterminate pin constraining system. 69

3.8 Achievable front-to-back artwork registration, including simulation data for the indeterminate constraining system, using 3x optical system and "T" targets. 69

3.9 Achievable front-to-back artwork registration, including simulation data for the indeterminate constraining system, using 3× optical system, "T" targets, and a precision stripper plate. 69

3.10 Current achievable front-to-back artwork registration including expose frame repeatability errors. 76

3.11 CTE, Poisson's ratio, and Young's modulus for clad and unclad laminates. 78

3.12 Typical values for FR-4 laminates.. 79

3.13 Stiffness of various copper-clad laminate constructions on a width per length basis. 82

3.14 Environmental contributions to layer-to-layer misregistration, neglecting post-etch punch errors. 84

3.15 Feature to feature registration between any two layers, neglecting post-expose punch errors. 84
3.16 Possible layer-to-layer registration using improved artwork alignment and punch techniques with more stringent humidity control. 85
3.17 Post-etch punch core alignment capability. 90
3.18 Layer-to-layer registration including artwork, post-etch punch, and lamination plate variances. 93
3.19 Top-to-bottom misregistration for various panel thicknesses pins tilts. 94
3.20 Inner-layer feature distribution for multiple stacked panels at drilling. 99
3.21 Required pad size for a particular drill diameter and specified annular ring. 100

5.1 Contact force calculations for given shearing stress. 165
5.2 Comparison of kinematically fixtured film to four pin system. 167
5.3 Comparison of new alignment and fixturing method to current technique. 172
5.4 Front-to-back registration capability using moiré interferometric alignment, kinematic film tooling, and kinematic die-set frame coupling. . . 183

A.1 Punch and alignment performance. 194
A.2 Estimated layer-to-layer registration performance using proposed laminate tooling. 198

Chapter 1

History and Thesis Overview

The work presented herein represents my continual effort to develop techniques for cost effectively producing electronic packages of decreased size. The broad term "electronic packaging" refers, in this instance, to the printed circuit board itself and subsequent assembly techniques. From 1992 through 1994, I had the opportunity to conduct research at M.I.T. with support from Motorola and MPM Corporation under the supervision of Professor Harry Asada. The goal of that research was to develop new methods for depositing solder paste onto copper pads of a printed circuit board. It was determined early on that the printing process was not particularly robust for printing fine pitch devices of sizes 0.012"- 0.015". Printing such pitches, often for quad flat packs (QFPs) and other high density components, required time consuming set-ups, and routine on-line maintenance. The question remained as to why the quality of printed pads degraded with aperture size. I hypothesized that as aperture dimensions were reduced, the interaction between the paste and stencil contributed significantly to print quality. Therefore, a study into the fluid and material mechanics of printing technology ensued.

Solder paste, which is largely a viscous resin media containing spherical solder particles, exhibited non-Newtonian, thixotropic behavior. Furthermore, its properties were strongly dependent on temperature, humidity, and environmental exposure time. While tremendous industrial efforts were directed toward environmental control schemes to minimize paste variations, my approach was different. In the spirit of Tagu-

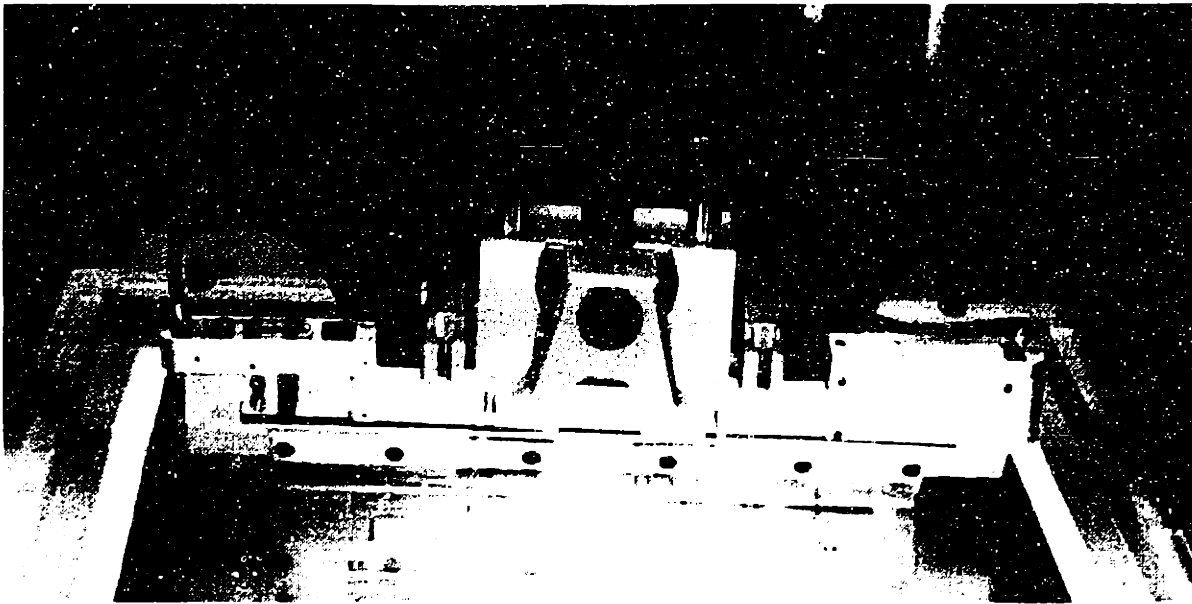

Figure 1-1: Strain gauges on monolithic flexures measure hydrodynamic and contact forces for calculating relevant paste properties.

chi [31], I attempted to make the process robust to material variations. However, the technique did not include rigorous design of experiments or data reduction. Rather, it worked under the premise that, given appropriate machine settings, acceptable printing is achievable under a variety of "paste conditions." Of course, pathologic paste conditions would not produce acceptable pads under any circumstance. It was deduced that if relevant material properties could be measured while printing, machine settings may be modulated in accordance with paste fluctuations, hence maintaining throughput.

The result of these endeavors was a new type of dispensing mechanism which would measure hydrodynamic forces generated during the printing cycle. Figure 1-1 shows the device. A model of the printing process, based upon viscous creeping flow of a power law fluid, simplified to a non-linear damper connected in series with a printing blade. Therefore, by measuring appropriate forces on- line, and relating those to printing speed, various paste properties such as instantaneous viscosity and power law exponent could be deduced [2]. These parameters were used in a feedback loop which would vary the angle of attack and velocity of the squeegee used to spread paste. In short, varying material parameters were measured and used to control appropriate

machine inputs to maintain print quality. This device and method was demonstrated at the National Electronics Packaging and Production Conference (NEPCON West) in early 1995 on an MPM semi-automatic printer. At the time of the demonstration, the duration over which printing occurred without intervention was approximately four times the duration without the device. Print quality was maintained and down-time was reduced. The device, known as SmartSqueegee^{TM}, has one pending patent and remains an active research project.

Impressive as the results were, it became evident that paste printing was sensitive to many other parameters not directly related to material properties. One area of particular interest was related to gasketing between the stencil and printed circuit board. Without proper gasketing, poor release of paste from the stencil would result, yielding unacceptable prints. The remedy for such a situation would often include increasing squeegee pressure, hence reducing attack angle. This had the effect of increasing hydrodynamic pressure, forcing paste through a poorly gasketed stencil. However, lack of a seal would often cause excessive paste to flow, sometimes causing shorts across successive pads. Out of plane distortions were considered the cause of poor sealing. Although possibly a significant factor, boards, stencils and squeegees are all reasonably compliant. Therefore, elastic deformation of the system should create a satisfactory seal.

Another well known, but perhaps underrated cause of poor gasketing, is related to registration of the PCB solder mask relative to the outer-layer image of the board, and hot air leveling. Hot air leveling is a process in which solder is applied to unmasked copper pads. Because of registration errors related to solder mask and outer-layer image, the mask image must be considerably larger than the outer layer image. This not only places restrictions on pad pitches, but also creates troughs in the vicinity of pads, resulting in a poor stencil to board seal. Similarly, hot air leveling produces non-uniform solder bumps on pads, that, when misregistered, contributes to gasketing problems. Unsatisfactory sealing may also be caused by mis-registration of solder leveled pads relative to stencils. In summary, one of many keys to successful printing is related to board registration, both among various processes of PCB manufacture,

and in board fixturing for subsequent assembly procedures.

Reasons for underlying variances of incoming printed circuit boards were not evident at the time of the printing research. Tooling variances could be accommodated by use of vision systems, but problems related to hot air solder leveling and solder mask registration remain. While active vision systems are currently the *de-facto* standard in high volume printers, their use contributes substantially to process cycle time. Indeed, the entire cycle time has been reduced in recent years due to rapid board delivery, fixturing, printing, and unloading, but this places further demands on automatic registration. If, perhaps, variances of incoming circuit boards could be reduced, use of active registration systems could be minimized; used for only the most demanding boards. This course of events eventually introduced me to printed circuit board manufacture.

I soon discovered that addressing specific issues of solder mask, tooling, and registration only began to address certain issues of circuit board production. Interestingly, the nature of my research at the time with Professor Slocum, in the Precision Engineering Research Group, was directed toward precision fixturing methods with application to semiconductor fabrication. Background research into circuit board manufacture revealed there were many critical processes that could benefit from new manufacturing methods, within a registration and tooling context. By applying some central tenants of deterministic design, many variances observed at paste printing and elsewhere could be reduced without substantial cost or dramatic change to equipment. This launched the research into precision methods for multi-layer printed circuit board manufacture described by this thesis.

1.1 Thesis Outline

Chapter 2 describes various measures of interconnectivity and outlines registration relevant processing steps in circuit board manufacture. This background establishes a vernacular and provides context for subsequent chapters. An error budget of a high-volume PCB manufacturing facility is contained in Chapter 3 along with sensitivity

analyses, beginning with inner-layer photo-plotting and ending with electrical test. Criteria for metrics such as minimum device pitch and minimum drill pad size are presented. Based upon the analysis of Chapter 3, Chapter 4 presents new methods for inner-layer film alignment. Theory of proposed optical techniques used for film and laminate metrology is presented, as are results from their implementation. Chapter 5 proposes new techniques for fixturing artwork. One particular tooling scheme is tested, using a measurement method from Chapter 4. Additionally, the design of a new type of coupling is described as it is applied to exposure frames. A repeatability study of the frame is presented. Chapter 6 concludes this thesis by discussing implications for board design based on the performance of the proposed alignment and fixturing designs. Directions for the circuit board industry are also discussed in light of these advances. Appendix A presents additional tooling concepts for other circuit board manufacturing processes.

Chapter 2

Interconnectivity and Manufacturing Processes

Continual efforts towards the miniaturization of electronic components have forced the manufacturing community to improve current technology and devise new methods for processing, packaging, and testing. In wafer processing, for instance, the drive to $300mm$ substrates, patterned with sub-micron line widths, has placed stringent performance requirements on the thermodynamic, chemical, and optical processes. This drive has often required mechanical infrastructures and material handling systems to be redesigned. Furthermore, testing of such devices has become a challenging task, forcing aggressive development of new technology in the area of probe cards, manipulators, and sockets. Within the packaging arena, ultra-fine pitch devices have spawned the development of precision processes within solder paste printing and component placement fields. Current soldering techniques, such as reflow soldering, are coping comfortably with the rapid pace of device engineering, placing the responsibility for joint integrity largely upon solder manufacturers.

The focus on device technology and associated assembly processes has to some extent caused a particularly important aspect of packaging engineering to be ignored. That aspect is the manufacture of the packaged device substrate itself, the circuit board. Clearly, this substrate is an essential component of the electronic product. The PCB largely determines product size, provides mechanical structure for circuitry, and

most importantly, provides means for discrete components to communicate with each other and to interface with peripheral devices. As in all processes, circuit board manufacturers have had to acknowledge and support increased line densities and decreased device pitches. However, these manufacturing specifications have been easily satisfied by existing circuit board assembly techniques. Manufacturers of these products, therefore, have not required substantial improvement to their technology. This comfort, however, will be short-lived. Forthcoming device pitches will force new methods for circuit board fabrication to be devised, especially with regard to artwork registration, core layer-to-layer registration, and board fixturing within exposure, drill, route, and test operations.

Additional motivation for this thesis stemmed from direct observations that printed circuit board variations contribute adversely to throughput of subsequent assembly processes, such as paste printing and chip placement. For example, by minimizing PCB tooling-to-image variations, use of active registration systems in paste printers may be reduced. This reduction may be by as much as 20% - 30% of the total cycle time.

Currently, registration for most PCB processes is accomplished largely through multiple hole/pin systems, requiring substantial operator skill during set-up and processing. Increased registration performance is achieved by decreasing manufacturing tolerances. Reliance on operator savvy and tooling tolerances will preclude manufacturers from satisfying new pitch and density requirements. Furthermore, material movement from various thermo-chemical processes introduces difficulties in maintaining registration. These difficulties, for example, are caused by stress relaxation during copper etch and strip, thermal cycling, and resin flow during lamination. Material shrinkage is a function of the artwork it contains, complicating registration schemes further. In short, there exists a tremendous need for a new approach for precision circuit board manufacture.

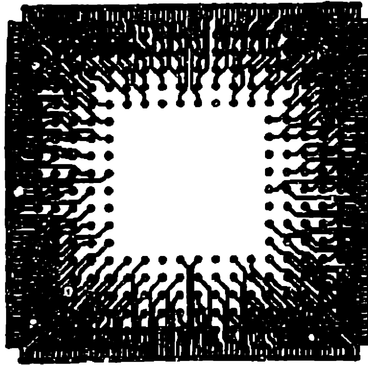

Figure 2-1: μBGA package type has as many a 500 I/Os on a $200mm^2$ package area. These and other devices, such as flip-chips, require interconnect densities not easily obtained using current manufacturing methods.

2.1 Connectivity

For a given circuit functionality, the ability to increase pattern density decreases the number of layers for a given board size, provided routing is achievable. The electronics market, however, is demanding greater functionality, requiring both increased densities and layer counts. Connectivity, a measure of connection density, is rapidly increasing. Technologies such as μBGA, shown in Figure 2-1 and direct chip attach are driving artwork patterns to increasingly smaller feature sizes [33].

Eight and ten layer boards are commonplace, with line/spacing patterns approaching 0.003"/0.003". Glass/epoxy core thicknesses of 0.002" with half-ounce copper are being used in 18"x24" panel sizes; widespread use of 0.010" pitch devices is forthcoming; and, dot patterns for photo-defined vias are approaching 0.004" diameters over 0.010"diameter pads. Clearly, registration of artwork and cores relative to each other and to various mechanisms is a challenging task, especially when perhaps twenty different mechanical and thermo-chemical operations are performed and yields greater than 95% are expected.

To quantify connectivity, metrics relating device area, pitch, number of I/Os, and the requisite wiring density have been established. The following empirical relationship has been proposed [26],

$$L = 1.5P\left(\frac{1.5}{2}N_T\right) \tag{2.1}$$

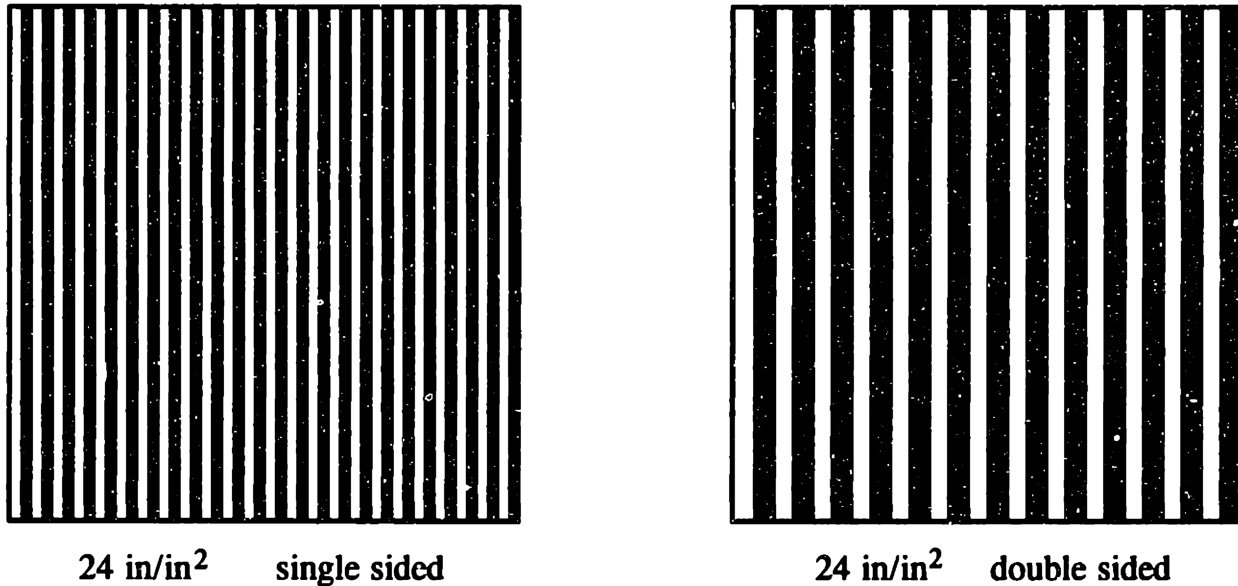

Figure 2-2: $25in/in^2$ could be accomplished with a single layer of 0.020" lines and spaces or two layers of 0.040" lines and spaces.

where L is the total wire length per chip site, P is the device pitch, and N_T is the total number of I/Os. For example, a 40 pad LCC on a 1 inch grid would require a wiring density of $45in/in^2$. This wiring demand, however, is not the metric PCBs are designed for. Rather, this value must be rated with a particular efficiency. For most PCBs and design systems, an efficiency of 50% [16] is widely accepted. For the above example, a wiring density of $90in/in^2$ should be specified. Wiring density is the total length of trace on an area basis. A density of $90in/in^2$ could be accomplished with a single layer of 0.005" lines and spaces. Alternatively, two layers of 0.010" lines and spaces could be used. Density as a function of layer count is illustrated in Figure 2-2.

One technology driving advances in wiring density is the μBGA. A fan-in package example is shown in Figure 2-1. These devices have a package to chip area of approximately 1.0 - 1.5, a footprint of $100 - 150mm^2$, and a bump pitch of $0.3 - 0.5mm$. 500 I/Os are attainable on $200mm^2$ packages.

A road-map for the μBGA is shown in Figure 2-3 [4]. The current pad pitch limit is indicated on this map. By applying Equation 2.1, using data in Figure 2-3, and assuming a device pitch twice the device edge dimension, a measure of connectivity may be obtained.

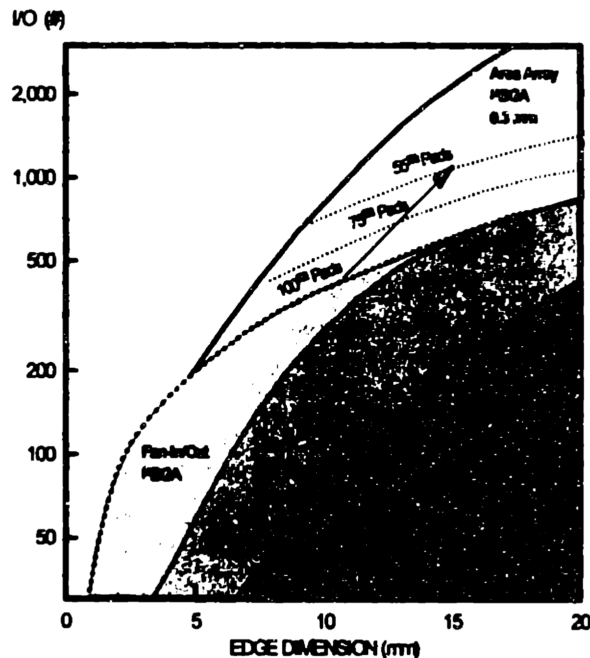

Figure 2-3: A road-map for μBGA. Forthcoming array packages exceed the board production capability.

A $15mm$ edge μBGA with approximately 200 I/Os requires approximately $1000in/in^2$, assuming an 80% layout efficiency. Board manufacturers may comfortably produce densities of $125in/in^2$ per layer, hence this particular device requires eight signal layers. Of particular importance, the pad pitch limit presented in Figure 2-3 will be extended beyond 500 IOs by manufacturing techniques developed through the course of this research.

Developments from this research aid in reducing variability among printed circuit boards by addressing tooling and registration issues; methods for increasing board connectivity necessarily followed. It was assumed that the *chemistry* involved in processes such as plotting, exposing, plating can produce densities the proposed registration and tooling schemes permit.

Since this thesis specifically treats board registration, a metric for measuring connectivity based on pad pitch and pad size should be developed. Beginning with

Equation 2.1, the line density of a PCB may be written as

$$\rho_{line} = \frac{L}{A} = \frac{1.125 P N_T}{A} \tag{2.2}$$

where A is the required area per IC. From [26], this area is simply P^2. This approximation, however, ignores the finite area required by actual pads. For densely placed devices with many IOs, this area can be significant. Consider a μBGA with pad diameter ϕ_{pad}. An array device edge dimension, ϵ, may be written as,

$$\epsilon = \zeta \phi_{pad} \sqrt{N_T} \tag{2.3}$$

where ζ is a scale factor for a particular device. Similarly, the pitch among devices may be written as a multiple, ζ' of the device edge dimension,

$$P = \zeta' \epsilon = \zeta' \zeta \phi_{pad} \sqrt{N_T} \tag{2.4}$$

Using this result, Equation 2.2, and subtracting the area required for pads, the line density reduces to,

$$\rho_{line} = 1.125 \frac{\zeta \zeta' \sqrt{N_T}}{\phi_{pad} \left(\zeta^2 \zeta'^2 - 1 \right)} \tag{2.5}$$

This relationship assumes that package edge dimension will scale with pad diameter. Note that for $\zeta^2 \zeta^2 \gg 1$, the equation reduced to

$$\rho_{line} = \frac{1.125 \sqrt{N_T}}{\phi_{pad} \zeta \zeta'} \tag{2.6}$$

which is Equation 2.1 using the area P^2. Referring to Figure 2-4, consider, for example, a 100 IO BGA, with 0.010" pad diameters. For a connect pitch twice the pad diameter ($\zeta = 2$), and a device distance twice the edge length ($\zeta' = 2$), the calculated line density from Equation 2.5 is $300 in/in^2$, compared to the slightly underestimated $280 in/in^2$ from Equation 2.1. For grid arrays with $\zeta = 1.5$ and component spacing $\zeta' = 1.5$, Equation 2.5 yields a density of $640 in/in^2$, while Equation 2.1 estimates $500 in/in^2$. Since board manufacturers may produce single signal layers with densit-

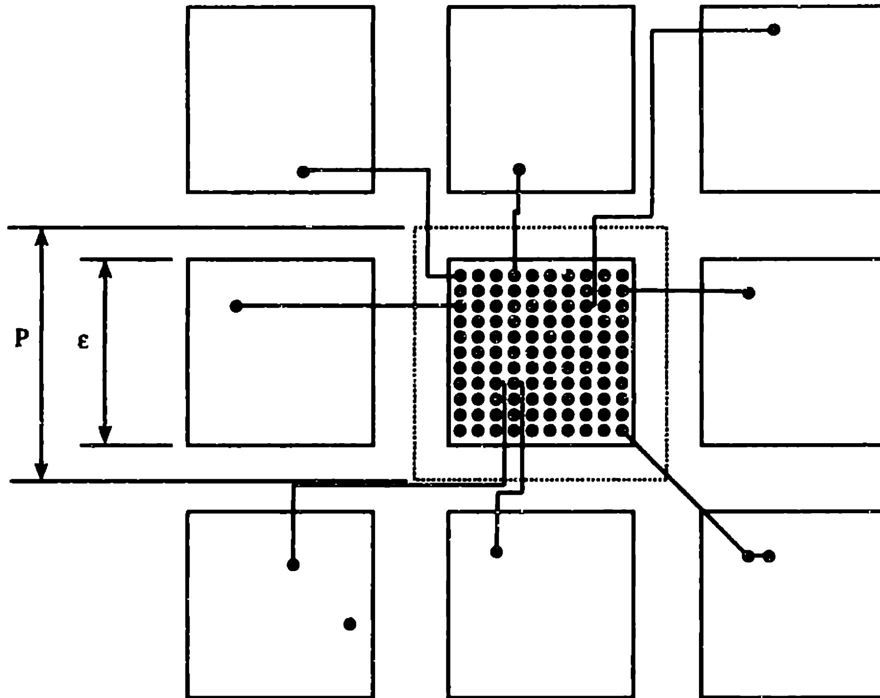

Figure 2-4: BGA populated board illustrating connectivity.

ies of approximately $125 in/in^2$, the different estimates for line density may mean the inclusion or exclusion of a layer. Interestingly, line densities calculated using Equation 2.1, divide by an additional factor. This factor is considered an "efficiency", which for particular board designs, may be 70% to 80%. This consideration raises the line density to the density calculated by Equation 2.5.

A 1992 price line follows a relationship which is inversely proportional to connectivity and proportional to the square of IOs N_T [15], [16]. By substitution, substrate costs C, per 1992 trends, may be written as,

$$C \sim N_T^{3/2} \phi_{pad} \tag{2.7}$$

which illustrates the relative weighting of IOs versus pad size.

This thesis develops enabling technology which significantly reduces pad diameters without substantial re-tooling costs. The results are fixturing and measuring techniques which permit higher package densities. Equation 2.5 will be revisited in the conclusions of this thesis when implications of the new techniques and designs are

discussed.

2.2 Printed Circuit Board Processes

The processes involved in producing a circuit board are numerous and varied. For purposes of presentation, however, the steps involved for the manufacture of *multi-layer rigid* boards with *plated through holes* will be discussed. Emphasis will be placed on registration critical processes, thus no treatise of various chemical procedures will be found. The following sections serve as a guideline for individuals not familiar with the methods involved in circuit board production.

2.2.1 Laminate Preparation

Core material for circuit boards studied in this thesis is a laminate structure of varied thickness FR-4 glass-epoxy, clad with copper of various thicknesses. These laminates are available in thickness from 0.002″ to 0.02″. Laminates are usually provided to a production facility in square sheets on the order of 16 ft^2, and are cut and trimmed to the desired dimension for a particular job. A typical size core is 18″ × 24″. On this single core, numerous circuit patterns will be produced, whereby actual boards are routed from large panels at the end of the production sequence. A recent product mix showing volume production of various panel sizes is shown in Figure 2-5.

Laminates are first cut to predetermined sizes from large blanks using a saw shown in Figure 2-6. These rough cut laminates are then trimmed to their final size using edging saws shown in Figure 2-7. Following edging, laminates are chemically cleaned to remove surface contaminants such as oil and epoxy dust, in preparation for application of a photo-resistive dry film.

2.2.2 Artwork

Artwork for exposure is created on large format polyester bases using laser photo-plotters like the drum type shown in Figure 2-8. Performance specifications may be

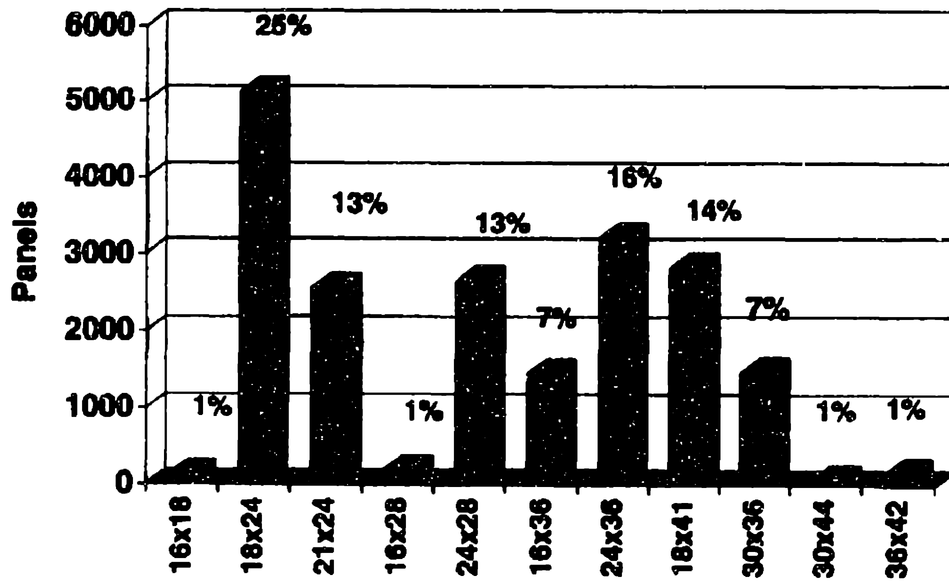

Figure 2-5: Distribution of panel size formats.

Figure 2-6: Saw for rough cutting laminates to size.

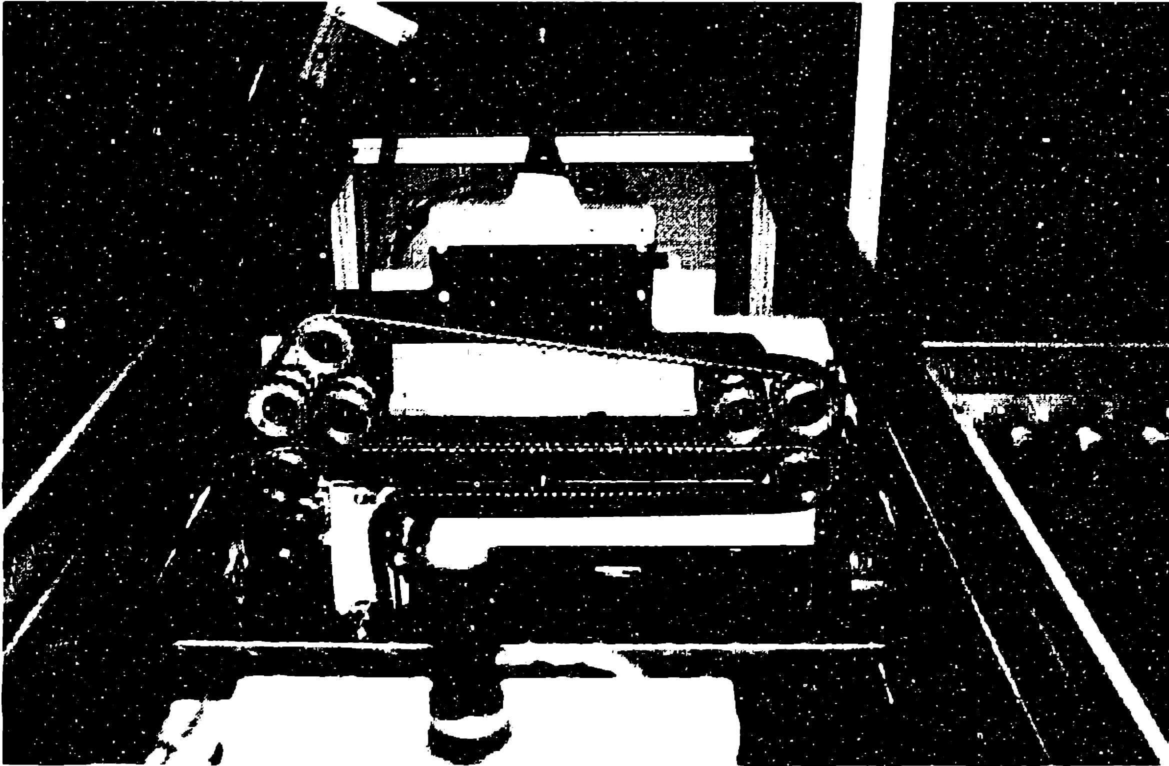

Figure 2-7: Laminates are captured by belts while being in fed to the edging blades (not shown).

found in Chapter 3.

After development and dry time, artwork patterns are measured to ensure proper scaling and plotter operation. Scale factors are necessary because lamination causes material shrinkage, as will be described later. Encoders on cameras measure the distance between target features on the artwork, as shown in Figure 2-9.

After measuring the artwork, it is placed onto a punch which creates tooling slots for the expose frames. Tooling features are required since two pieces of artwork must be registered with respect to each other for exposing the top and bottom of an inner-layer laminate simultaneously. Artwork is fixtured to the punch table via vacuum, and manually aligned to fixed reference fiducials. A punch table with artwork is shown in Figure 2-10. In this case, punches along the top and bottom edge produce tooling features. Figure 2-11 shows the entire film punch, manufactured by Multiline Technology.

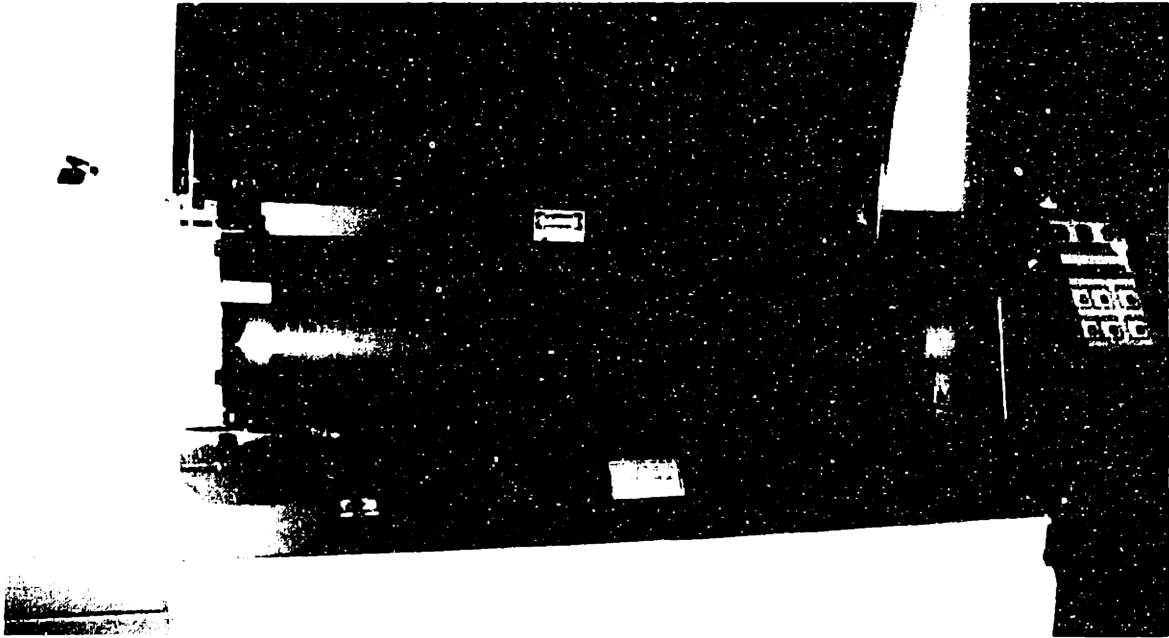

Figure 2-8: Drum Plotter for producing inner and outer-layer artwork.

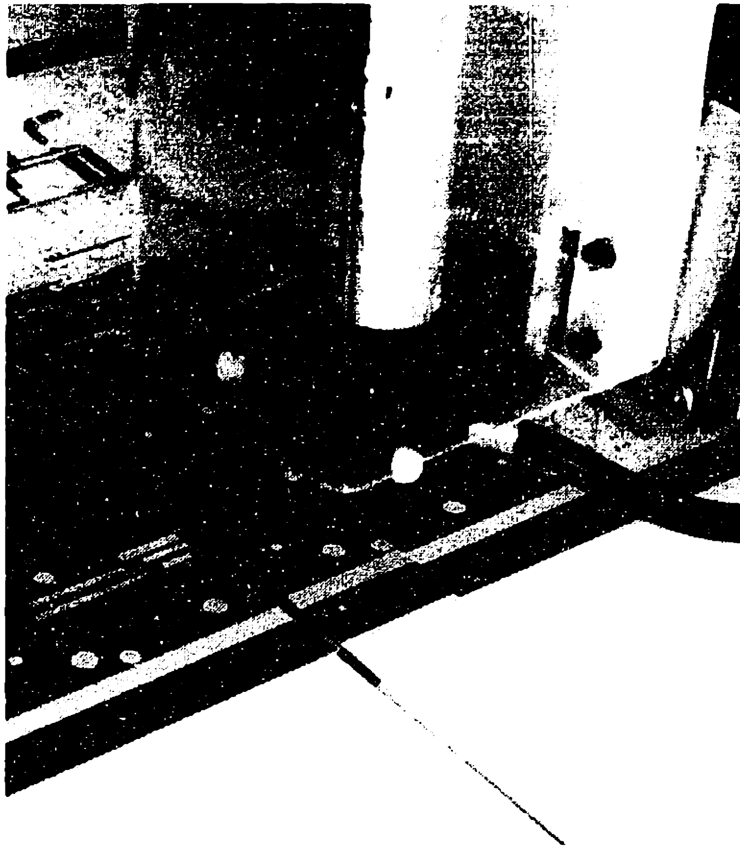

Figure 2-9: Cameras are aligned to targets on the edge of the artwork to verify correct scaling.

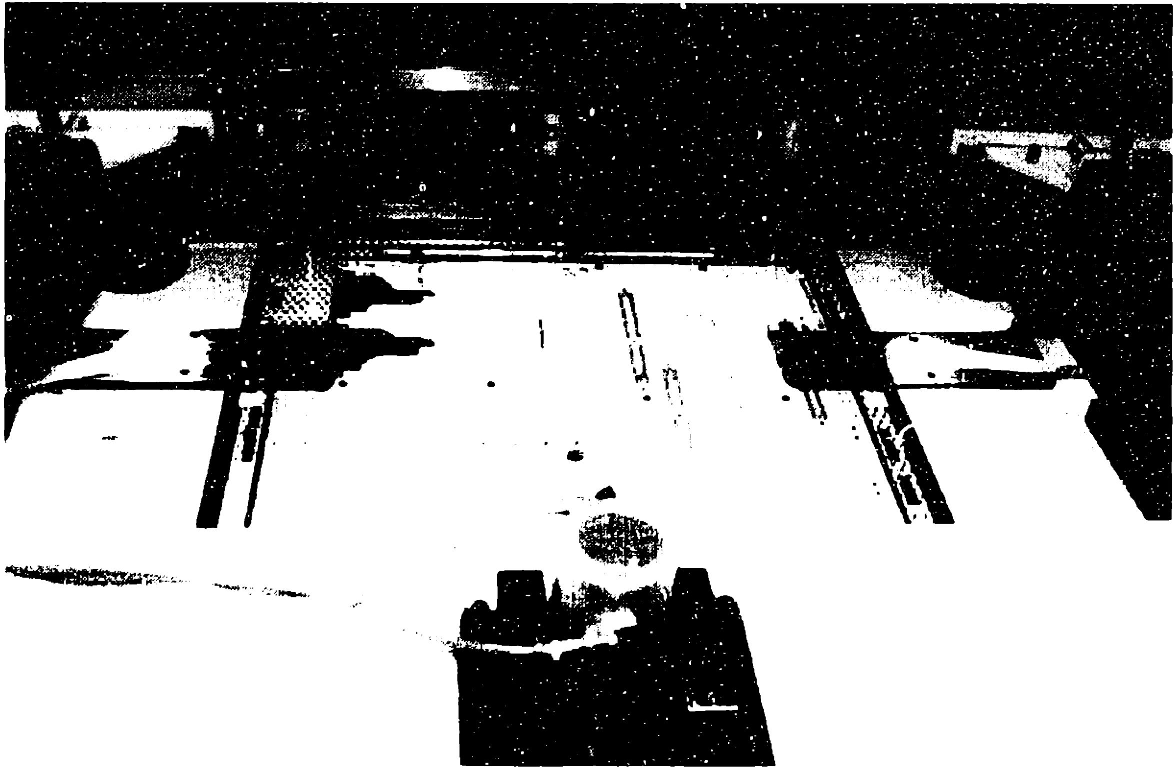

Figure 2-10: Artwork is aligned to reference targets and punched with tooling features for fixturing during laminate exposure.

2.2.3 Inner-Layer Processes

Clean and dry laminates pass through a preheat process and then through rollers that apply dry film, as shown in Figure 2-12. Roller temperatures of 100°C are typical, necessitating a cooling time prior to exposure. A cutting mechanism automatically cuts the film to the correct length as the laminates are unloaded and allowed to cool. The area available for circuits is maximized by applying the film to the outermost edges of cores. Typically, a $1mm$ perimeter of copper is all that remains. The dry film may be a positive or negative type, depending on the application. Film thicknesses are on the order of $30\mu m$ with an additional $125\mu m$ mylar base that protects the film and provides structure. Following dry film application, cores are ready for inner layer expose.

At exposure, front and back artwork is fixtured together in frames which simultaneously expose the circuit pattern onto cores. Artwork is held to top and bottom glass plates by vacuum, while cores are located between the film, as shown in Figure 2-13.

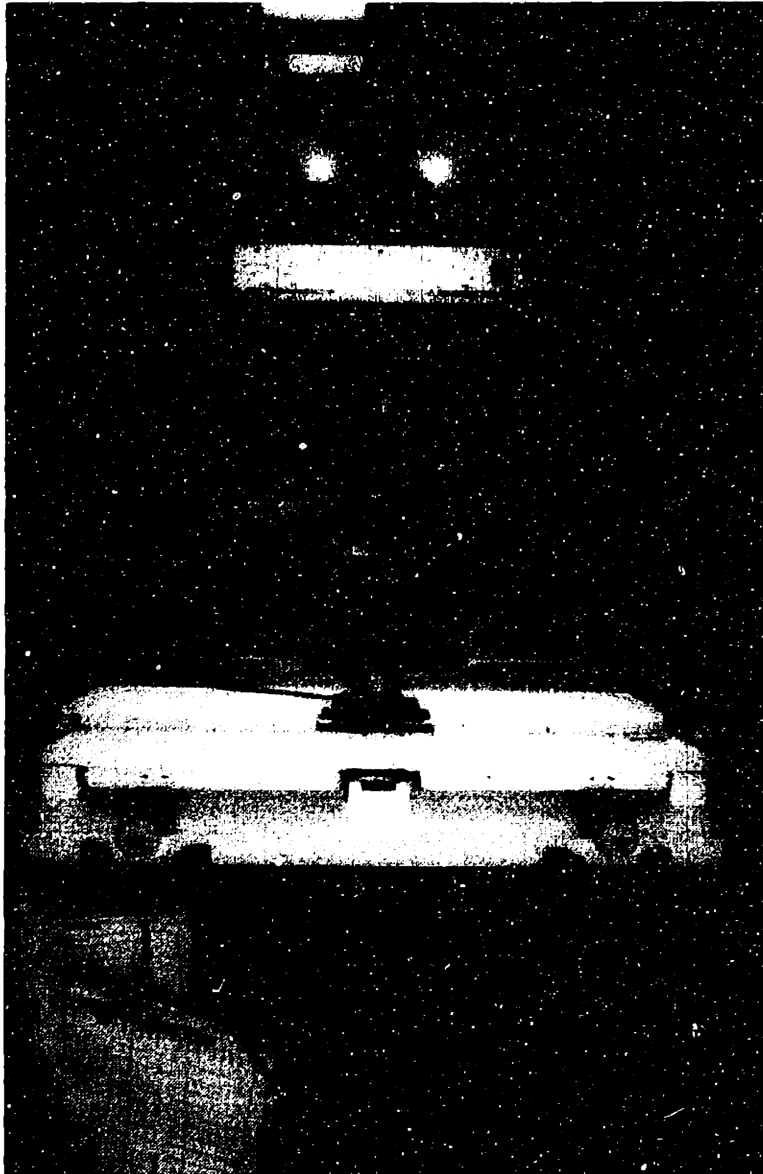

Figure 2-11: Multiline Technology artwork punch.

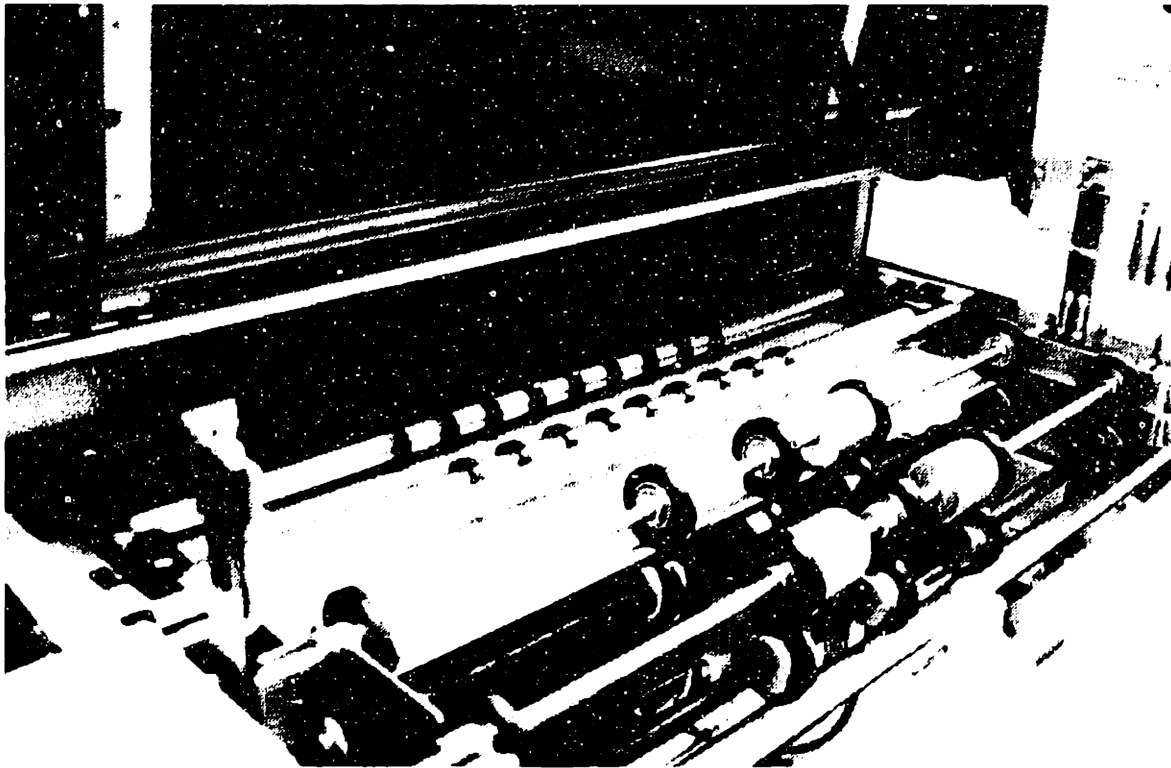

Figure 2-12: Following edging and cleaning, dry-film photo-resist is applied to both sides of the laminates with hot rollers.

An open exposure frame without laminate is shown in Figure 2-14. Frames are closed and vacuum preloaded before the laminates are exposed to UV light. Following exposure, laminates are removed from exposure frames, the mylar is removed from the dry film, and cores undergo a develop, etch, and strip procedure (DES). Note that at exposure, laminates are not tooled. Tooling of laminates occurs after DES because of material movement during chemical processing. The profile of the core after DES is shown in Figure 2-15.

Post-etch punching is the process which produces tooling holes in laminates, after material shifting has occurred. An automatic laminate punch is shown in Figure 2-16. Tooling features in cores are used to align board layers for lamination. A punch and die set used to produce the slot in Figure 2-17 is shown in Figure 2-18.

Inner-layers are now tooled and ready for kitting. Press plates with precision bushings contain pins onto which inner-layers of a board are sequentially stacked. Figure 2-19 shows a bottom press plate with pins ready to accept cores. Inner-layer

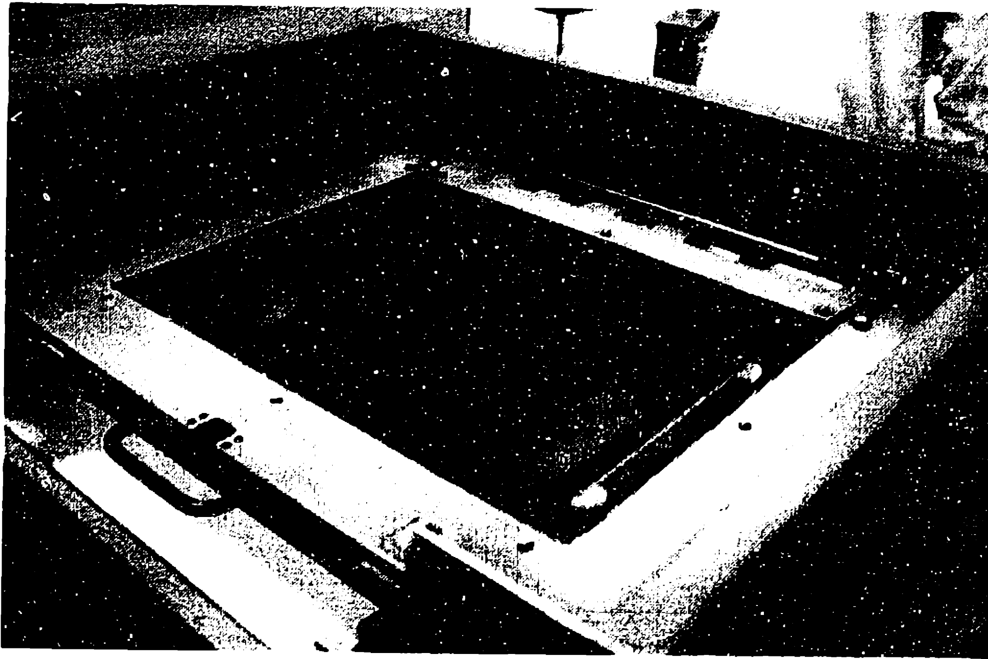

Figure 2-13: Inner-layer expose process. Top and bottom film must be registered precisely to align top and bottom features on laminates.

cores are stacked in correct order as shown in Figure 2-20. using prepreg material between layers. Multiple boards are stacked onto the same plate separated by thin separation plates to create a book. which are then sent to presses for lamination.

The lamination cycle ramps the temperature of the books above the melting point of the epoxy. while applying pressure. The epoxy crosslinks at the elevated temperature. forming a bond between the layers. At the correct time. the temperature is ramped down. and the pressure relieved. Fixturing pins are removed. cores are de-booked and re-edged. and prepared for drilling. The bonded inner-layer cores are referred to an panels. the profile of which is shown in Figure 2-21. The processes up to this point are referred to inner-layer processes. while manufacturing steps following lamination are referred to as outer-layer processes.

2.2.4 Outer-Layer Processes

Panels are fixtured to drill tables. using the tooling slots left after removal of the lamination pins. Multiple spindle CNC drills are used for drilling panels as shown in Figure 2-22. Panels are stacked on top of each other. The number of panels in a

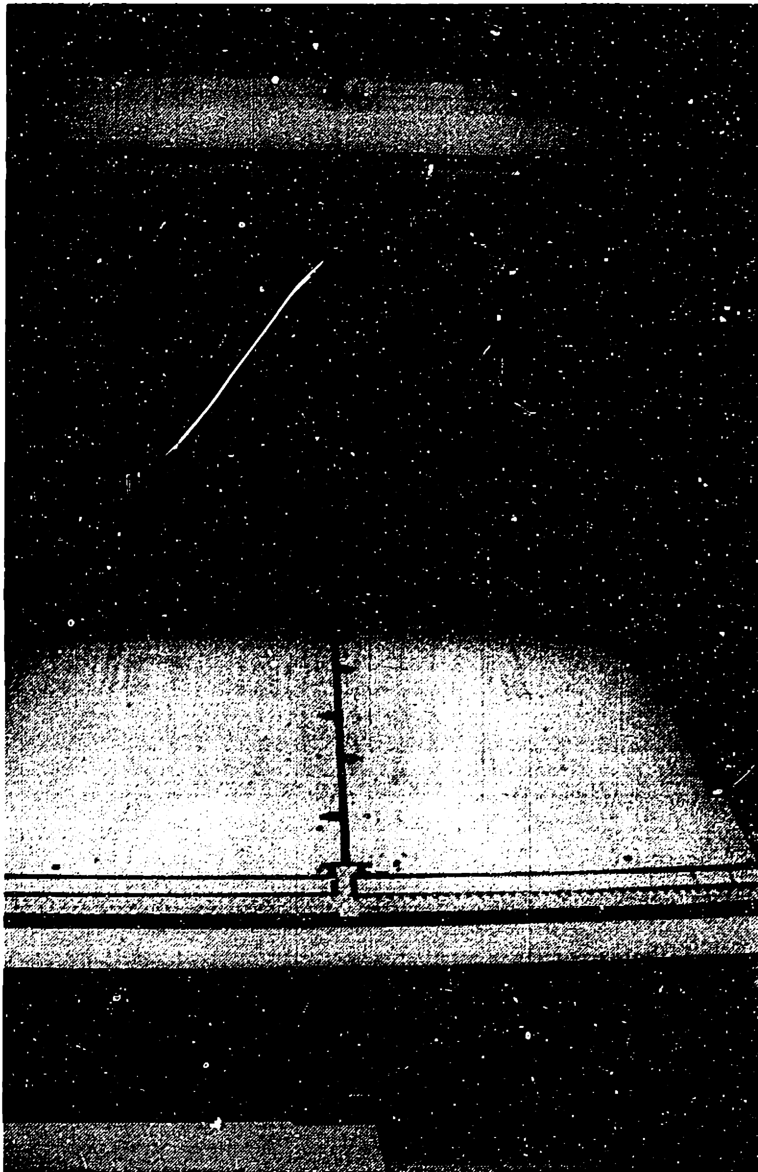

Figure 2-14: Frame to frame repeatability is as important as initial film registration. A proposed method for maintaining frame registration will be presented in Chapter 5.

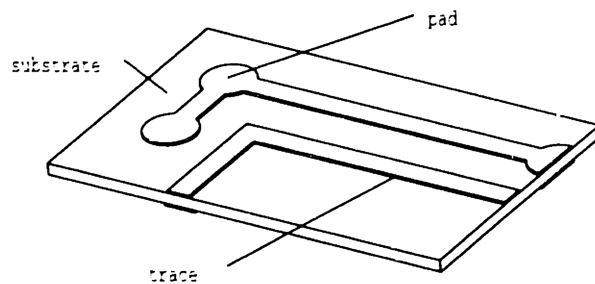

Figure 2-15: Core profile after inner-layer expose and DES.

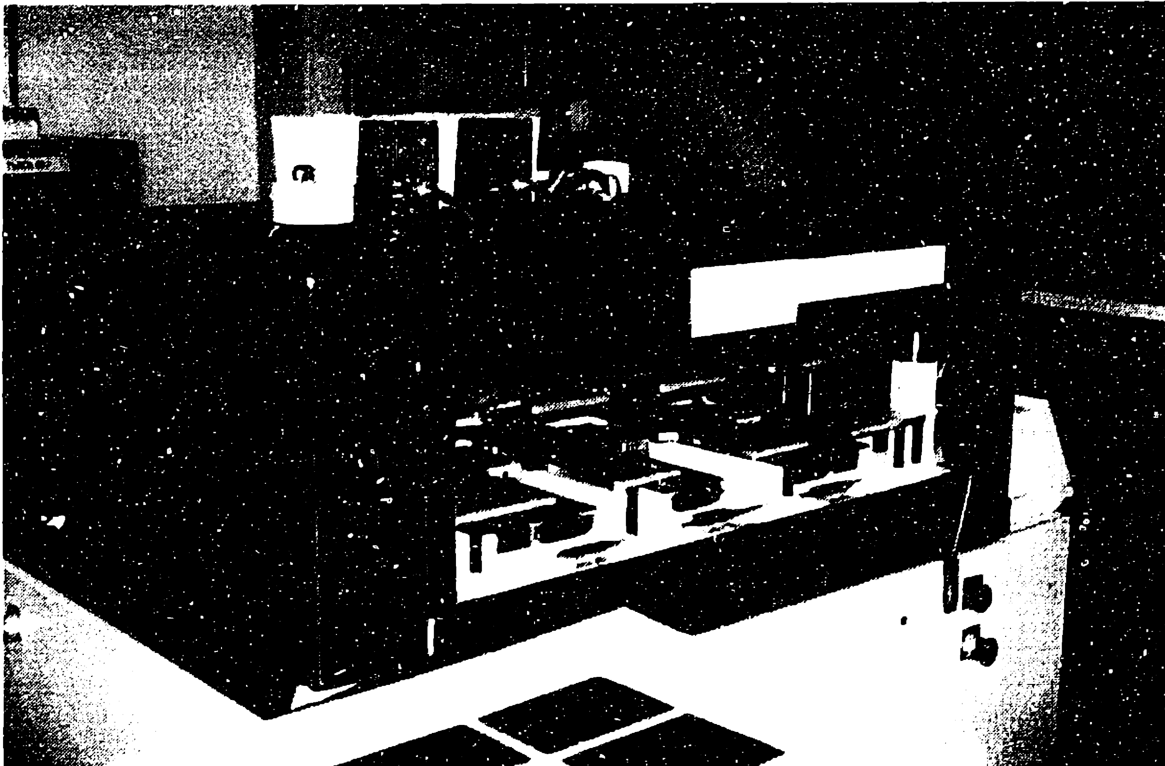

Figure 2-16: Post-etch punching after material movement has occurred from DES.

Figure 2-17: One of four punched slots in the laminate. These are used for fixturing the cores during lamination.

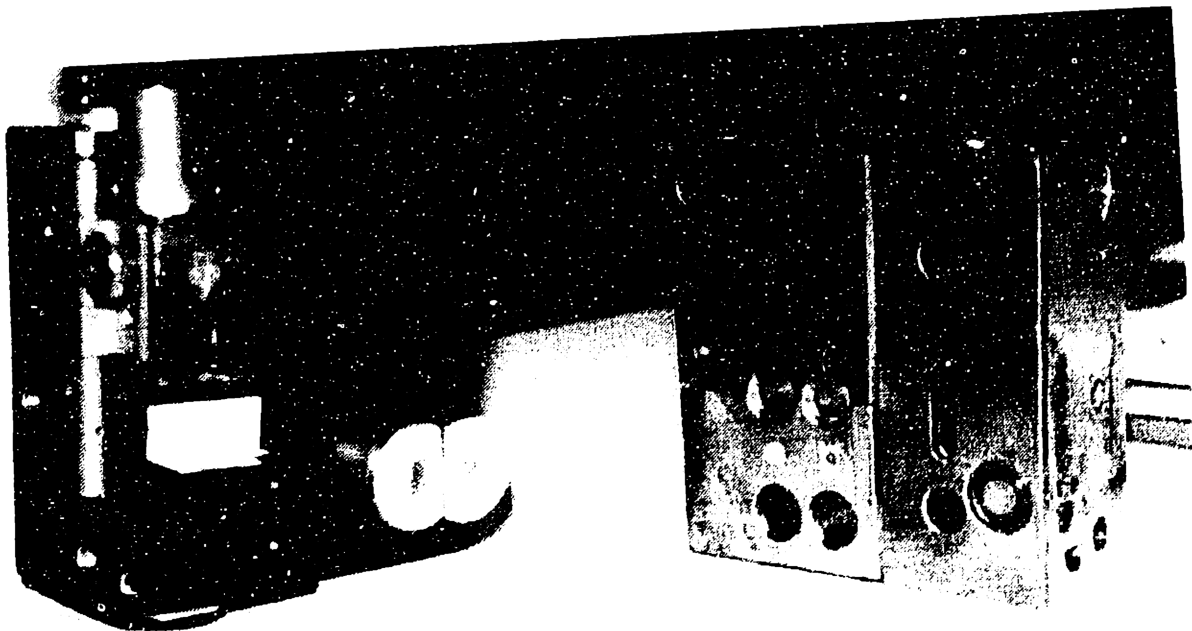

Figure 2-18: Punch and Die used in the post-etch punch. A CCD camera is attached to the punch which measures the position of a target on the laminate for registration.

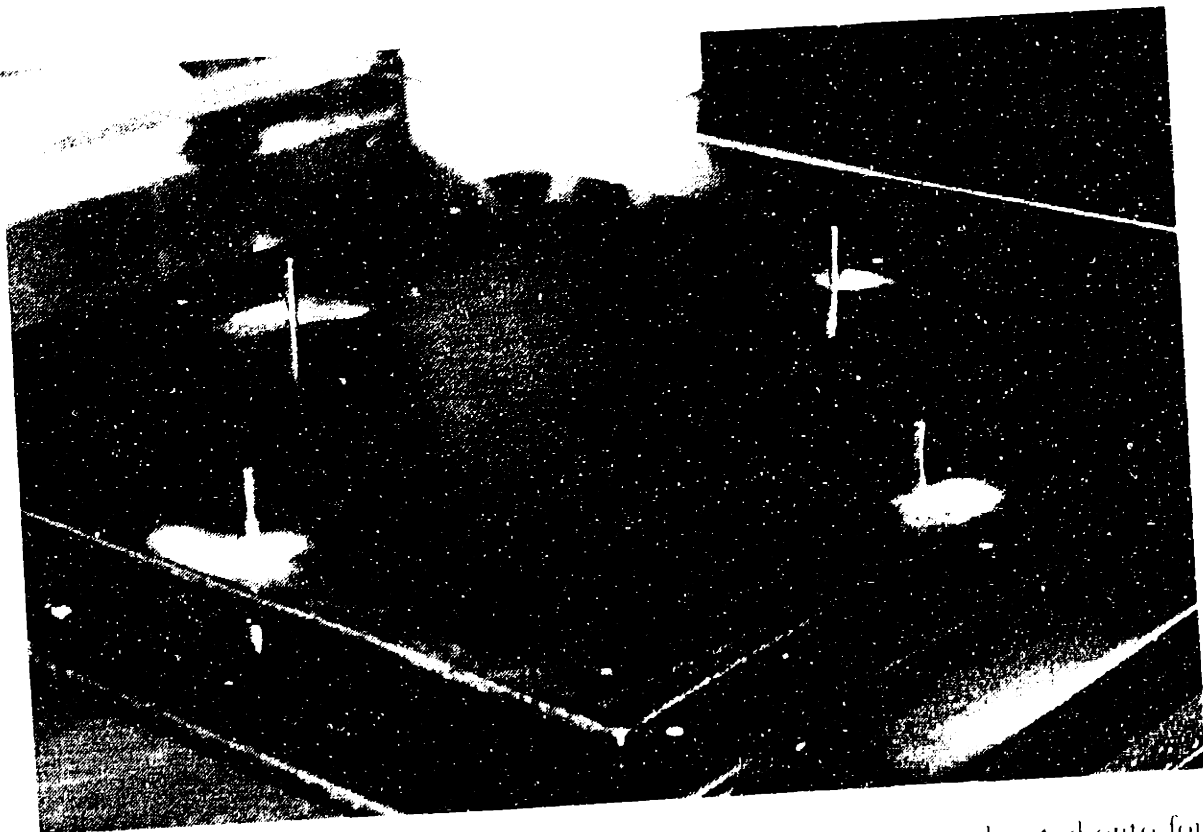

Figure 2-19: Four slots punched in cores by post-etch punching are located onto four tooling pins of a lamination plate.

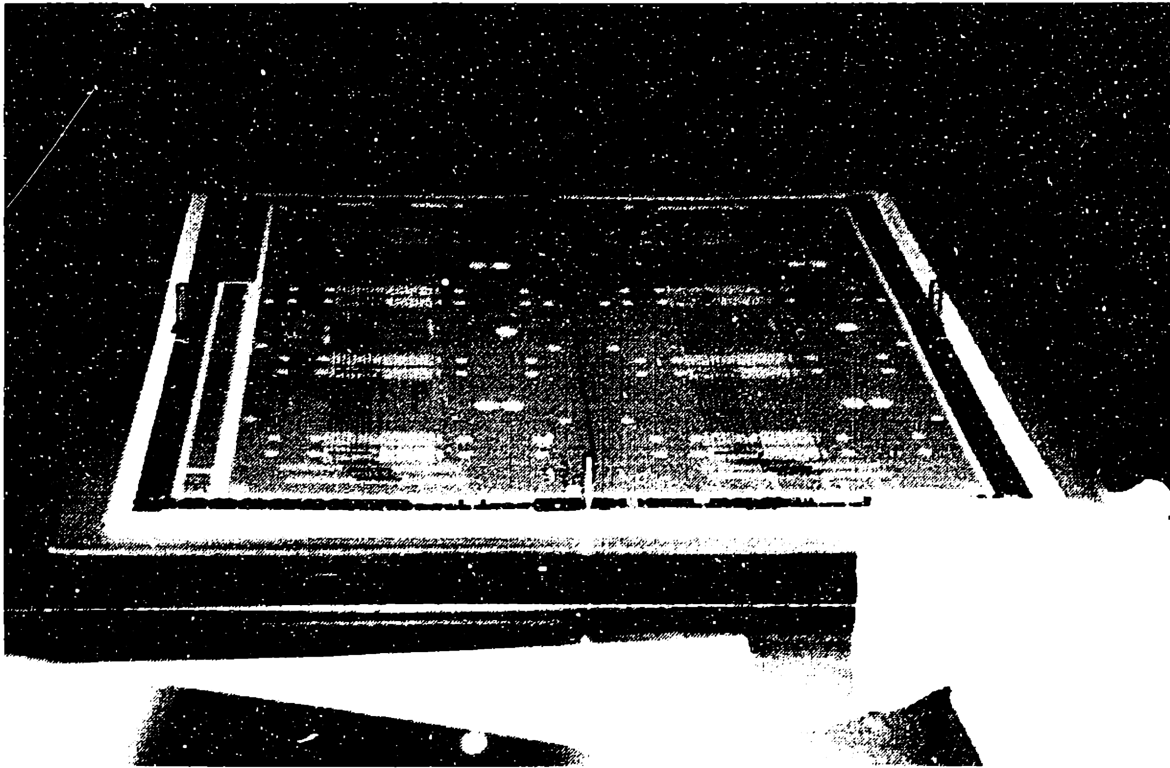

Figure 2-20: Stacking the various layers before lamination.

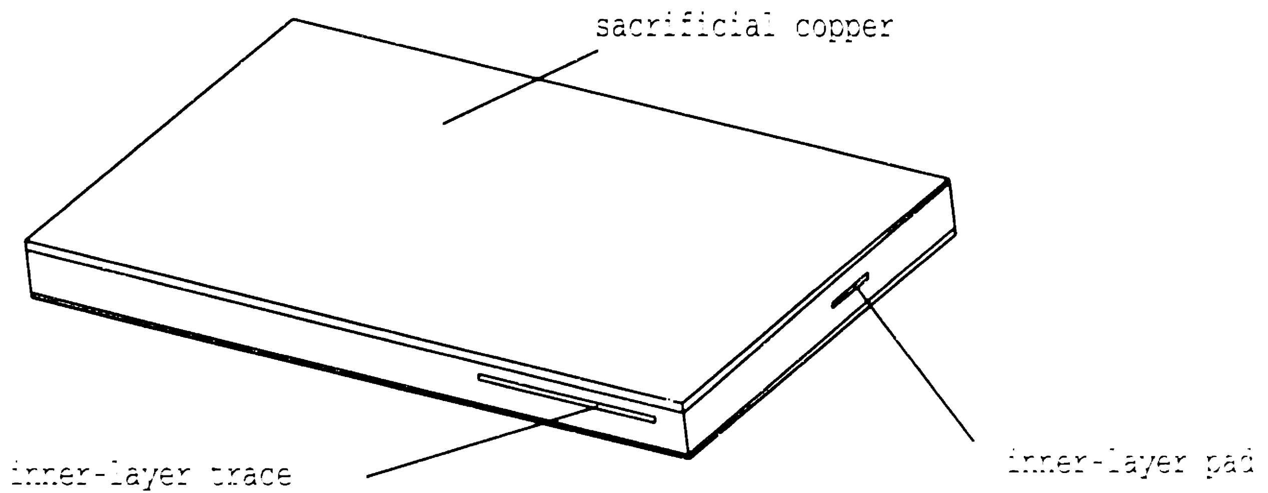

Figure 2-21: Profile of an inner-layer panel ready for drilling and outer-later expose.

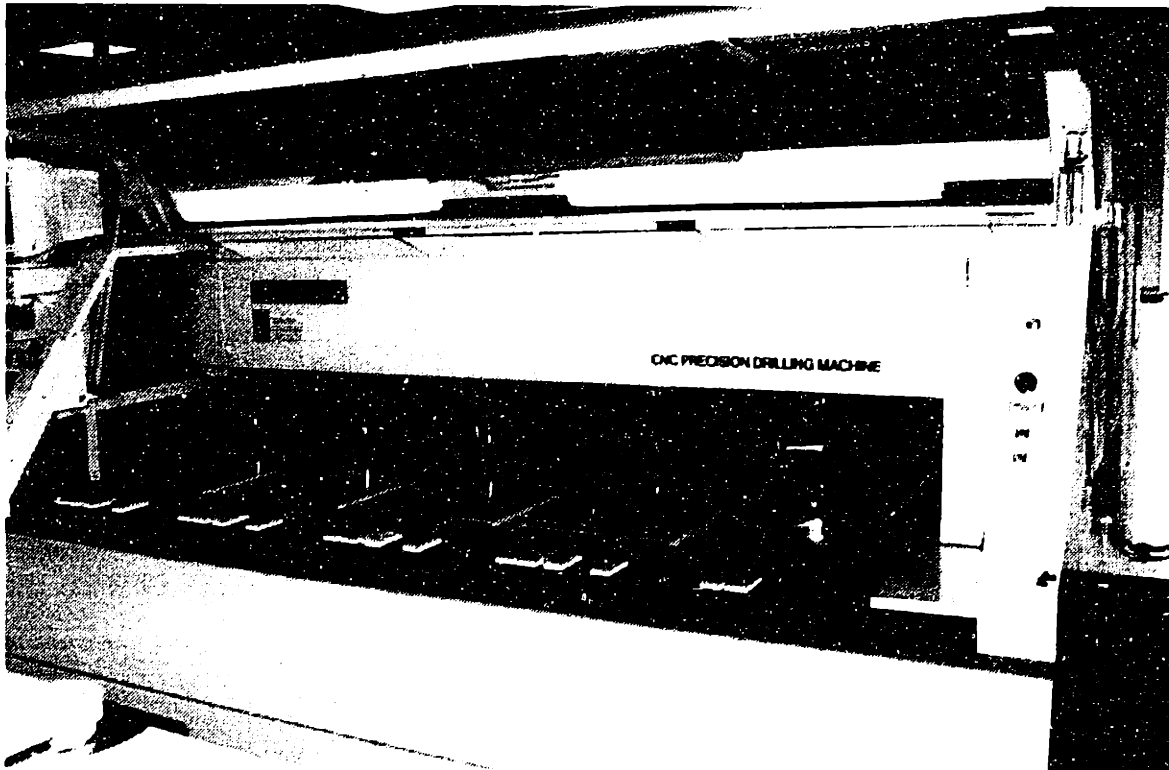

Figure 2-22: Multiple spindle CNC drills may drill approximately twenty panels simultaneously.

stack depends on the thickness. Typically 3-5 panels will be drilled together. With the five spindle drill shown in Figure 2-22, 15-25 panels can be drilled simultaneously. A drilled panel with cover plate is shown on Figure 2-23. Drilling creates the vias by which the various layers will communicate. After drilling, panels are electroless-plated to plate the vias.

Outer-layer image processes are similar to inner-layer expose, except that panels must be registered to outer-layer artwork. Dry-film resist is applied to the panels, where the film is tented over the plated through holes. Panels being off-loaded from the dry-film laminator are shown in Figure 2-24. These panels are fixtured to an expose frame for exposure of the outer-layer image. This is typically a negative process whereby the outer-layer artwork is a negative of the outer-layer board image. After exposure, panels are developed, then solder electro-plated. Photo-resist is stripped, and the electroless plate and sacrificial $1/2oz$ copper are etched, leaving a profile as shown in Figure 2-25.

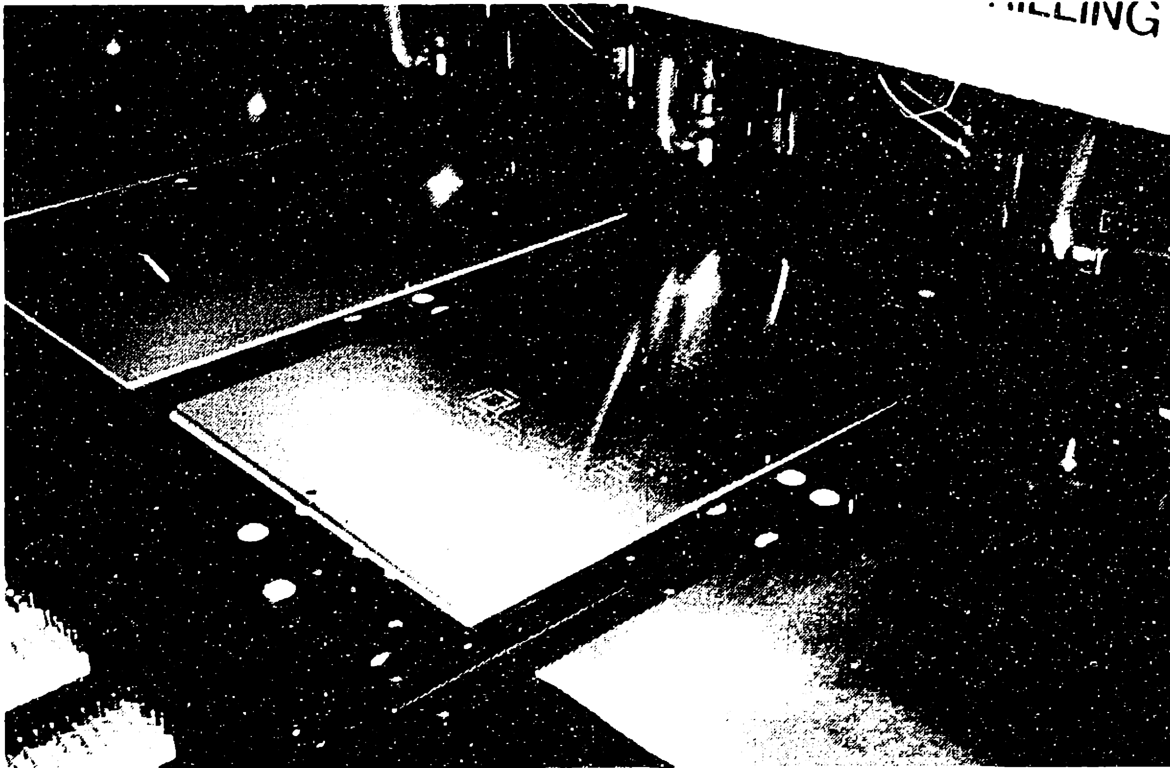

Figure 2-23: A panel with sacrificial top plate is shown. Note the drill holder in foreground.

The electro-plated solder is stripped, leaving only the copper traces and pads on the outer-layer. The panels are curtain coated with a solder mask material on both sides, via spray nozzles, and land patterns for boards components are exposed through another imaging process. Panels are developed, leaving only device pads exposed. These pads are solder plated via hot air leveling. Figure 2-26 shows a panel after hot-air leveled. Finally, individual boards are routed from the larger panels and electrically tested using bed-of-nails equipment with board specific fixtures.

2.3 Chapter Conclusions

Having outlined the various processes and described particular metrics for evaluating "connectivity", it is clear a tolerance study to identify critical processes is necessary. A description of such a study is contained in Chapter 3, where error contributions from production equipment are determined. One particular facility was studied, the

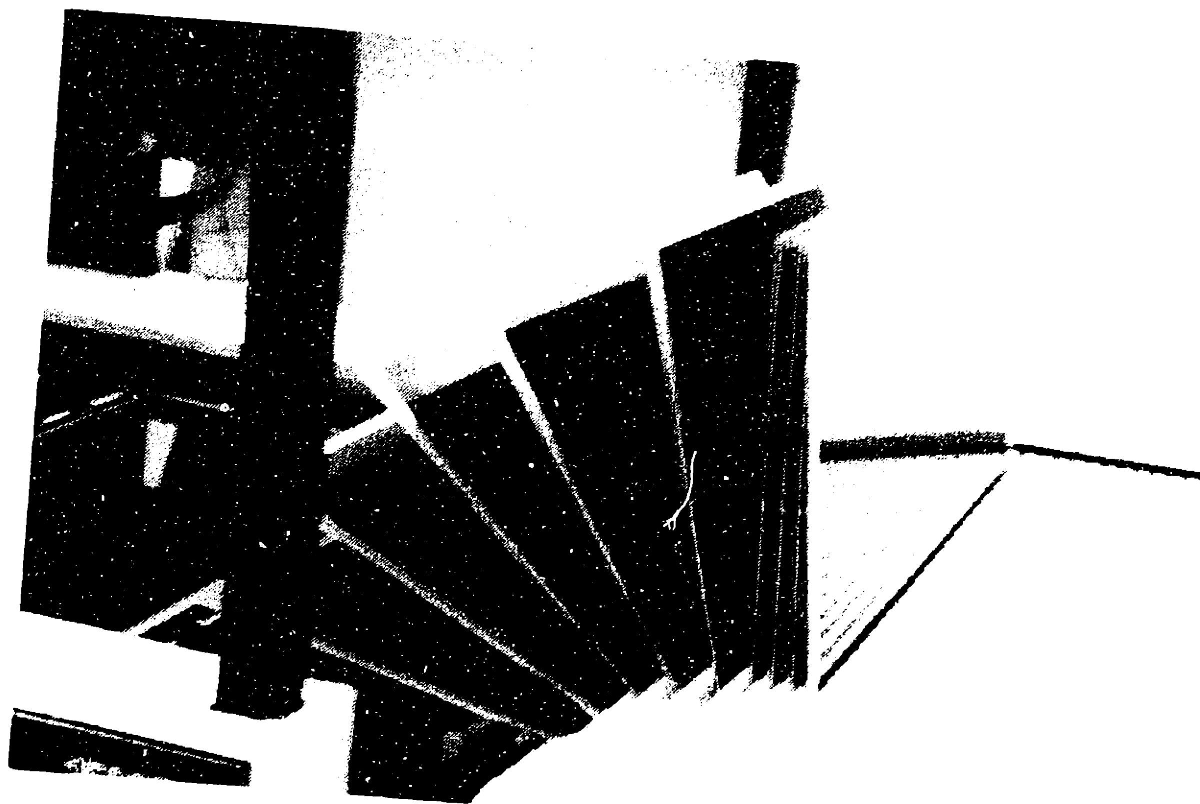

Figure 2-24: Panels being loaded from outer-layer dry-film and prepared for outer-layer expose. Dry-film tents drilled holes, although tooling slots on the perimeter are not covered, since they are used to fixture the panels in the expose frames.

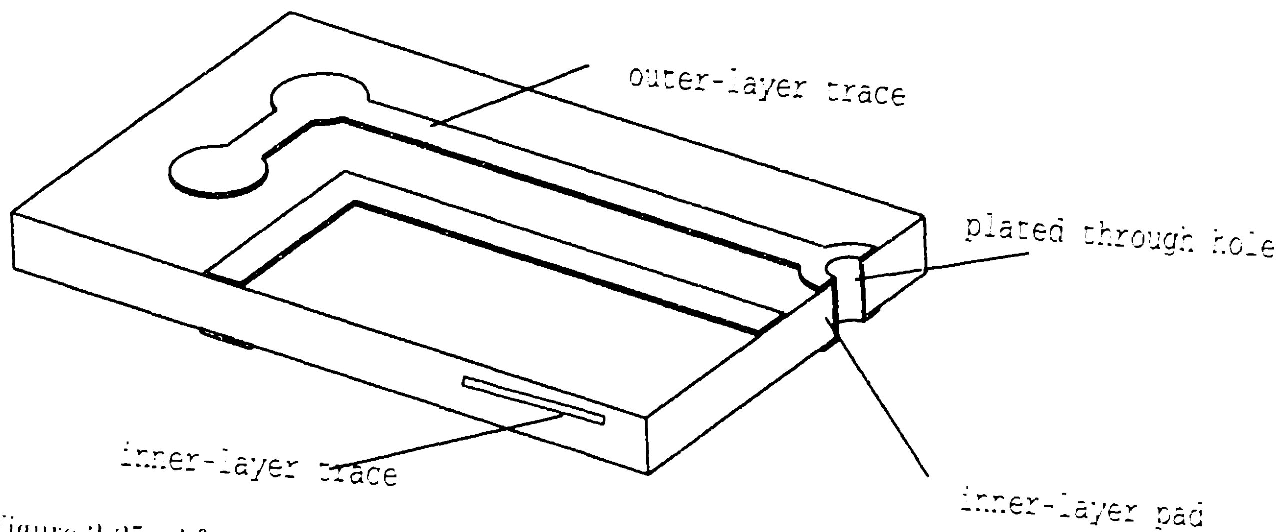

Figure 2-25: After resist is stripped, the electroless plate is etched, leaving the board profile as shown.

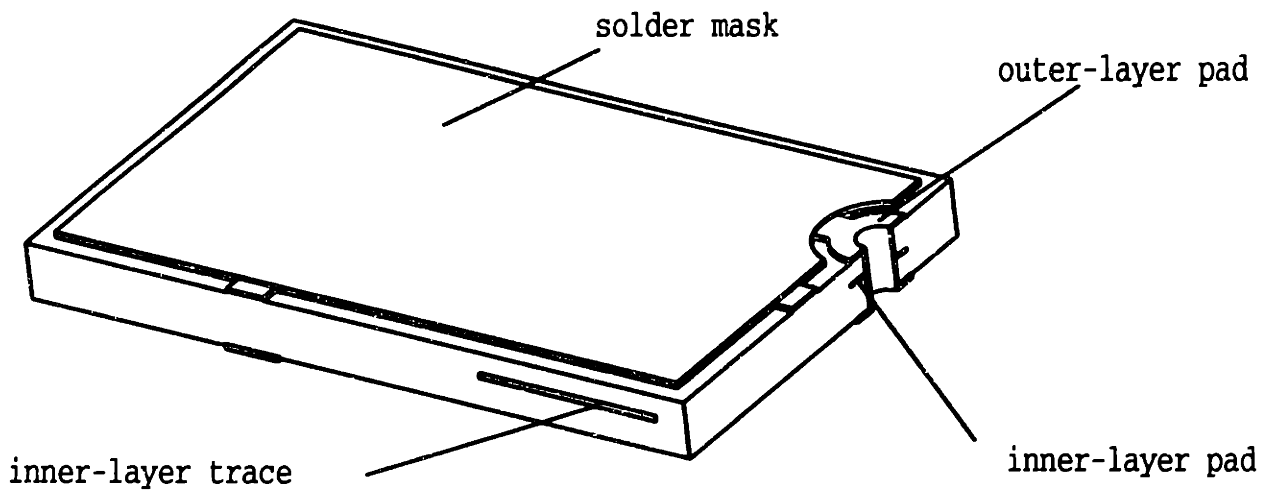

Figure 2-26: A final exposure process exposes only the pads of the devices, which are then hot-air leveled.

results from which were used to determine relationships among various manufacturing tolerances and registration errors of inner and outer-layer images. Most importantly, conditions and estimates for minimum device pitch and pad size are established, based on current state of the art.

Chapter 3

Production Facility Registration Errors

The following chapter is the result of a four month investigation of a particular production facility's current registration systems. Having already identified the need for new tooling methods, this chapter describes the sensitivity of board registration to manufacturing variances. Each production step is covered, and the contributing errors are calculated. Recommendations for discovery purposes and simple improvements are also outlined here. Except here otherwise noted, errors are assumed to be random independent variables, normally distributed about a nominal point. Process capability does not enter into the model presented herein, since tolerance control limits were not specified. Rather, the complete normal distribution is used, whereby total errors are calculated as geometric mean. Predicted results correspond with observable results, testimony to the accuracy of the model. Since the performance is predicted through the physics of the process, the alchemy of circuit board manufacture is significantly reduced.

3.1 Artwork Material Considerations

Mechanical and thermal properties of the artwork dictate film behavior when subjected to various environmental conditions and mechanical stresses, as in, for example,

Specific Gravity	1.39	
Young's Modulus	6.8×10^5	psi
Poisson's Ratio	0.25	
Tensile Strength Yield ASTM D882-67	13,500	psi
Tensile Strength Break ASTM D882-67	25,600	psi
Elongation at Yield ASTM D882-67	5.5	%
Elongation at Break ASTM D882-67	115	%
Tear Strength Initiation Graves Tear ASTM D1004-66	24	lbs.
Tear Strength Propagation Tongue Tear ASTM D1938-67	0.5	lbs.
Toughness ASTM D882-67	21,500	lb./in^3

Table 3.1: Mechanical properties of polyester film base.

punching and constraining the material. Table 3.1 outlines many of the relevant physical properties of a commonly used film base. This information was provided by Eastman Kodak [7].

For the analysis of the polyester film base, it is assumed that the material is strictly Hookean, and that at small strains, Young's modulus and Poisson's ratio will describe the stress response. This assumption is critical since it will govern the tooling designs for expose frames and punches to minimize stress, while maximizing stiffness. This optimization will maintain material integrity and permit extreme levels of precision in film placement.

The mechanical properties of the film, e.g. Young's modulus and Poison's ratio, will determine how the film deflects under applied loads, such as a fixturing preload. Mechanical properties alone, however, do not fully characterize the film's static deflection. Thermal properties become increasingly important as feature densities increase and precise registration is required. With certain assumptions about the operating environment, and the thermal conductivity, capacity, and expansion of the film, exchange of energy between the film and surroundings may be predicted. Important aspects of this energy exchange include thermal transients within the film, due to environmental fluctuations, and thermal gradients within the film. Spatial and temporal thermal behavior will determine dimensional behavior of the film, due to its inherent thermal expansion. Thermal properties are given in Table 3.2.

Thermal Coefficient of Expansion	0.0018	% / °C
Humidity Coefficient of Expansion	0.0005	% / %RH (measured at 50% RH)
Coefficient of Conduction	0.13	W/mK
Heat Capacity	1900	J/kgK

Table 3.2: Thermal properties of various polyester film bases.

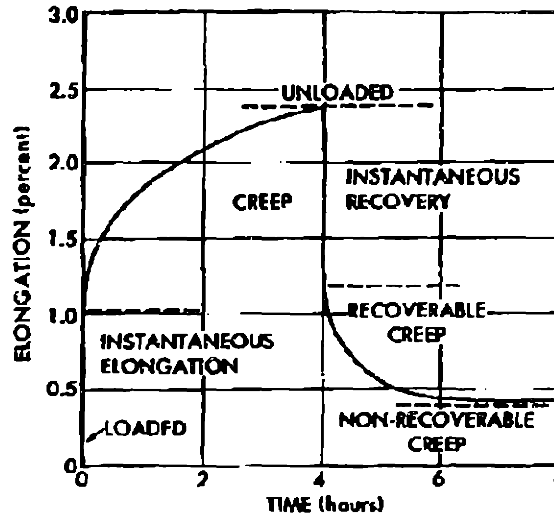

Figure 3-1: Creep and recovery for a typical film, under 6000 psi tension.

Primary and secondary creep behavior of a typical Kodak film is shown in Figure 3-1. The visco-elastic properties; however, were not considered for design purposes.

To determine whether internal thermal gradients contribute to material deformation during thermal cycling, the dominant mode of heat transfer must be calculated. In order to do this, certain assumptions about the operating environment must be made; specifically, the degree to which exchange of heat between the film and surroundings is facilitated. Therefore, the coefficient of convection, assuming free convection of a horizontal surface, will be estimated. From the convection coefficient, validity of a lumped parameter model is tested. If the film base within the operating environment may be treated as a lumped parameter material, then internal thermal gradients may be negligible, and it may be assumed that artwork expands and contracts uniformly based on its thermal expansion coefficient. Furthermore. thermal time constants may

be calculated.

To calculate the convection coefficient, the nature of the thermal boundary layer must be determined. For this, the Rayleigh number was calculated by the following equation, using parameters for air at 21°C,

$$Ra = \frac{g\beta \Delta T L^3}{\alpha \nu} \tag{3.1}$$

Since $Ra < 10^7$, the thermal boundary layer is laminar, and the convection coefficients for warm and cool surroundings, respectively, are given by the following relationship,

$$\overline{h} = \frac{k\overline{Nu_L}}{L} \tag{3.2}$$

where $\overline{Nu_L}$ is determined from semi-empirical relationships involving the Rayleigh number. For warmer surroundings, the convection coefficient, h is approximately $1W/m^2K$, and for cooler surroundings is $2W/m^2K$.

To determine whether thermal gradients dominate the behavior of the film, the ratio of convective heat exchange with the surroundings to internal conduction is calculated. This dimensionless quantity, the Biot number, is defined as,

$$Bi \equiv \frac{\overline{h}L}{k} \tag{3.3}$$

where L is the thickness of the material, $\overline{h}$ is the convection coefficient as above, and k is the thermal conductance of the film. For a conservative estimate, the lower of the convection coefficients previously calculated is used. The thermal conductivity of the polyester film base is approximately $0.13W/mK$, and is 180 mm thick, yielding an approximate Biot number of 2.7×10^{-3}. Since this number is significantly less than 1, the material conducts heat internally more easily than it convects heat with the surroundings. Therefore, within the film, thermal gradients can be neglected, and a lumped parameter model for the transient thermal behavior will be used.

The transient thermal behavior of the film behaves as a simple first order system,

where the response is given by,

$$\frac{T - T_\infty}{T_i - T_\infty} = e^{-t/\tau} \tag{3.4}$$

where T is the temperature of the film, T_∞ is the surrounding temperature, and T_i is the initial temperature of the film. Notice an electrical analogue of this system is a capacitor (thermal mass) and a resistor (convection). Of importance, is the time required for the temperature to reach a particular value. The temperature at most circuit board photo facilities are controlled to $\pm 0.5°C$. Recall that the convection coefficients for heating the film, due to an increase in surrounding conditions is approximately half of that to cool the film, due to a decrease in surrounding temperatures. Therefore, the time constants for heating and cooling are different. Using property values listed in Table 3.2 and the appropriate convection coefficient, the time constant for heating is calculated as 0.5 s, and for cooling is 0.25 s. These are the times required to reach 63% the steady state surrounding temperature. For 86% of steady state, these times are doubled. Interestingly, these times are relatively short, despite the large thermal capacitance of the film. These fast transients are because the films are only 0.18 mm thick. It is assumed that large environmental thermal variations occur over long time scales as compared to film time constants; therefore, it may be assumed that film temperatures track surrounding temperatures without significant delay. That is, thermal dynamics may be ignored, and the problem is reduced to a quasi-static process.

Finally, from the expansion data provided, variation in film dimension can be calculated. Given a film coefficient of expansion of 18 ppm/°C, environmental variation of $\pm 0.5°C$, and film width and length dimensions of 0.53m $\times$ 0.64m, absolute thermal growth is 4.8 mm x 5.7 mm. Since thermal gradients can be neglected, expansion or contraction is uniform, occurring with time constants determined above.

Note that during process operations, artwork is in contact with a machine table of considerable thermal mass, in which case, environmental temperature fluctuations minimally affect the thermal condition of the tables. Because of this, the film surface in contact with the machine is at the machine temperature. Therefore, a thermal gradient

in the z-direction does exist, however, because the film is thin, this gradient has negligible affect on the dimensional stability, and certain phenomena, such as cupping, can be ignored, especially since induced thermal stresses are dominated by the body forces of the films. As an aside, thermal gradients, as those just described, in silicon wafers cause undesirable dimensional responses during processes like lithography and resist deposition. Fortunately, however, the processing of large format polyester films is more robust than that of silicon wafers.

Material expansion and contraction is also a function of humidity, which for unprocessed ALI-7 is 6 ppm/%RH and 5 ppm/%RH for processed ALI-7. Kodak provides a humidity coefficient specification which is obtained by linear interpolation from 15% RH to 50% RH. The humidity expansion is, in fact, non-linear with relative humidity, and within $\pm5\%$ RH within the particular facility studied, the expansion is 5 ppm/%RH. Expansion coefficient within this small region will be used throughout this thesis. Humidity control within $\pm5\%$ contributes approximately $\pm13\mu m$ of movement for a $0.5m$ film dimension. Figure 3-2 shows typical elongation of various film bases as a function of relative humidity. Note that material movement due to humidity fluctuations can be 2.5 times as great as movement caused by temperature fluctuations. Although ppm stability of the temperature induced variability is greater than the humidity expansion rate, humidity is only controlled to $\pm5\%$. Therefore, efforts towards increased humidity control capabilities are warranted. should be implemented.

3.2 Photo-Plotting

Since registration of printed circuits is based on optical alignment of target patterns to fixed references, alignment performance will largely be limited to that of the photoplotter. Optical techniques that average plotter error for alignment will be presented in later chapters. For now an understanding of limitations of photo-plotting must be understood.

Plotter performance is measured in terms of resolution, dimensional tolerance of plotted features, and feature to feature locational tolerance. Table 3.3 outlines these

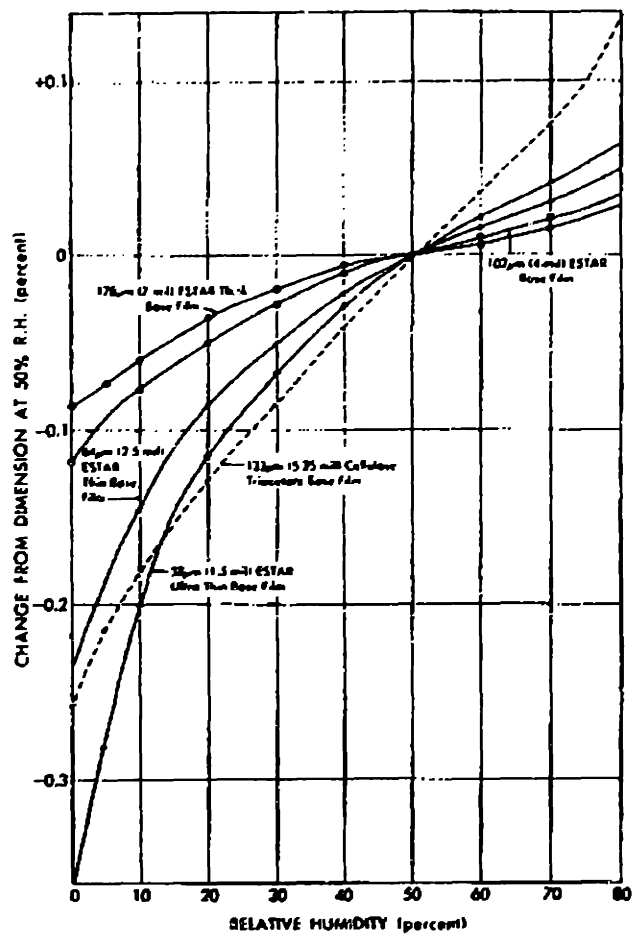

Figure 3-2: Dimensional variations of unprocessed Kodak film. Measurements taken at 21°C

Plot Resolution (low)	6.4	μm
(high)	3.2	μm
Edge Roughness	± 25.4	μm
Accuracy	± 7.6	μm
Repeatability	± 3.8	μm
Line Width Variation	± 3.8	μm
Minimum Plotted Line Width	50	μm (low resolution)
	19	μm (high resolution)

Table 3.3: Performance specifications for an Optrotech Golden Plotter.

and other performance specifications for a high resolution Optrotech Golden plotter.

Repeatability, or precision, is a measure of the statistical spread of a number of measures. For plotting, Gaussian distributions are assumed, hence an average (accuracy), and sigma (precision), will define a particular probability density function. Confusion arises from the loose usage of these terms in image quality specifications above. When one film is plotted, the x position (defined as the drum circumferential direction) and the y position (linear laser guide axis) of each feature's center location is measured and nominal dimensions are normalized. Average position and spread for that one film are recorded. The location of any one feature to another is centered about an average, with a $|3\sigma|$ of $7.6\mu m$ (Golden plotter). The average defines the per film accuracy and repeatability (σ) for that one film The same operation for successive exposures is performed. The average point positions per film is averaged, and the distribution of those per film averages is determined. This distribution of per film average positions is centered about zero, with a $|3\sigma|$ of $3.8\mu m$. Notice that film to film accuracy is perfect since an absolute reference does not exist. That is, the average of the per film averages is zero because data is measured with respect to a plotted feature rather than another datum. Figure 3-3 illustrates the notion of per film accuracy and precision, and film to film accuracy and precision. Difficulty arises in measuring printed features, not only because of the accuracy to which they must be measured, but also in that the film must be developed, which introduces additional errors.

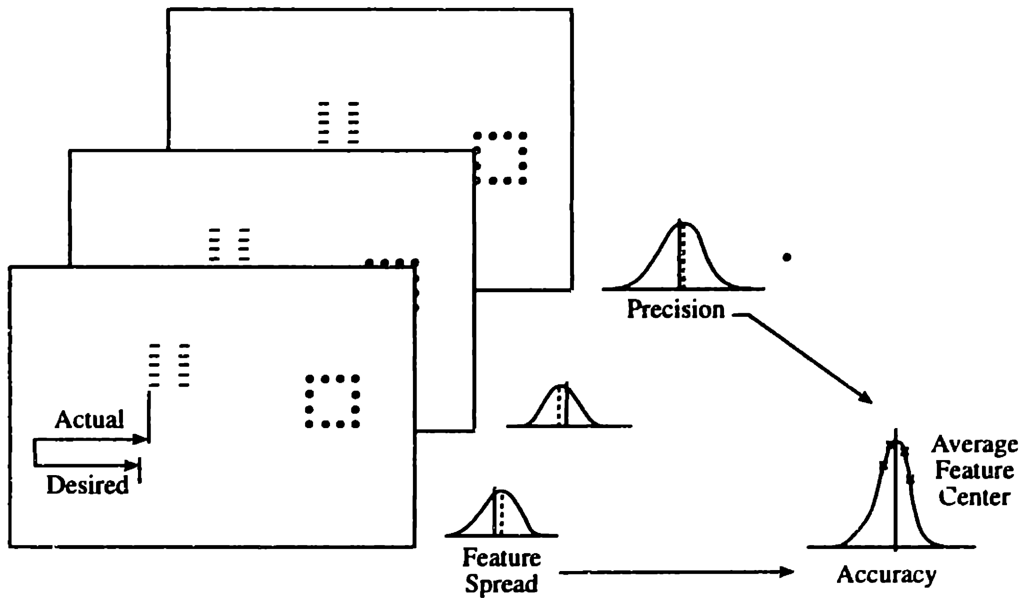

Figure 3-3: Accuracy and precision of plotted features.

Whether the film is underdeveloped or overdeveloped, plays a significant role in the final size of the printed features. Plotter errors aside, features may be undersized or oversized approximately $\pm 2.5\mu m$. The development process is a function of many process factors, such as processing duration, temperature, and replenish rate. Note that unlike plotter error, which produces random errors of all features on a film, under or overdeveloping contributes uniformly to the entire film.

The film, at this point, does not contain any mechanical tooling features. Following developing and verifying, the artwork is punched with tooling features by manually aligning artwork features to the punch dies. Historically, post-plotting punching has not been the case. Previous to post develop punching, tooling features prior to expose were used to achieve front-to-back registration. However, because of printer positioning accuracy and repeatability limitations in tooling features, registration capabilities were limited. This was one motivation for the current procedure of post-expose punching.

Again, the limits of punch registration are being reached. A technique based on kinematic tooling of artwork will be described in Chapter 5. Repeatability results are also presented in Chapter 5.

3.2.1 Sources of Error

The sources of the above described errors are due to a number of electrical, mechanical, and optical factors, and it is difficult to assign attributable causes without rigorous study of the particular design. Therefore, the degree to which a factor contributes to a particular error will not be estimated; instead, possible sources of error will be qualitatively discussed within the general context of opto-electrical- mechanical systems.

Drum related errors include geometrical errors in the drum itself and error motions due to bearing runout and compliance. As in most spindles, the dominant contributing factor to error motions is bearing compliance. The accuracy of a bearing is a function of its type (rolling element, contact, aerostatic, hydrostatic, or magnetic), size, preload, and constructional integrity. The plotter drum uses rolling element bearings, whereby the error motions will largely be periodic in nature, with a spatial frequency equal to the spatial frequency of the balls or rollers. The spatial frequency of the rolling elements can be determined from the size of the bearing and the number of rolling elements it contains. The periodic errors will be in the radial direction at both ends of the drum, combinations of which producing radial, yaw, and pitch error motions, as shown in Figure 3-4.

The specific design, selection, and installation of the bearings is critical to minimize bearing error motions. Without further study of the actual plotters, however, bearing selection and mounting issues are inconclusive.

Transmission and actuator dynamics also play a significant role in the performance of the plotter drum. Oscillations resulting from gearing and stator/rotor dynamics can cause errors in the velocity and position tracking of the drum. Since the drum may operate in both synchronous and asynchronous modes, control of the drum is critical. Compliance in transmission elements, such as timing belts, will often contribute to endpoint (drum rotation) errors. Closing the feedback loop based on a drum encoder is used to minimize such errors.

Although axial stiffness of the drum is important, it is also of equal importance

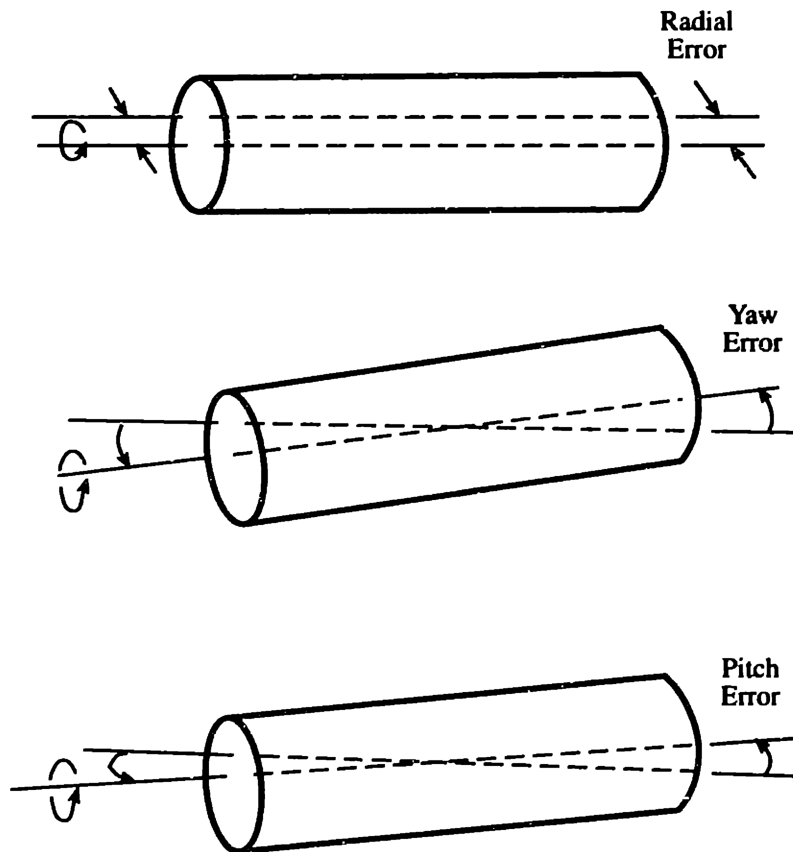

Figure 3-4: Radial, yaw, and pitch errors of plotter drum.

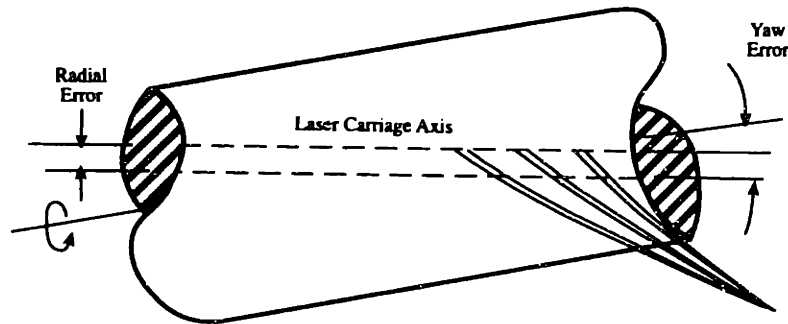

Figure 3-5: Sensitive error motions of plotter drum.

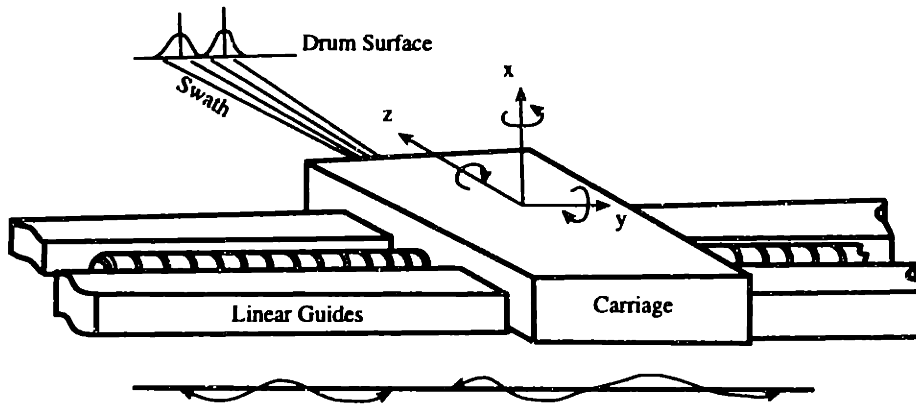

Figure 3-6: Laser carriage error motions.

to appropriately design the axial constraints so that thermal expansion of the drum or bearing shaft does not apply excessive preload on the bearings. This will cause error motions in the radial directions since over-constraining the drum in the axial direction will alter radial bearing preload, hence affecting its compliance. Because of the small distance from the laser head to the film and the beam collimation, plotter performance is robust to radial error motions in the plane of the laser swath. However, the plotter is sensitive to other drum error motions, either strictly radial or yaw errors, as illustrated in Figure 3-5.

The carriage assembly scans the laser swath across the length of the rotating drum; hence, its positional repeatability and resolution will determine the $y$location of exposed features. Further, other error motions due to bearing, actuator, transmission, and structural compliances as well as geometric errors will cause errors in both the x and y directions. The carriage assembly with an associated coordinate system is illustrated in Figure 3-6.

The previous discussion on bearings applies to the carriage, except that in this instance, bearings used are for linear travel. Bearing compliance and friction play an important role in the positional accuracy and precision of the print head. Vibrations from recirculating elements may also contribute to plotter error. Since the print head is close to the surface of the films, feature positions are relatively insensitive to rotational errors of the head, as compared to translational errors in the x and y directions. The loads acting on the print head are strictly inertial, and since the accelerations are small, the inertial forces are low. However, the significant print head error motions are probably due to vibrations caused by the stepping action of the motor. The frequency of stepper vibration is of particular importance, since it may excite certain structural modes in other mechanical elements.

The primary subassemblies of the plotter include the drum and the laser carriage; however, the actual structure is important, in that constructional details determine thermal stability and natural modes. It has been the author's experience that many errors in machined parts, or otherwise produced, could be related to structural vibrations.

Errors in feature location are primarily due to the mechanical design of the various subassemblies. Often, errors can be reduced significantly by designing a structure with well damped modes and by selecting and properly installing bearings with appropriate stiffnesses. Although a sound mechanical design will reduce and often eliminate errors, electrical support systems must also perform well. The synchronization of the acoustic-optic modulator with the rotational speed of the drum is critical for accurate location of plotted features in the direction of rotation. Synchronization of the carriage with the drum is important for feature placement in both rotational and translational directions. The speed with which the plotter operates is limited by data transfer rates and controller bandwidth. Tracking ability of the system is a function of the controller, amongst other factors, and its robustness to external disturbances. Errors in feature size and location are also due to the stability of the acousto-optic modulator and the related drive electronics. The Optrotech plotter splits the laser beam using 32 frequencies and the degree to which any one of the laser spots is in the correct

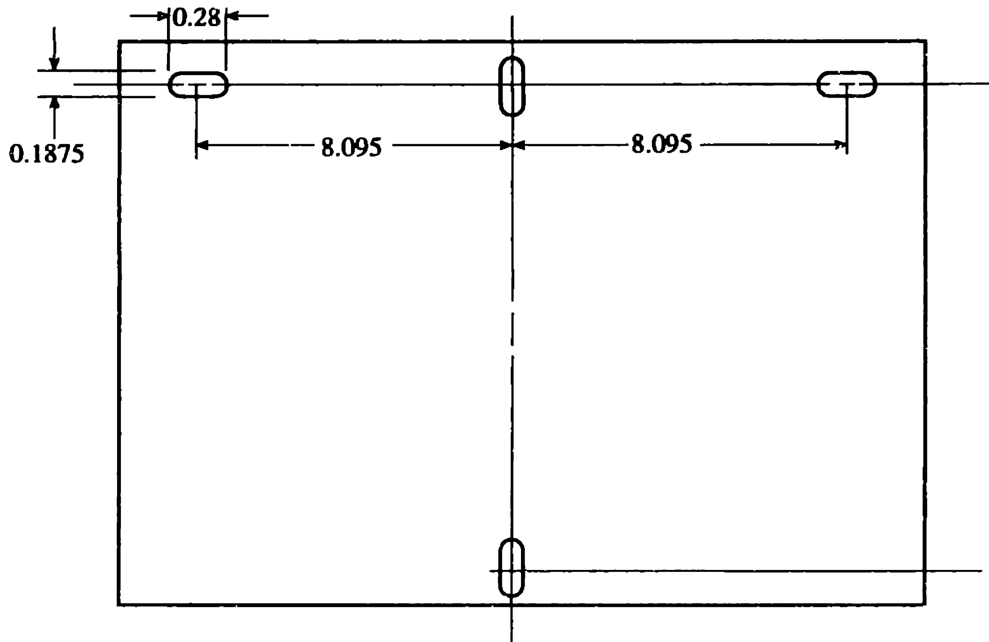

Figure 3-7: Current artwork tooling scheme (dimensions in inches).

location is a function of the integrity of the acoustic signal and the crystal material.

3.3 Artwork Tooling

Having outlined the error contributions from environmental effects and photo-plotting, tooling errors may now be estimated. The artwork punch, shown in Figure 2-11, is used for tooling the artwork. Film is vacuum fixtured against the tooling table and manually aligned to fixed targets using a 1.85× optical system. Printed targets on the film define centerlines, *within* the errors introduced by the plotter itself. This fundamental alignment limitation will be addressed in Chapter 4.

The tooling pattern for inner-layer artwork is shown in Figure 3-7, with appropriate dimensions. The only difference between inner-layer and outer-layer artwork tooling is in the additional clearance holes for panel constraining pins.

The motivation for this film tooling hole configuration is to define the orthogonal centerlines of the film, hence any material movement occurs with respect to the datum defined by the intersections of these lines. Process capability requirements, call for $\pm 2.54 \mu m$ hole position-to-position accuracy, with a $\pm 12.7 \mu m$ repeatability. Slot

widths, although not measured, were required to be $4.76mm \times 7.11mm, +7.6\mu m/-0.0\mu m$ with a $\pm 7.6\mu m$ repeatability.

The artwork is constrained using the pins of the expose units, with locational tolerances for the upper three pins along the axis are held to $\pm 12.7\mu m$, assuming the pin locating holes are jig ground using a pinning template. The y axis tolerance for these three pins and the forth bottom pin are $\pm 12.7 \pm m$. Pin dimensional tolerance is not given, but it assumed that the pins are ground to $4.76mm$ flats $+0.0\mu m/-5.0\mu m$.

3.3.1 Film Placement Simulation

Solution of the film placement problem with variation in multiple slot/pin pair sizes and locations is non-trivial. Therefore, a numerical simulation was devised that created tooled film, and pinned tables. Film was placed on tables with the goal to minimize the squared error among the pins and slots. Clearance or interference fits were calculated based on the simulated slot and pin size and final film position and orientation. It is important to realize that film positions and orientations are dependent on previous pin conditions. Numerical techniques can determine the statistical distribution of the clearances interferences and material mechanics will determine the equilibrium position of the film when interference conditions are encountered. Elastic averaging of hole deformations leads to a non- repeatable, indeterminate structure where positional precision is a strict function of manufacturing ability. The point of the discussion is that the factors which determine the registration capabilities are not deterministic. Using known manufacturing tolerances, film and frames were created. The goal of the simulation was to place slot centers over pin centers. This was accomplished by appropriate translational shifts and rotations. The coordinates of a point in a corner of the film was tracked during the simulation. Figure 3-8 shows the distribution of the "ideal" point after all four slots were placed over the pins. This data includes the distribution of a random sample of film fixtures to a random sample of frames.

Figure 3-9 shows the distribution of an "ideal" point for a random sample of film on the same frame, and Figure 3-10 shows the distribution of an "ideal" point of the

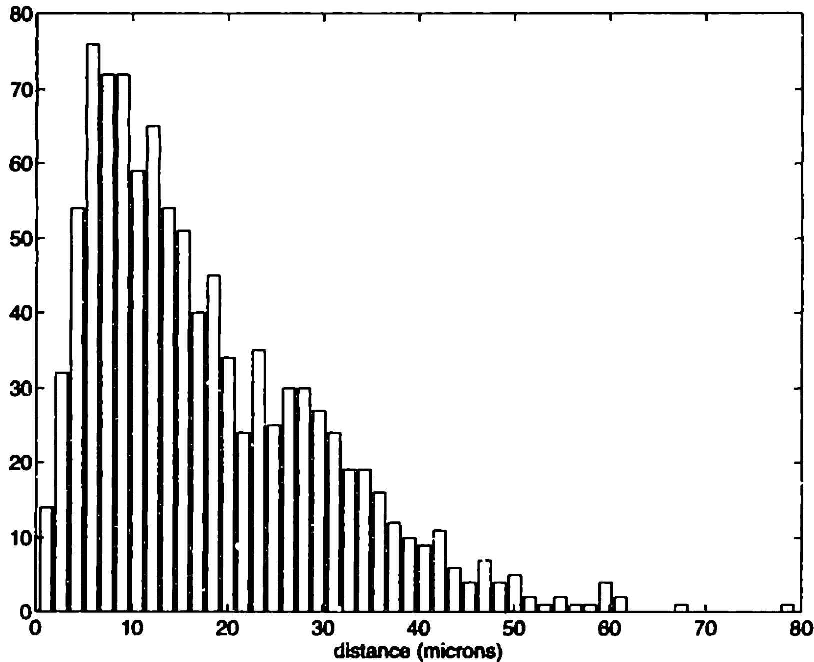

Figure 3-8: Distance distribution of an "ideal" point on a film from nominal (zero) position after being fixtured to four pins.

same film placed onto a random sample of frames.

Interestingly, the simulation demonstrates that registration performance of the four slot system (film or cores) is limited due to the ill-defined constraints and their non-deterministic nature. A kinematic film fixturing system, which will be described later, is limited only by punch and alignment repeatability. The physics of the kinematic fixturing does not further contribute to registration error as does the four slot system. Variations from frame-to-frame are non-existent for the kinematic system, even in the presence of frame variations.

During this investigation, some operators stated that there was substantial tooling clearance to permit hand alignment of the films. For many types of artwork, manual alignment due to tooling error is adequate, although undesirable, and it would be best to eliminate any human factors for registration accuracy and precision.

Because excess clearance is not desirable from a fixturing standpoint, the hole to pin tolerances are held to the tightest tolerances manufacturing allows. The non-deterministic nature of the current pin/slot interfaces, will frequently cause local de-

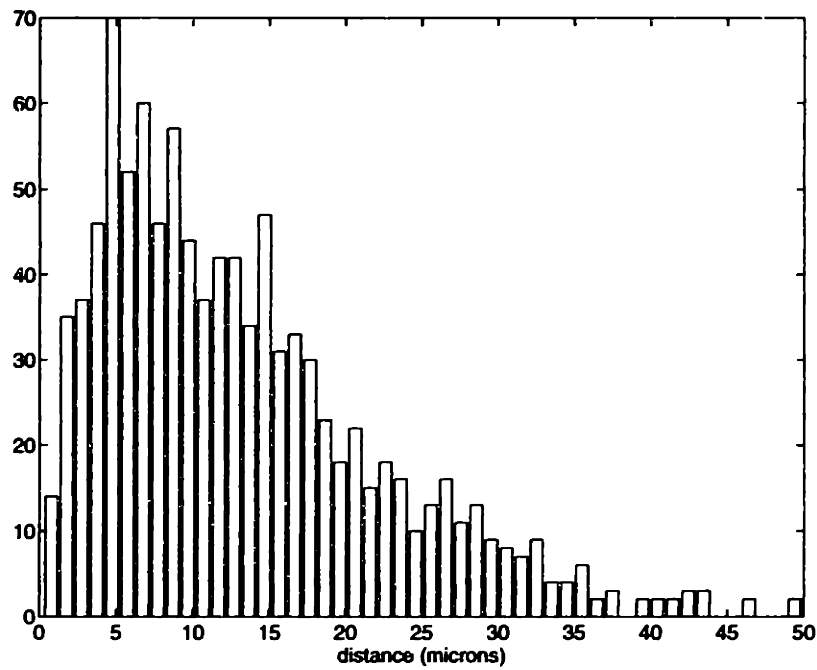

Figure 3-9: Distance distribution of an "ideal" point for different film sets placed onto the same "perfect" frame, illustrating the contribution from punch variations alone.

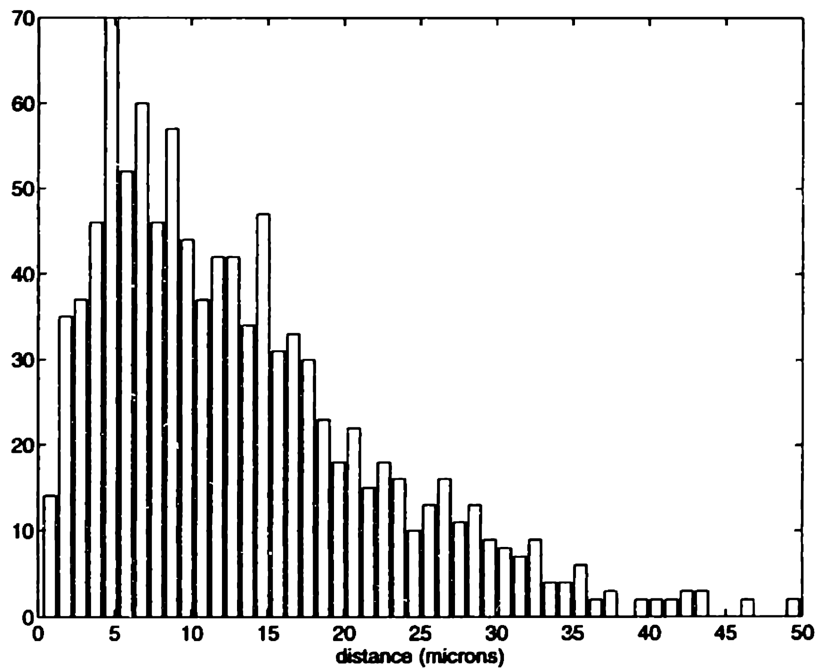

Figure 3-10: Distance distribution of an "ideal" for the same "perfect" film set placed onto different frames, illustrating frame variance contribution to placement errors.

formation of the films in the vicinity of the slots. Such deformations affect registration, since hole integrity is compromised by the repeated interference fits of the four individual constraints, especially due to negligible film bending stiffness. Tooling schemes to achieve increased registration accuracy and precision, while maintaining slot integrity, would be desirable.

3.3.2 Sources of Error

Alignment of artwork depends on the capability of the punch to precisely create accurately sized tooling features, while expose frames require accuracy in pin location, size and orientation. Without both machine elements matching tolerances, accurate and repeatable film registration is not possible. This section will only address sources of punch related errors.

Absolute position of the holes does not affect registration of front-to-back artwork. The relative position of the slots does, however, affect registration, since film slots must fit onto expose frame pins. Given that an absolute datum is inconsequential, the first source of punch error, would be the operators' film alignment repeatability. Because the practice is to split the difference in target location, including artwork scaling, temperature, and humidity effects, alignment involves repeatability in optically dividing the two targets between the reticle position, as shown in Figure 3-11.

A conservative estimate for operator alignment is $\pm 38.1\mu m$ in x direction. Because errors are not divided in the y direction, reticle alignment is easier, hence a 3σ operator estimate of $19\mu m$ is reasonable. Recall that artwork feature to feature positioning is limited to $\pm 10.2\mu m$, so that the centerline created by splitting the difference has $|3\sigma|$ limits of $39.4\mu m$, with a $|3\sigma|$ rotational error caused by misalignment of y targets of approximately $50 mrad$, and y translational error of $\pm 25.4\mu m$. These values are summarized in Table 3.4.

Although operator error is the limiting factor in aligning film, consider that the field is approximately 3.8 mm, in which case, the operator can align objects to 1% of the field of view. If film targets are reduced in size, and a higher magnification lens is used, deviation in film alignment can be significantly reduced. Smaller circular targets

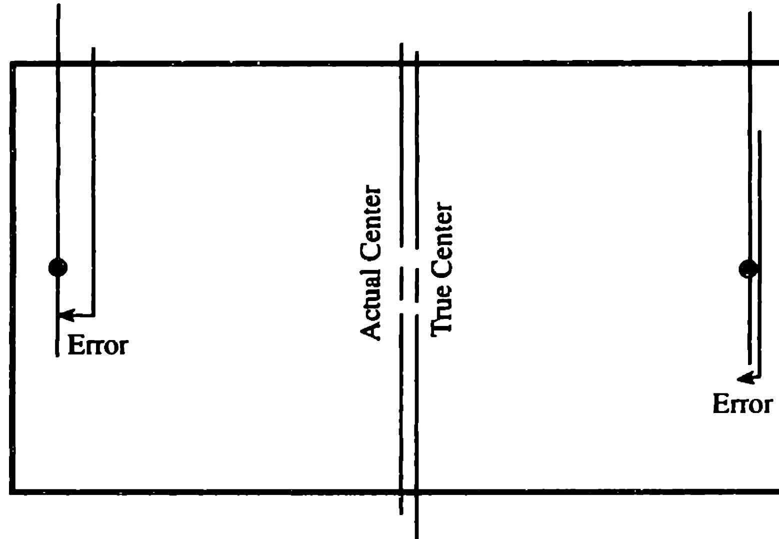

Figure 3-11: "Splitting the difference" based upon two plotted features.

Measure	$3\sigma(\mu m)$	**% Contribution**
Feature-to-feature position (assuming centroid measurement)	7.6	3.8
Operator alignment of features to reticle ("splitting the difference")	38.1	96.2
Total film alignment	38.6	100

Table 3.4: Current film alignment capabi!ity.

Measure	$3\sigma(\mu m)$	**% Contribution**
Feature-to-feature location	7.6	22
Feature size	6.35	15
Developing	2.5	2
Operator alignment	12.7	61
Total film alignment	16.3	100

Table 3.5: Alignment capability based on smaller field of view and "T" targets.

are difficult to plot, hence "T" targets identical to those used by the Ceco Confirmer may be used. By reducing the field of view to 1.25 mm, operator deviation would be $12.7\mu m$. For the case of a "T" target, since a cross-hair reticle will be aligned to a feature edge, feature size variations affect alignment ability. These results are shown in Table 3.5.

Alignment of the film may be improved by approximately 2.4 times the current capability, although it should be noted that initial placement of the film within the field of view will be more difficult for the operator.

Errors introduced by operators are further compounded by errors of punch and die blocks. The accuracy of punch and die locations are only important in that they must be within the tolerance of the expose frame pin locations. Repeatability of a punch and die, however, is critical and is generally limited to their relative clearances, and the amount of preload applied by the stripper plate. The particular artwork punch does not use a stripper plates, which causes film to be drawn into the die from the surrounding region, reducing punch precision. Additionally, the punch itself and its housing are loosely located on the punch table. The punch table contains guides, rather than a stripper plate, to direct the punch into the die. Die wear caused by the absence of a precision stripper plate, may contribute to film breakage and size repeatability issues. Inspection revealed numerous nicks in the cutting edges of the punches, as shown in Figure 3-12, and is best attributed to mishandling when changing format sizes, and the repeated driving through guide blocks. A punch placed in a guide block is shown in Figure 3-13. Notice the chamfered edge of the punch guide for the unused format position.

Figure 3-12: Punch removed from guide. Nicked edges can cause film tear and degraded punch repeatability.

Measure	$3\sigma(\mu m)$	**% Contribution**
Film Alignment	38.6	76 (currently)
	16.3	36 ("T" target, small field)
Punch Repeatability	21.6	24 (currently)
		64 ("T" target, small field)
Total repeatability	44.2 (currently)	100
	26.9 ("T" target, small field)	100

Table 3.6: Tooling features to circuit board artwork deviation.

Inspection data measuring the relative position of punched features indicates a 3σ positional deviation of $20.3\mu m$ in punched aluminum. Punching polyester film without a stripper plate further contributes to feature location and size errors. Introducing the alignment errors from previous tables, the deviation of the relative positions of punched features to the artwork can be calculated. These results are summarized in Table 3.6 through Table 3.9.

Notice that increasing alignment performance, through the use of "T" targets for instance, without improving punch repeatability, causes the punch to become the dominant factor in tooling-to-artwork precision. Such an increase in alignment capability

Figure 3-13: Punch in upper guide block. Removal and refitting can cause punch damage due to insertion.

Measure	$3\sigma(\mu m)$
Tooling to artwork	44.2
Film to frame	38.1
Front-to-back film	2 pieces of film
Total front-to-back registration capability	82.3

Table 3.7: Achievable front-to-back artwork registration capability, including simulation data for the indeterminate pin constraining system.

Measure	$3\sigma(\mu m)$
Tooling to artwork	26.9
Film to frame	38.1
Front-to-back film	2 pieces of film
Total front-to-back registration capability	66

Table 3.8: Achievable front-to-back artwork registration, including simulation data for the indeterminate constraining system, using 3x optical system and "T" targets.

will place new emphasis on punch performance. Intuitively, use of a stripper plate will reduce punch errors, in which case a total tooling to artwork 3σ deviation of approximately $19\mu m$ may be achievable, using a higher magnification optical system.

The indeterminate nature of the four pin constraining system dominates registration performance; however, errors may be reduced 20% by aligning the film using a $3\times$ optical system and "T" targets. Increased difficulty in initial placement of artwork may require course locating cameras in addition the $3\times$ system.

Measure	$3\sigma(\mu m)$
Tooling to artwork	19.5
Film to frame	38.1
Front-to-back film	2 pieces of film
Total front-to-back registration capability	42.8

Table 3.9: Achievable front-to-back artwork registration, including simulation data for the indeterminate constraining system, using $3\times$ optical system, "T" targets, and a precision stripper plate.

3.3.3 Artwork Tooling Summary

Since film sets are punched on the same punch, precision, not necessarily accuracy, is critical for establishing and maintaining front-to-back registration.

Operator alignment repeatable to 1% of the camera field of view. However, because of the low magnification system (approximately 3.8mm field), operator alignment is limited to 38μm.

Four pin fixturing comprises an indeterminate system, and as such, film registration error can be determined either experimentally or through numerical simulation. Numerical simulations agree well with observed film registration errors, and demonstrate that the four slot system is fundamentally performance limited due to ill-defined constraints. Registration 3σ deviation is 59μm for different film sets fixtured to different frames. Registration 3σ deviation, from simulation, is 38μm for different films sets on the same frame. Registration 3σ deviation, from simulation, of the same film set on different frames is 36μm. This final value was experimentally determined by measuring with a microscope relative positions of a film set on different frames. The experimental 3σ was approximately 30$/mum$, indicating agreement within 16% the simulated value. This particular experiment, however, was only conducted once over a limited population of frames, using a microscope with 5μm resolution. Further, since only one corner feature was measured, plotter error contributed a measurement deviation of 7.5μm. This experiment did demonstrate that the model used is consistent with actual registration capabilities.

Inclusion of artwork and alignment errors with simulation data predicts a 3σ overall registration deviation of 82μm. That is, 95% of the film registers to $\pm$55μm. *This is in close agreement with acquired data and anecdotal evidence.* By increasing the magnification of the alignment optics to approximately 3$\times$, and aligning a reticle to "T" targets, registration errors may be reduced 20%, from 82μm to 66$\mu m(3\sigma)$, all else remaining the same. Additionally, a stripper plate may be able to further reduce the 3σ deviation to 43μm, approximately halving the current deviation.

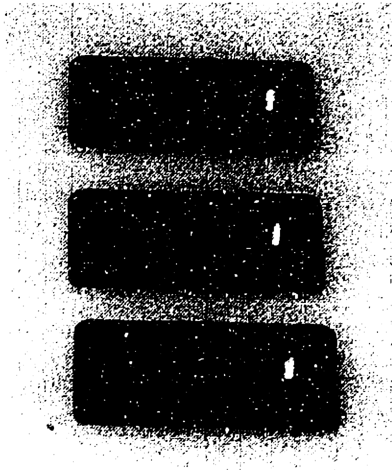

Figure 3-14: Carlson pins used to verify front-to-back artwork registration.

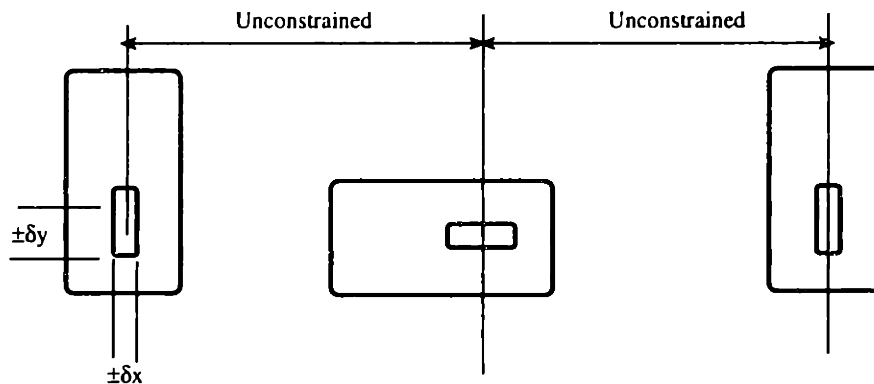

Figure 3-15: Three (of four) unconstrained Carlson pins. Since the pins are not constrained relative to each other, the registration measurement does not account for pin positional errors.

3.4 Registration Measurement

Front-to-back registration is verified using individual Carlson pins, as shown in Figure 3-14. The difficulty in using this particular method, is that, like any manufactured part, the individual pins have size tolerances, which will determine, to some probability, the type of fit. Furthermore, notice that since the Carlson pins are not constrained to each other, the pinning scheme, in this instance, is only subject to size error, not locational errors, as depicted in Figure 3-15. Because of this, the films are more readily constrained to each other, but the registration value is questionable, since it does not account for errors from constrained sets of pins.

The only valid registration measure would that obtained from a particular expose frame the film sets will be fixtured to. The relation between film tooling and pin size and locational tolerances in expose units is not deterministic, hence registration values vary from one expose frame to another using the same set of films, as confirmed by both experiment and simulation. Again, operators noted that with Carlson pins, artwork could be adjusted to satisfy the $50.8\mu m$ tolerance.

Point-wise measurements may be deceiving, since the four corners measured do not constitute a statistically significant data set. Averaging many points is not practical, but a measuring technique described in Chapter 4 will perform artwork feature averaging automatically, yielding a measure more representative of the feature population. Further, note that since front-to-back measurement is a measure of relative location, temperature and humidity effects are *negligible*, assuming both films have been exposed to identical conditions. Therefore, the limit to which registration can be measured from a small population of features is limited by plotter error alone, and is found to be, from previous sections, $\pm 7.6\mu m$. Since two films are registered relative to one another, the 3σ deviation of the relative position of any two particular features is $10.8\mu m$, neglecting any errors introduced by the punch. Accounting for an approximate comfortable operator resolution of $\pm 13\mu m$ through a $60\times$ scope, the 3σ positional deviation of a point-wise optical measurement of any single feature is $19\mu m$, again neglecting punch error.

3.5 Exposure Frames

Front and back artwork is registered to each other by placing each film over four pins located in a glass plate of the exposure frames, as depicted in Figure 3-16. Errors in film registration are caused by initial misregistration on the pins, movement of the film when the top frame is lowered but before being held by vacuum, and repeatability errors of the top and bottom frame coupling. Because previous discussions outlined the tolerances of the slot/pinning system, this section will be primarily limited to top and bottom frame repeatability.

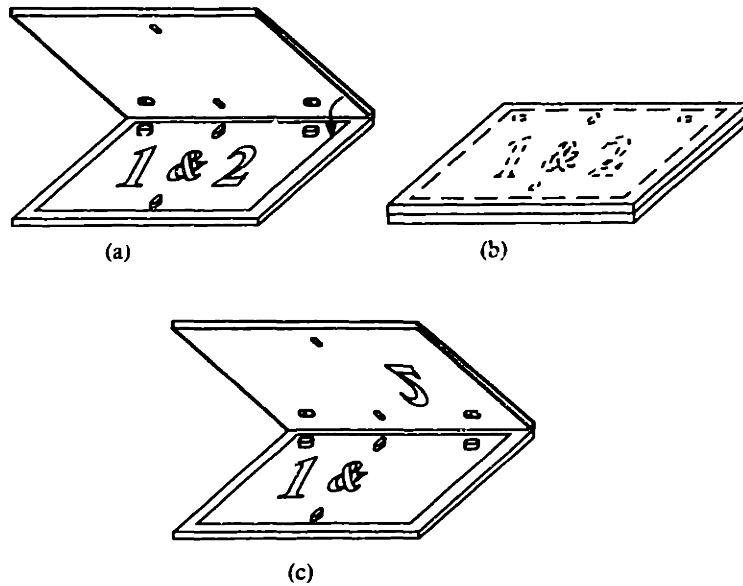

Figure 3-16: Fixturing a film set to the glass of an exposure frame.

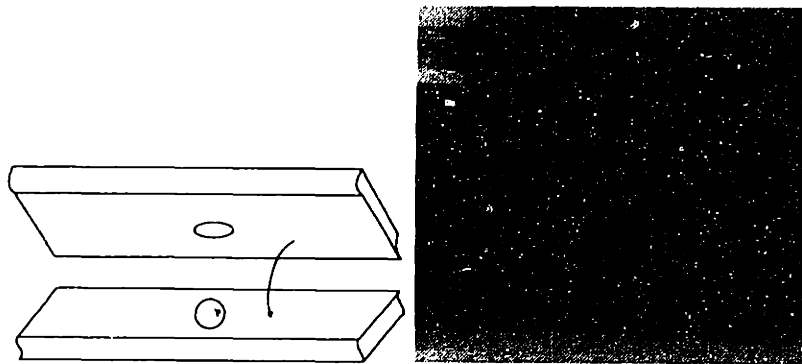

Figure 3-17: Ball in hole constrains x and y frame position.

Once artwork is registered and vacuum fixtured to the respective glass plates, front-to-back registration is presumably maintained by the repeatability of the two expose frames. Registration for the frames as achieved by constraining the upper frame position by a hardened ball in a hole, and rotation with a square pin in a matching square hole, as pictured in Figure 3-17 and Figure 3-18. These elements are supplied as matched sets to provide high repeatability. The specification for the individual fits is unknown and variable from wear.

During this study, it was noted that replacement of these matched sets required a certain run-in time, and that on occasion, sets were excessively difficult to engage and release. Repeatability of these constraints, like any pin/hole type of constraint,

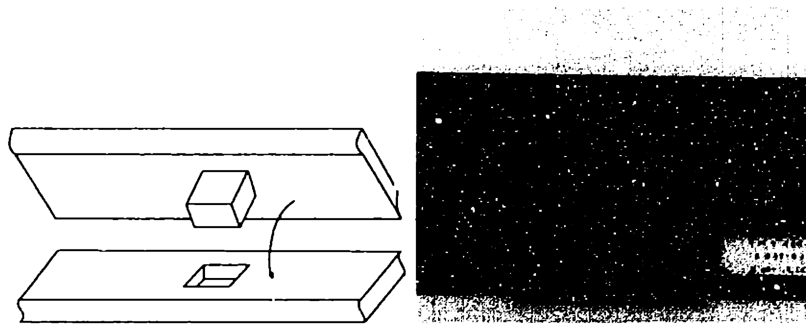

Figure 3-18: Peg in hole constrains frame rotation.

requires tight tolerances. The tighter the particular fit, the better the repeatability is assumed to be. However, since this arrangement is over-constrained, repeatability is not necessarily assured because friction, which is often non-repeatable, will dominate. Furthermore, wear of the components adversely affects registration performance. Additionally, overconstraints hinder smooth opening and closing of a delicate piece of equipment. The use of kinematic coupling elements to achieve higher repeatability, will be introduced in Chapter 5. A test system and acquired data is also presented in Chapter 5.

The issue of glass plate flatness was raised on many occasions throughout this study. It seems that the consequences of glass warp on image quality is uncertain. Instead one cause of glass warp will be described. An important aspect of glass deformation is not solely the effects of image quality, but also the extraneous stresses imposed on the glass by overconstraints. A lower glass plate is attached to a frame as shown in Figure 3-19. A gasket seals the glass against the frame, so that it can be vacuum preloaded against the surface. The upper plate is the same, with the addition of bolt holes which prevent the glass from falling, should there be a vacuum failure.

This design requires the glass/frame interface to be sealed since the frame halves themselves are vacuum preloaded against each other during the expose cycle. It is important to note that the frame surface will never be planar due to manufacturing tolerances; hence, constraining the glass plate to the frame perimeter by the vacuum preload will cause some deflection. Furthermore, since frame planarity is unknown, the form of the deformation is unknown, and is, in fact, indeterminate. That is, this par-

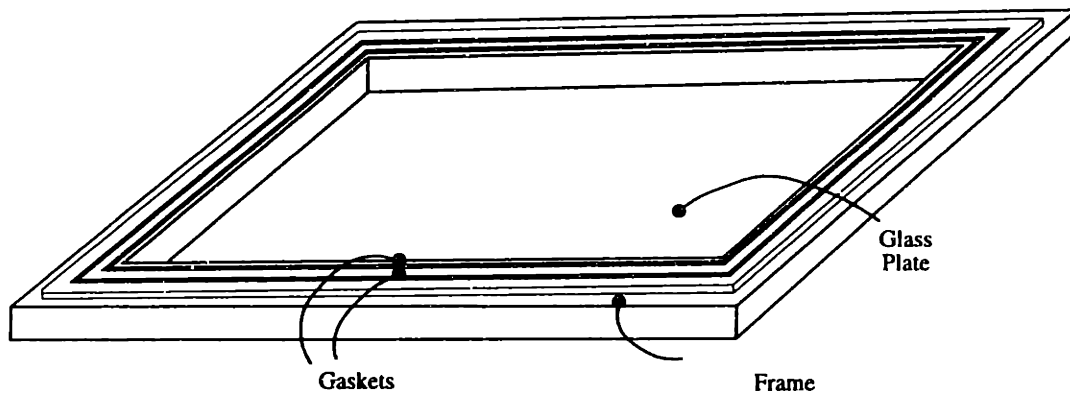

Figure 3-19: Over-constrained glass along its perimeter causes glass warp, requiring large vacuum pressure and draw time to achieve contact printing.

ticular mounting is over-constrained. Each glass plate suffers from overconstraints, so when the frames are brought into contact, a large frame vacuum is required to achieve full contact across the artwork surface. *If deformation is minimized, lower vacuum pressures may achieve adequate contact, and cycle times may be shortened.* Note that hardening glass adds some warp, but unlike warp introduced by overconstraints, it cannot be eliminated. To define a plane, only three points are required; therefore, to maintain planarity, within the limits of glass warp and sagging under its own weight, the glass should be constrained at precisely three locations. This is easily accomplished by mounting the glass against three spherical surfaces, as shown in Figure 3-20. Fixturing against three spherical surfaces will define the plane of the glass, but for locational repeatability, in the event the glass has to be removed, and, more importantly, for lateral stiffness and fixture preload, a six point kinematic coupling is recommended. Furthermore, note that spherical surfaces on the glass will cause large contact stresses. For this reason, metal inserts could be used for constraining the glass to frames.

By placing coupling elements on monolithic flexures, frames can be vacuum sealed against each other when the frames are closed, via a lightly preloaded gasket around the perimeter of the glass. Because individual glass plates have identical sag and they are kinematically located to the frames, deformation is minimized. As stated earlier, minimized deformation will lead to lower vacuum, which will lead to smaller deform-

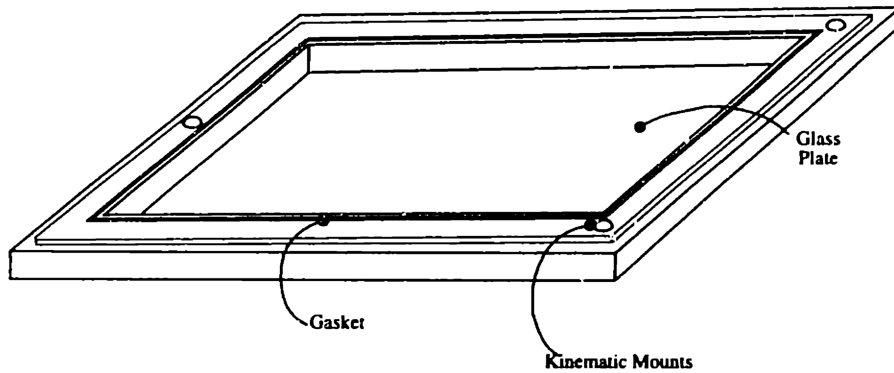

Figure 3-20: Kinematically constrained glass may reduce glass warp. The coupling may be a 6-point contact type to ensure lateral and transverse stiffness.

Measure	$3\sigma(\mu m)$
Film front-to-back	82.3
Top to bottom frame	42.0
Total front-to-back registration capability including frames	92.4

Table 3.10: Current achievable front-to-back artwork registration including expose frame repeatability errors.

ations from the gasket seal, which may ultimately reduce cycle times and contribute favorably to image quality.

Errors in film registration are caused by initial misregistration on the pins (as described in Section 3.3, movement of film when the top frame is lowered before being held by vacuum, and repeatability errors of the top and bottom frame coupling. Frame-to-frame repeatability is limited to manufacturing tolerances and wear of the ball and post. Repeatability of this non-deterministic system degrades with use, and on one randomly sampled frame was limited to approximately a positional σ of $14\mu m$, as shown in Figure 3-21. Data was acquired at one position on a frame for multiple opening and closing cycles.

Using data from Figure 3-21 and Table 3.7, front-to-back registration error may be estimated, as calculated in Table 3.10

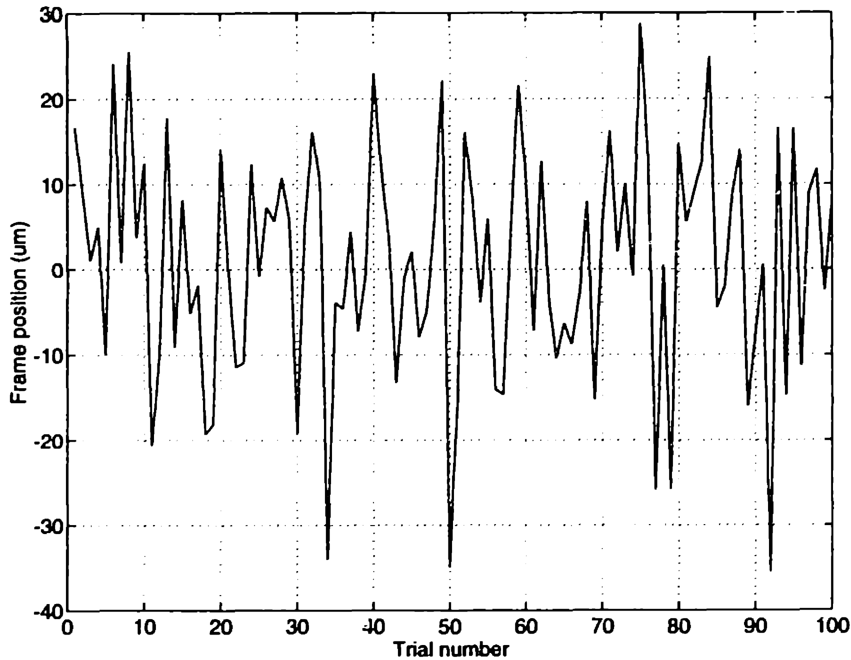

Figure 3-21: Ball and post frame repeatability.

3.6 Laminate Material Considerations

Mechanical properties of the glass/resin matrix are a strong function of weave orientation. However, the copper foil covering the laminates dominates the lamination's mechanical properties. The copper modulus is approximately 17 times the modulus of the glass/resin weave. For simplicity, the material was assumed Hookean and isotropic.

Stresses throughout an etched laminate caused by fixturing are negligible compared to the stresses in the regions of the pins. Because of this, copper should remain in the vicinity of any constraint, i.e. slot. Thermal expansion is a function of the particular artwork a laminate contains, however, as an estimate, the clad expansion is dominated by the copper foil, and is approximately 16 ppm/°C, a signal plane is approximately 10 ppm/°C, and a ground/power plane is approximately 14 ppm/°C. These estimates were calculated using equations provided by Polyclad Corporation, originally derived

α_{glass}	5.0 ppm/°C	ν_{cu}	0.36
α_{resin}	69 ppm/°C (pre-T_g)	ν_{unclad}	0.25
α_{cu}	17 ppm/°C	ρ_{glass}	$2.54g/cc$
E_{glass}	10.5 Mpsi	ρ_{resin}	1.31 g/cc
E_{resin}	0.5 Mpsi (T ¡ 90°C)	K	0.52
E_{cu}	17 Mpsi	K*	0.60
h	volume fraction of cu foil	RESIN%	resin weight %

Table 3.11: CTE, Poisson's ratio, and Young's modulus for clad and unclad laminates.

at Bell Labs. For reference, these are,

$$\alpha_{unclad} = \alpha_{glass} + \frac{\alpha_{resin} - \alpha_{glass}}{1 + K\frac{\rho_{resin}}{\rho_{glass}}\frac{E_{glass}}{E_{resin}}\frac{1-\nu_{resin}}{1-\nu_{glass}}\frac{1-RESIN\%}{RESIN\%}} \tag{3.5}$$

$$\alpha_{clad} = \alpha_{cu} + \frac{\alpha_{unclad} - \alpha_{cu}}{1 + K\frac{E_{cu}}{E_{unclad}}\frac{1-\nu_{unclad}}{1-\nu_{cu}}\frac{h}{1-h}} \tag{3.6}$$

for the values listed in Tabletab:bell-labs.

Resin content weight percentage is obtained by,

$$RESIN\% = \frac{\rho_r(h_f - h_g)}{\rho_r(h_f - h_g) + w_g} \tag{3.7}$$

where w_g is the glass weight per unit area (g/in^2), h_f is the final pressed thickness (inches), h_g is the theoretical glass compression thickness, which equals $0.024w_g$, ρ_r is the resin density (22.1 g/in^3), and ρ_g is the glass density ($41.6g/in^3$). The glass volume fraction, x_g, and resin volume fraction, x_r, may be calculated from,

$$x_g = \frac{1}{1 + \frac{\rho_g}{\rho_r}\frac{RESIN\%}{1-RESIN\%}} x_r = 1 - x_g \tag{3.8}$$

Different glass weights are available, and different types of printed boards will require different weave styles. Two typical weaves, 104 and 1080, have w_g of $0.0121g/in^2$ and $0.0303g/in^2$ respectively.

From a fixturing point of view, an understanding of the mechanical behavior of the cores and the laminated panels is critical for designing systems to satisfy stringent re-

Property	Value
Tensile Strength, MPa	
lengthwise	275
crosswise	240
Compressive Strength, MPa	
in-plane	410
out-of-plane	240
Modulus of Elasticity, GPa (tensile)	
lengthwise	17
crosswise	14
Poisson's Ratio	
in-plane	0.20-0.25
out-of-plane	0.10-0.15
Density, g/cc	1.85
Thermal Expansion, ppm/°C	7 (unclad) 16 (clad, 50mm 1080, 1/2-1/2)
Thermal Conductivity, $Cal/s/cm^2/C/cm$	1.2×10^{-3}
Specific Heat, $Cal/g/°C$	0.26
T_g,°C (by TMA for PCL-226)	132.5
Moisture expansion, ppm/$\%H_20$	200

Table 3.12: Typical values for FR-4 laminates.

gistration specifications. For instance, stress-strain behavior of panels will determine how they deflect against fixturing points when subjected to transverse loads, such as those generated during routing, hence affecting route-to-image registration. From the discussion on fixturing and preload in previous sections, it should be clear there is a strong relationship between the mechanical properties of the medium being constrained and its response to loading conditions. The mechanical properties also describe material movement due to environmental fluctuations, and the fluid mechanics during lamination.

The dependence of the mechanical properties on glass weave size, number, style, and orientation, precludes a rigorous analytical treatment of core behavior; however, copious experimental data exists. Some typical values of mechanical and thermal properties for FR-4 laminates (provided by Polyclad Laminates, Inc.) are outlined in Table 3.12.

Figure 3-22 qualitatively illustrates the dependence of the modulus on weave ori-

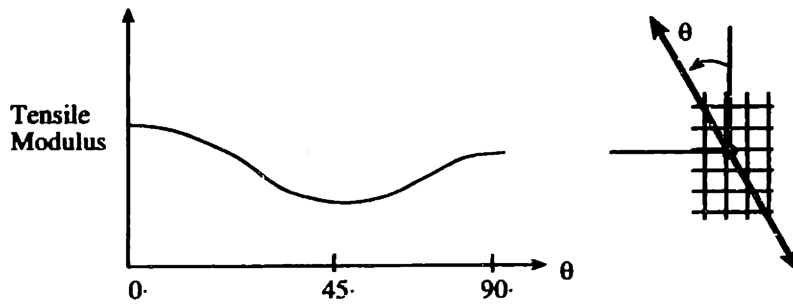

Figure 3-22: Dependence of modulus on weave orientation.

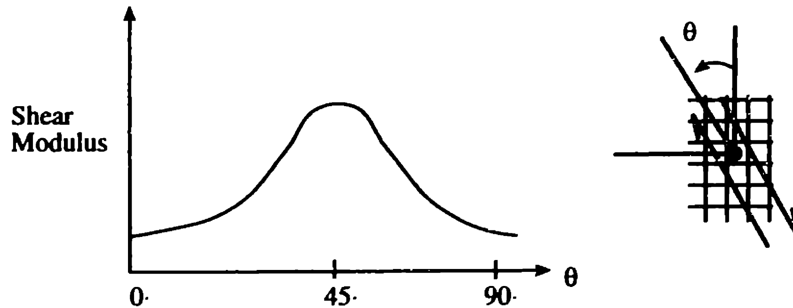

Figure 3-23: Shear modulus as a function of load direction.

entation. Note that the maximum moduli occur in the directions aligned with the glass fibers, since the uniaxial tensions of these respective directions is strengthened by the fibers.

The difference in moduli in the crosswise and lengthwise directions can best be attributed to a tensile preload which is created during the manufacture of the cores. At 45° from these principal directions, the tensile modulus is a minimum, since the fibers are in pure shear. Consequently, at this angle, the shear modulus is a maximum, and is minimum at 0° and 90° since fibers are aligned with applied shear and act as slip planes, as illustrated in Figure 3-23.

The above properties apply to copperless glass/epoxy composites. However, since the modulus of elasticity of copper is approximately 7 times that of the glass/epoxy itself, the stiffness of the cores in the transverse direction is significantly enhanced by the thin copper foil. This is especially true for the thin core materials ($50\mu m$ glass/epoxy), where the copper foil dimension, for example $1/2oz$ over $1/2oz$ copper ($18\mu m/18\mu m$), accounts for 42% of t Under uniaxial tension, as shown in Figure 3-24, the stiffness of the copper clad composite is the parallel arrangement of laminate and

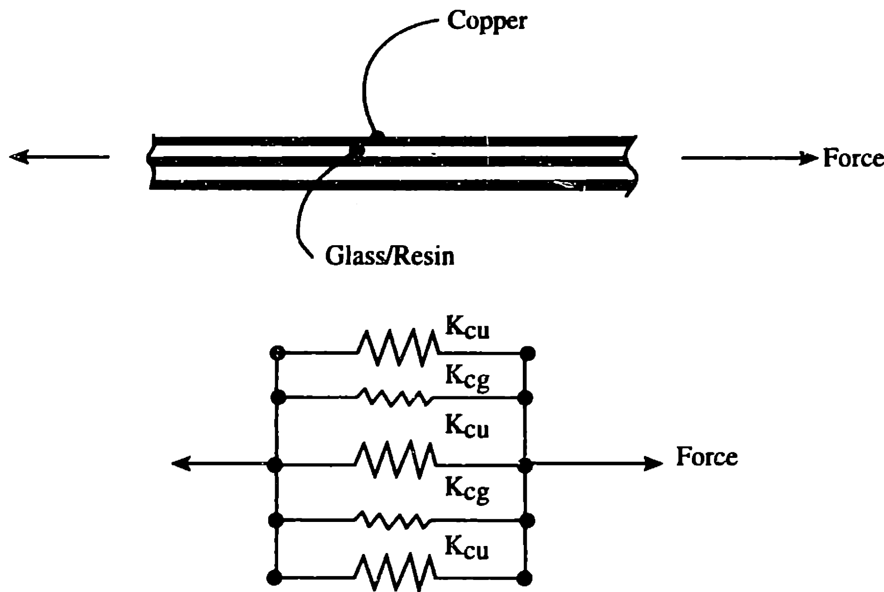

Figure 3-24: Modulus of laminates is significantly enhanced by copper cladding.

copper "springs", given by the relationship,

$$k_{eff} = \frac{E_{cu} E_{lam} t_{cu} t_{lam}}{E_{cu} t_{cu} + E_{lam} t_{lam}} \tag{3.9}$$

on a width/length basis, where E_{cu} and E_{lam} are the copper and laminate moduli, respectively, and t_{cu} and t_{lam} are the total copper and laminate thickness, respectively. It is important to recognize that the copper modulus dominates the system stiffness for all practical core thickness. The contributions of the copper and composite material moduli on system stiffness become comparable when the core thickness is 7 times larger than the total copper thickness. As a conservative estimate, for $1/2oz$ over $1/2oz$ copper, glass/epoxy thickness would have to be $0.25mm$ to satisfy this criteria. System stiffness of parallel combinations of glass/epoxy and copper, for various constructions is shown in Table 3.13. It is assumed that the tensile and compressive moduli are equal. Furthermore, note that since the copper is isotropic and its material stiffness dominates system stiffness, modulus variations of the copper clad laminates due to orientation are assumed to be negligible.

This discussion, however, is limited to laminates with copper over the entire surface. When copper is etched to produce the particular artwork, the core stiffness is

Construction		Stiffness, $N/\mu m$
$50\mu m$ core	$18\mu m/18\mu m$ copper	0.71
$100\mu m$ core	$18\mu m/18\mu m$ copper	1.2
$100\mu m$ core	$36\mu m/36\mu m$ copper	1.4
$150\mu m$ core	$18\mu m/18\mu m$ copper	1.6
$150\mu m$ core	$36\mu m/36\mu m$ copper	1.9
$200\mu m$ core	$18\mu m/18\mu m$ copper	1.9
$200\mu m$ core	$36\mu m/36\mu m$ copper	2.4

Table 3.13: Stiffness of various copper-clad laminate constructions on a width per length basis.

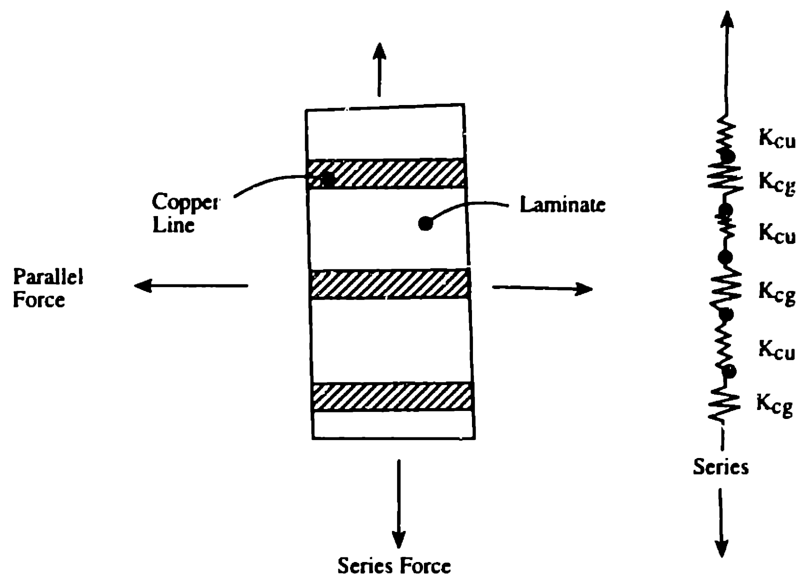

Figure 3-25: Series and parallel combination of stiffnesses after artwork is etched into the laminates.

degraded. Consider, for example, a series of lines etched in the laminate under tensile loading, as illustrated in Figure 3-25.

Notice that the stiffness of this system is the series connection of stiff (copper and laminate) springs and compliant (laminate) springs. For tensile loading parallel to the copper traces, copper stiffness dominates. For designing fixturing systems, it is important to identify the compliant and stiff directions of a particular laminate, so that the strains produced by preloading or machining can be minimized. It is also important to recognize that the artwork patterns are complex, hence the stiffness of

any particular etched core cannot be determined analytically. For design purposes, a range of stiffnesses, from typical ground and power planes, to typical signal planes, for various thicknesses should be determined. These stiffnesses may be obtained experimentally.

In the vicinity of tooling features, where the stresses will be largest due to point contact, copper will not be etched away. Copper clad tooling features is the current, intuitive, practice. Rigorous treatment of the anisotropic stress-strain behavior of artwork-etched laminates will generate incremental improvement over the significant progress made from conservative estimates of mechanical properties, assuming an isotropic Hookean material. Additionally, since contact stresses are restricted to the immediate (copper-clad) regions of the tooling, copper stiffness will dominate composite stiffness.

3.7 Inner-Layer Expose

Front-to-back registration of inner-layer expose is achieved through correct registration of the respective films, as was described in previous sections. At inner-layer expose, the individual cores are not tooled. Rather, the panels are manually placed within the field of the artwork; hence, the images are not exposed in any particular location. Post-etch punching creates the tooling features with respect to the etched pattern, in the same manner in which the tooling slots are created in the artwork following laser plotting. Prior to the advent of post-etch punching, panels were tooled and fixtured relative to the artwork; however, yields decreased as registration demands increased, due to errors in the fixturing technique and material stability issues. Since an automated optical system could align and punch the panels with better repeatability than the expose unit tooling could provide, post-etch punching became the standard practice. Another reason post-etch punching became the standard method was that the core dimensions varied due to stress relaxation during the develop, etch, and strip processes. Furthermore, stress relaxation is a function of the particular artwork, making modeling impossible. Therefore, dimensional stability issues, inadequate tooling,

Measure	$3\sigma(\mu m)$	% Contribution
Thermal expansion	0.2-0.3	negligible
Humidity expansion	5 - 8	100
Total layer-to-layer registration limit aligning from centerline (neglecting PE punch errors)	5 - 8	100

Table 3.14: Environmental contributions to layer-to-layer misregistration, neglecting post-etch punch errors.

Measure	$3\sigma(\mu m)$	% Contribution
Front-to-back (film)	94	99
Layer-to-layer (core)	8	1
Total registration limit of any single feature of one layer to that of another layer	94.3	100

Table 3.15: Feature to feature registration between any two layers, neglecting post-expose punch errors.

and the ability to service a multitude of core formats, were motivations for post-etch punching.

Relative positions of the film and frames will determine the front-to-back artwork registration, while humidity and temperature fluctuations will affect the absolute size of the image, hence affecting the layer-to-layer registration. Assuming etched laminates have been equilibrated prior to lay-up, temperature and humidity fluctuations during inner-layer expose contribute to layer-to-layer misregistration as shown in Table 3.14.

Neglecting PE-punch errors, the 3σ deviation in layer-to-layer image registration is limited to approximately $8\mu m$ (at the perimeter) under current environment controls. Recall from previous sections that front-to-back registration is limited to $94\mu m(3\sigma)$, which will dominate the layer-to-layer registration limit as shown in Table 3.15; again neglecting errors introduced by the PE-punch.

By implementing more stringent humidity control ($\pm$2.5%RH), using a higher magnification film alignment system and targets as described in previous sections, with a punch stripper plate, the expected layer-to-layer registration will be as shown in Table 3.16.

Measure	$3\sigma(\mu m)$	**% Contribution**
Front-to-back (film)	42	99
Layer-to-layer (core)	4	1
Total registration limit of any single feature of one layer to that of another layer	42.2	100

Table 3.16: Possible layer-to-layer registration using improved artwork alignment and punch techniques with more stringent humidity control.

For a detailed description of front-to-back registration of artwork, the reader is referred to previous artwork section, Section 3.3. Although relative positions of film will determine front-to-back artwork registration, humidity and temperature fluctuations affect image size, hence affecting layer-to- layer (i.e. core-to-core) registration.

In summary, assuming etched laminates have been equilibrated prior to lay-up, temperature fluctuations during inner-layer expose contribute $\pm 0.25\mu m \times \pm 0.6\mu m$ image variation for core dimensions of $0.45m \times 0.60m$. Similarly, humidity fluctuations during inner-layer expose contribute $\pm 11\mu m \times \pm 15\mu m$ image growth for the same core dimensions. Note that material movement due to ***humidity*** fluctuations dominates image size. This is attributable to matched thermal coefficients of clad laminates and film, as compared to mismatched humidity coefficients.

Neglecting post-etch punch errors, the 3σ deviation for layer-to-layer image registration is limited to approximately $7\mu m$ (at the perimeter, "splitting the difference") under the current environment control. Recall from previous sections that front-to-back registration is limited to $92\mu m, (3\sigma)$, which will dominate layer-to-layer registration limit, neglecting errors introduced by post-etch punching.

3.8 Post-Etch Punch

Aside from specific errors introduced by the punch, the nature of the four slot tooling system is fundamentally limited for reasons discussed with reference to artwork tooling. The registration capability of the four slot scheme is largely determined by the manufacturing tolerances of the hole and pin size, relative locations, and orientations.

Furthermore, the sliding fits for the pins into the press plates introduce registration errors, but such fits are required specifically because of the uncertainty of core slot positions and sizes, caused by punch errors. With reference to the current punching operation, the punched slots must be repeatable within individual machines, and the location of the slots must be accurate from machine to machine, so that cores punched on different machines may be registered against each other during lamination. The primary areas which cause concern are related to the relative position of the cameras to the punch blocks, the relative positions of the die blocks themselves, the repeatability of the optical alignment method, the repeatability of the punch and die block locating mechanism, and the dynamic response of the suspended stage.

Since the camera is used for locating the core targets relative to the punch and dies, each camera/punch pair should be calibrated; however, it is uncertain if this is done, instead relying on manufacturing to establish a "known" camera to punch position. Deviations in camera to punch location should be measured for each machine and used for establishing the origin of the punches. Theoretically, once the cameras have been rigidly constrained and the origin established, the location of the slots relative to the targets should be known. However, this is not the case primarily because of the locating mechanism of the individual punch/die pairs. The punch and die blocks are located by a pin fit into table holes, as shown in Figure 3-26. This type of coupling is underconstrained, since clearance is required to move the punch and die blocks into and out of position, accommodating various panel formats. Although difficult to measure, the total clearance is estimated at $25\mu m(3\sigma)$. Because this clearance is present in both the punch and die blocks the relative position of the two may be as much as $35\mu m$ off-center. Note, however, that the punch position will determine the location of the slot, but the difference in die block clearance will cause variation in slot width since the core will be extended differently on either side of the punch. Clearance along the axis of the slot does not contribute to misregistration since this direction is a desired degree-of-freedom; however, clearance perpendicular to the slot will have a negative effect on registration because it is a sensitive direction, as illustrated in Figure 3-27. Furthermore, it is estimated that the nominal block-set position error is

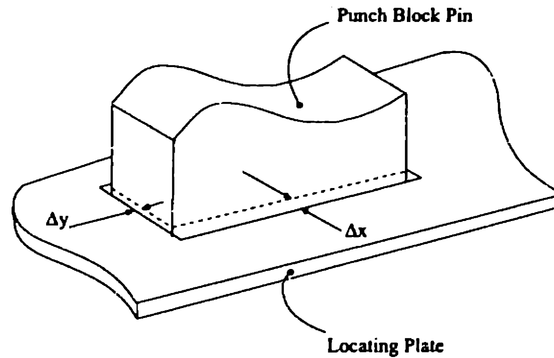

Figure 3-26: Block locating mechanism limits punch repeatability.

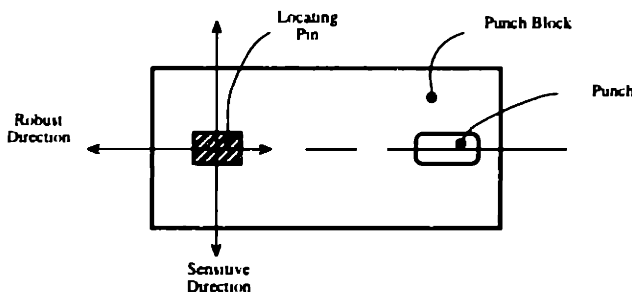

Figure 3-27: Sensitive punch/die block locating direction.

$12\mu m(3\sigma)$. This estimate will also be used as the machine-to-machine accuracy.

The current practice when changing the position of the punch and die pairs is to push the blocks against an edge of the hole to minimize misalignment of the blocks. Consistency in this action will help the positional repeatability, but this method does not preload the blocks into position so the coupling stiffness is nonexistent. Because of this coupling compliance, punch repeatability cannot be assured. Simply put, the blocks move, requiring the punch to be recentered. Recentering is a matter of entering offset values to the controller; however, these values are obtained by the verifying system which has its own errors. Further, excessive recalibration by operators has caused tremendous variation in positional accuracy, and has been limit[illegible] erification and action by the engineer in charge. Additionally, the blocks are not guaranteed to remain in place for subsequent punching, due to the clearances. Recentering addresses the symptom, rather than the cause of repeatability error. Once calibrated,

punches should not require recentering, even when allowing the blocks to be moved for a multitude of format sizes.

Because positional errors are inherent to the locating mechanism, the clearance between the punch and die must be at least as large as the locational tolerance to avoid striking the punch against the die edge. Since this clearance must be designed to accommodate block positional repeatability error, the actual punch hole location may be anywhere within the clearance region, even if, for a particular instance, the punch and die blocks are well registered. As will be discussed later, stiff and repeatable coupling elements between the punch and die blocks and the machine bases need to be implemented. Such a coupling will ensure positional repeatability and stiffness when format sizes are changed, and will permit the punch and die clearance to be reduced, hence reducing the positional uncertainty of the punched slots.

Slot size is another factor which will determine the registration capabilities. Data obtained from punched cores demonstrates that the slot size is also a function of core thickness. Slots punched in thin cores are larger than those of thicker cores, as shown in Figure 3-28. A difference of as much as $0.75\mu m$ in slot width was measured from cores 0.05 mm to 0.46 mm thick. For more common thickness of 0.05 mm to 0.2 mm, a discrepancy of approximately $50\mu m - 75\mu m$ was noted.

This phenomena is difficult to describe, but is related to the bending and elongational stiffness, and the shear strength of a loaded plate with large deformations. The theory is further complicated by the fact that one material is an anisotropic composite material. It suffices to say that this problem is similar to an extrusion problem, and that in fact the punched hole dimension will be related to the material thickness and punch/die geometry. The extension of the lamination prior to shear failure is related to the clearance between the punch and die, as shown in Figure 3-29, and can be minimized by methods which will be described later. If extension is minimized, the hole sizes will be more uniform. Average 3σ deviation in slot widths for a particular laminate was $40\mu m$. For thin-core material ($50\mu m$), average slot width was $4.745mm$. Lamination pins are $4.763mm$ wide $+0/-0.75\mu m(3\sigma)$. The above figures will be used later to simulate layer-to-layer registration. It should be noted that the quoted

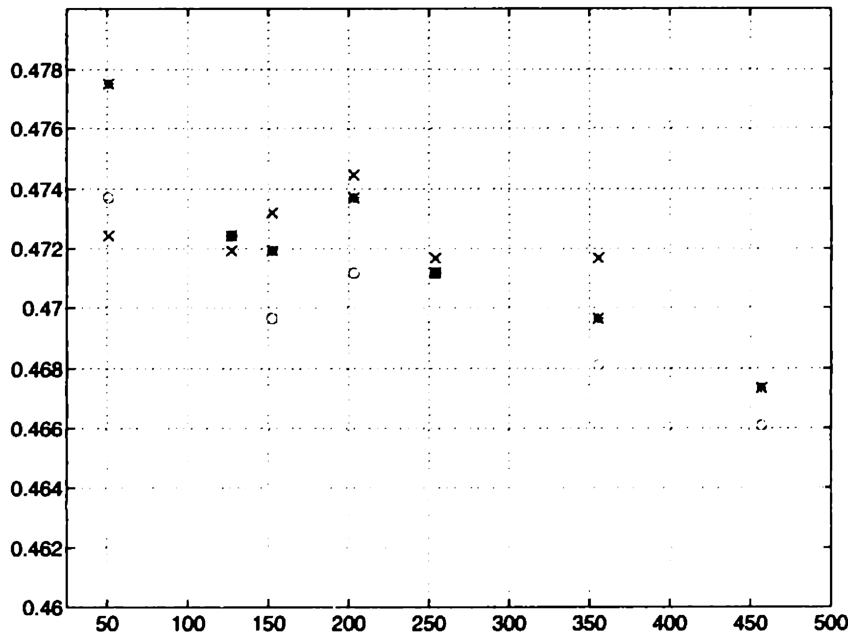

Figure 3-28: Slot width as a function of core thickness.

data was obtained using a dial calipers, and is subject to debate.

Alignment of the cores to the punches is automatic and is based on the positions of targets on one side of a core. As in any point-wise measurement, the ability to align the core is limited by the feature-to- feature distribution and the optical alignment system. Table 3.17 describes the total alignment capability of the post-etch punch.

Another area for the introduction of errors is related to the dynamics of the punch. Although the punching operation alone is a quasi-static operation, the rapid alignment

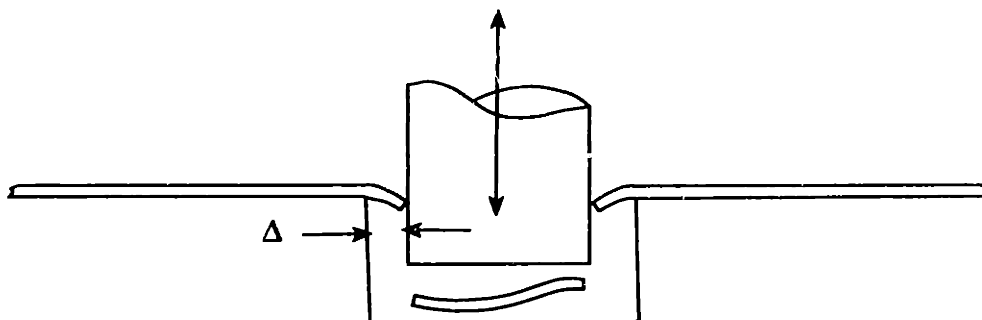

Figure 3-29: Extension of cores during punching causes slot size variations as a function of core thickness.

Measure	$3\sigma(\mu m)$	% Contribution
Copper targets to other printed circuit features (assuming centroid measurement)	7.6	20
Automatic alignment of features to reticle ("splitting the difference")	15	80
Total core alignment	16.8	100

Table 3.17: Post-etch punch core alignment capability.

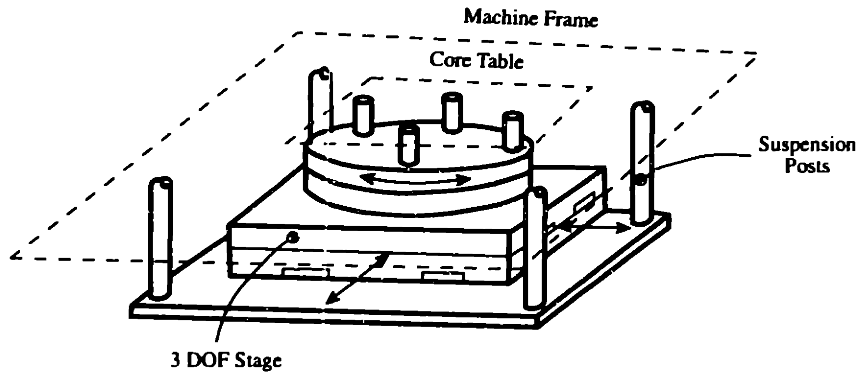

Figure 3-30: Suspended stage may cause punch errors due to vibrations.

of the laminates into position most likely excites certain structural modes. If these vibrations are not damped prior to punching, the slot positions will vary from core to core. Similarly, if the stripper plates strike and constrain the cores before vibrations have settled and the frame has reached its equilibrium state, slot positions will be displaced. Without conducting an experimental modal analysis of the punch it is difficult to determine the dominant mode shapes and their respective frequencies; however, examination of the stage mount construction reveals an area of most probable compliance. The $xy\theta$ stage is suspended below the machine frame by four corner posts, as shown in Figure 3-30.

The connections of these posts to the stage base and machine are bolted; therefore they are compliant as compared to the bending stiffness of the posts themselves. As a conservative approximation; however, bending mode frequency may be estimated from the mass and bending stiffness the posts.

For an aluminum post, $0.3m$ long, $10cm$ radius, with $2mm$ wall thickness, the

stiffness is approximately $50kN/m$. Assuming a concentrated end mass per post of approximately $8kg$, the estimated frequency of vibration is $12Hz$.

The important point is that underdamped, low frequency modes may be excited during the core alignment, causing repeatability errors in tooling feature positions. To quantitatively characterize the dynamic behavior of the punch; however, an experimental modal analysis is highly recommended. Thermal errors may also be responsible for errors in slot location. The sources of thermal gradients are the thermally unshielded drive amplifiers and transformers immediately below the stage. Without further study of the heat distribution within the punch, a quantitative description of the thermal errors is impossible.

In summary, centerline alignment of the laminates is limited to an approximate $17\mu m(3\sigma)$ deviation. Due to the under-constrained die and punch block locating mechanism, the position of any given slot is limited to a 3σ deviation of $25\mu m$. Machine-to-machine accuracy is estimated as $12\mu m(3\sigma)$.

Slot width variations for a particular laminate are caused by worn punches, punch size variations, and the indeterminate extension of the laminates while punching due to the indeterminate punch/die clearances. Width variations observed among different laminate thicknesses are primarily to the extrusion of the material into the die prior to piercing. The average 3σ deviation of slot width was $40\mu m$. These variations would be reduced by sharpening punches more frequently, and more importantly, reducing punch/die clearance by improving the repeatability of the respective block's locating mechanism. This could be accomplished by redesigning a block to machine base coupling.

3.9 Lay-Up

Lay-up of cores prior to lamination is a massively elastic averaging process. The pins are only hammered into position after the cores have been placed over them, indicating that final position of pins is largely determined by average location of individual core slots. Since positions of slots are normally distributed about their nominal (zero)

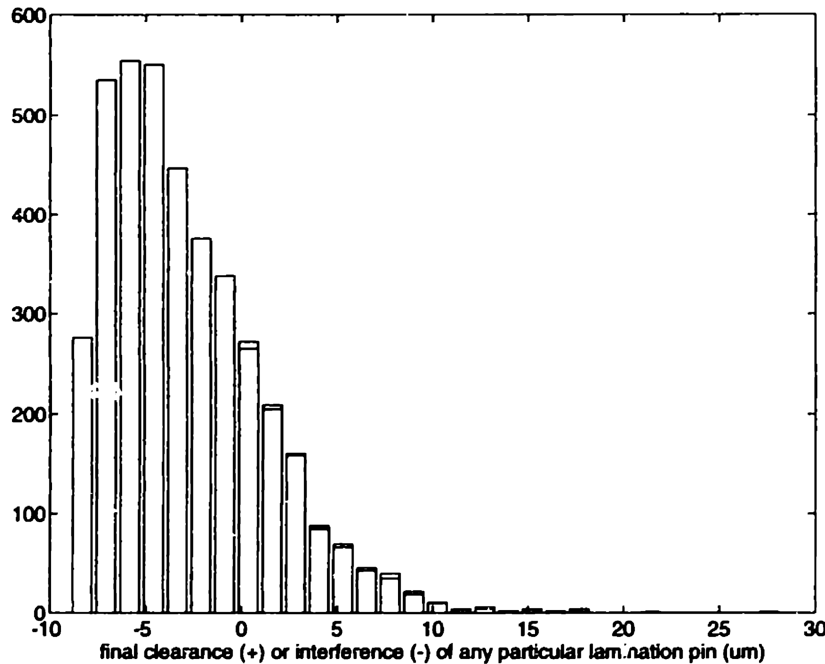

Figure 3-31: Pin/slot clearances at lay-up.

location from any particular punch, and that punch-to-punch accuracy errors are random, final pin position is the average (zero) position of all of the laminates, even if this means core slot yielding. However, deviations of the core position of *any* two cores in a panel will determine its misregistration. Because the tooling method is indeterminate, layer-to-layer registration must be determined numerically. The simulation technique is identical to that used for determination of artwork tooling. Figure 3-31 illustrates the types of fit encountered during lamination. Based on the slot dimension data, most pin/slot fits are interference fits, as indicated by Figure 3-31.

Approximately 25% of fits are clearance fits with average clearance of $2\mu m$. These underconstrained instances are inconsequential, because not only are they small, but they occur (statistically) with three other interference fits. Rigid body movement on the pins during lamination is negligible. Figure 3-32 shows the distribution of an ideal etched feature once a laminate has been fixtured. The measurement is a distance measurement; hence strictly positive.

The 3σ deviation of an etched point from its nominal position is $24\mu m$. Accounting

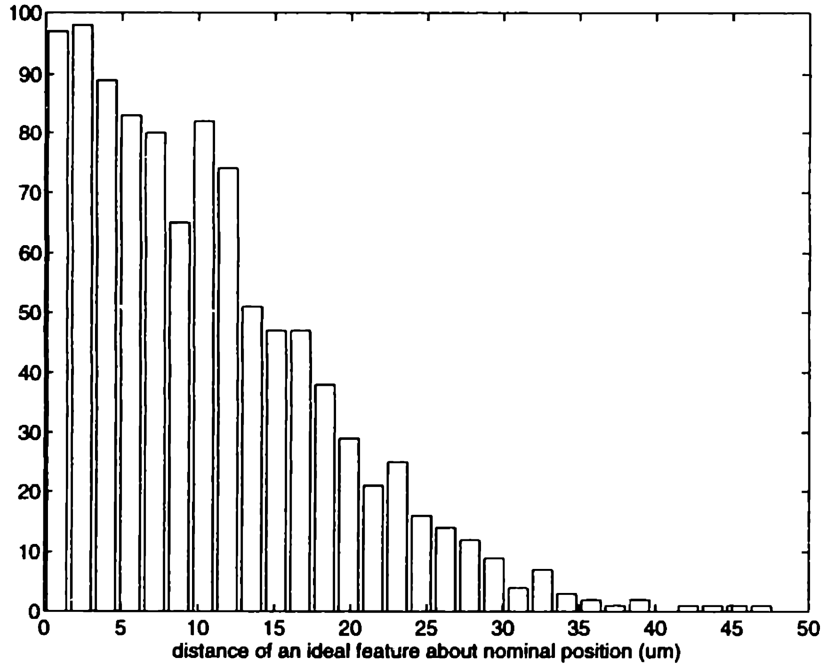

Figure 3-32: Distance distribution of an ideal etched feature from its nominal position.

for rigid body alignment errors during punching and uncertainty due to point-wise feature alignment, the layer-to-layer registration 3σ distribution is $30\mu m$. The total registration is shown in Table 3.18, including the front-to-back artwork registration error.

Note that top-to-bottom feature deviation is $66.5\mu m$ rather than the previously quoted $94\mu m$, because the $\sqrt{2}$ factor is applied to the sum of variances above.

The use of a top press plate minimizes pin tilt during hammering; however, the

Measure	$3\sigma(\mu m)$	**% Contribution**
Environmental effects	8	1.2
Core alignment	16.8	5.3
Distribution of an ideal point	24	10.8
Top-to-bottom feature spread (Section 3.3)	66.5	82.8
Any two laminates	factor of 1.4	
Total layer-to-layer registration	103	100

Table 3.18: Layer-to-layer registration including artwork, post-etch punch, and lamination plate variances.

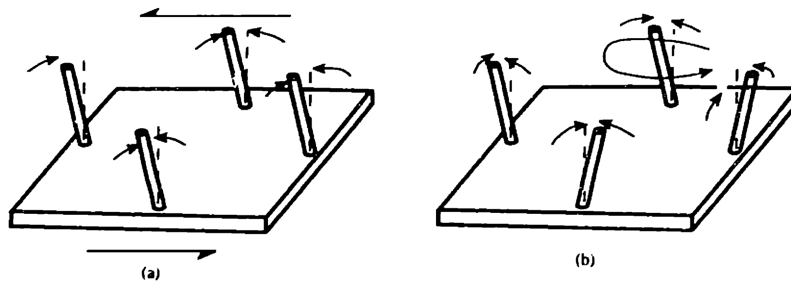

Figure 3-33: Lamination pins tilt by hammering.

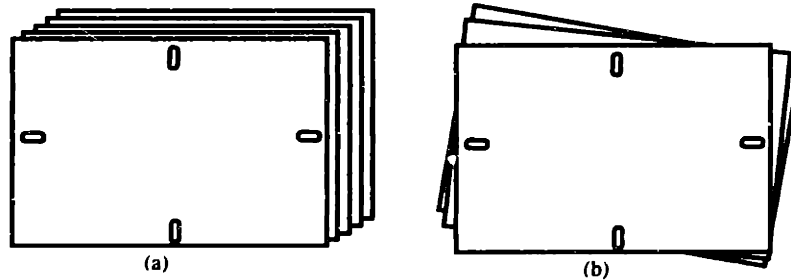

Figure 3-34: Translation and rotation of cores due to skewed lamination pins.

plates, and therefore the pins, may still be tilted or rotated as a group, as indicated in Figure 3-33.

Tilting as a group has the effect of rigid body translation and rotation of the cores relative to each other as shown in Figure 3-34. The amount of core misregistration depends on pin tilts and panel thickness, as shown in Table 3.19. Calculations are based on an assumed 5 cm book thickness, and estimated plate displacements.

Since the top plate is hammered into position by a single operator in a particular position, it is likely that the pins are tilted as a rigid body, rather than tilted at random. Furthermore, the tilt most likely causes core-to- core translational errors. The same

	2mrad	5mrad	10mrad
0.25mm panel	0.7mm	1.3mm	2.5mm
0.50mmpanel	1.3mm	2.6mm	5mm
0.75mm panel	1.9mm	3.9mm	7.5mm
1.5mm panel	3.8mm	7.5mm	15mm

Table 3.19: Top-to-bottom misregistration for various panel thicknesses pins tilts.

may be true of the soft tooling used for drilling. These are systematic errors and are not included in the distribution data of Table 3.19. The additional $1 - 15\mu m$ error must be weighed against the $103\mu m, 3\sigma$ error.

In summary, by simulation, the 3σ distribution of an ideal core feature is $24\mu m$. This represents the fundamental limitation of the four-slot tooling system. Core alignment 3σ deviation is $17\mu m$, and considering front-to-back artwork errors, the total layer-to-layer 3σ deviation is approximately $100\mu m$. *Of the total layer-to-layer error, approximately 20% is associated with the post etch punch and tooling, while 80% is associated with artwork misregistration.* Note that environmental factors only contribute 1.5% to layer-to-layer registration error.

3.10 Lamination

It is assumed that all layers shrink at the same rate regardless of the artwork it contains. Because of this, the relative positions of the individual cores remain the same through this process, not affecting registration. However, since the degree to which the laminates shrink is difficult to assess, the position of the tooling slots created by the curing resin relative to the artwork is uncertain. The effects of overconstraining panels during lamination has been recently investigated [35]. Naturally, rigid body motion of artwork relative to tooling causes registration errors at drill. Because scaling is uncertain, lamination creates problems for electrical test. Lamination as a process was not dealt with as it is primarily a material scaling issue.

Because of the unmatched thermal expansion coefficients of the laminate and the pins, during the cure cycle at 200°C, average slot clearance, from simulations, is $2.2\mu m$ on each side ($4.4\mu m$ overall), with a 3σ deviation of $24\mu m$. Approximately 65% of the slots are clearance fits at the cure temperature, which means the cores may be positioned uniformly within that tolerance. The clearance distribution is shown in Figure 3-35.

The total 3σ deviation of registration error, accounting for possible material movement from slot-to-pin clearances per the above distribution, is $105\mu m$.

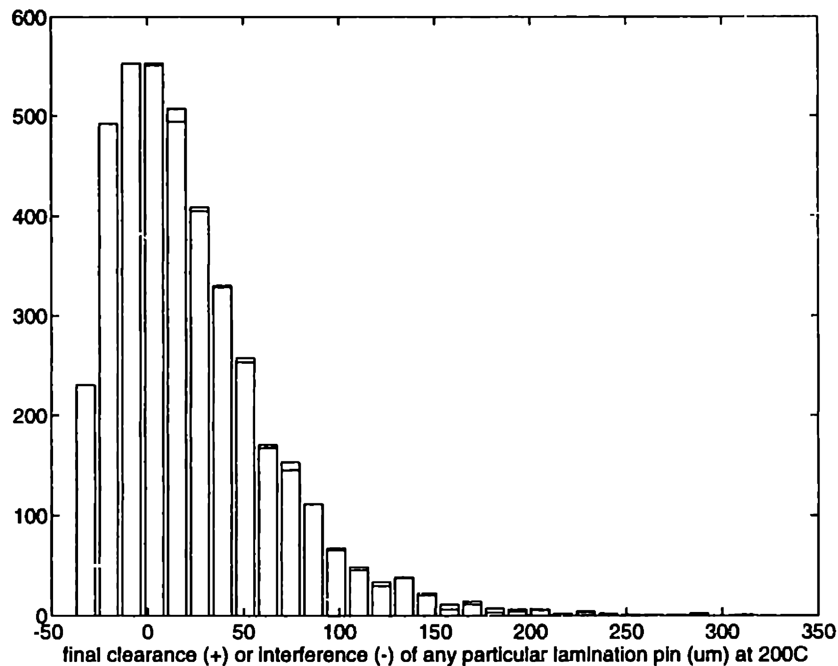

Figure 3-35: Pin and slot fit at cure temperature.

3.11 Drill

Numerous technical challenges exist with regard to the drilling operation, many of which are related to machine dynamics, as in dynamic spindle and structural stiffness, to motion control, and to tool mechanics. Generally, the errors caused by these elements will be on the order of less then $10\mu m$, with the exception of tool deflection, which, for smaller diameter holes may be as much as $75\mu m$. Drill deflection is the dominant cause of machine related errors and is attributed to excessive radial forces caused by contact with glass fibers.

Machine specific errors aside, tooling of the panels to the drill tables is another source of error. The tooling scheme involves drilling holes into Delren plugs which are threaded into the drill bed. Pins are then hammered into the Delren plugs and the panels are placed over these. Tooling features in panels are four slots formed from resin replication of tooling pins during lamination.

As in all previous discussions of the four slot tooling scheme, the fixturing technique in this instance is indeterminate. The pins themselves designed to fit into the replicated

slots, but with the variation of slot and pin diameter, any one particular fit may be either a clearance or interference fit. The combination of four such constraints creates an elastically averaged system, where the static equilibrium position of the panels is a function of the size and location of the pins and slots. Since these size variations are stochastic, panel fixturing is not deterministic. In fact, while watching operators during set-up, it was observed that many panels were difficult to fixture, indicating interference or variation in location of the slots and pins, while other panels were placed easily. Solving the contact forces for this system is impossible because there exist more constraints than equations. Recall that for the case of a body constrained to a plane, three equations for static equilibrium are available. Because this system is statically indeterminate, the location of the panels relative to bed cannot be calculated; which is the same problem currently existing for film and core fixturing. Furthermore, for this particular case of panel fixturing, the location of the image is not known with respect to the tooling slots because of material movement during lamination. Without measures to reduce material movement, or without adequate modeling of such motions, the registration of the drill to image is limited. To determine where the image is relative to tooling features, an x-ray vision system is recommended, in which new tooling features may be drilled with respect to the average center position of inner-layer features. It is further recommended that kinematic tooling features as shown in Figure 3-36 be profile ground based on x-ray measurements.

Currently, pins are hammered into position once Delren plugs have been drilled. Similar to lamination, pin tilt is an important consideration. For lamination, however, the pins would rotate or tilt as a group, as previously shown in Figure 3-33 and Figure 3-34. Because the pins in the drilling operation are not end constrained, as is the case with the top press plate, individual pin tilt is independent; however, since the pins are hammered by the same operator in the same position, pins may tilt in a preferred direction. The tilt is most probably caused by hammering them into position. For a $15mmpin$, end deflection caused was measured to be, on average, $0.125mm$, as shown in Figure 3-37. Although the ratio of length to deflection is greater that 100:1, consider that two stacked $1.6mm$ panels may be misregistered, on average, by as much

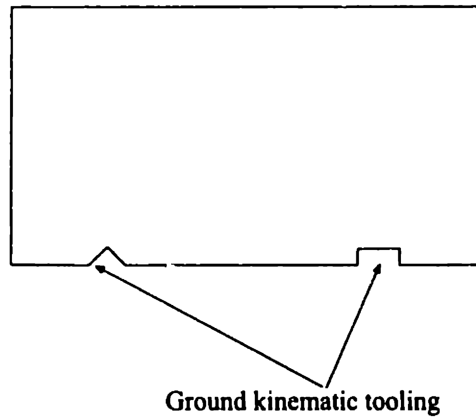

Figure 3-36: Proposed profile ground tooling features for primary drill and route.

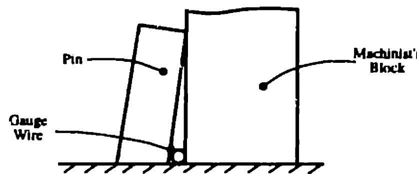

Figure 3-37: Measuring tilt of drill tooling pins with a machinists square.

as $16\mu m$.

The sensitive direction of tilt is in the direction perpendicular to the tooling slots. In tooling scheme where panels are to be stacked, it is imperative to maintain squareness of the tooling pins to maintain panel- to-panel registration. Fixturing stiffness should also be considered, since the panels are subjected to forces, albeit small, during drilling. The stiffness is a function of the materials and their interface preload. The table is made of cast aluminum, and based on its thickness can be considered a rigid body. Delren, on the other hand has approximately 1/3 the stiffness of aluminum, and based on their dimension and threaded connection, are the most compliant element of the chain of elements. Care should be practiced while inserting the plug. The correct torque should be applied and the design of the plugs should require sufficient threads to engage the bed. The press fit of the hardened steel pins couples the panels to the plugs, and the preload of the slot/pin interface is critical. However, because the

Measure	$3\sigma(\mu m)$	**% Contribution**
Environmental effects	2	negligible
Inner-layer features	105	64
Drill error (runout, wander, etc.)	77	34
Fixturing (estimated)	20	2
Total	131	100

Table 3.20: Inner-layer feature distribution for multiple stacked panels at drilling.

system is overconstrained, this preload is unknown, hence the overall fixture stiffness cannot be determined. Panel position relative to the drill head, therefore, cannot be determined to any accuracy. Aside from fixturing panels in the $(xy\theta)$ positions, they should also be preloaded in the lateral direction. Currently, an aluminum top sheet is held against a stack of panels and taped to the table as shown in Figure 2-23. Panel warp due to oveconstraining can lead to excessive tool wear, breakage, and registration problems if not preloaded flat against the table. The spindles themselves contain a preloading collar to hold the panels flat in the vicinity of the particular drilled hole. However, repeated loading and unloading, especially of a warped panel, will cause small panel motions, hence affecting tool-to-panel and panel-to-panel registration.

Table 3.20 shows the various error contributions and their relative importance.

Registration deviation for inner-layer and stacked panels is approximately $130\mu m(3\sigma)$. Using this figure, an estimate for the smallest pad size may be obtained for the case of drilling stacked panels. Minimum pad size may be calculated using the above tolerance. According to Figure 3-38, the inner-layer pad diameter is given by the equation,

$$\phi_{pad_{inner-layer}} > \phi_{via} + 2t_{ring} + 2(130\mu m) \tag{3.10}$$

where t_{ring} is the radial thickness of the required annular ring. Assuming that the annular ring is 20% the pad diameter,

$$\phi_{pad_{inner-layer}} > \frac{\phi_{via} + 260\mu m}{0.6} \tag{3.11}$$

For example, a $0.2mm$ diameter via requires a $0.77mm$ pad diameter; a $0.4mm$ via

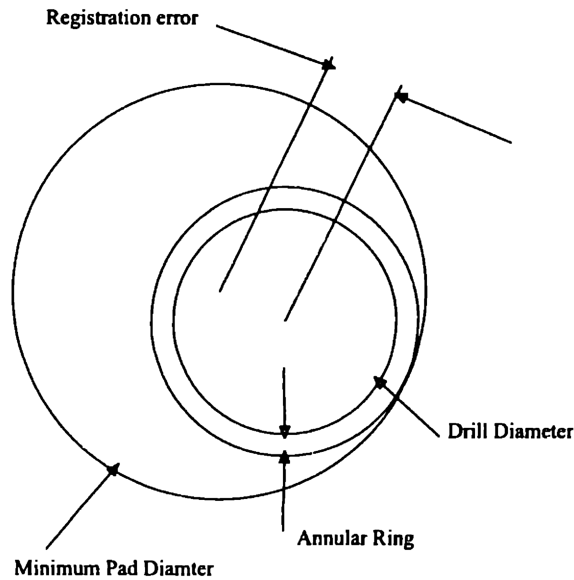

Figure 3-38: Registration error, specified hole diameter, and annular ring determines the required pad size.

requires a 1.1mm hole.

Table 3.21 shows the minimum pad size required for various diameter holes and required annular rings using the above equation.

Hole diameter (mm)	Annular ring (mm)	Pad diameter (mm)
0.20	0.025	0.500
0.20	0.050	0.550
0.25	0.050	0.600
0.25	0.100	0.700
0.30	0.050	0.650
0.30	0.100	0.750
0.40	0.100	0.850
0.40	0.150	0.950

Table 3.21: Required pad size for a particular drill diameter and specified annular ring.

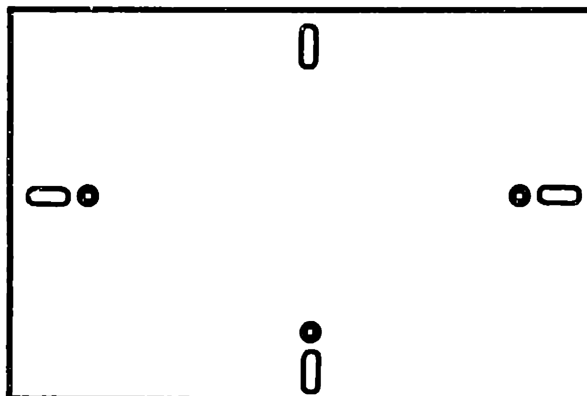

Figure 3-39: Outer-layer frame tooling.

3.12 Outer-Layer Imaging Processes

3.12.1 Outer-Layer Image

The outer-layer exposure process is similar to inner-layer expose, and the issues pertaining to front- to-back film registration, frame-to-frame repeatability, glass flatness, and film constraints are discussed extensively in previous artwork sections. Most of the inner-layer discussion is directly applicable to outer- layer expose. The primary difference between inner and outer-layer expose is that panel positions relative to the artwork is critical to ensure that component land patterns and traces register to the drilled vias. Therefore, precision *and* accuracy are issues. Panels are registered to the artwork by fitting three 0.157" diameter holes in the panels over 0.157" diagonal square pins, as shown in Figure 3-39.

As in all process fixturing techniques, this system, too, is indeterminate. Fixturing accuracy and precision is a function of the size and location of holes and pins. Tooling holes and vias are drilled at the same time, based on an x-ray inspection system, so that tooling features are registered with respect to the artwork. The 3σ positional accuracy of the drilling operation is approximately $16\mu m$, as previously noted, neglecting tool deflection. Because outer-layer tooling holes are large compared to the via holes, tool deflection is negligible, and positional accuracy is limited to the x-ray inspection system resolution and the drill repeatability. Hole and pin sizes and locations must be accounted for. Considering these additional factors, the panel to tooling 3σ position

deviation is, by simulation, $40\mu m$. This represents the uncertainty in panel positioning with respect to the frame. Artwork on each side contributes $66\mu m$ (Section 3.3), while for smaller diameter drilled vias, drill wander causes $75\mu m$ of drilled via-to-tooling hole uncertainty. The overall artwork-to-via registration deviation (3σ) is approximately $105\mu m$. Outer-layer pad positions are limited by this error, and are given by the equation,

$$\phi_{pad_{outer-layer}} > \phi_{via} + 2t_{ring} + 2(105\mu m) \tag{3.12}$$

where t_{ring} is the radial thickness of the required annular ring. For example, a 0.2 mm hole with a specified minimum annular ring of 0.05 mm, requires at least a 0.5 mm pad. Similarly a 0.4 mm hole with a specified minimum annular ring of 0.1 mm, requires at least a 0.8 mm pad.

Due to overconstraints, panels are elastically averaged when fixtured to the glass. Each hole is elastically averaged over a pin, and the panel itself is averaged to find its equilibrium position. If a positional misregistration between a pin and hole of more than $10\mu m$ exists, the hole integrity is compromised by local yielding and abrasive damage. Abrasion will affect pin life and image quality, when particles from repeated abrasion migrate to the image area. Because, ultimately, the registration capability relies on the positional accuracy of pins relative to artwork and tooling features relative to inner-layers, it is not conclusive if this particular instance of overconstraining will be inferior to a kinematic system; however, a proposed methods will be described later. Furthermore, the dominant cause of outer-layer image error is drill wander for smaller vias, and artwork errors. Fixturing error contributes approximately 15% to the total outer-layer image uncertainty.

3.12.2 Solder Mask and Photo-Defined Vias

The process of applying Probimer interferes with registration since curtain coating solder resist affects tooling hole integrity. It nonuniformly coats the interior edges with thick material. Without either protecting the holes from coating or drilling new features after the solder mask is applied, passive fixturing of the panels with respect

to the photo-tool will not be achievable for panel-to-artwork registration. Active vision systems are becoming an alternative to passive tooling for precisely this reason; however, the lower throughput and high cost of these systems is an issue. Currently, the artwork is manually aligned to the outer-layer image using a loupe and fixed to the panels using tape. Manual registration for tighter tolerances will no longer be an acceptable technique.

Without kinematically fixturing the outer-layer artwork, thereby reducing the top-to-bottom misregistration, fixturing the photo-defined via artwork with a passive registration system will not be beneficial. This is primarily because the current technique, consisting of manually taping artwork to the outer-layer image, can account for any outer-layer misregistration. That is, each panel is aligned to fit. Introducing the kinematic fixturing will reduce the outer-layer registration error significantly, as will be shown later, in which case kinematic tooling of photo-via artwork is feasible. However, as is the case with outer-layer imaging, accuracy of tooling pins relative to the fixtured artwork is critical since this will determine registration performance of the image to panel. But because the coating process alters panel tooling features, even with accurately placed pins, panel registration is questionable. The alternatives to active registration are to either create new features following each coating process, or, as will be described later, the existing features should be protected during the coating process.

Assuming drilled tooling features have been protected from coating, the outer-layer image to solder mask image registration is limited to by the uncertainty in fixturing ($40\mu m$), the uncertainty in the outer-layer image relative to tooling holes ($71\mu m$), and the uncertainty in the artwork position ($66\mu m$). The total uncertainty in solder-mask image to outer-layer image is $105\mu m(3\sigma)$. The smallest pad size may be calculated using Equation 3.12, from which the minimum pad pitch may be calculated by specifying the amount the solder mask should be oversized and the minimum solder mask web. By Figure 3-40, the minimum pad pitch p is,

$$p > w_{web} + 2t_{oversize} + \phi_{pad} + 2(105\mu m) \tag{3.13}$$

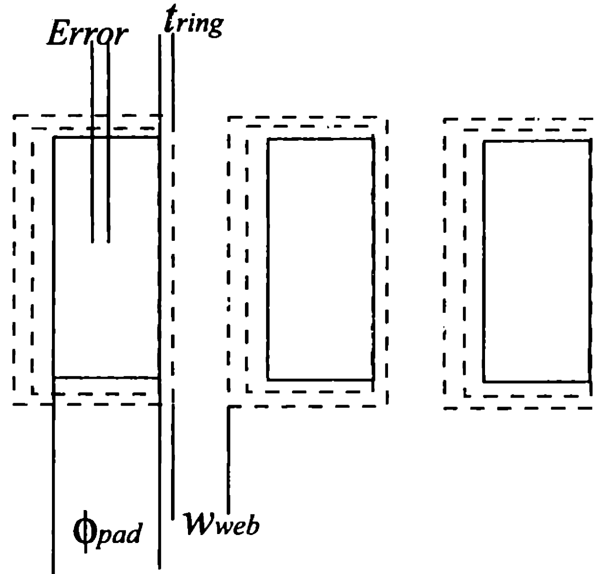

Figure 3-40: Determination of minimum device pitch from solder mask.

For the case where component pads are over plated holes, ϕ_{pad} would be given by Equation 3.10.

Similarly, the size of an outer-layer dot for a specified photo-defined via is readily determined since the outer-layer pad to via artwork uncertainty is 105 mm.

For a specified 0.1 mm via and a 50 mm annular ring, the minimum dot size is 0.4 mm, assuming passive fixturing techniques and protected tooling features. Currently, the desire to create 0.1 mm vias over 0.25 mm pads with a 50 mm minimum annular ring will be satisfied at a rate of approximately 53%, assuming tooling features are protected from the coating process.

3.12.3 Outer-Layer Summary

The dominant cause for misregistration at outer-layer expose is uncertainty in via position due to drill wander and uncertainty in outer-layer artwork position due to punch and fixturing errors. Panel fixturing accuracy accounts for approximately 15% error, artwork 35%, and drill 60%. Note that drill error contribution is large in this case because small drill bits $0.2mm - 0.3mm$ are used as a benchmark. Currently, the desire to create 0.1 mm photo-defined vias over 0.25 mm pads with a 50 mm minimum

annular ring will be satisfied at a rate of approximately 50%, assuming tooling features are protected from the coating process.

3.13 Route

Routed features were reported as having an overall tolerance of 0.125 mm. It is doubtful that a significant portion of this tolerance is attributed to tool deflection or spindle runout. A tolerance of $55\mu m$ may be attributed to spindle, tool, laminate stiffness, and tooling clearance. Routed feature to outer-layer image 3σ deviation is $120\mu m$. It is estimated that at least 80% of route errors are caused strictly by panel fixturing, either at route itself, or due to uncertainty in outer-layer image location.

3.14 Electrical Test

The fabricated boards are electrical tested using top and bottom probe fixtures which interface to the board being tested and to a programmed bed of nails. The probes themselves are $0.5mm$ diameter piano wire which can test device pitches down to $0.4mm$. The test fixture is fabricated using the router for profiling, and the drill head for probe holes and fixturing holes. The Acrylic sheets used are first drilled with three $4.75mm$ diameter holes as fixturing holes for subsequent routing. Fixturing pins are $4.7mm$ in diameter; some clearance is needed for ease of placement in the route fixture since three hole and pin connections are present. Accuracy and precision is required for drilling, since the hole to hole positioning of the test fixture will largely determine probe to board registration.

As previously discussed, routed feature deviation is approximately 0.125 mm. Although this has been attributed to compliance in the spindle, most of this error can be attributed to fixturing error and outer-layer image to tooling error. Panel and test fixture members contain clearance fits with router pins; hence the stiffness is zero until transverse cutting forces push the parts against a pin. This motion is not repeatable and causes most of the reported error. It is also likely that panels and fixtures are

vibrating against the tool as they are cut. Because the drill does not apply transverse cutting forces, better repeatability is observed on drill than route. To reduce the errors associated with these operations, a more repeatable fixturing technique is needed.

Once test fixtures are made, other registration issues remain. Related to the board, these are:

1. Position of the board fixture holes relative to each other, and

2. Position of the image with respect to fixturing holes.

For the probe fixtures, the issues are:

1. Probe to probe positioning,

2. Probe to board pinning, and

3. Top to bottom fixture registration.

Position of the fixturing holes on the board relative to each other will determine the type of fit between the board and fixture [10]. Unlike the case of fixturing panels to the drill table, where panel features were slots, features on the board are drilled holes which do not permit any relative displacement of the pin and feature. This is the same problem associated with outer-layer image, where the panels are fixtured to the expose units over three square pins. In any event, like all previously discussed fixturing techniques, multiple pin and hole arrangements create an indeterminate system, which is severely limited in its placement repeatability by the manufacturing tolerances involved in creating tooling features. However, similar to outer-layer imaging, accuracy is also required, since the board test sites must be located with respect to the probes. The accuracy will depend on the ability to locate constraining pins relative to the probe pattern, while repeatability is more a function of the type of constraining system used. Because of this, a kinematic fixture-to-fixture coupling is appropriate, while the performance of a kinematic board-to-fixture coupling will have to be determined experimentally.

Minimum device pitches which can be tested are ultimately limited by wire size and probe geometry; however, registration issues currently impact the process. Approximately 25% of the fine-pitch thin cards report false alarms because of probe misregistration caused by fixture to board or fixture to fixture registration errors. Registration error of board tooling features to outer-layer components is approximately $71\mu m$ and, although indeterminate, board placement repeatability to the test fixture is estimated as $50\mu m$. This is primarily due to the compliance of the spring-loaded coned fixturing pin. The total component pad position uncertainty is $87\mu m(3\sigma)$. Pin position uncertainty is $125\mu m$ and fixture position uncertainty is $50\mu m(3\sigma)$. Probe to component pad uncertainty is $160\mu m(3\sigma)$, 60% of which is caused by the uncertainty in probe location. Temperature fluctuations contribute 0.1% to the total error. For example, a pad would have to be at least 0.36 mm wide to avoid a false alarm caused by probe to pad error. For 3σ certainty, this would correspond to a $0.6mm$ pitch device. A 75% success rate (reported for fine-pitch thin cards) corresponds, approximately, to a $0.125mm$ pad, or a $0.2mm$ pitch device. Testing of $0.4mm$ pitch devices should be valid for approximately 1.8σ, or 92.8 % of the boards. Registration specific problems were not recorded, so it is uncertain if above estimates are satisfied. To reduce registration errors considerably, smaller probe hole clearances should be specified when making the fixtures.

3.15 Sensitivity Analysis

Each registration critical process has been studied, and specific errors have been documented for the particular production facility studied. The model used to calculate these errors was one which assumed each process could be represented as a random independent variable, the normally distribution about a nominal value. Additionally, since all tooling schemes were indeterminate, numerical simulations were incorporated into the model for determining locational and rotational variances of artwork and panels. Predicted results agree with experimental data and anecdotal evidence. Percent contributions of each process were calculated to determine the relative importance of

each step. In this section, the variances of the production line are summarized to concisely describe the relative significance of each process. Furthermore, the model is generalized to study the sensitivity of certain metrics to process variations. Registration sensitivities were calculated using nominal values determined from previous error analysis. Output metrics include, inner-layer pad diameter, outer-layer pad diameter, minimum pitch for solder mask over drilled pads, minimum solder mask pitch over undrilled pads, and minimum pitch of photodefined vias over outer-layer pads. Contributions to these measures from process deviations are calculated.

The sensitivity of each criteria may be written as a function of the deviation of any particular process,

$$\frac{\partial \phi_{pad}}{\partial \sigma_i} = \frac{\sigma_i}{\sqrt{\sum_k \sigma_k^2}} \tag{3.14}$$

Equation 3.14 shows that an output measure, such as pad diameter ϕ_{pad} is most sensitive to processes with the largest variance. This is intuitive, since the largest reduction in an error is accomplished by reducing its most significant contributor.

Data in Figure 3-41 through Figure 3-45 displays the error contribution to a particular measure, as a function of various process deviations. Figure 3-41 shows that the largest reduction to inner-layer pad diameter may be most effectively accomplished by reducing errors from inner-layer expose. These errors have been listed in Table 3.10. Environmental variations have negligible impact on inner-layer pad diameters. Notice that drill errors are also significant contributors to required inner-layer pad dimension. This is primarily due to drill wander. For larger drilled holes, this error is reduced. For this and other plots, the y axis represents the contribution of process variations, which does not include pad specifications, such as annular ring and drill size. The pad diameters are given by the sum of the specifications *and* the error contributions.

Conversely, drill deviations are the most significant contributing factor for the required size of outer-layer pad diameters, as shown in Figure 3-42. This differs from the inner-layer pad diameter case, since for outer-layers, positional uncertainty relates only to the outer surface, as opposed to drilling which required alignment of all inner-layer pads.

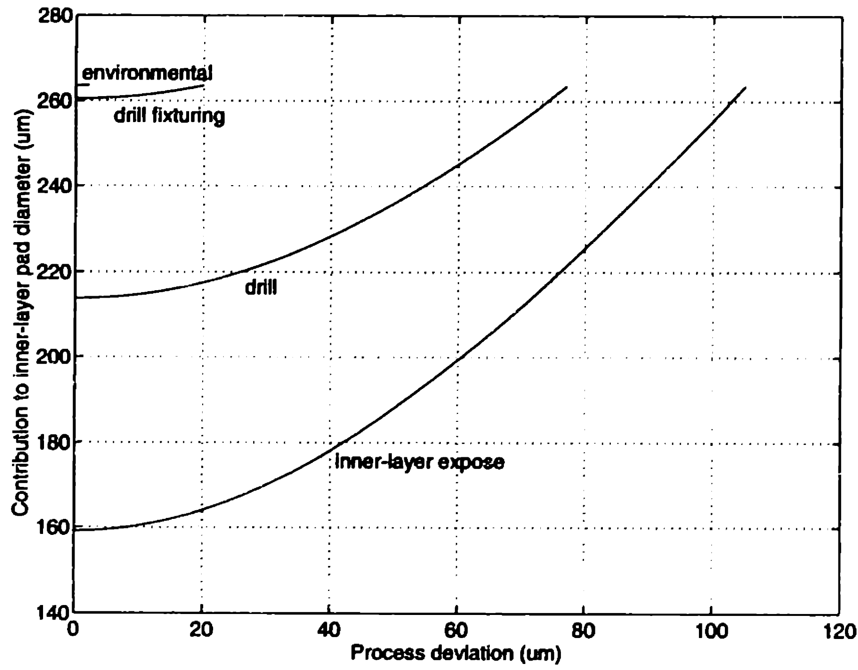

Figure 3-41: Process deviations and their impact on inner-layer pad diameter.

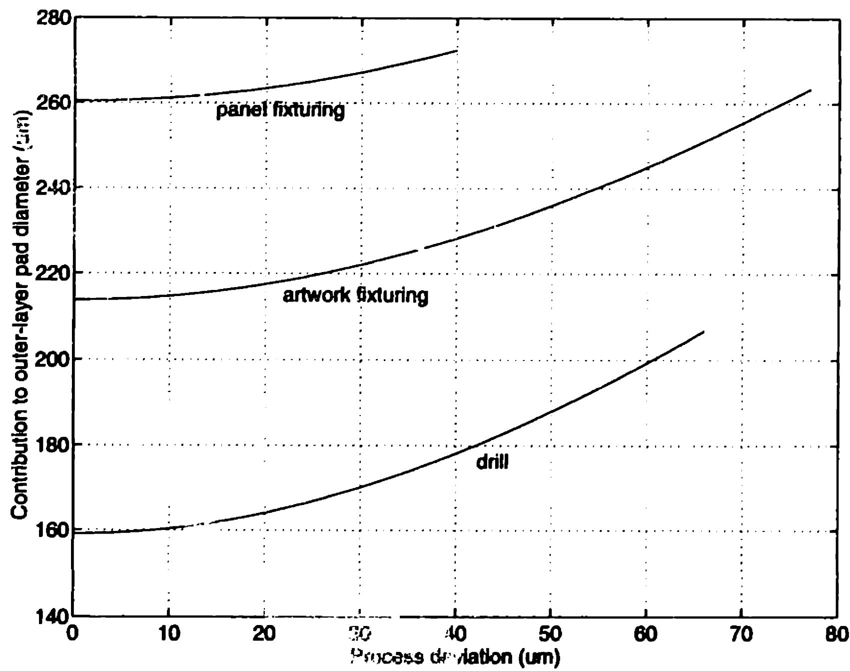

Figure 3-42: Process deviations and their impact on outer-layer pad diameter.

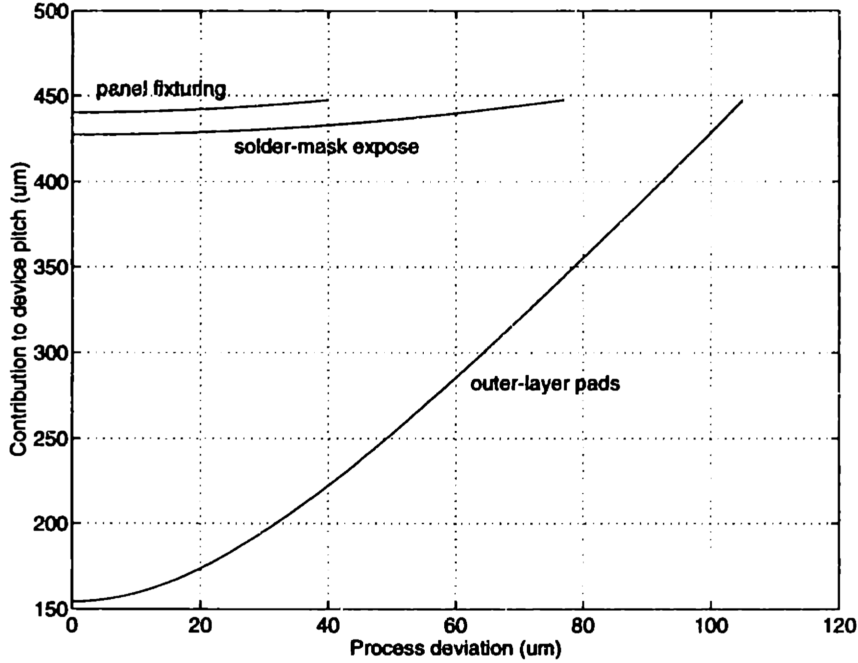

Figure 3-43: Process deviations and their impact on pad pitch. Solder mask over drilled outer-layer vias was used as the criteria.

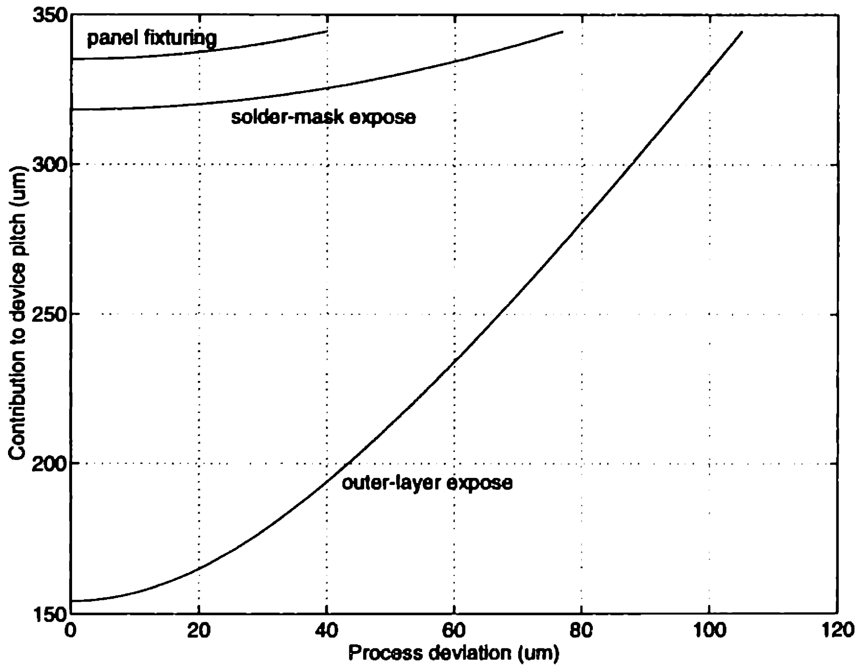

Figure 3-44: Process deviations and their impact on pad pitch. Solder mask over undrilled vias was used as the criteria.

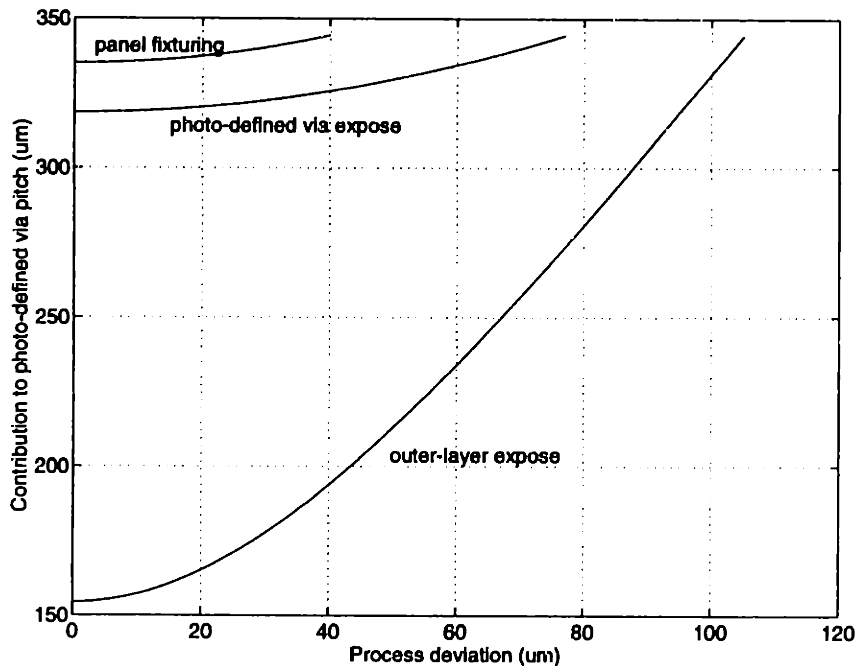

Figure 3-45: Process deviations and their impact on photo-defined via pitch.

Process deviation contributions to minimum device pitch may be determined from the uncertainty in panel fixturing, outer-layer pad position uncertainty, and solder mask artwork positional uncertainty. Figure 3-43 shows outer-layer pad positional uncertainty is the dominant contributor to solder mask imaging, hence pad pitch. This data represents the error contribution to minimum pad pitch for pads that contain drilled vias. Often, drilled vias (outer-layer pads) are connected to devices by traces in fan-in or fan-out configurations. Because of this, Figure 3-44 shows the sensitivity of device pitch to process deviations, where the solder mask is exposed over a device without drilled vias. The contributing errors in this instance do not include the requisite larger outer-layer pad dimensions for drilled holes.

Figure 3-45 also shows process impact on the pitch of photo-defined vias. This scenario is identical to the solder mask process, whereby outer-layer pads do not contain drilled vias. Note that these processes are highly dependent upon outer-layer image variations, which are, in turn, most sensitive to inner-layer expose processes.

The error contributions to inner and outer-layer pad diameter, and outer-layer pad

pitch from processes noted range from approximately $0.25mm$ to $0.35mm$. These 3σ contributions are consistent with current limitations in production of fine pitch boards. For example, μBGAs with fan-out configuration may have pitches of $0.3mm$. Boards for these devices are not produced using conventional techniques, nor are yields as high as for sparsely populated boards. Since special methods are required, and yields are low, product cost is high. It is the goal this thesis to develop new methods within a conventional PCB manufacturing framework which will facilitate production of these μBGA and other fine pitch components.

The inner-layer expose process was targeted for improvement because of the sensitivity of subsequent processes. Advances in this area will significantly reduce the requisite inner and outer-layer pad diameter, which impacts favorably outer-layer images and permissible device pitches. Furthermore, improvements to the exposure process are applicable to outer-layer imaging processes, further reducing diameter and pitch limitations.

Before proceeding to actual designs, however, the issue of film measurement must be considered. Since this thesis develops fixturing techniques that surpass the resolution of the current fiducial type of measurement, new measurement methods are developed. This is the subject of Chapter 4. Once a suitable measurement scheme is developed, fixturing and coupling designs for improving inner-layer registration will be presented.

Chapter 4

Artwork and Laminate Metrology

Feature-to-feature repeatability error of photo-plotters used in the creation of circuit board artwork, limits measuring and alignment repeatability of film to external references such as tooling holes or with respect to another piece of film. Fiducial based measurement schemes are limited by variances of plotted features themselves.

For the case where registration is assessed based on measurements of multiple features, the standard deviation of the mean position is inversely proportional to the square root of the number of features sampled. This technique requires individual measurements of numerous features if a registration result is to be reported with a higher resolution than the plotter error.

Practically, however, such a method would be difficult. Consider, for example, that many printed features could be measured within the same field of view. A rectangular grid of features such as those illustrated in Figure 4-1 may be used. For the standard deviation of the mean of measured positions to be ten times smaller than that of the deviation of any single feature, one hundred samples are needed in the field of view. A ten by ten square grid would accomplish this task. Since the desired resolution of a registration measure is on the order of a few microns ($5 - 10\mu m$), the measurement itself should have a resolution of five to ten times that, requiring a resolution of $0.5 - 2\mu m$ and a dynamic range on the order of $20\mu m$. The grid shown in Figure 4-1 may satisfy this specification, if imaged onto a high resolution CCD array. Twenty micron squares are assumed to satisfy the dynamic range requirement, with a

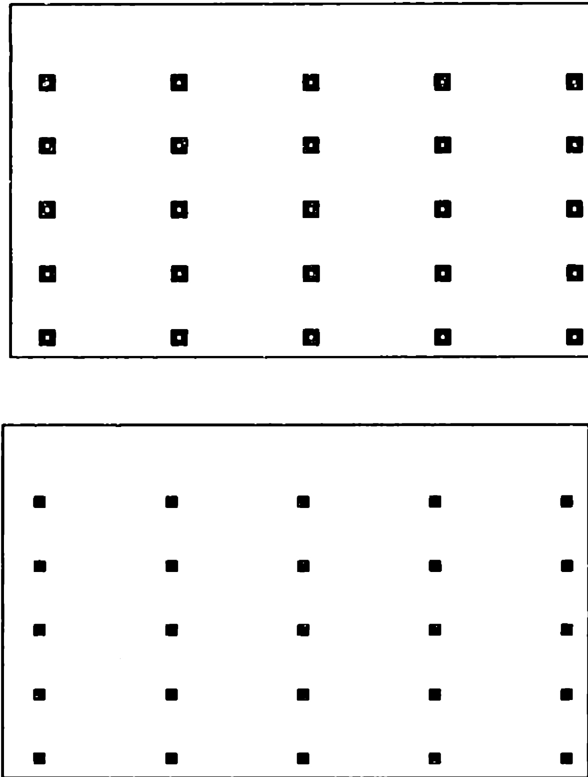

Figure 4-1: Rectangular grid of printed features for obtaining an average measure of artwork position and rotation.

measuring resolution of approximately $\frac{1}{20}$ of a square. Considering the requisite gap between printed squares, an 800×800 array would be required. The total object dimension is approximately $0.5mm \times 0.5mm$, which would call for a $15\times$ optical system using a practical CCD format. Image processing techniques to parse the image space into evenly spaced grids would calculate the relative displacement of individual squares and boxes, determining the mean position and rotation of the film, along with the respective variances. One substantial difficulty is that the plotting and developing systems have a realistic printing resolution of approximately $40-60\mu m$, precluding the use of such a finely spaced pattern. By tripling the size of the pattern, the dynamic range is increased, but the measurable position resolution has been degraded. A simple technique which will yield superior displacement resolution given the feature size restriction imposed by plotting and developing is desired.

Two candidate methods are proposed and tested in the following sections. These are both techniques which use binary gratings to measure artwork displacement. As

such, the optical effects are the outcome of the interaction between light and numerous features, minimizing the contribution of plotter uncertainty to the measurement. Furthermore, the implementation of such systems is such that system parameters other than feature size and optical magnification will determine measurement resolution. These techniques are based on fringe patterns generated by overlapping binary gratings at relative angles, and on Fraunhofer diffraction patterns generated by coherent light passing through multiple narrow slits.

In this chapter, the theory of each method is presented along with a description of the implementation within the context of circuit board manufacture. Experimental results are presented.

4.1 Moiré Interferometry

4.1.1 Theoretical Treatment

Moiré fringes are patterns which can occur when either two gratings are rotated or displaced relative to each other, or the gratings have different line frequencies. Fringing is a beat phenomenon, and can be easily understood by describing gratings as a sum of sinusoidal patterns, without any loss in generality. Using a Fourier approach, the transmittances of two gratings can be expressed as [22],

$$T_1(x,y) = a_0 + \sum_{m=1}^{\infty} a_m \cos(\frac{2\pi}{d_1} m \left[x - f_1(x,y) - \delta_1\right]) \tag{4.1}$$

$$T_2(x,y) = b_0 + \sum_{n=1}^{\infty} b_n \cos(\frac{2\pi}{d_2} n \left(\left[x - f_2(x,y) - \delta_2\right] \cos\theta - y \sin\theta\right)) \tag{4.2}$$

The $f_i(x,y)$ terms account for local distortions of the grating lines. Current etching and evaporation techniques employed for manufacture of gratings eliminates these distortions in the gratings themselves; however, these terms represent *any* departure from straightness. For instance, in topography the out-of-plane displacement of the subject will distort the grating lines, causing fringe patterns in the absence of any relative displacement or rotation of the gratings themselves. The a_i and b_i terms are

the Fourier coefficients of the intensity distribution, d_i are the grating periods, δ_i are grating displacements, and θ is the relative rotation angle of the gratings. The gratings can be overlayed, shadowed and viewed through itself, or one grating remotely viewed through the other; in all these cases the transmittance of the gratings are multiplicative. The individual gratings can also be projected onto a diffuse viewing screen whereby the intensity of the fringe patterns are additive. Each method has advantages and disadvantages.

When two gratings are overlapped, the transmittance is the product of the individual transmittances,

$$T_M = T_1 T_2 \tag{4.3}$$

Performing this operation, neglecting higher order frequency summations, and equating the arguments of the cos() terms to integer multiples of π, the following scalar expression for the spacing and orientation of the moiré fringes is obtained,

$$r = \frac{M}{d_1}\{x - f_1(x,y) - \delta_1\} - \frac{1}{d_2}\{[x - f_2(x,y) - \delta_2]\cos\theta - y\sin\theta\} \tag{4.4}$$

where M is an integer multiple line spacing of grating 2. For example, in the case where $f_i(x,y) \neq 0, \delta_i = 0, \theta = 0$, the fringes are contours caused strictly by the deformation of the gratings, $f_i(x,y)$, and are given by the family of curves,

$$\frac{d_1\cos\theta - d_2 M}{d_1 d_2}x - \frac{\sin\theta}{d_2}y - \frac{f_2(x,y)\cos\theta}{d_2} + \left\{\frac{M}{d_1} - f_1(x,y)\right\} + r = 0 \tag{4.5}$$

Typically, $f_2(x,y) = 0$, where the distorted grating is imaged through an undeformed grating to acquire contours. Such is the case in moiré topography, where $f_1(x,y)$ represents the surface profile of the sample to be contoured [11], [6], [25], [24].

The projection of the grating onto this surface, $f_1(x,y)$, generates an intensity pattern according to Equation 4.1. When this distribution is viewed through another grating, intensity patterns are multiplicative.

Additive Moiré

With additive moiré, the intensity distributions of the projected gratings are summed. This is realizable by individually projecting gratings onto a common diffuse surface. Additive moiré is used in double projection systems and the fringe patterns are viewed in real time through a third optical system, [34].

The intensity distribution of two sinusoidal gratings can be expressed as,

$$I_1 = 1 + \sin\frac{2\pi}{d_1}x \tag{4.6}$$

$$I_2 = 1 + \sin\frac{2\pi}{d_2}x \tag{4.7}$$

where d_i are the grating spacings. When summed, the intensity distribution becomes,

$$I_0 = I_1 + I_2 = 2 + 2\sin\left(\pi x\left(\frac{1}{d_1}+\frac{1}{d_2}\right)\right)\cos\left(\pi x\left(\frac{1}{d_1}-\frac{1}{d_2}\right)\right) \tag{4.8}$$

The main disadvantage of additive moiré is that the contrast is poor between the carrier wave and the moiré pattern. That is, the optics has to resolve the carrier wave to observe the moiré pattern. The poor contrast may make analysis difficult. This can be resolved by squaring the intensity distribution. When this is done, an additional moiré term is not modulated by the carrier. The contrast is thus enhanced.

Multiplicative Moiré

When one grating is viewed through another, either in a projection system or when placed in contact, the intensity distribution is simply the product of the individual intensity patterns. That is,

$$I_0 = I_1 I_2 \tag{4.9}$$

Using equations 4.6 and 4.7, the intensity distribution of the multiplicative case is.

$$I_0 = 1 + 2\sin(\pi x\left(\frac{1}{d_1}+\frac{1}{d_2}\right))\cos(\pi x\left(\frac{1}{d_1}-\frac{1}{d_2}\right)) + \tag{4.10}$$

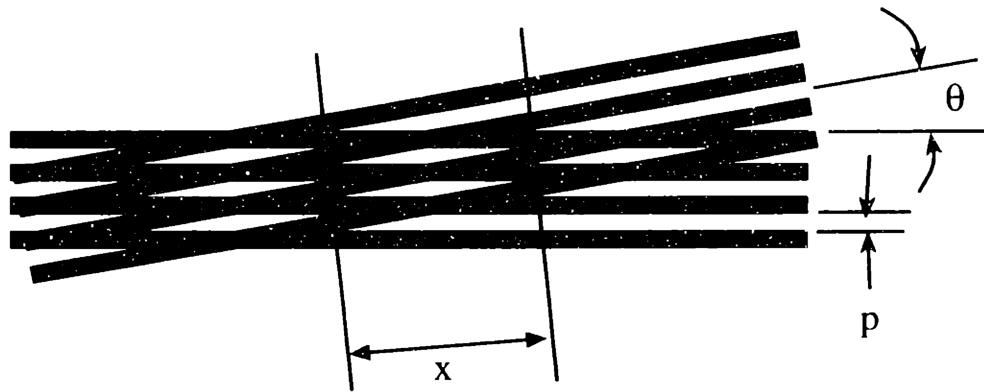

Figure 4-2: Two binary gratings at relative angle θ creates a fringe effect.

$$\frac{1}{2}\left(\cos(2\pi x\left(\frac{1}{d_1}-\frac{1}{d_2}\right))-\cos(2\pi x\left(\frac{1}{d_1}+\frac{1}{d_2}\right))\right)$$

Notice that with multiplicative intensity distributions, the moiré term is isolated from the carrier. The contrast is enhanced without a nonlinear transformation, as was the case for additive moiré. The single projection moiré topography system, presented later, makes use of the higher contrast which results from the multiplication of the intensity distributions.

Subtractive type moiré can be achieved; however, it is difficult to realize, making use of gratings which have alternating polarizing regions. Subtractive moiré does, however, generate the highest contrast moiré fringes.

Consider two linear binary gratings of pitch p, rotated an angle theta with respect to each other, as shown in Figure 4-2. According to multiplicative moiré, the transmittance of the pattern is zero along the locus of points where the lines are out of phase, and is full along the locus of points where the lines intersect.

Defining x as the distance between fringes, the equation describing the locus of fringes is given by,

$$x = \frac{lp}{2\sin(\theta/2)} \tag{4.11}$$

where $l = 0, 1, 2, \ldots$ and the fringe number. For small angle θ, Equation 4.11 reduces to,

$$x \approx \frac{lp}{\theta} \tag{4.12}$$

Notice that the fringe separation is $1/\theta$ times the grating pitch, p. As one grating is translated relative to the other by an amount x', the fringe moves by an amount $x'/2\theta$; therefore the fringe effect creates a transmission ratio between the actual grating displacement and the fringe displacement. This technique can be applied to circuit board artwork by laser plotting one grating on a film, and placing it in contact with a precision glass reference grating. To align film, two translational and one rotational measurement are needed. Printing three gratings on the film perimeter, two translational and one rotational degree-of-freedom can be registered by resolving the phase of the fringe pattern.

4.1.2 System Overview

Although three planar degrees of freedom can be determined from one radial target [19], this type of pattern is not well suited to film alignment. The reason for this is because the plotters used for producing artwork cannot print features with the necessary angles. The plotters are best suited for straight lines normal and parallel to the printing axis, corresponding to vertical and horizontal lines on the artwork itself. Because of this restriction, simple straight line binary gratings were considered for measuring position and rotation of the artwork. The alignment and measurement systems developed in this study employed a Ronchi grating printed on the film which would be held against another Ronchi grating, fixtured at a slight angle creating the vernier effect illustrated in Figure 4-2. For alignment of the film prior to punching, repeatability is essential while accuracy is not a significant consideration. Therefore, as a proof of concept, the system consisted of a reference glass grating fixtured flush with a tooling table. Another Ronchi grating was bonded to half of the reference grating, creating a reference fringe pattern as shown in Figure 4-3.

When the film is placed onto the table, the plotted film grating creates a fringe pattern on the other half of the reference grating as shown in figure 4-4. For repeatable alignment, the pattern generated by the film is to match that of the reference fringes by moving the film with respect to the glass grating. By using three such gratings around the perimeter of artwork, three degrees of freedom may be measured. A heterodyne

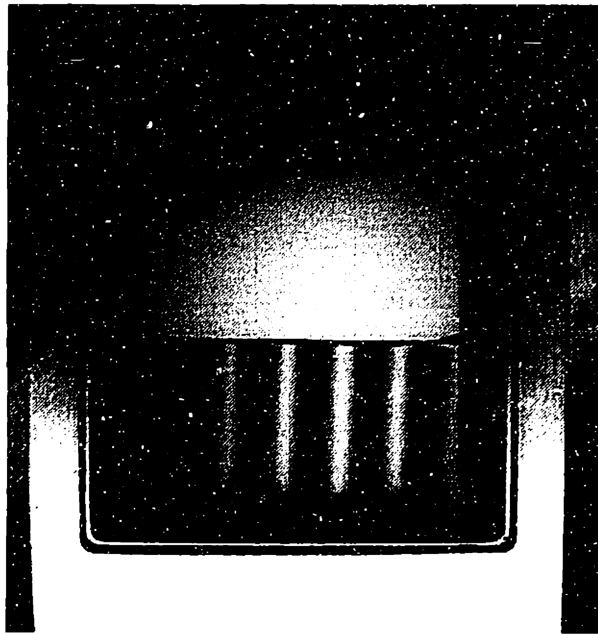

Figure 4-3: A $1'' \times 2''$ grating is bonded to a $2'' \times 2''$ grating to create the reference fringe pattern against which all measurements will be made.

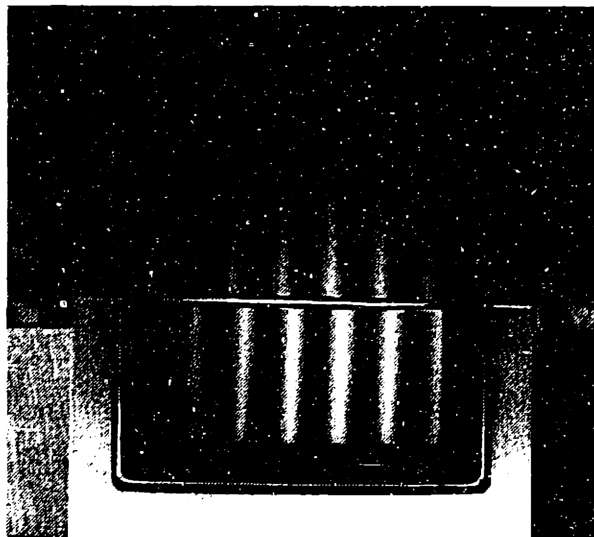

Figure 4-4: The $250lp/in$ film grating against the reference grating creates a fringe pattern. Fringes are compared to determine relative position and rotation of the film with respect to the reference.

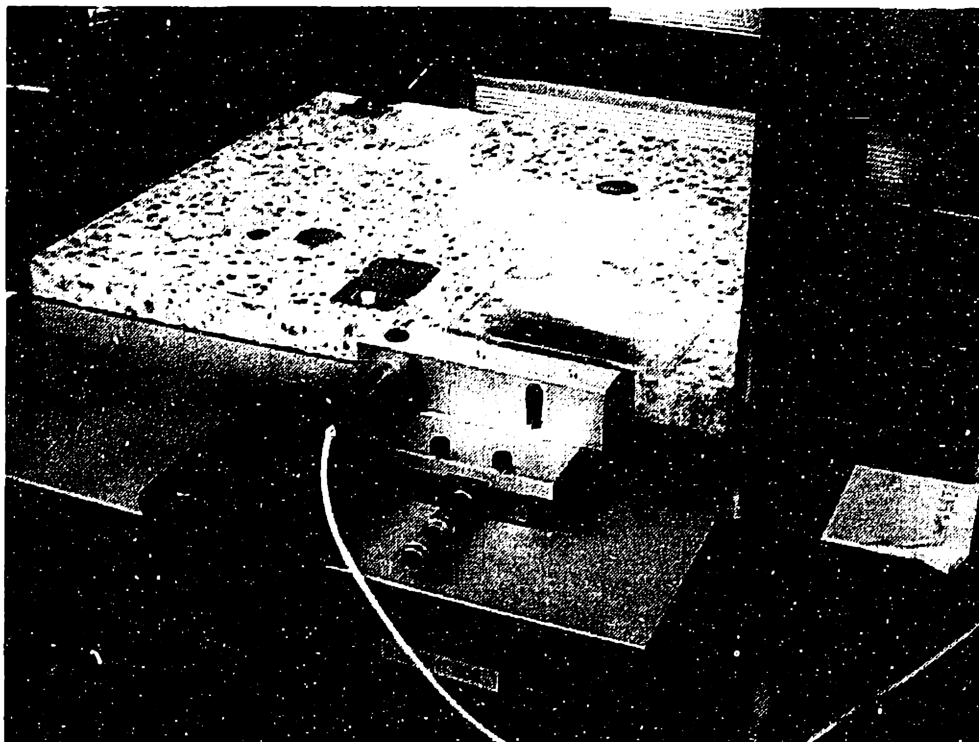

Figure 4-5: The system used to measure the gauge capability of the optical alignment methods.

method which uses the fringe phase and frequency information was also developed, with a redundant rotational measurement.

The system shown in Figure 4-5 was used for a gauge capability study of the proposed moiré technique. Only one film grating was used, measuring displacement along a single axis, with the assumption that extending the system to include multiple degrees of freedom would readily follow. A 250 lp/in Ronchi grating was used as the reference since this is the smallest pattern the film photo-plotter can comfortably produce. The reference grating was $2'' \times 2''$ soda lime glass, etched and filled with black opaque material. An additional $1'' \times 2''$ glass grating was bonded to one half of the square grating to produce a reference fringe pattern as shown in Figure 4-4. This glass subassembly was bonded to three steel spheres press fit into an aluminum carrier. The carrier was kinematically located within a housing assembly, using a 3-2-1 scheme, and was ultimately bolted to a single axis manually driven stage with differential micrometer adjustments. The film with the printed grating was fixtured to the tooling table, with the grating overlapping the glass reference previously described. The

linear stage was adjusted, with the film fixed, to produce the relative phase difference of the film fringe and reference fringe. A lens assembly imaged the fringe patterns onto a Sony XC-75 CCD array which was captured using a MATROX 512 $\times$ 512 frame grabber board. A rotational adjustment to the film was provided so that the frequency of the film fringe pattern matched that of the reference fringe pattern. Once both patterns were of the same frequency, only the phase difference needed to be determined for calculating displacement. The half-wavelength of the fringe pattern represented 0.002", since that was the pitch of the gratings. Actual film-to-reference displacement was determined from the fractional fringe phase difference, given by

$$\delta = \frac{p\Delta\phi}{\pi} \tag{4.13}$$

where p is the grating pitch and $\Delta\phi$ is the phase difference. For example, a $\Delta\phi = \frac{\pi}{4}$ would correspond to 0.0005" displacement. To determine the capability of the measuring technique, the stage movement was measured using a capacitance probe with $5\mu m/V$ gain and 20 V range. Millivolt resolution was readily attainable without sophisticated signal processing, yielding a displacement resolution on the order of nm.

4.1.3 Resolving Phase

Numerous methods for determining the phase of an interferogram exist [5], [3],[28], and [18], for example. While these methods have been used to determine the full phase distribution of an interferogram to make an accurate measurement of the desired quantity, in the particular case of the film grating, the frequency range of the fringe pattern is known *a-priori*. Furthermore, the pattern generated is a simple periodic function in one dimension, and constant in the second, orthogonal, direction, as shown in Figure 4-4.

Therefore, the image information is sliced along the fringe axis, and averaged with subsequent fringes. This averaging takes place over the fields defined by the film and reference fringe, respectively, thus generating two vectors of data, each representing the average of multiple slices of fringe patterns in their respective fields. It thus remains

to analyze the two periodic vectors. The methods for analysis include, single point heterodyning. Fourier transform method, correlation, and heterodyning for frequency and phase modulated interferograms.

Homodyne Method

Homodyning is a simple way to measure the phase difference of a pattern of known frequency. The method involves multiplication of the fringe signal by $\sin(kx)$ and $\cos(kx)$, respectively, and integration of the results over one period. Assuming that the intensity pattern, $I(x)$, may be represented by

$$I(x) = I_0 + I_1 \sin(kx + \phi), \tag{4.14}$$

multiplication and averaging yields,

$$I' = \frac{k}{2\pi} \int_{\frac{-\pi}{k}}^{\frac{\pi}{k}} \sin kx \, [I_0 + I_1 \sin(kx + \phi)] \, dx \tag{4.15}$$

which ultimately reduces to,

$$I' = \frac{I_1}{2} \cos \phi \tag{4.16}$$

Multiplication of the same intensity pattern by $\cos(kx)$ and averaging gives,

$$I'' = \frac{k}{2\pi} \int_{\frac{-\pi}{k}}^{\frac{\pi}{k}} \cos kx \, [I_0 + I_1 \sin(kx + \phi)] \, dx \tag{4.17}$$

which reduces to,

$$I'' = \frac{I_1}{2} \cos \phi \tag{4.18}$$

The phase, ϕ is obtained by division, and is,

$$\phi = \arctan\left(\frac{I''}{I'}\right) \tag{4.19}$$

Resolutions on the order of $1/200 - 1/500$ of a fringe have been reported using this homodyning procedure [13].

This technique, common to radio frequency receivers, requires knowledge of the fringe frequency. For the case of aligning of measuring circuit board artwork, the frequency of the signal is not known exactly. In this instance, only a range of frequencies are known, due to possible rotational error of the film. To determine frequency, a Fourier transform may be employed. Since, however, the spectral content of the pattern would then be known, the interferogram phase could be determined directly.

Fourier Method

From Section 4.1.3, the intensity pattern created by evenly spaced Ronchi gratings rotated relative to each other was assumed to be sinusoidal. Actually, the pattern is a periodic triangle wave. Over one period, T_0, the intensity pattern is,

$$I(x) = \frac{2I_0}{T_0}x, x \leq \frac{T_0}{2} \tag{4.20}$$

$$I(x) = \frac{2I_0}{T_0}x - 2\frac{2I_0}{T_0}\left(x - \frac{T_0}{2}\right), \frac{T_0}{2} < x \leq T_0 \tag{4.21}$$

The intensity spatial pattern may be expressed as a linear combination of harmonically related complex exponentials of the form

$$I(x) = \sum_{k=-\infty}^{k=+\infty} a_k e^{jk\omega_0 x} \tag{4.22}$$

To calculate the Fourier coefficients a_k, Equation 4.22 is multiplied by $e^{jk\omega_0 x}$ and integrated over one period. The result yields solutions for the coefficients,

$$a_k = \frac{1}{T_0}\int_{T_0} I(x)e^{-jk\omega_0 x}dx \tag{4.23}$$

Note that the integration may be performed over *any* period of the function $I(x)$. For the particular case of a periodic triangle wave as described by Equation 4.21, by applying Equation 4.23 the coefficients a_k are,

$$a_k = -\frac{2I_0}{\omega_0^2 k^2 T_0^2}\left\{1 + e^{-jk\omega_0 T_0}\left(1 + 2jk\omega_0 T_0\right)2e^{\frac{-jk\omega_0 T_0}{2}}\left(jk\omega_0 T_0 - 1\right)\right\} \tag{4.24}$$

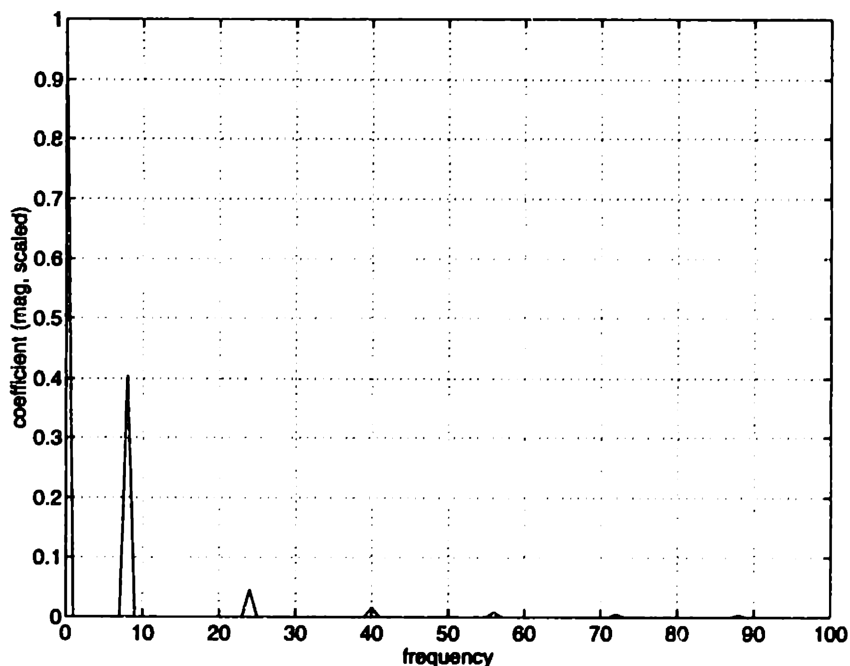

Figure 4-6: Magnitude of the first 5 Fourier coefficients of a triangle wave. Note that the even harmonics are zero.

By substitution of $\omega_0 = \frac{2\pi}{T_0}$, Equation 4.24 reduces to,

$$a_k = \frac{I_0}{2\pi^2 k^2} \left\{ 1 + e^{-jk2\pi} \left(1 + 4\pi jk\right) - 2e^{-jk\pi} \left(2\pi jk - 1\right) \right) \right\} \qquad (4.25)$$

The magnitude of the first five coefficients are shown in Figure 4-6 for a unity maximum intensity, I_0, and spatial period T_0. A moiré interferogram is shown in Figure 4-7, of two crossed equally spaced binary gratings. The intensity pattern $I(x)$, projected onto the y, represents the average of the image raster lines, as shown in Figure 4-

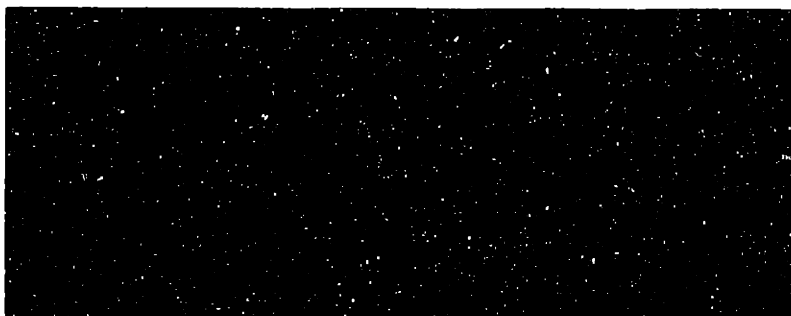

Figure 4-7: Moiré interferogram of two crossed binary gratings.

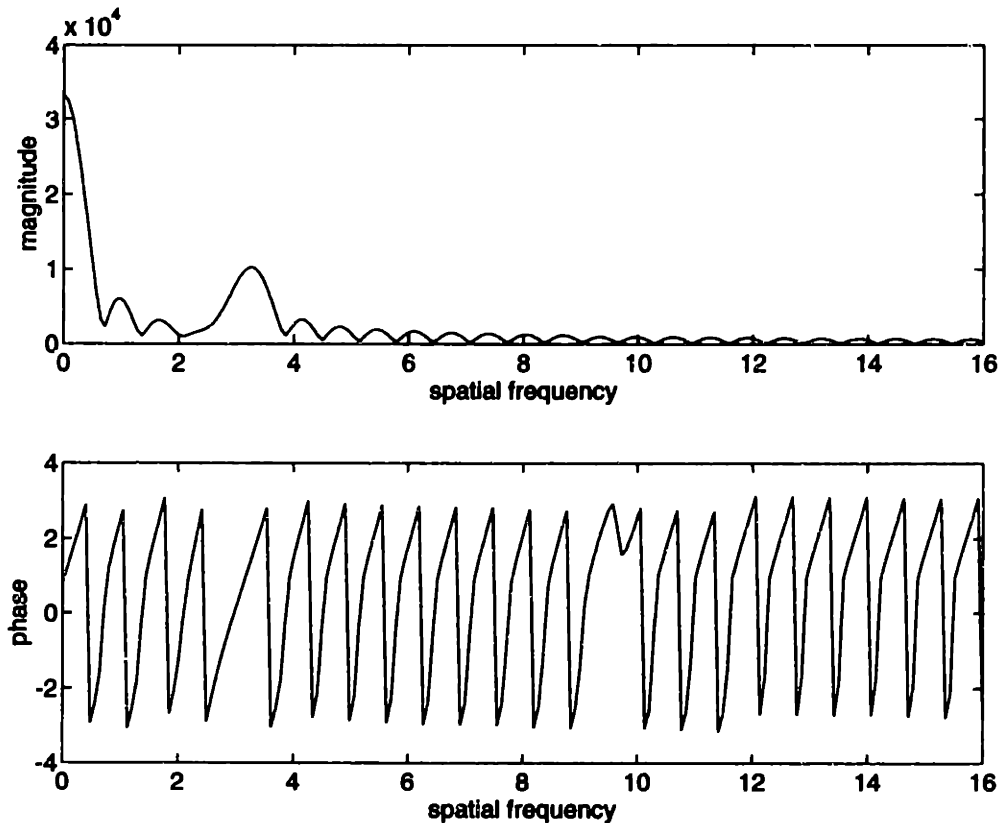

Figure 4-8: Spectral content of a triangular intensity pattern.

9(b). The magnitude and phase of the discrete Fourier transform of this signal is shown in Figure 4-8, for a triangle wave with spatial sampling of $64 samples/2\pi$ and a field spatial frequency of 8π. The resulting 512 point DFT provides 128 points below the Nyquist frequency, each point representing the Fourier coefficient at the corresponding frequency [21]. As expected, the even harmonics are zero. Use of Fourier methods in resolving interferogram phase has been presented in [1], [27], and [17]. A moiré interferogram obtained from the system described in Section 4.1.2 is shown in Figure 4-9 along with the projected intensities from the upper and lower fringe patterns. Note that unlike the data obtained through simulation, the actual image contains additional frequency components due to variations in the illumination across the field and system noise. High frequency random noise is minimized by averaging the raster lines. The low frequency components remain; however, since a range of frequencies for the fundamental mode is known *a-priori*, distinguishing

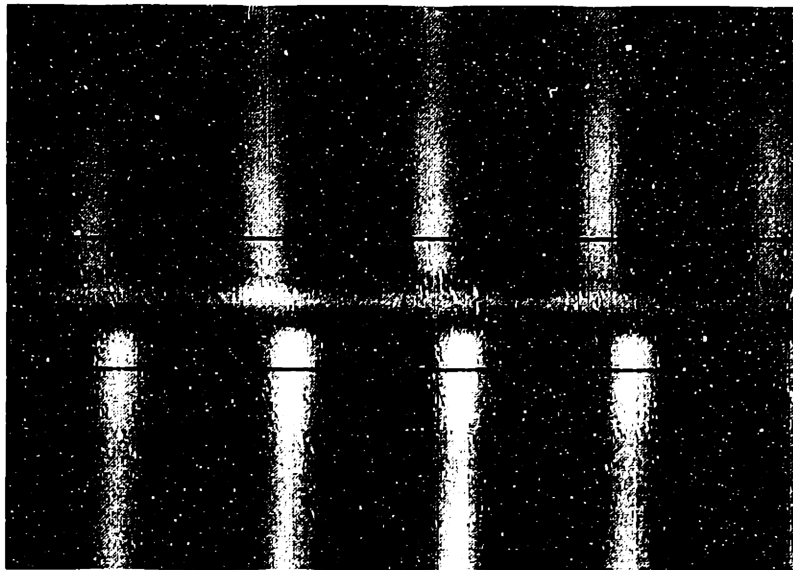

(a)

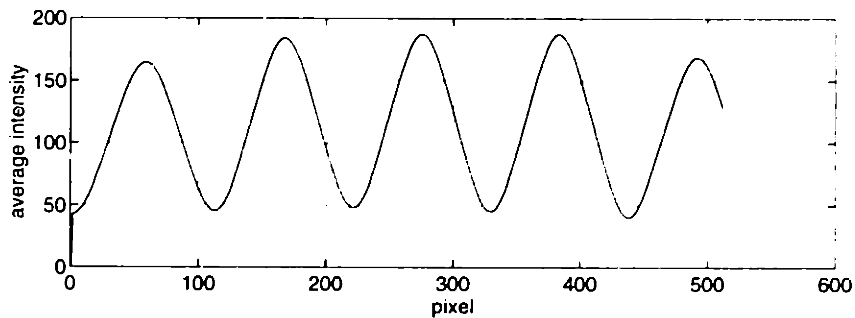

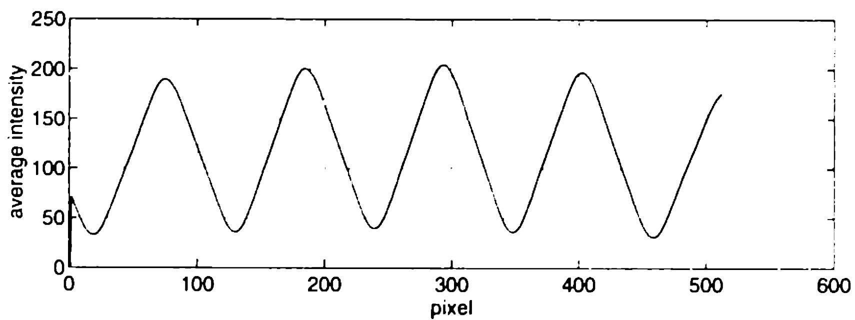

(b)

Figure 4-9: (a) Moiré interferogram from the film grating and the reference pattern. The phase difference between the two fields represents the displacement of the film relative to the reference. (b) The averaged rasters of each field are used for analysis.

the signal from any background contribution is readily accomplished. Movement of a grating will cause uniform phase shifting of all harmonics, therefore, it suffices to track the phase of the interferogram at the fundamental frequency.

For resolving fine motions of a grating, a low frequency fringe pattern is desired. Since the fundamental frequency and related harmonics will seldom be an increment of spatial sampling frequency, the fringe data must be zero padded. Zero padding in space domain corrupts the frequency data because of the convolution with $sinc\left(\frac{\omega T_0}{\pi}\right)$ in frequency space. Although this has the effect of smearing the non-windowed data, the maxima of the corrupted signal still correspond to the signal's harmonics. The fundamental mode may be found using a peak detection scheme and curve fit in the vicinity of the maximum for sub-pixel frequency resolution [8]. For simplicity, however, the fundamental mode was found by equating it to the maximum of the magnitude response within a predefined range of frequencies. The phase corresponding to this frequency can then be used to infer grating displacement. The spectral content of the patterns in Figure 4-9 are shown in Figure 4-10. Note the nearly identical magnitude response. The phase shift is determined by subtraction of the phase at the fundamental frequency. Also note the linear phase contribution from the window. The linear phase terms, unfortunately, make the Fourier method sensitive to slight frequency modulation, which will be discussed in Section 4.1.3. Phase modulated signals for various grating displacements are shown in Figure 4-11. Displacements are calculated using Equation 4.13.

Correlation

As previously stated, the Fourier approach to resolving phase can be sensitive to frequency modulation because of the linear phase contribution of the space domain windowing. Another method to resolve phase difference, which is closely related to convolution involves the correlation of the fringe patterns. Again, raster lines are averaged to acquire one dimensional signals of the upper and lower fields of view. The projected intensity signals from the interferograms in Figure 4-11 are shown in Figure 4-12. The discrete correlation of the upper and lower intensity signals, $I_1(x)$

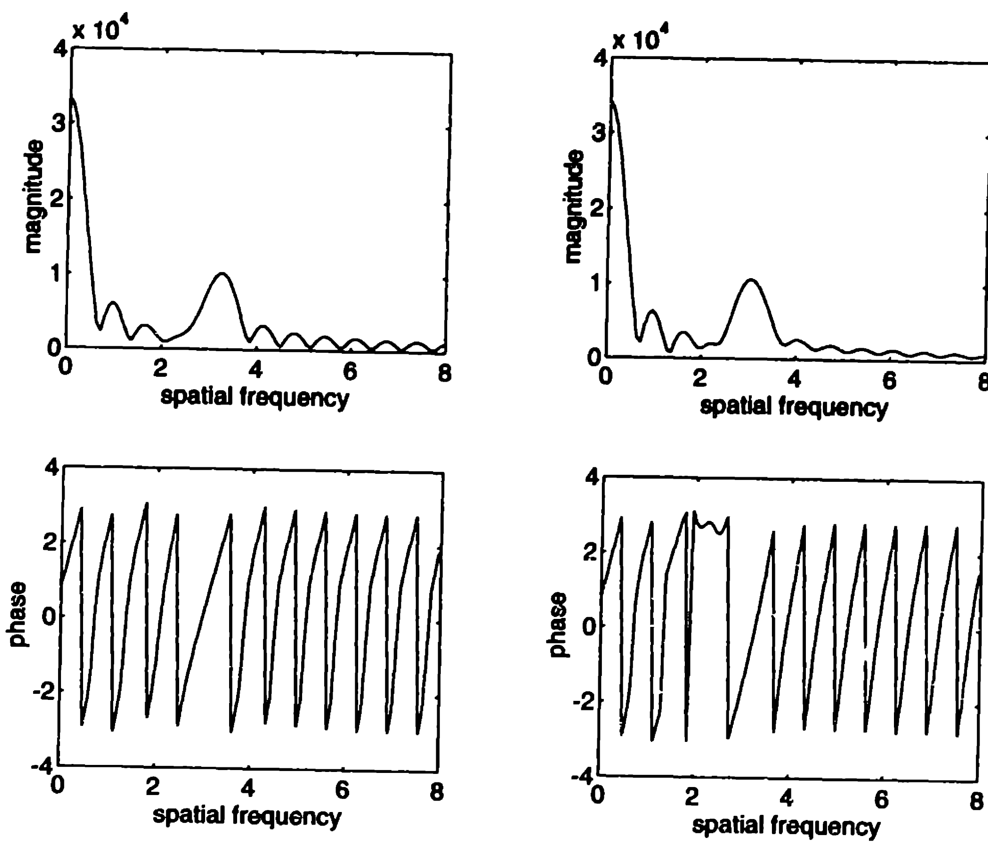

Figure 4-10: Spectral content of the averaged image. The magnitude response yields the fundamental mode of the fringe pattern, which will be used for determining the phase difference of the signals.

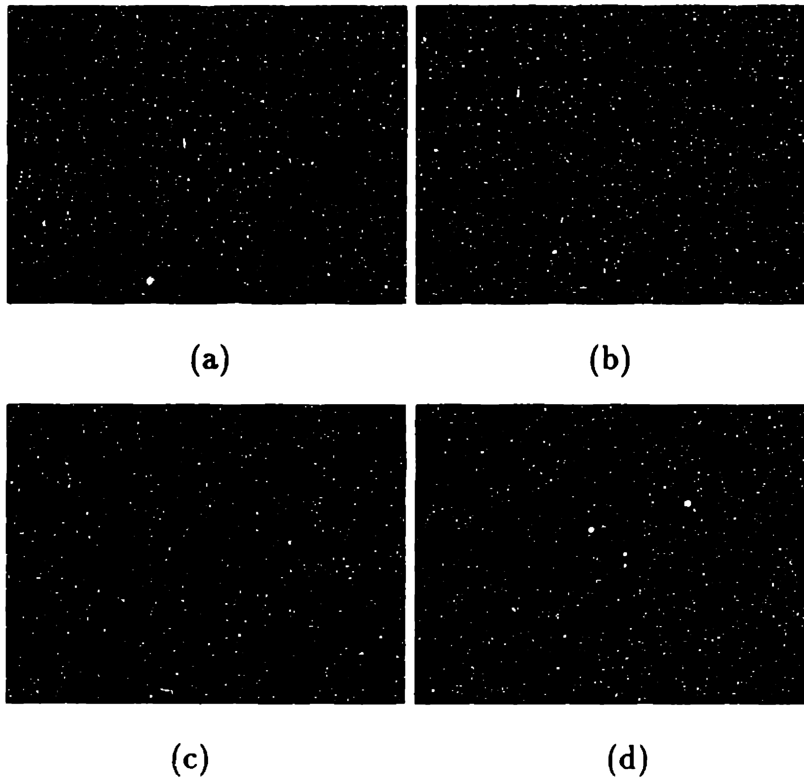

Figure 4-11: Four interferograms illustrating the phase shift for displaced gratings. (a) Displacement = $\pm 50.8\mu m$; (b) displacement = $5.1\mu m$; (c) displacement = $-2.3\mu m$; and, (d) displacement = $12.6\mu m$.

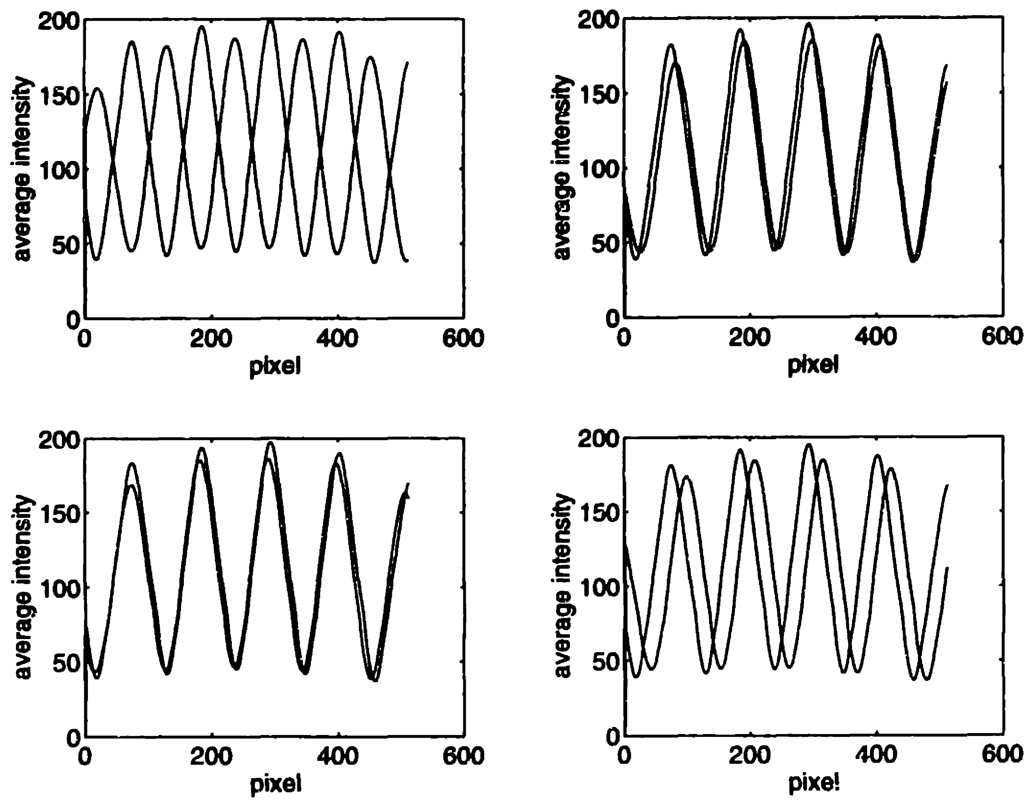

Figure 4-12: Intensity patterns corresponding to the interferograms in Figure 4-11.

and $I_2(x)$ respectively, is defined by,

$$Corr(I_1(x), I_2(x))_j \equiv \sum_{x=0}^{N-1} I_1(x+j)I_2(x) \tag{4.26}$$

for $I_1(x), I_2(x)$ periodic, with period N. As a convolution in spatial domain, the correlation can also be represented as a multiplication in the frequency domain,

$$Corr(I_1(x), I_2(x))_j \equiv I_1(\omega)I_2^*(\omega) \tag{4.27}$$

where it is assumed that $I_1(x), I_2(x)$ are real. The correlation compares the signals when directly superposed as well as phase shifted. The maximum of the correlation function represents the requisite phase shift for the signals to be "most overlapping". Correlation methods are used often in dynamic analysis because of their relative insensitivity to frequency modulation as compared to Fourier approaches. Figure 4-13 shows the correlation of the signals of Figure 4-12. To increase the phase resolution, the signals can be oversampled. For this study, the 512 point pattern, with an approximate fringe fundamental frequency of 5 fringes/field, gives a resolution of approximately $100 samples/T_0$, or a $1\mu m$ resolution for the 250 lp/in grating. Oversampling in this instance was not considered necessary, which had the further advantage of being computationally easy.

To investigate the sensitivity of the correlation and Fourier methods to frequency modulation, interferograms were obtained whereby the patterns were deliberately frequency shifted. Frequency modulation was accomplished by rotating the film relative to the grating. The range of rotation used for this experiment was based on the expected placement and alignment errors of the circuit board artwork. For a common film format of $18'' \times 24''$, the expected allowable error is $O(0.0015'')$, giving a rotational error $O(0.15mrad)$. The reference gratings, as described in Section 4.1.2, have a relative rotation of $5mrad$. Therefore possible artwork errors contribute 3% frequency modulation. For this experiment, the center of rotation was located 10" from the center of the grating. Therefore, the Abbe error would introduce a linear error of $0.0015''$,

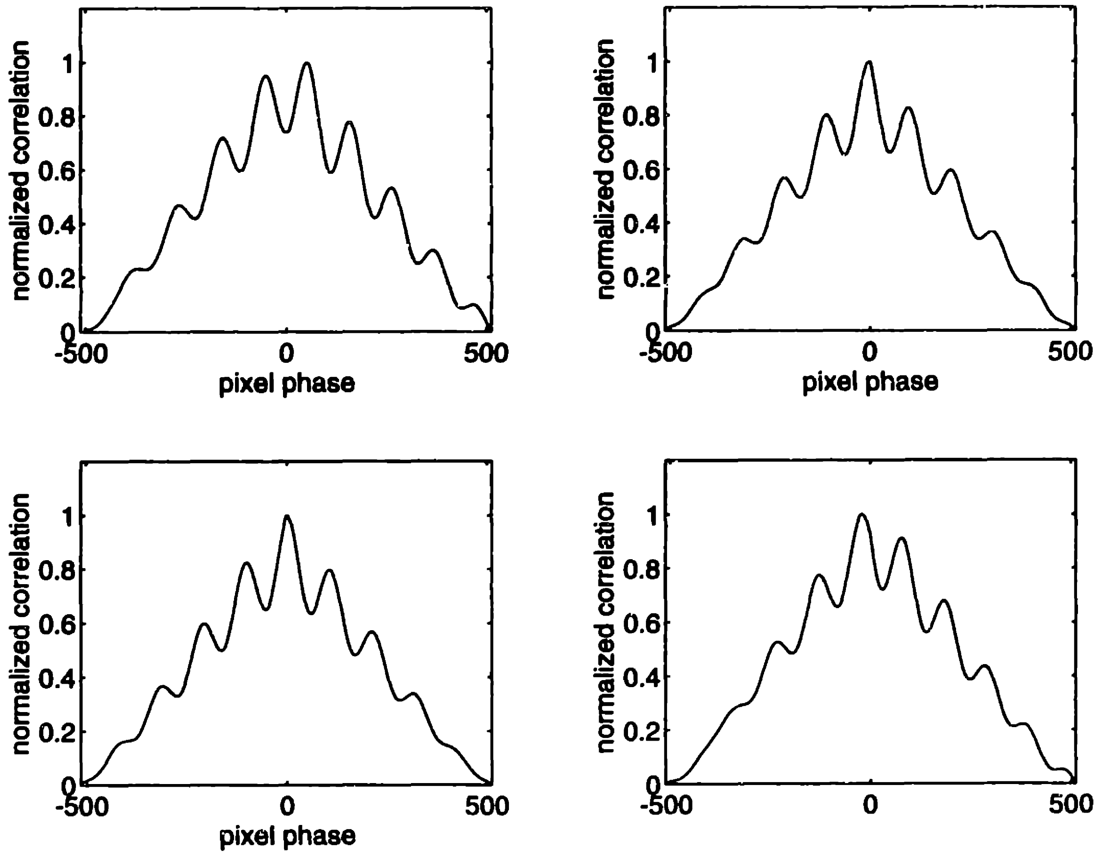

Figure 4-13: Four correlation signals for different intensity patterns. The displacement can be calculated from the location of the maximum of the correlation. (a) Displacement = $5\mu m$; (b) displacement = $0\mu m$; (c) displacement = -$7\mu m$; and, (d) displacement = $15\mu m$.

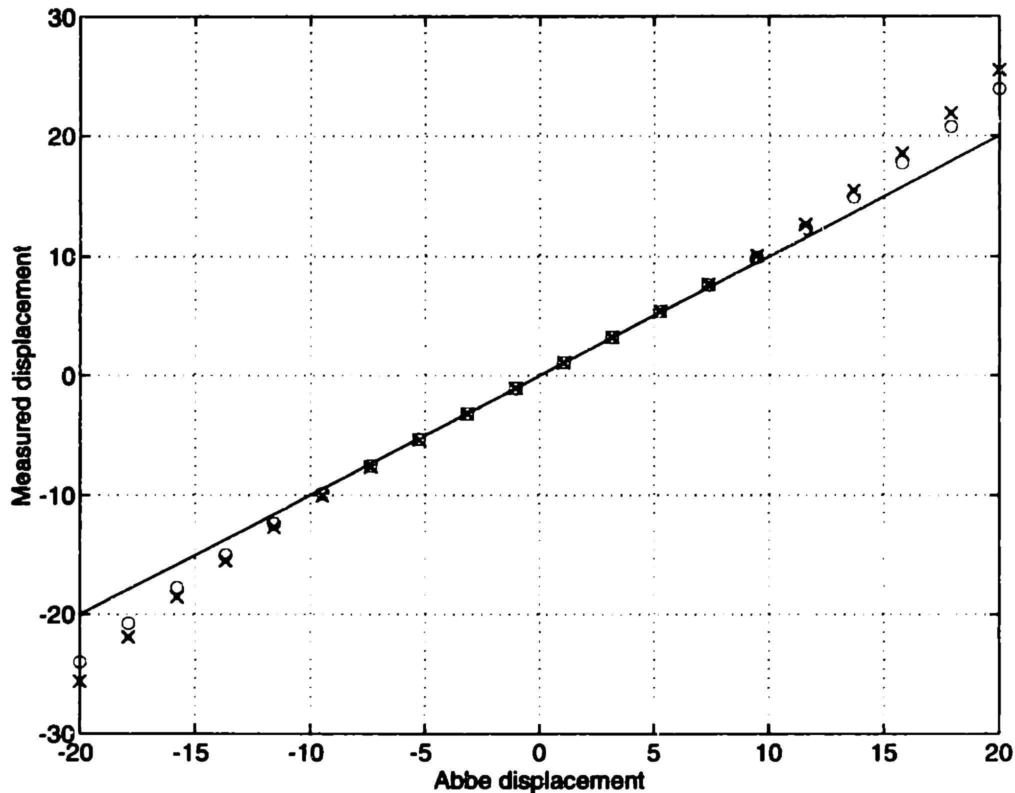

Figure 4-14: The reported displacement of the Fourier and correlation methods, compared to the Abbe displacement caused by rotation about a remote point indicates the relative sensitivity of the algorithms to frequency modulation. (0-correlation, x-Fourier, - - ideal

resulting in a $\frac{3}{4}\pi$ phase shift, and a $0.12 fringe/field$ frequency change.

The Abbe motion of the grating as a function of the reported displacement is shown in Figure 4-14. The reported displacements are those calculated by the indicated methods. For reasons noted previously, the images were not oversampled for increasing correlation resolution.

Heterodyne Method

Up to this point, concern was directed toward the sensitivities of various phase resolving algorithms to frequency modulated interferograms. Rather than dismiss the frequency content, a heterodyne approach exploits the added information to determine the displacement and rotation of the circuit-board artwork.

Consider again, the projected intensity patterns from the two fringe patterns. These signals, $I_1(x)$ and $I_2(x)$ may be written as periodic sinusoids,

$$I_1(x) = I_1' + I_1'' \sin(k_1 x + \phi_1) \tag{4.28}$$

$$I_2(x) = I_2' + I_2'' \sin(k_2 x + \phi_2) \tag{4.29}$$

where k_1 and k_2 are $2\pi/T_0\omega_1$ and $2\pi/T_0\omega_2$, respectively. The summation of these two signals gives,

$$I(x) = I_1(x) + I_2(x) = (I_1' + I_2') \tag{4.30}$$

$$+2I_1'' + I_2'' \sin\left(\frac{k_1 + k_2}{2}x + \frac{\phi_1 + \phi_2}{2}\right) \cos\left(\frac{k_1 - k_2}{2}x + \frac{\phi_1 - \phi_2}{2}\right) \tag{4.31}$$

$$-I_1'' \sin(k_2 x + \phi_2) - I_2'' \sin(k_1 x + \phi_1) \tag{4.32}$$

For the special case where the $I_1'' = I_2''$, Equation 4.32 reduces to a form that contains only the DC and modulated signal. For the above general case, the modulated signal contains the ripple of the third and forth terms, although the phase is invariant. The low frequency beating of the second term of Equation 4.32 contains the useful information pertaining to rotation of the film. The fringes are in phase when the cos() term is a maximum. The maximum occurs when,

$$\cos\left(\frac{k_1 - k_2}{2}x + \frac{\phi_1 - \phi_2}{2}\right) = 1 \tag{4.33}$$

For this condition to be satisfied,

$$\frac{k_1 - k_2}{2}x + \frac{\phi_1 - \phi_2}{2} = N\pi, N = 0, \pm 1, \pm 2, \ldots \tag{4.34}$$

Solving for x to obtain the locations of the modulated maximum,

$$x = \frac{\pm 2\pi N + (\phi_1 - \phi_2)}{(k_1 - k_2)}, N = 0, \pm 1, \pm 2, \ldots \tag{4.35}$$

Rotation about locus of points defined by x, normal to the grating axis, will generate

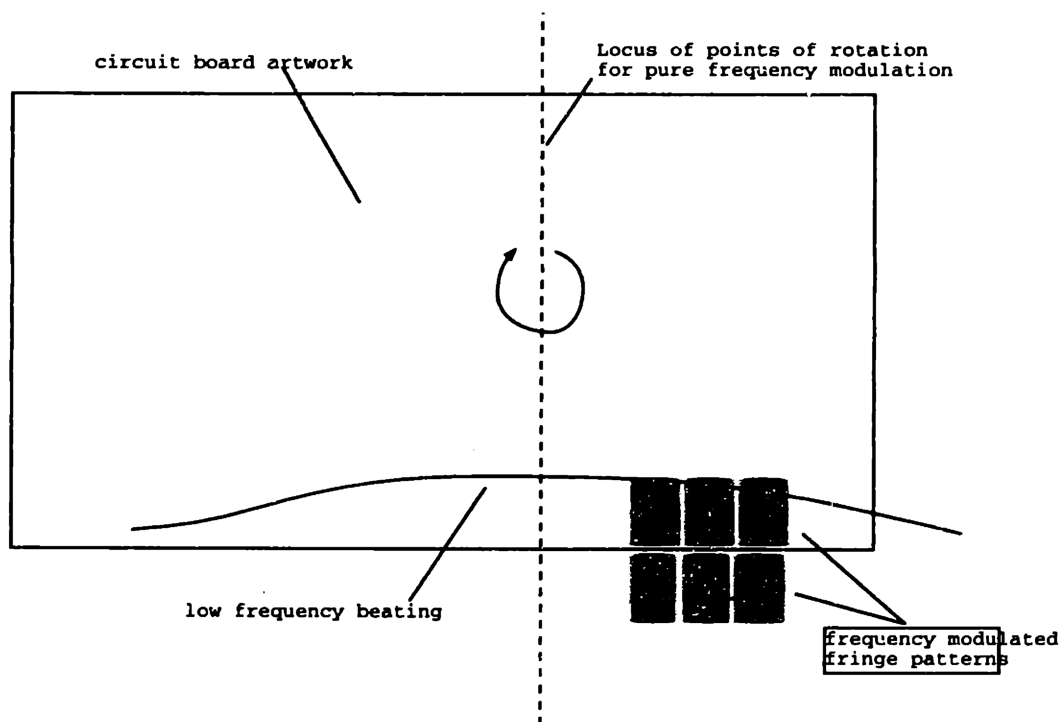

Figure 4-15: Rotation about the locus of points normal to the grating axis and at the low frequency maximum causes a pure frequency shift for the case where $N = 0$ For all other N, a phase shift of $2\pi N$ is introduced because of the Abbe displacement.

pure frequency modulation. For $N = \pm 1, \pm 2, \ldots$, the fringe pattern is frequency modulated *and* phase modulated by $2\pi N$. The phase modulation is a consequence of the Abbe displacement about the remote maximum. Figure 4-15 illustrates the effect of such a rotation.

The Fourier transform of the individual intensity components gives the frequency and phase of each, enabling direct calculation of the locus of rotation points by Equation4.35. The zeroth order maximum of the low frequency modulation from intensity patterns of the moiré fringes defines the rotation locus for frequency modulation of the film fringe pattern. The loci are relative to the field of the camera, making them sensitive to camera position, although implementation details could make the process robust to such variations.

Determining the locus of points about which frequency modulation occurs is a powerful result. Performing the same analysis on an additional interferogram not collinear with the original grating, forms another locus of points. The intersection

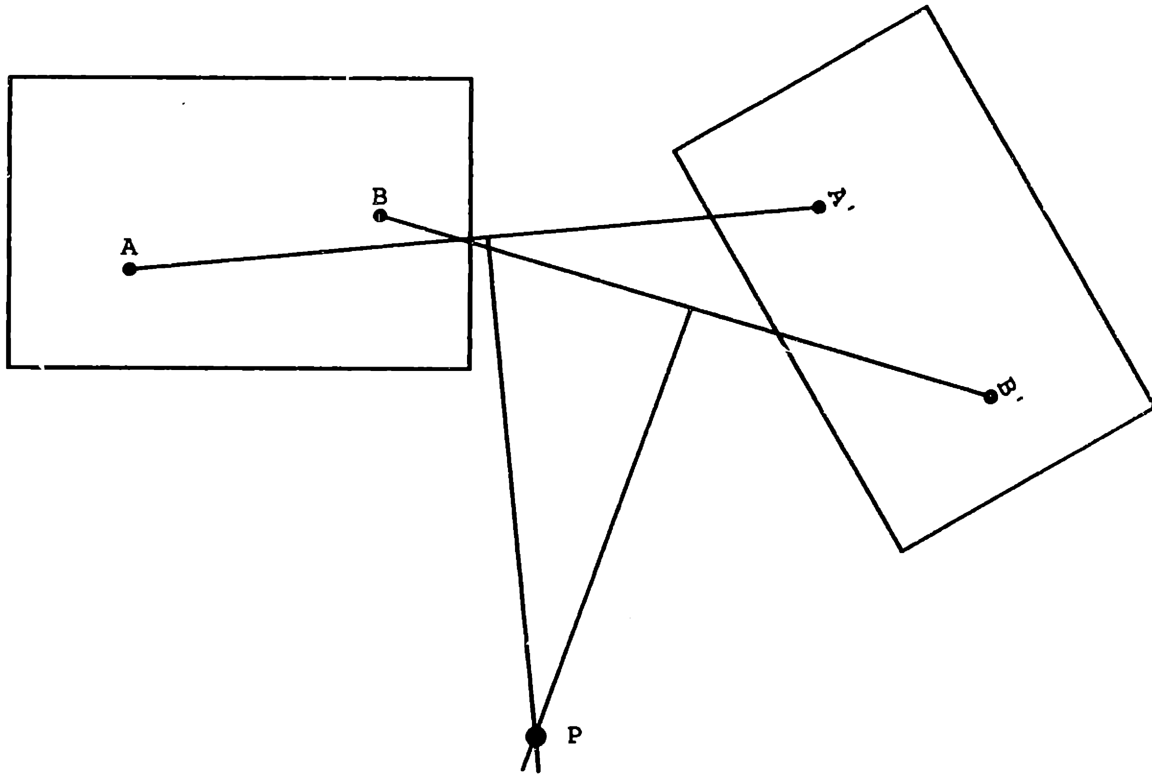

Figure 4-16: Any planar motion of a lamina can be represented by pure rotation.

of the loci formed by both fringe patterns *is* the center of rotation of the artwork, which aligns and orients the film. This is true because *any planar motion of a lamina is equivalent to a pure rotation* [23]. The proof follows by considering any two non-coincident points on a rigid body, A and B, as shown in Figure 4-16. The motion of A to A', can be accomplished by rotation about the perpendicular bisector drawn from A to A'. Similarly, the motion of B to B', can be accomplished by rotation about the perpendicular bisector drawn from B to B'. Simultaneous solution determines the pole of rotation for the body. An implementation of the method using two gratings is shown in Figure 4-17. The use of two fringe interferograms provides redundant information. The amount of rotation about the center of rotation is given by both gratings. The reference fringe patterns must be identical, which is readily accomplished by bonding gratings prior to cutting. This ensures that the rotational information is the same from both gratings. The rotation necessary to register the film is given by,

$$\Delta\theta_2 = \frac{\omega_2 - \omega_1}{\omega_1}\theta_1 \tag{4.36}$$

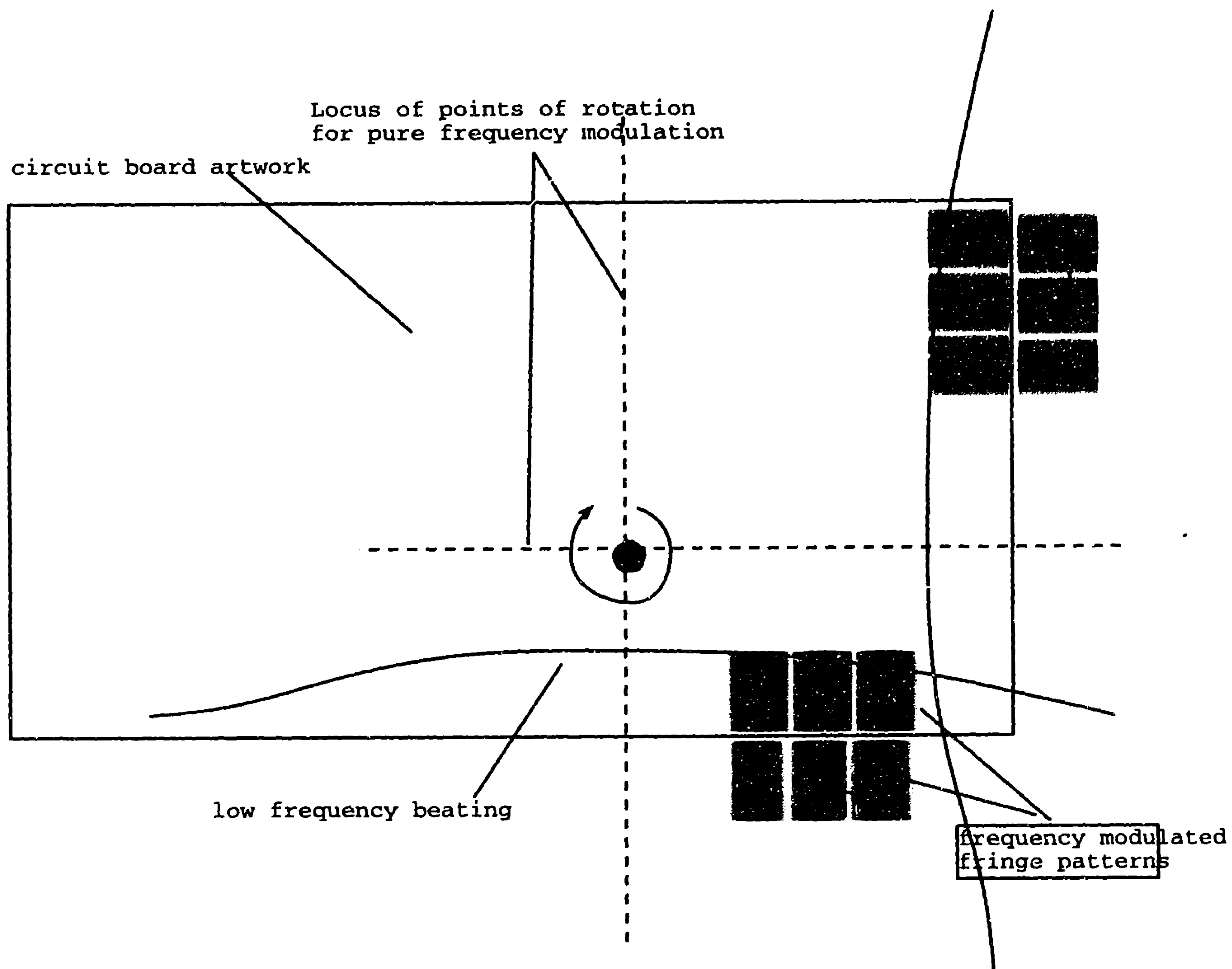

Figure 4-17: The intersection of two loci of rotation points for frequency modulation of the heterodyned moiré patterns is the center of rotation for the film. Rotation of the film about this point will register the artwork with respect to the reference grating positions.

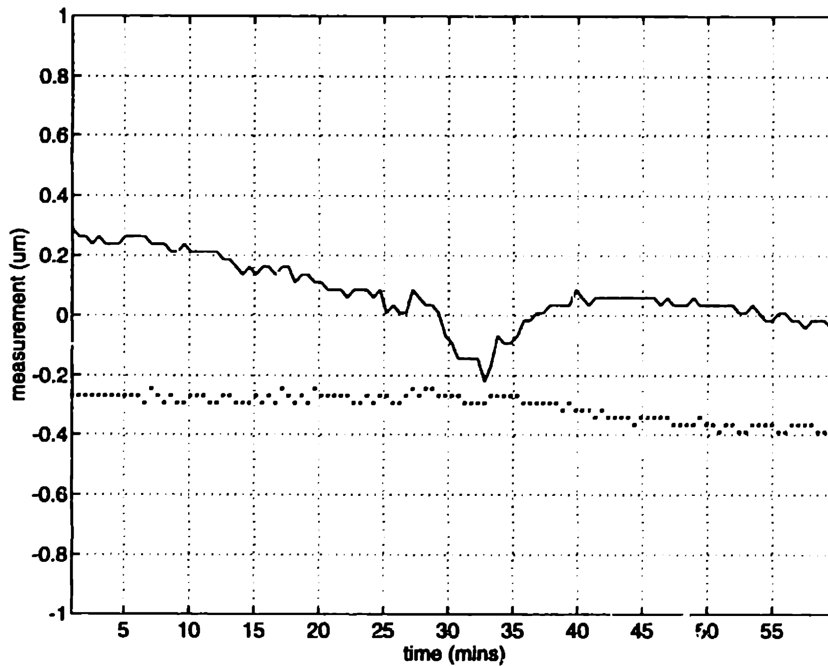

Figure 4-18: Time series data from the capacitance probe and optical measurement illustrates the repeatability of the moiré technique (solid-moiré, dashed- capacitance probe).

where $\Delta\theta_2$ is the required film rotation, θ_1 is the fixed angle of the reference grating, and ω_i are the spatial frequencies of the reference moiré pattern (1) and the film moiré pattern(2).

4.1.4 Testing

The repeatability of the moiré method was tested by comparing a capacitance probe measurement to the calculated value from the moiré image. For this test, the Fourier method of Section 4.1.3 was used. This method was chosen, since the reference and film fringe patterns were not frequency modulated. Strict displacement was measured, making the Fourier approach appropriate. Tests were conducted over approximately a one hour duration in 30 second intervals. Time series data for this experiment is shown in Figure 4-18. Histograms for the data are shown in Figure 4-19.

Note the stability of the measurement. The reading repeatability is reportable to a $\sigma = 0.08\mu m$.

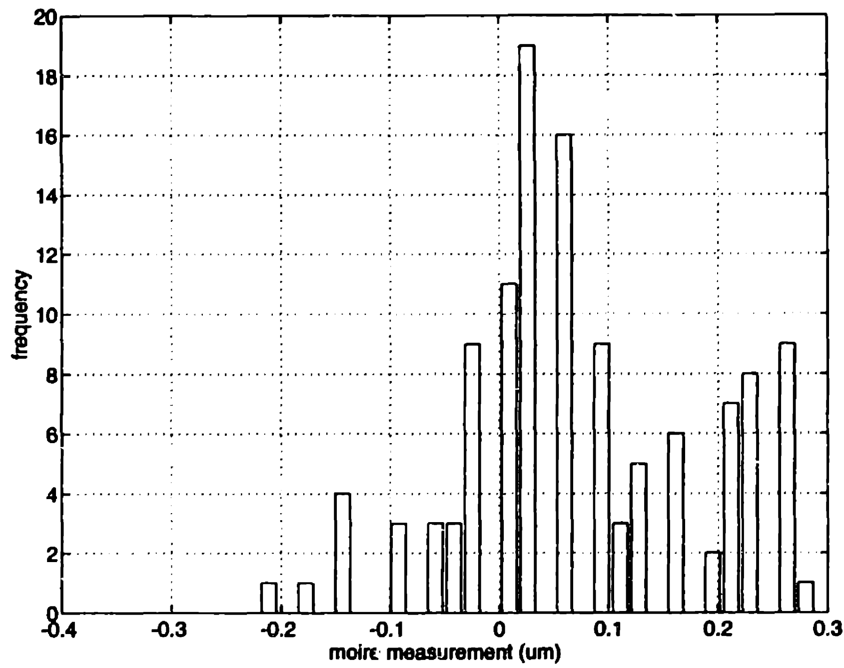

Figure 4-19: Histogram of the moiré time series data from Figure 4-18. $\sigma_{moire} = 0.08\mu m$

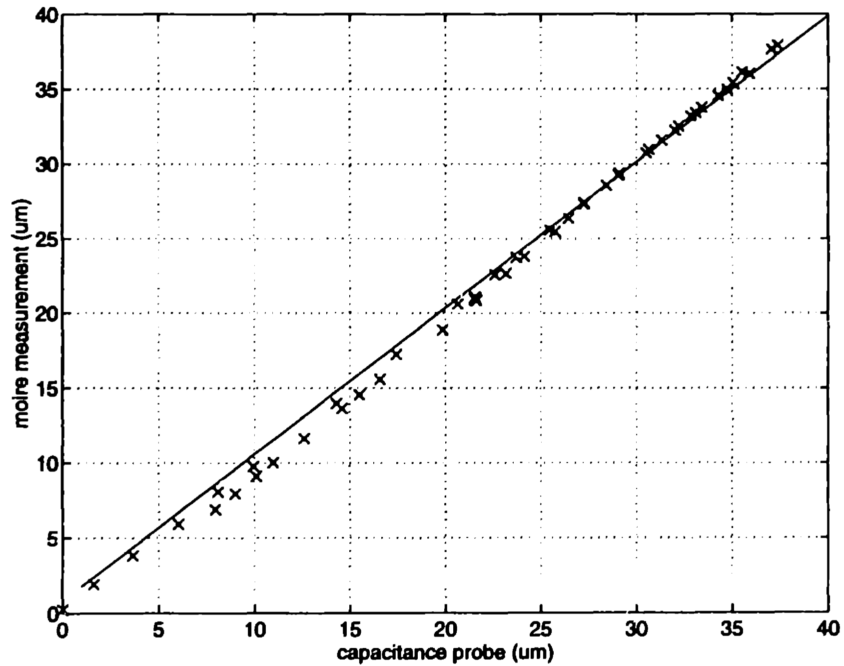

Figure 4-20: Comparison of the capacitance probe reading and the moiré method. Trial day 1.

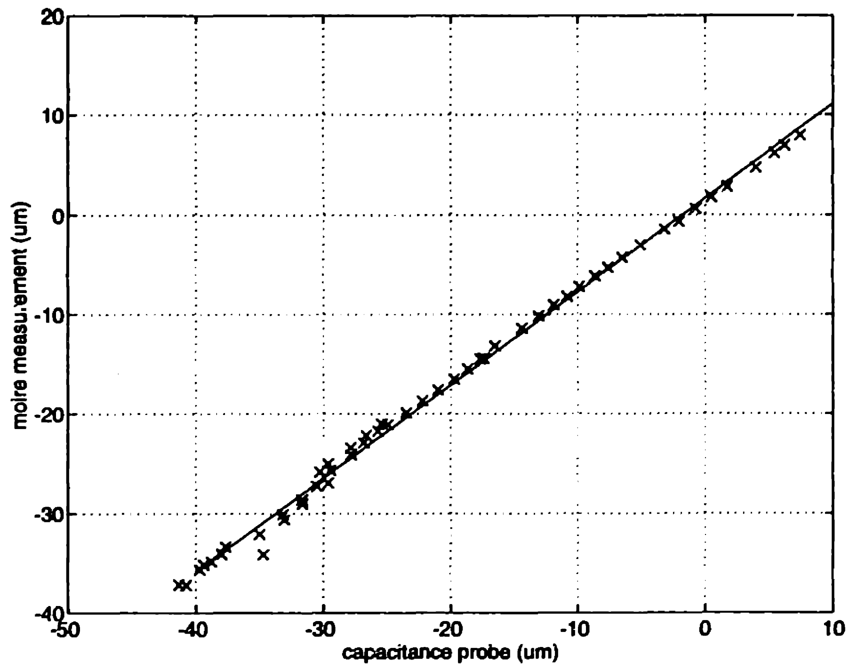

Figure 4-21: Comparison of the capacitance probe reading and the moiré method. Trial day 2.

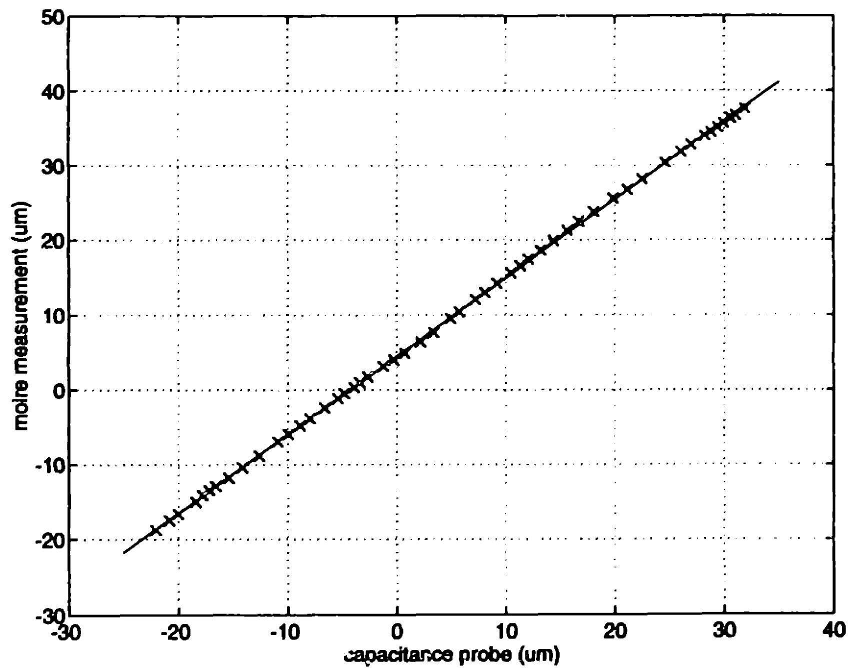

Figure 4-22: Comparison of the capacitance probe reading and the moiré method. Trial day 3.

The accuracy of the method was determined by moving the stage, recording the corresponding capacitance readings and the fringe phases at each position. Data was acquired while moving the stage into and away from the fixed film. This experiment was conducted over the course of three days, two trials per day. The data is shown in Figure 4-20 through Figure 4-22. In all cases capacitance probe readings agree with fringe data. The average slope of the data is 0.956 $\mu m/\mu m$. The intercept is meaningless, since it only indicates that the signals require nulling. Based on linear curve fits to the data, accuracy may be reported to $\sigma = 0.2\mu m$. For this particular instance, whereby the line deviation is $\sigma_{line} = 7.5\mu m$, for 100 lines, $\sigma_{\bar{x}_{line}}$, is 0.75 μm, markedly improved from the standard two fiducial technique. The total deviation of the measurement is $\pm 0.78\mu m$. It was concluded from this gauge capability study that the moiré fringe technique provides a repeatable measure, with sufficient resolution for circuit board film alignment and position and rotation measurement.

4.1.5 Proposed Implementation

Alignment to Punches

Because space on the film is valuable, extraneous use of the perimeter area is undesirable. A fiducial alignment approach does boast a large dynamic range and required small film area. Typical dot pattern diameters are 0.030". However, since positional accuracy and repeatability are desired, and the current specifications are approaching the fiducial method's capability, film area for the moiré pattern should be allocated. For testing, a 2" long swath 0.5" wide was used. This size permitted 125 lines of 0.002" pitch.

Additional gratings must be used to measure all three degrees of freedom. Furthermore, since the measurement must be made at the film perimeter, any thermal expansion of the film will cause a bias in measuring, if the measured along a single edge. Therefore it is suggested that in order to have a thermo-centric alignment and measuring system, gratings should be placed on opposing edges of the film for alignment of the film to the tooling punch, as illustrated in Figure 4-23. By orienting

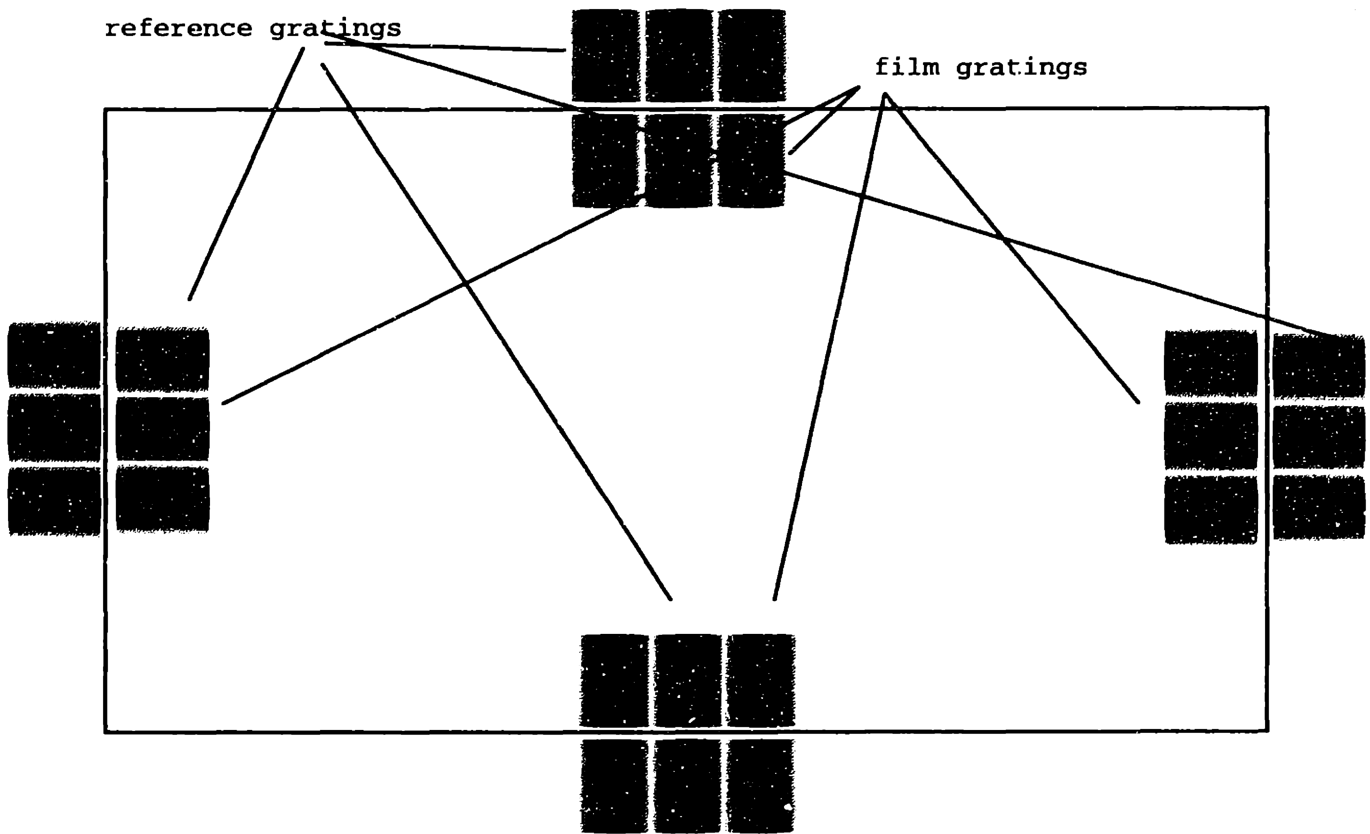

Figure 4-23: Gratings placed along the perimeter of the film can be used to center the artwork with respect to reference fringes for a thermocentric design.

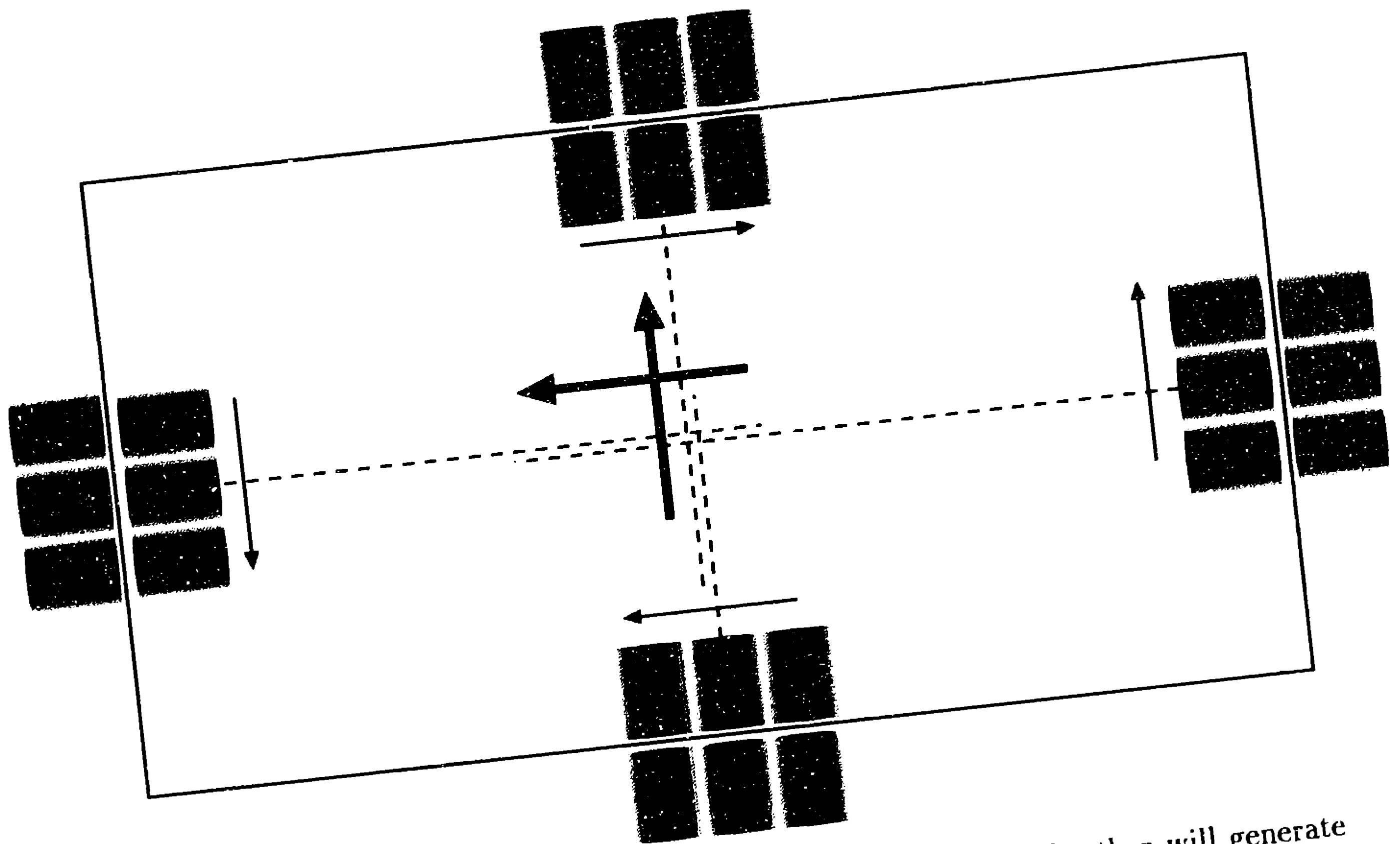

Figure 4-24: Gratings placed at opposite angles relative to each other will generate opposing fringe motion as the film is moved. By aligning the fringes on opposite sides of the film, the artwork is centered. Note that centering is achievable in the presence of thermal errors or artwork scaling.

opposing reference gratings at opposite angles, film displacement will cause opposing motions of the fringes, as depicted in Figure 4-24. The film is centered when the fringe patterns from the opposing edges are aligned. Note that in this implementation, the alignment is invariant to artwork scaling, facilitating its use in certain production environments, where border artwork is scaled with the circuit image. Rotational alignment can simply be obtained by matching the fringe frequency to a predetermined value. Since this scheme does not use reference gratings, it is sensitive to camera position. Although repeatability, rather than accuracy, is the critical constraint, long term camera movement is acceptable, provided that artwork is punched in sets. Alternatively, reference gratings may be used, in which case the relative measure renders camera placement inconsequential. As in the previous case, this technique is insensitive to film scaling.

Registration Measurement

One approach for measuring the registration of two pieces of film relative to each other, would be to analyze the resulting fringe pattern when the respective film gratings are brought into contact. Ideally, film gratings would overlap with no relative rotation. At infinite fringe mode, only one fringe over the entire field would be noticeable. The transmission through the overlapping gratings would be a direct measure of the relative displacement. A more robust technique employs a reference grating whereby the film gratings are offset from each other such that each film generates its own unique interferogram. Note that if the gratings are to be offset, the alignment of the film prior to punching must accommodate different grating positions depending on layer number. By using any permutation of the moiré technique for film alignment and registration measurement, positions and orientations may be resolved to approximately $\pm 0.8\mu m$, unlike the current fiducial method which is fundamentally limited to $\pm 7.8\mu m$.

4.2 Diffraction Method

Another optical alignment scheme, which has the advantage of averaging plotter error, again uses binary gratings printed onto the film. In this instance, however, the gratings are used to generate diffraction patterns rather than moiré fringe interferograms. Artwork alignment is achieved by tracking the relative intensities of the diffraction orders. This method has a number of compelling reasons for its use. Namely, the required size of the grating is considerably smaller than that of the moiré grating, and the method is not as computationally demanding as the fringe methods. The following sections describe the theory of operation, the results of simple experiments, and suggested implementation for circuit board alignment.

4.2.1 Theoretical Background

Derivations of near an far field diffraction are found in numerous texts, most notably [12], [9], and [14]. For completion, Fresnel and Fraunhofer approximations are

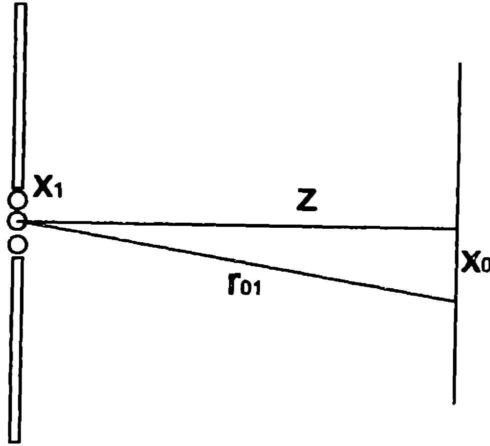

Figure 4-25: The observation field $\mathbf{U}(x_0, y_0)$ can be described by the superposition of point sources emanating from the pictured aperture.

reviewed.

The Huygens-Fresnel principal states that a field at an observation point $\mathbf{U}(x_0, y_0)$ may be expressed as the superposition of a collection of point sources emanating from point (x_1, y_1). Mathematically this is,

$$\mathbf{U}(x_0, y_0) = \int\int \mathbf{h}(x_0, y_0; x_1, y_1)\mathbf{U}(x_1, y_1)dx_1dy_1 \tag{4.37}$$

where $\mathbf{h}(x_0, y_0; x_1, y1)$ is the impulse response function of spherical waves from point $(x_1, y1)$ evaluated at point (x_0, y_0), given by,

$$\mathbf{h}(x_0, y_0; x_1, y_1) = \frac{1}{j\lambda}\frac{e^{jkr_{01}}}{r_{01}}\cos(\mathbf{n}, \mathbf{r}_{01}) \tag{4.38}$$

From Figure 4-25, the distance r_{01} may be approximated by a binomial expansion as,

$$r_{01} \approx z\left[1 + \frac{1}{2}\left(\frac{x_0 - x_1}{z}\right)^2 + \frac{1}{2}\left(\frac{y_0 - y_1}{z}\right)^2\right] \tag{4.39}$$

neglecting higher order terms in the expansion. For large distances z, the approximation $\cos(\mathbf{n}, \mathbf{r}_{01}) \approx 0$ may be used. Substitution of these approximations into Equation 4.37, and expanding quadratic terms gives the Fresnel diffraction approximation,

$$\mathbf{U}(x_0, y_0) =$$

$$\frac{e^{jkz}e^{jk(x_0^2+y_0^2)/2z}}{j\lambda z}\int\int_{-\infty}^{\infty}\mathbf{U}(x_1,y_1)e^{jk(x_1^2+y_1^2)/2z}e^{-j2\pi(x_0x_1+y_0y_1)/\lambda z}dx_1dy_1 \qquad (4.40)$$

Fraunhofer diffraction places the further requirement that,

$$z \gg \frac{k(x_1^2+y_1^2)}{2} \qquad (4.41)$$

When this condition is satisfied, the quadratic phase term of Equation 4.40 is small, hence $e^{jk(x_1^2+y_1^2)/2z} \approx 1$, and the field distribution at the observation point is given by the Fourier transform of the aperture. The observed field becomes,

$$\mathbf{U}(x_0,y_0) = \frac{e^{jkz}e^{jk(x_0^2+y_0^2)/2z}}{j\lambda z}\int\int_{-\infty}^{\infty}\mathbf{U}(x_1,y_1)e^{-j2\pi(x_0x_1+y_0y_1)/\lambda z}dx_1dy_1 \qquad (4.42)$$

The Fourier transform is evaluated at spatial frequencies, $f_x = x_0/\lambda z$ and $f_y = y_0/\lambda z$.

It can be shown by either vector summation [12] or by the above Fourier description, that the binary grating used for the moiré analysis of previous sections, as depicted in Figure 4-25, will generate an intensity pattern in the far field,

$$I \sim \frac{\sin^2\beta}{\beta^2}\frac{\sin^2 N\gamma}{\gamma} \qquad (4.43)$$

where $\beta = (\pi/\lambda)b\sin\theta$, $\gamma = (\pi/\lambda)d\sin\theta$, b is the slit width, d is the slit pitch, θ is the angle from the optical axis, and λ is the wavelength of light.

The spatial signal of the grating can be generated by convolving a single square slit with an impulse train of delay T. The resulting signal is then rectangularly windowed to obtain N number of openings. In the frequency domain, this procedure is identical to multiplying a *sinc*() function (corresponding to the single slit) with an impulse train of frequency $2\pi/T$. This is a sampling procedure, whereby the sample interval is determined by the grating pitch. Finally, the sampled *sinc*() function is convolved with a (narrow) *sinc*() function corresponding to the wide window of containing N slits [20]. Using this argument, it becomes clear that the diffraction order width is a function of the number of slits N, that the modulation of the orders is governed by the slit width b, and that the frequency of the orders is a function of the grating pitch d.

Theoretical diffraction patterns for various grating widths, pitches, and number of slits are shown in Figure 4-26. Note that the horizontal axis has been nondimensionalized.

4.2.2 System Considerations

Since the modulation of the narrow *sinc*() train is a function of grating slit width, circuit board artwork registration may be determined by measuring the intensity ratio of various diffractive orders. As in the moiré technique, a film grating is placed over a reference grating. Coherent light passing through the grating will generate a diffraction pattern, the modulation of which is a function of the relative displacement of the film and reference. The sensitivity and dynamic range of this technique is a function of the nominal modulation, selection of diffractive orders, and grating geometry.

From Equation 4.43, the maxima and minima of the modulation envelope and diffrative orders can be determined. The location of such points are important design considerations. For instance, to achieve the largest measurement range, the modulation of a diffractive order should vary between unity and zero. Unity response is achieved when the slit is infinitesimally small, approaching a Dirac delta function. The frequency response of this slit would be a DC signal. Therefore, as the film grating phase approaches *pi*, the resulting diffraction pattern is unmodulated, as illustrated in Figure 4-27.

Similarly, zero intensity of a particular diffractive order is achieved when the zero of the $\frac{\sin^2\beta}{\beta^2}$ modulation is located precisely at the diffractive order's maximum, as illustrated in Figure 4-28. Missing orders are generated by the relation,

$$\frac{d}{b} = \frac{m}{p} \tag{4.44}$$

where d and b are the grating pitch and slit width, respectively, and m and p are the diffraction order and modulation minimum. For this investigation, p is always 1, hence the grating pitch must be a multiple of the diffractive order. Nominal position of the film grating is $\pi/2$ out of phase with the reference, as illustrated in Figure 4-29.

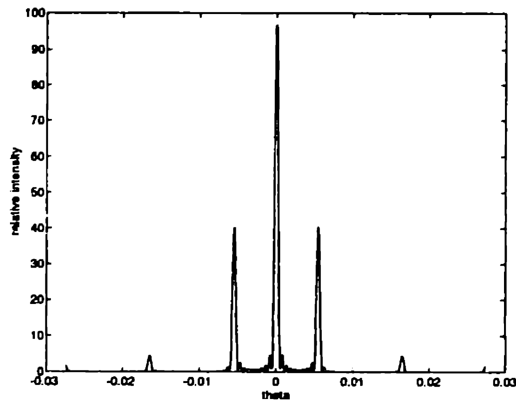

(a)

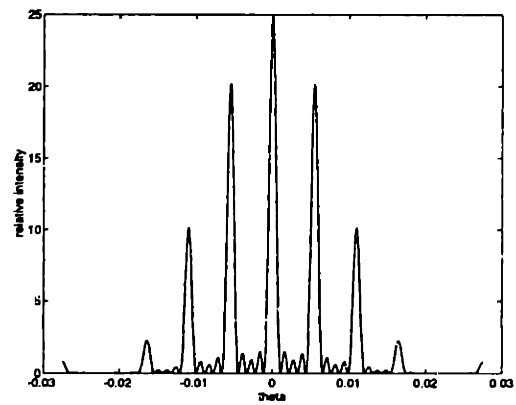

(d)

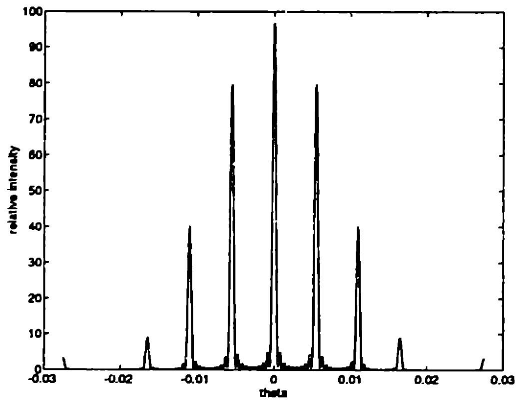

(b)

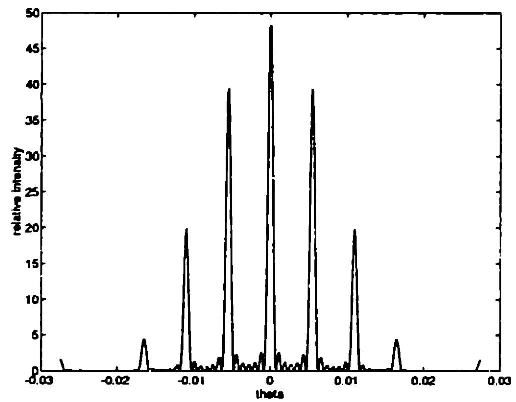

(e)

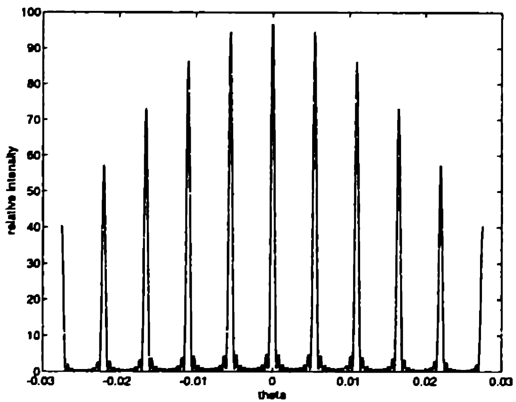

(c)

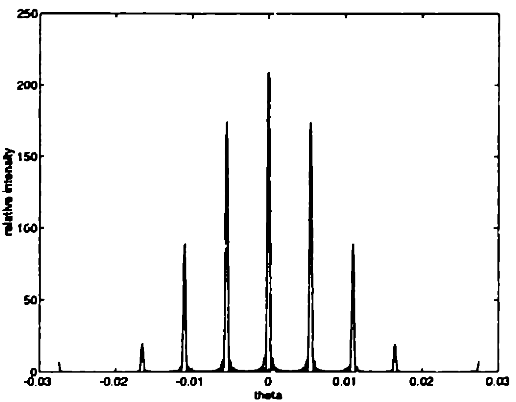

(f)

Figure 4-26: Diffraction patterns of linear binary gratings for various design parameters. (a)$d/b = 2$, (b)$d/b = 4$, (c)$d/b = 10$, (d)$N = 5$, (e)$N = 7$, (f) N=15.

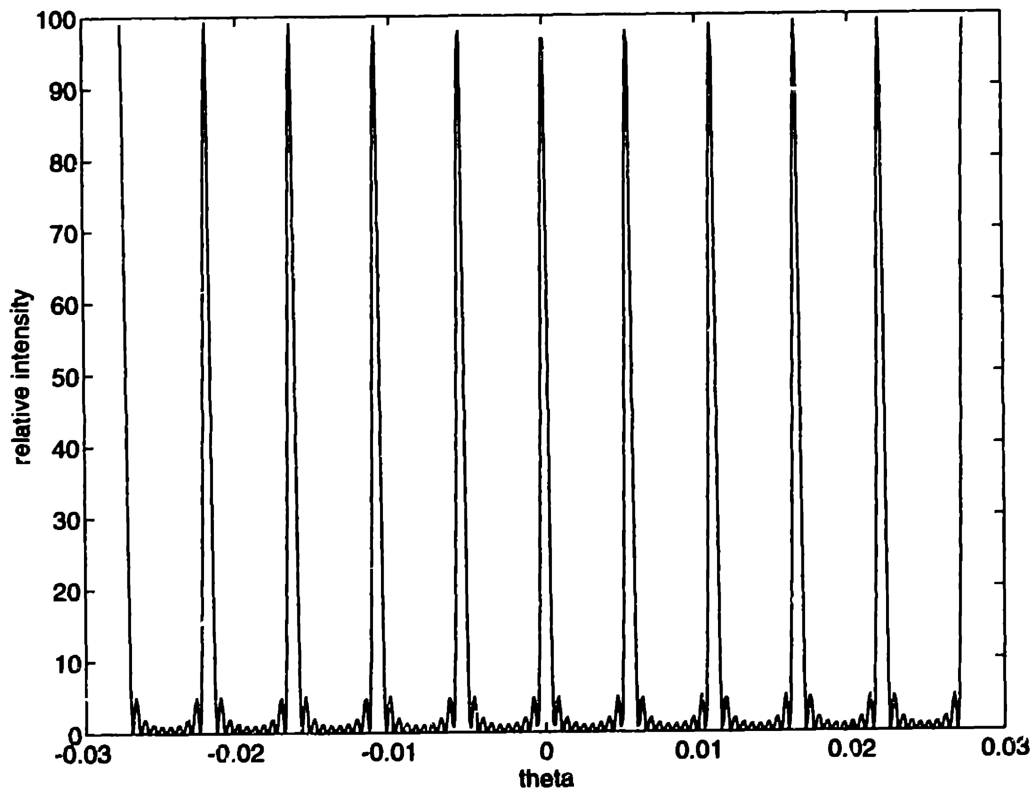

Figure 4-27: As the grating slits become infinitesimally small, approaching a Dirac delta function, the modulation approaches unity, hence the ratio of successive diffraction orders is also unity.

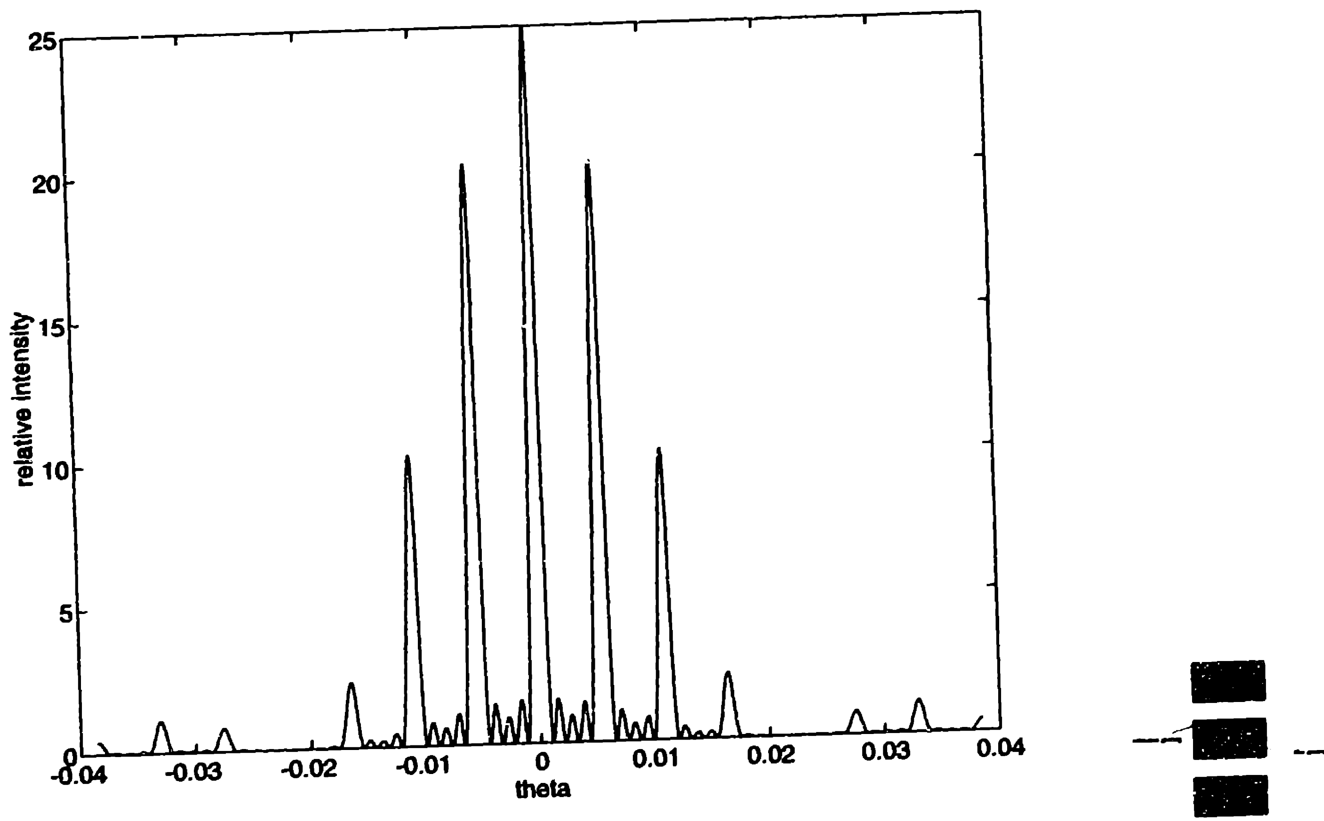

Figure 4-28: When the reference grating is unobstructed, judicious selection of pitch and slit width causes certain diffraction orders to be zero.

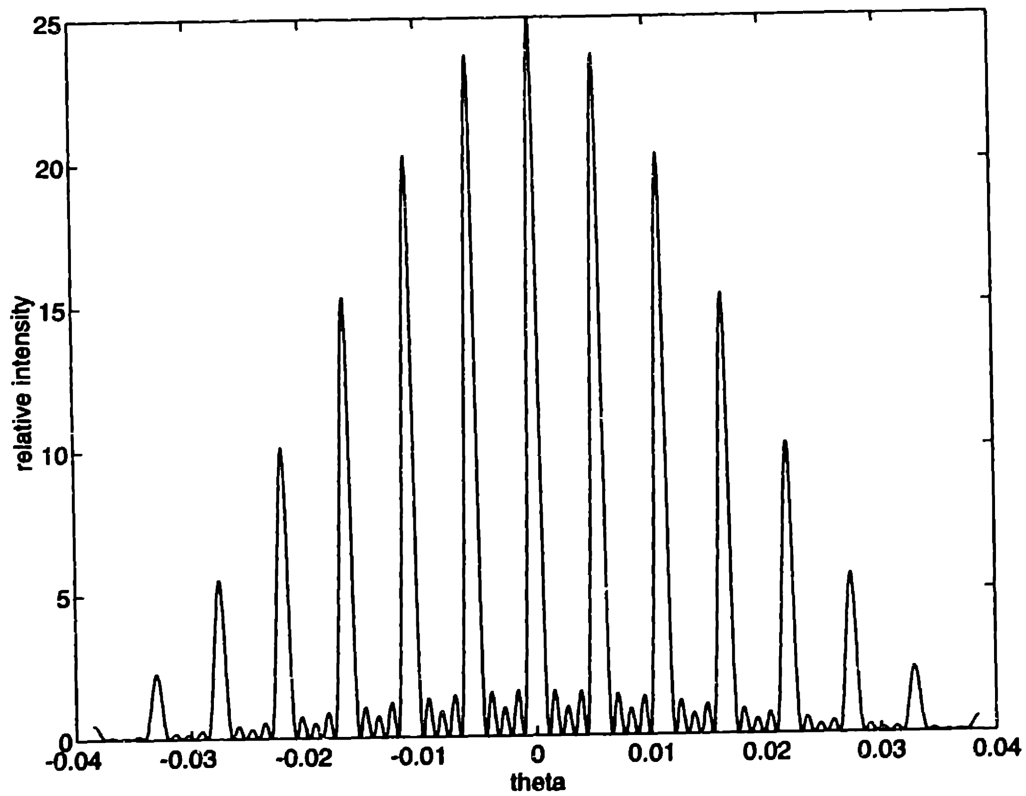

Figure 4-29: Nominal center grating position places the measured diffractive order near the 1/2 the center intensity.

Dynamic range is determined by the slit width, while the pitch is determined by selection of diffractive order to measure. This selection is not arbitrary. Instead it is based on a practical consideration related to maintaining directional information of the registration measurement.

Consider two overlapping gratings of pitch equal to twice the slit width. These grating have lines and spaces of equal value. To obtain a missing order within the first lobe of the modulation response, by Equation 4.44, the first diffractive order must be measured. Notice that if the gratings are completely out of phase, the direction for correcting registration error is indeterminate. Motion in either direction will create the desired diffraction pattern, although the film may be 2π radians times the grating pitch misregistered. This phenomenon is identical to the dynamic range issue of the moiré fringe patters discussed in previous sections. If, however, the film lines, l_{film} are wider than the reference spaces, s_{ref}, and the reference lines, l_{ref} are larger than the lines of the film grating, l_{film}, i.e.,

$$l_{ref} > l_{film} > s_{ref} \tag{4.45}$$

then the direction for registration correction is known, provided the initial registration error is within an amount δ from the mid-line of the reference grating, given by,

$$\delta < \frac{s_{ref}}{2} + l_r + s_r - l_{film} \tag{4.46}$$

These conditions are illustrated in Figure 4-30. Note that s_{ref} equals the requisite slit width b. Provided the δ condition is satisfied, then opacity demands the film be moved in the direction indicated in Figure 4-30. Similarly, a missing order indicates necessary motion in the opposite direction. The nominal position has the film grating edge vignette half the reference slits. Note that film and reference gratings have identical pitches.

Since a condition on d/b is imposed by the missing order criterion and b_{max} is determined from dynamic range requirements, d may be calculated using Equation 4.46. The maximum initial registration error must be evaluated based on knowledge of the

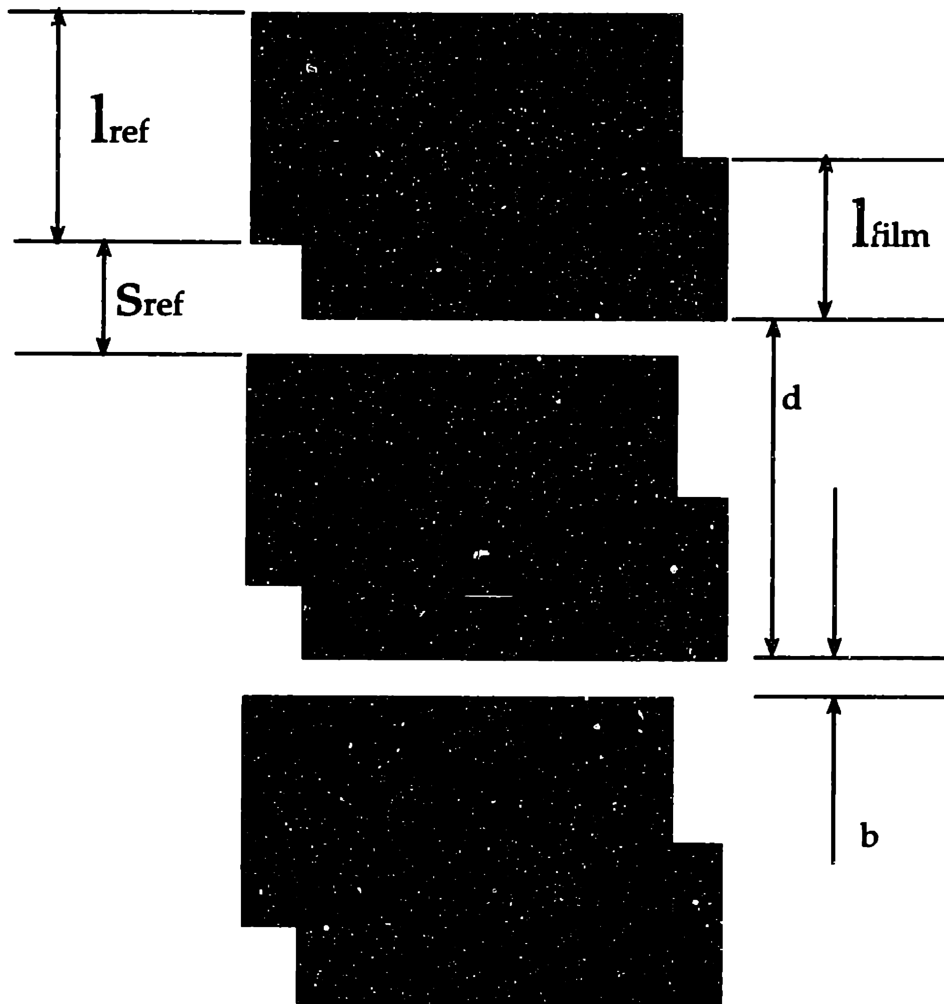

Figure 4-30: Grating geometry can be designed to satisfy dynamic range requirements. Furthermore, from conditions of Equation 4.45 and Equation 4.46 directional information can be maintained, unlike the moiré alignment method.

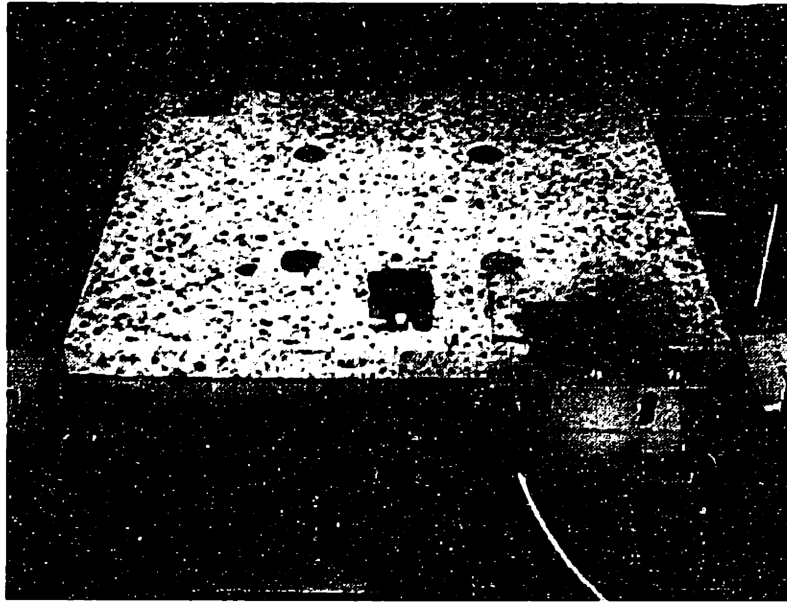

Figure 4-31: Experimental setup for qualifying the diffraction based measurement method.

particular application.

The only parameter that remains to be determined is the number of slits in the gratings, which control the width of the diffrative orders and plotter error averaging. Other considerations for determining the number of slits relates to the detection scheme. The ratio of the zeroth and n^{th} order should be measured by the same sensor. The easiest sensors include a CCD linear array, in which case the intensity profile is spatially sampled, or a quad-element photo-transistor. For this study, a CCD array was used because of its availability. The image plane distance must satisfy the Fraunhofer condition, and is located by the linear distance between the optical axis and the nth order being measured. These are all system specific design parameters.

Figure 4-31 shows the system used for measuring the gauge capability of the diffraction method.

This apparatus is the same as the system used for the moiré study; however, the CCD zoom lens was removed and replaced with a neutral density filter. Furthermore, the diffuse light source beneath the grating subassembly was replaced with a 5mW He-Ne laser, λ = 550 nm. A laser expander was used to illuminate the 250 lp/inch grating. An opaque mask 1/16 inch long and approximately 1mm wide served as a

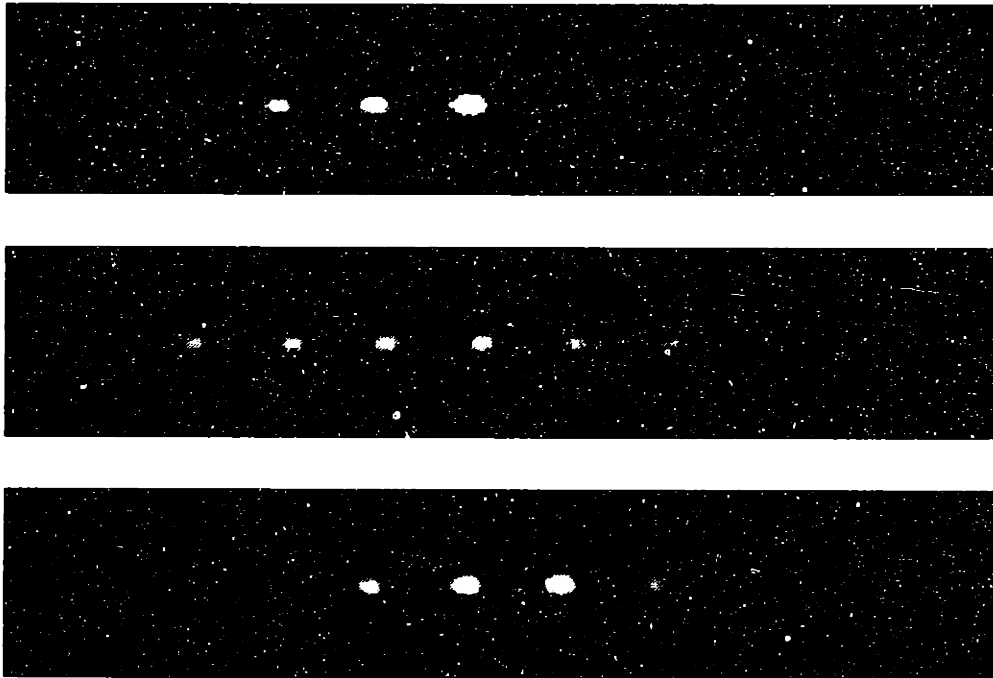

Figure 4-32: Diffraction patterns created by a $250 lp/inch$ grating using a He-Ne laser and an OD3 filter.

field mask.

The diffraction pattern generated by the grating is shown in Figure 4-32, with corresponding scaled intensity profile shown in Figure 4-33.

To determine the intensity of the center and first diffractive order, the actual pixel values were used; although, for further resolution, curve fitting algorithms should be employed.

Displacement may either be calculated by a linear coefficient from a linearization of the intensity distribution in the vicinity of the nominal position, or from the actual modulation envelope. Since the envelope is governed by a transcendental equation, solution for position may be calculated by successive approximation.

4.2.3 Implementation

For measuring three planar degrees of freedom, three displacement measurements are required. Since measuring patterns are constrained to the perimeter of artwork, and grating patterns must be orthogonal to the printing axes, two x and one y, or two y and one x measurements will suffice. This may be accomplished by the placement of

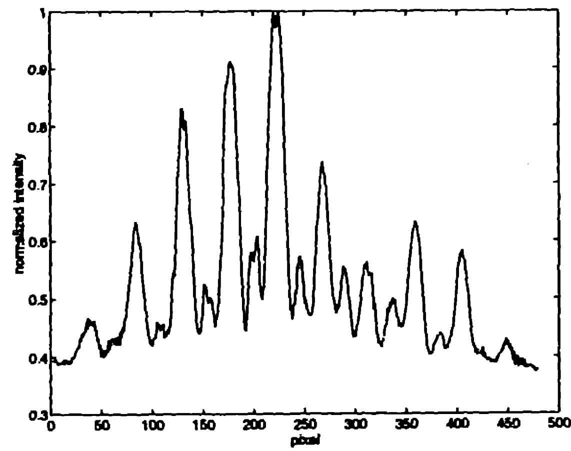

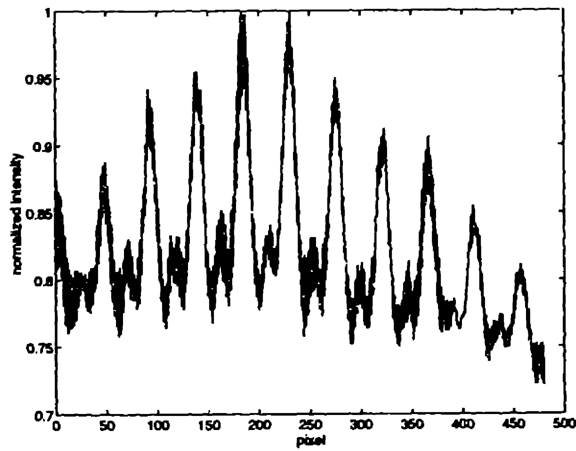

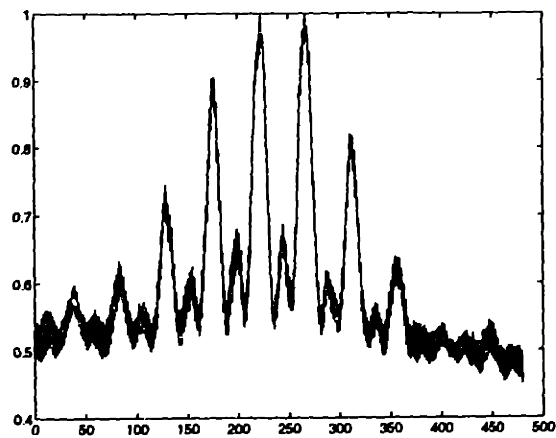

Figure 4-33: The intensity profile of the pattern of Figure 4-32 shows the diffraction orders and the $\sin^2 \beta/\beta^2$ modulation.

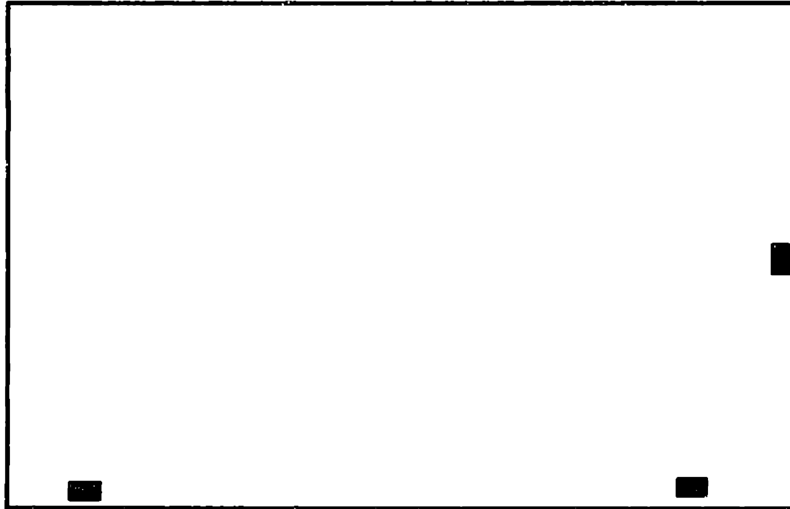

Figure 4-34: Diffraction grating placement for measuring three degrees of freedom.

gratings as shown in Figure 4-34.

This design, however, is not thermocentric. That is, since position is referenced from an edge, thermal expansion causes twice the error at the opposing edge. Expansion about the center splits registration errors at the film perimeter. center the film, the pattern similar to one proposed for moiré alignment may be used as shown in Figure 4-35 Notice that for this arrangement of diffraction gratings, diffraction measurements are invariant to artwork scaling and thermal variations.

4.3 Discussion

This chapter introduced the theory and developed methods for optically registering circuit-board artwork. The need exists to develop new methods, since the required measurement accuracy and alignment repeatability are approaching the fundamental limits of the current fiducial approach. The moiré method demonstrated a measurement resolution of $\pm 0.8\mu m$ and $\sigma = 0.82\mu m$. This technique is computationally intensive requiring frequency domain analysis of the signals to determine phase of fringe patterns. A fringe heterodyne method was developed which was used to locate the rotation center of the artwork to achieve registration. This method exploited the phase and frequency information provided by the fringe pattern. One less desirable trait of

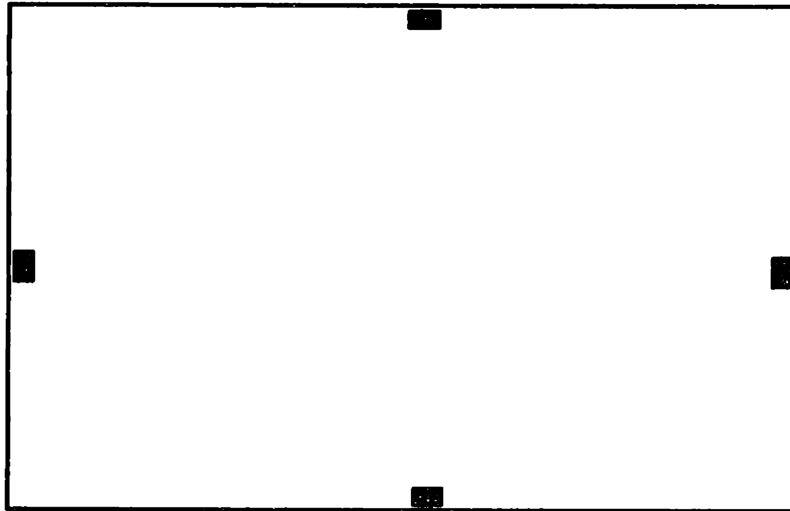

Figure 4-35: Film alignment using a thermocentric design is invariant to artwork scaling and thermal errors.

the method is the required film space for the gratings. For a thermocentric design, four gratings are needed, each grating requiring a swath approximately $1/2'' \times 1''$.

A measuring and alignment method based on diffraction gratings was also developed, whereby the modulation of various diffractive orders were measured to calculate the film position. This technique requires substantially less film real estate (approximately $0.03'' \times 0.06''$). Furthermore, the grating design is readily parameterized for increasing dynamic range, and the periodicity problems encountered with the moiré method can be eliminated through grating design. Since diffraction patterns are aligned with the grating itself, the method is insensitive to film rotation, i.e. film rotation is measured as a pure Abbe error. Abbe errors measured by the gratings determine the necessary rotational adjustments.

Chapter 5

Kinematic Artwork Tooling and Expose Frame Design

In Chapter 3 alignment and fixturing limitations of current tooling methods were described. In those sections, it was determined that pad dimensions and pitches are most sensitive to inner-layer processes, indicating that improvements to inner-layer artwork alignment and fixturing would contribute most favorably to reductions in pad dimensions. Furthermore, the new methods can be directly applied to other imaging processes, such as outer-layer expose, solder mask, and photo-defined vias.

Of key importance, is an understanding that current methods rely solely on stringent machine tolerances to achieve registration. Tolerance in size, location, and orientation of slots and pins are limiting factors for front-to-back registration. Numerical simulations suggested that dominant sources of error were variations in multiple slot fixturing and target alignment. Registration error between two patterns was found to have a 3σ deviation of $94\mu m$. This figure agrees well with actual registration results.

This chapter will describe a new method for constraining artwork. This technique is based on a kinematic constraining system, whereby film tooling features provide precisely three constraints: two translational, and one rotational. Data demonstrating the repeatability of this type of film coupling is presented using moiré interferometry developed in Chapter 4.

Additionally, a kinematic coupling design using die set bushings for use in expos-

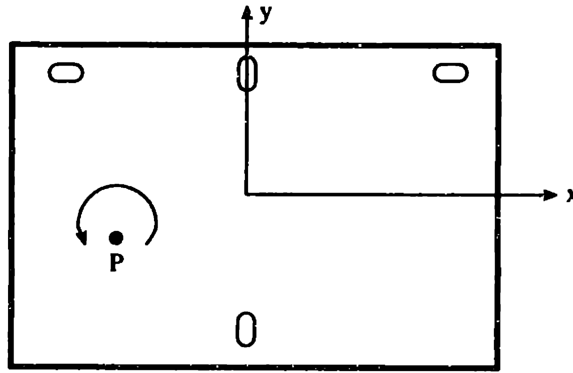

Figure 5-1: Coordinate system definition for artwork.

ure frames is presented. Reduction of constrains by the use of die sets is needed, since frames must accommodate many board thicknesses. The range of thicknesses precludes use of monolithic flexures.

5.1 Film Fixturing

For a system to be deterministic, the number of independent equations for static equilibrium has to equal the number of unknown quantities. The four slot tooling scheme is indeterminate because the number of unknown quantities is greater than the number of equations. To deterministically constrain a plane, three equations must be satisfied for equilibrium. These are,

$$F_x = 0 \tag{5.1}$$

$$F_y = 0 \tag{5.2}$$

$$M_p = 0 \tag{5.3}$$

which state that the sum of the forces in the x and y directions, and the sum of the moments about any point, must be zero, as defined in Figure 5-1. To uniquely solve these equations, there can be at most three unknown quantities.

As opposed to kinematic fixturing, constraints of the four slot tooling scheme are non-repeatable, and numerous. Because of this, contact forces cannot be calculated; contact stresses and strains are therefore indeterminate, limiting information

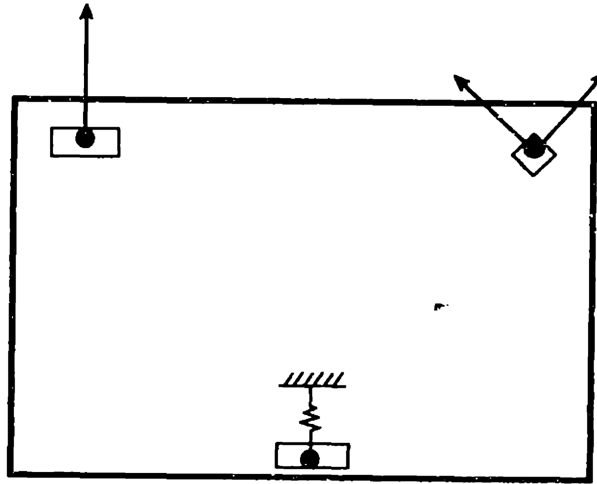

Figure 5-2: One proposed kinematic constraining scheme.

for precise fixture design. Additionally, since constraint preloads are not solvable, the stiffness and stability of the system is also indeterminate. Performance cannot be predicted.

Design of precise fixtures requires understanding of the strain fields. Strain fields are solvable from stress fields, which are obtained from knowledge of applied forces, geometrical considerations, and material properties. Contact forces, which provide constraints, can be calculated for a kinematic system. These constraints can be generated in a plurality of ways, but the proposed method does so through the use of a vee shaped hole, and a flat, as shown in Figure 5-2. The additional hole located at the bottom of the film provides a desired preload by a spring, solenoid, or other means. It is emphasized that this hole is not a constraint: it is a force source. The preload ensures that the constraints, i.e. contact points, are maintained. Artwork remains registered in the presence of external disturbances or environmental fluctuations.

The vee hole provides exactly two constraints when placed onto a round pin, since there are precisely two point of contact. When contact is made, this interface constrains x and y translation of the film. Rotation is constrained by placing the slot over a round pin. To maintain contact, a preload pin is provided. In this configuration, contact points are well defined, and the induced stresses may be calculated. Other kinematic designs may be implemented as shown in Figure 5-3.

In any one configuration of Figure 5-3, there is precisely one location a film can

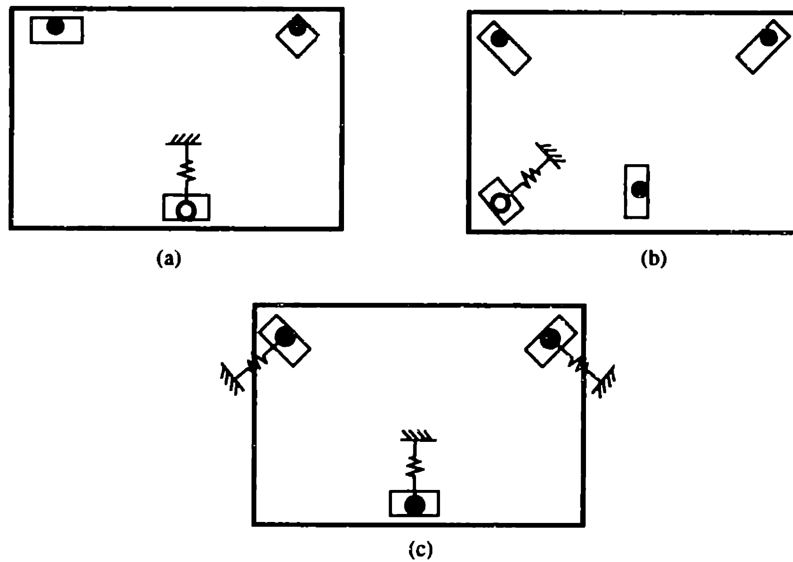

Figure 5-3: Three different kinematic systems. (a) Vee and flat, corner origin; (b) center origin with oblique preload pin; and, (c) center origin, each pin location with opposing force source.

occupy, regardless of the position and size of either the pins or the holes. Accuracy specifications for sizes and positions of pins can be relaxed, as their values are of no consequence to artwork registration capability. Because hole diameters can be substantially larger than pin diameters, film placement is facilitated; inadvertent hole deformation from interference fits may be avoided; and, tool and film wear is reduced, prolonging film life. Furthermore, kinematic tooling features eliminate the need for operator savvy. Longer film life and faster set-up times are additional compelling reasons to implement a kinematic tooling scheme for artwork registration.

When film is preloaded against pins, the coupling stiffness is that of the polyester film itself. As depicted in Figure 5-4, the coupling is a series spring arrangement involving the polyester film and steel pin. Because film compliance is significantly larger than pin compliance, (0.7 Mpsi versus 30 Mpsi, respectively), the modulus of the film material limits coupling stiffness. However, since artwork is not subjected to any in-plane forces, stiffness is not a limiting factor as it may be, for example, in a machining center.

The design procedure for this system involves limiting the maximum shearing stresses near the contact points for a given preload force. Hertzian point contact

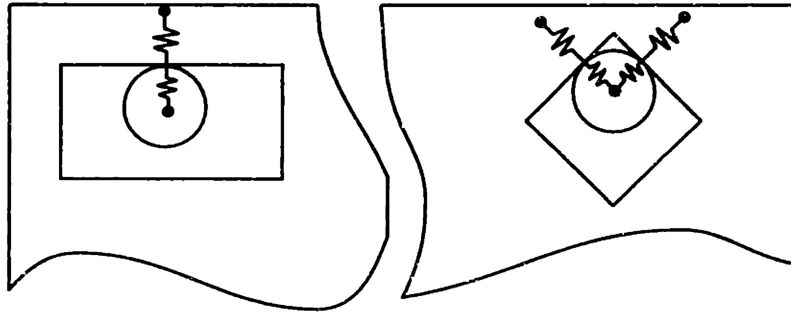

Figure 5-4: Preloaded coupling stiffness is calculated from the series connection of springs.

theory for two cylindrical bodies in contact is used to determine the contact stresses and resulting footprint [32]. Because there are no in-plane forces applied to the film, there is no predetermined value for coupling preload. Rather, an estimate of the requisite force to overcome friction between the film and the glass it rests on is used. The remaining contact forces are calculated from equations for equilibrium. Each stress field is calculated, and the strains are determined. Table 5.1 displays results from spreadsheet calculations. Algorithms for determining the stress fields are found in [29] and [30].

For a conservative factor of safety, the coupling was designed for a maximum shearing stress of 1000 psi, using 3/16" diameter hardened constraining pins, and a compliant 0.25" diameter Teflon preload pin. From Table 5.1, the preload pin will be designed to exert 0.5 lbs. force. Stresses are confined to the immediate areas about the contact points; induced strains throughout the film are negligible.

Additional factors of practical consideration, which will affect repeatability, are contaminants on pins or hole edges, table friction, hole edge profile, and preload variation. Also, local buckling of the film at the pins may occur. To prevent such buckling, light vertical (clamping) preloads using low friction materials around the pins are recommended. The clamping action of the top and bottom glass itself serves this purpose well. Coupling repeatability is expected to be within $5\mu m(3\sigma)$ deviation. If so, emphasis shall be placed on the repeatability of the punch and operator alignment.

An assumption in the preceding analysis was contact between two semi-infinite bodies. This assumption implies a contact footprint of significantly smaller dimension

Film		
Material	polyester	
Stiffness	6.80×10^5	psi
Poisson's Ratio	0.25	
Specific gravity	1.39	
Thickness	0.007	in
Preload Pin		
Material	Teflon	
Stiffness	6.00×10^4	psi
Poisson's Ratio	0.25	
Radius	0.125	in
Constraining Pins		
Material	Steel	
Stiffness	3.00×10^7	psi
Poisson's Ratio	0.292	
Radius	0.09	in
ASSUMING CYLINDRICAL SEMI-INFINITE BODIES		
τ_{max}	1000	psi
Load/thickness	74.19034671	lbs/in
Preload pin footprint	0.014	in
Load at preload pin	0.52	lbs.
Load at flat pin	0.26	lbs.
Load at vee pin (each)	0.37	lbs.

Table 5.1: Contact force calculations for given shearing stress.

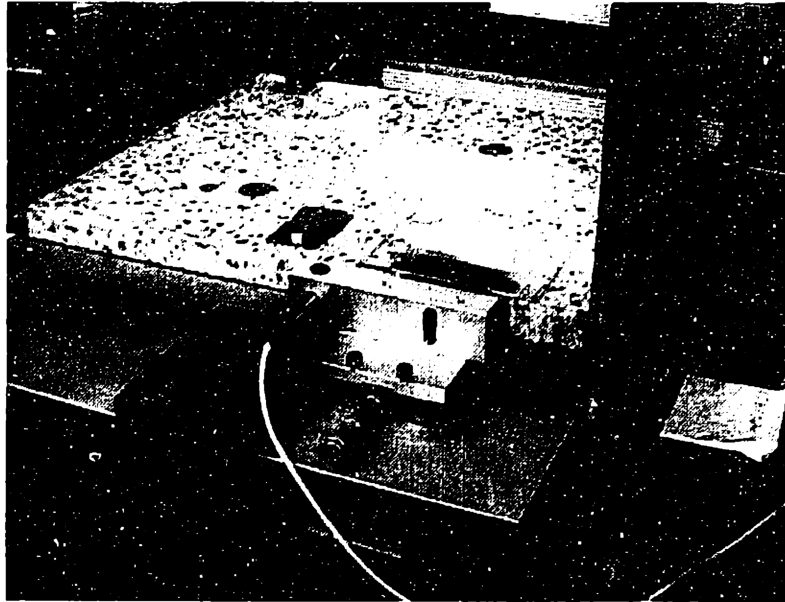

Figure 5-5: Test fixture for measuring repeatability of kinematically fixtured film.

as compared to the body dimension itself. The calculated footprint, however, was twice the thickness of the film. The plane strain formulation is not valid. Poisson expansion should be considered. Since, however, artwork is not subjected to in-plane forces, the coupling stiffness is not necessarily a design constraint. For purposes of locating film on frames, existence of kinematic constraints is rather than an accurate description of stress fields is needed. This constraint condition is satisfied regardless of the particular geometry of the pin and film edge. Front-to-back registration will be maintained for similar stress fields of the two films.

5.1.1 Repeatability Results

For testing, the vee and flat configuration of Figure 5-3 (a) was used. The moiré method using the Fourier transform to resolve phase was used. The vee and flat arrangement does not constitute a thermocentric design, however, it was assumed repeatability results for any of the kinematic configurations will be similar, if not, identical. A test table was constructed from granite as shown in Figure 5-5.

Aluminum inserts along the rear edge of the table held two 0.375" hardened steel constraining pins. One aluminum insert was attached to a linear stage. This stage

Measure	$3\sigma(\mu m)$
Kinematic film repeatability	Four slot system repeatability
3	38

Table 5.2: Comparison of kinematically fixtured film to four pin system.

controlled rotation of the film about the other fixed pin. A spring Teflon pin preloaded the film in tension with 0.5 lbs force, ensuring contact among the pins and slots. Since these tests measured repeatability of film placement, the shape and location of slots were not important. The tooling features were cut using a razor blade. The assumption on accuracy from film to film is that tooling features will be placed as accurately as the punches and alignment are. Because a moiré or diffraction method will center the film to the punches with a resolution below one μm, punch repeatability will be the dominant cause of error. Punch error is currently $21\mu m$, 3σ. Alignment errors are no longer a contributing factor as the accuracy of the method has been improved by more than an order of magnitude.

Another assumption was that film repeatability in one degree of freedom will be the same in the other two degrees of freedom. By this, only one moiré pattern was measured. To negate the effects of frequency modulation prior to the experiment, the film was rotated to match the fringe pattern of the reference grating.

Film was placed onto the fixturing assembly, position measured via moiré interferometry, and removed. This procedure was repeated for several trials. Time series analysis for the kinematically tooled film is shown in Figure 5-6. Figure 5-7 is a histogram of the time series data. For 150 trials, which incidentally is many more removals a film set undergoes in production, the position is normally distributed with a 3σ deviation of $2.5\mu m$. Tests were performed on a separate occasion, the time series and histogram of which are shown in Figure 5-8 and Figure 5-9. For the second trial, the 3σ deviation in film position from center was $3.2\mu m$.

These placement results are compared with those of the four slot tolling system described in Chapter 3. Table 5.2 summarizes the comparison.

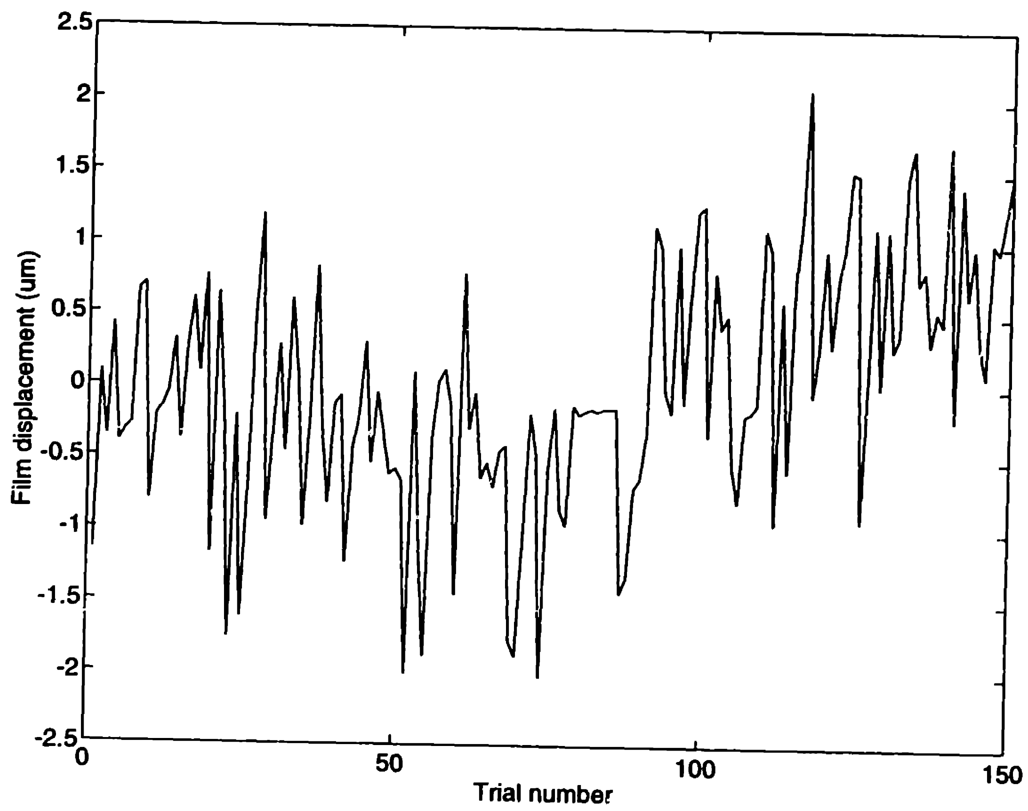

Figure 5-6: Time series position data of kinematically tooled film.

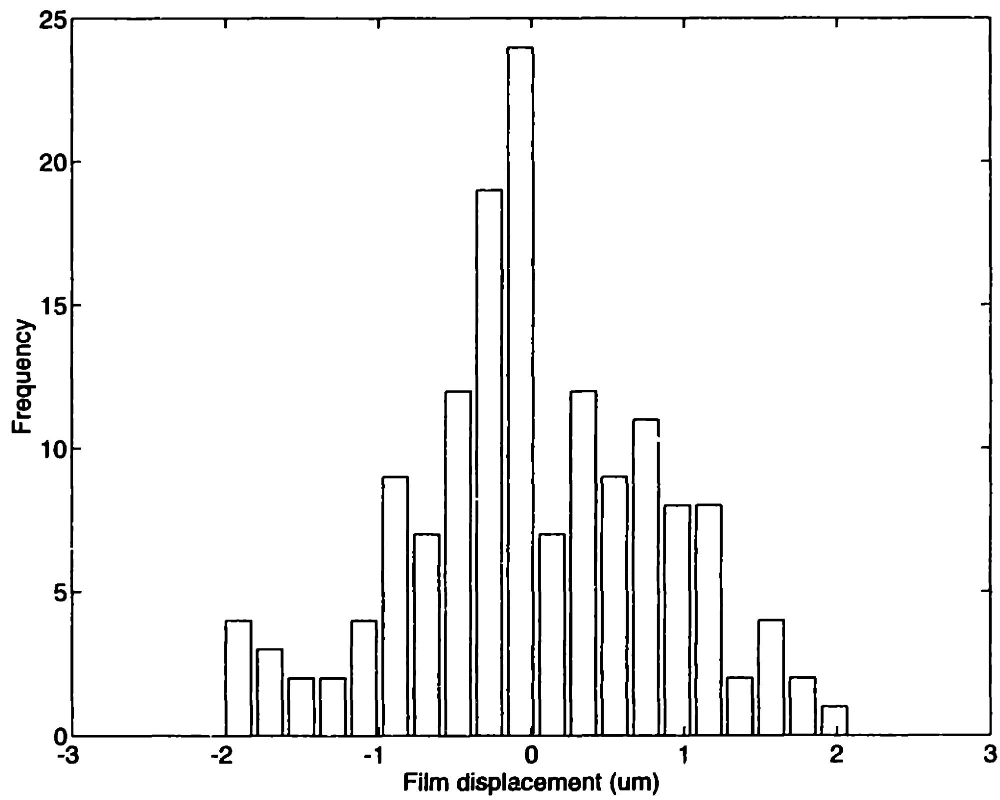

Figure 5-7: Histogram of kinematically tooled film, $3\sigma = 2.5\mu m$.

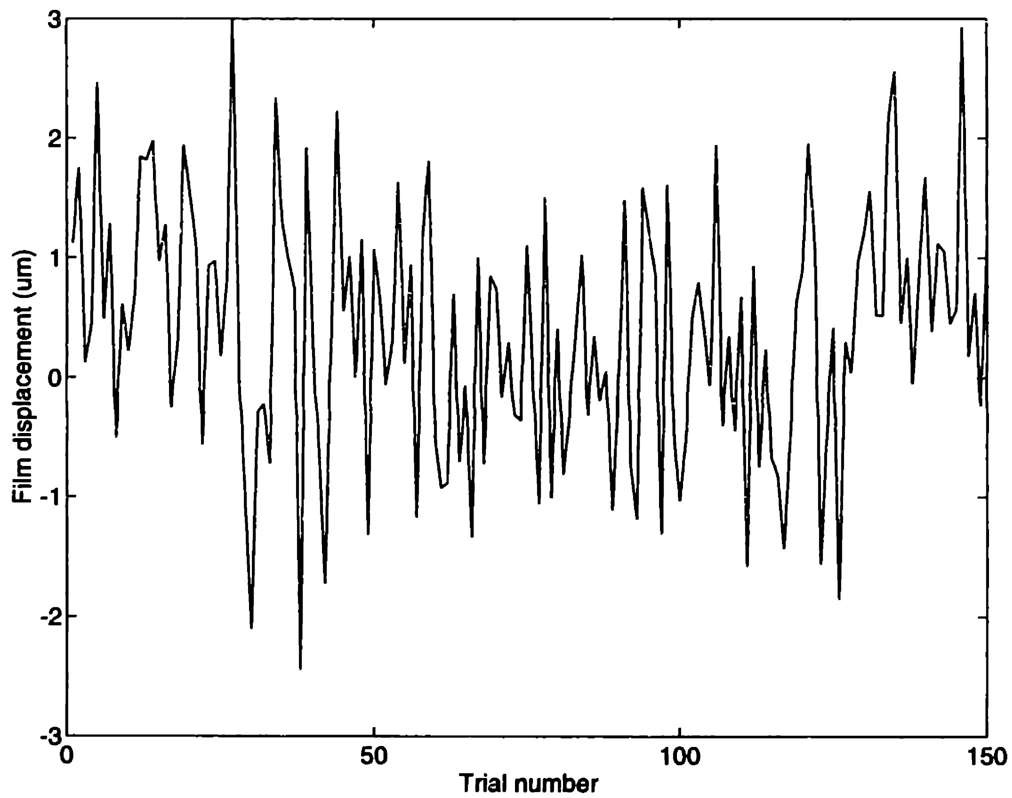

Figure 5-8: Time series data for second experiment of kinematically tooled film.

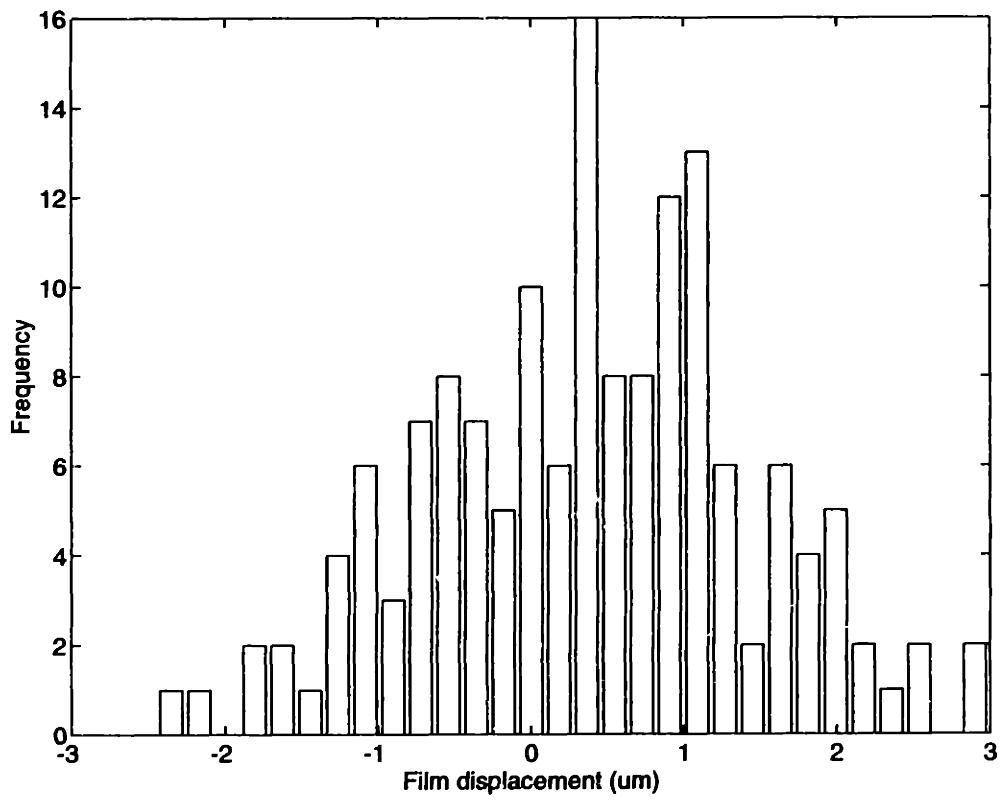

Figure 5-9: Histogram of second experiment, $\sigma = 3.2\mu m$.

Measure	Moiré Alignment, Kinematic Tooling $3\sigma(\mu m)$	Fiducial Alignment, Four Slot Tooling $3\sigma(\mu m)$
Tooling to image	21.8	44.4
Film to frame	3	38
Front-to-back	2 pieces of film	2 pieces of film
Total Registration	22	82.3

Table 5.3: Comparison of new alignment and fixturing method to current technique.

An order of magnitude improvement in positional repeatability is achieved through kinematically fixturing the film. Aside from the dramatic improvement in repeatability, manufacturing tolerances on the position and sizes of the constraining pins may be relaxed as their dimension has no impact on film placement. Further, the $36\mu m, 3\sigma$ deviation is position of a film fixtured to different frames is eliminated. The benefits of a kinematic film fixturing system are evident.

Punch repeatability becomes the dominant source of error. A few proposed designs are contained in Appendix A that may reduce these errors. It is left as another research project to improve punch technology. In any event, assuming that the same punch is used with new alignment methods, and that kinematic tooling is adopted, the expected improvement in front-to-back film alignment is as shown in Table 5.3

Of the $22\mu m$ 3σ deviation in front-to-back registration, 98% is due to punch limitations. Efforts in improving punch repeatability will greatly enhance registration performance. Furthermore, once constrained, front and back artwork must remain registered after opening and closing exposure frames. As described in Chapter 3, frame repeatability (3σ), is limited to approximately $40.8\mu m$. For the existing artwork tooling scheme, frame deviation only contributes an additional 20% to the total front-to-back error. For the moiré alignment and kinematic film fixturing methods, this frame error contributes 77% to the total registration error. Because this is a significant contributing factor, a new coupling for use in exposure frames is proposed. This coupling is the subject of the following section.

5.2 Exposure Frames

Incentive to investigate alternative designs for exposure frames was derived from the excessive contribution of frame repeatability to artwork registration error. Current frames, which use sliding fits among mechanical elements, are repeatable to approximately $41\mu m$. Wear of the mechanical constraining elements degrades frame performance with time. A ball fixtured to the lower frame fits into a hole of the upper frame, thereby constraining location. Similarly, a square pin on the upper frame mates with a square hole of the lower frame, constraining rotation. Because frames are to be used to expose cores of varying thicknesses, out-of plane travel must be permitted.

Rigid ball-groove type kinematic couplings have long been known to provide a means to achieve sub-μm positional repeatability between two rigid bodies [29]. Exposure frames differ from traditional kinematic coupling applications because a means to permit out-of-plane motion must be provided to accommodate different core and panel thicknesses. A coupling with the benefits of kinematic coupling for planar positioning, but with a reduced constraint set is to permit necessary motion is needed.

To permit out-of-plane motion, either monolithic flexures or die-set bearings were proposed to be used at each ball-groove interface. A flexure may be designed for pure translational motion, while the die-set only permits single degree of freedom motion. The reduction of a degree of freedom per ball-groove pair frees three degrees of freedom. These are, translational motion normal to the plane containing the coupling elements, and rotation about two axes contained in the coupling plane. Since, for example, exposure frames are held together by vacuum, the translational and rotation degrees of freedom are constrained. The remaining constraints, x, y, and θ, in the plane of the printed circuit board are constrained by the kinematic coupling elements.

For frames which need to accommodate limited laminate thicknesses, a coupling with monolithic flexures may be used.

In the event that larger displacements are required, as is necessary to accommodate thick panels, die-set bushings with crowned posts may be used as shown in Figure 5-10. Note that the bushing coupling is different than traditional die-set bushings in that

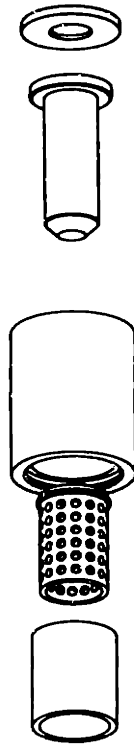

Figure 5-10: Kinematic coupling using die-set bushings and ball cages for large out of plane travel.

for traditional systems, posts are rigidly attached to one assembly, while the bushing is rigidly attached to the other body. This system is naturally overconstrained limiting repeatability and causing material wear. The post and bushing of the die-set coupling system are part of the same assembly, which is in turn coupled kinematically through the crowned post to grooves of the mating part. Hence ball cages are not subjected to eccentric loading. Because of this, bearing life of the kinematic die-set coupling will be lengthened. Repeatability of the individual die-sets are estimated, $\sigma < 5\mu m$.

Design of the kinematic elements follows procedures described in [29] and [30]. Preload will dictate the spring used to preload the die-sets, while load capacity and stiffness requirements will determine the size of the ball cage. Hertzian contact theory [32] is used to calculate the stress and strain fields of the bodies in contact. Stiffness and load capacity of the die-set bearing system may be obtained.

Figure 5-11 shows a conceptual model of the proposed frame design. The lower glass plate contains the two film constraining pins and the preload pin, the crowned

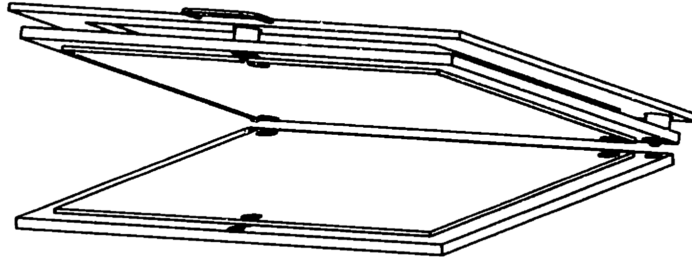

Figure 5-11: Exposure frame concept based on die-set kinematic couplings.

coupling elements of the upper frame are shown seen, as are the coupling grooves of the lower frame.

As seen in Figure 5-12 through Figure 5-15, the force and moment stiffness of the die sets are a strong function of the number of rows of the cage and the number of balls per row. This should be evident since the load is distributed among the balls. Similarly, the more rows the cage contains, the higher the moment stiffness. The is due to the larger lever arm of the long cages.

To determine the repeatability of the die-set kinematic coupling, a test system was designed. Ball cages with $19mm$ diameter, 6 ball rows, and 14 balls per row were used. Balls had a $0.0001in$ diameter tolerance, and a $25\mu in$ sphericity tolerance. The post was designed with ISO h3 tolerance. A $3in$ radius crown was hard turned onto the post. Bushings were cylindrically ground for a light preload. Posts and vee blocks were hardened to a Rc 55 hardness. The die-sets, crowned posts and vee-blocks are shown in Figure 5-16 through Figure 5-18. A test plate used to measure coupling

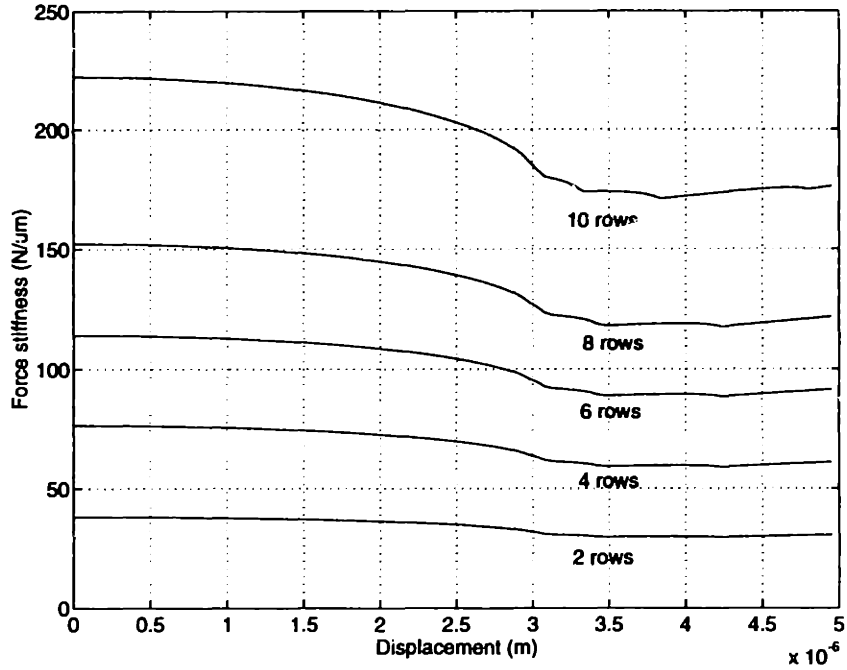

Figure 5-12: Force stiffness of die set bushings of different numbers of rows.

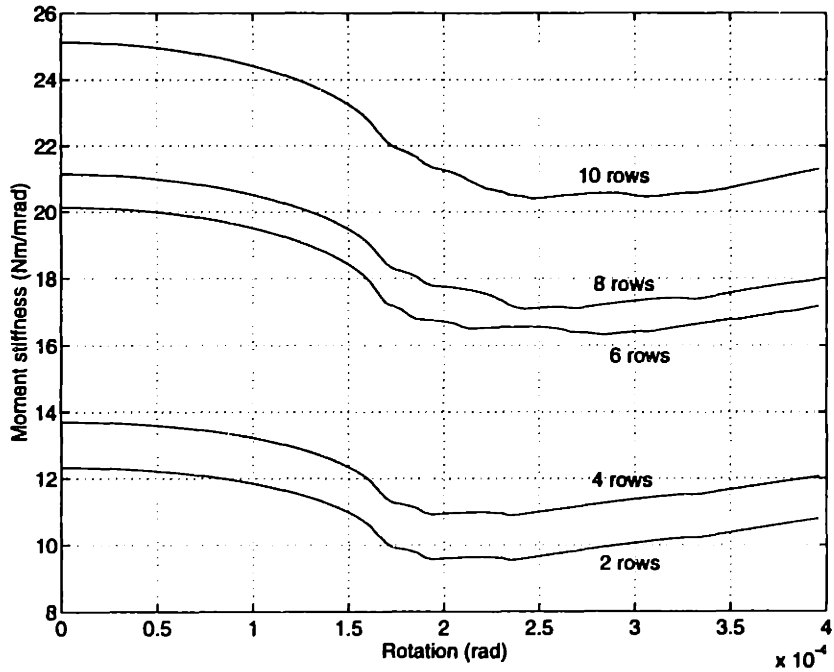

Figure 5-13: Moment stiffness of die set bushings of different numbers of rows.

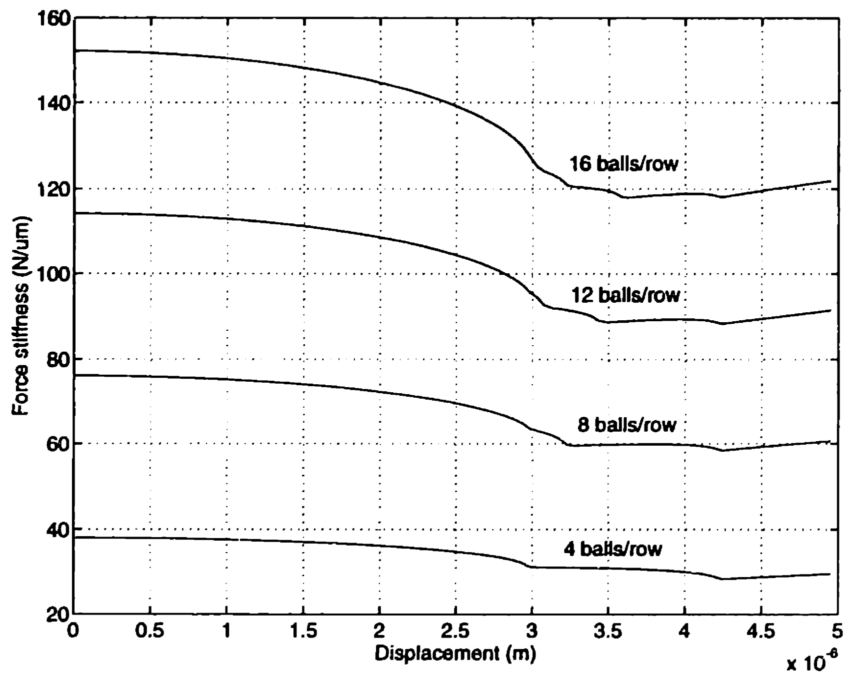

Figure 5-14: Force stiffness of a six row die set bushings of different numbers of balls per row.

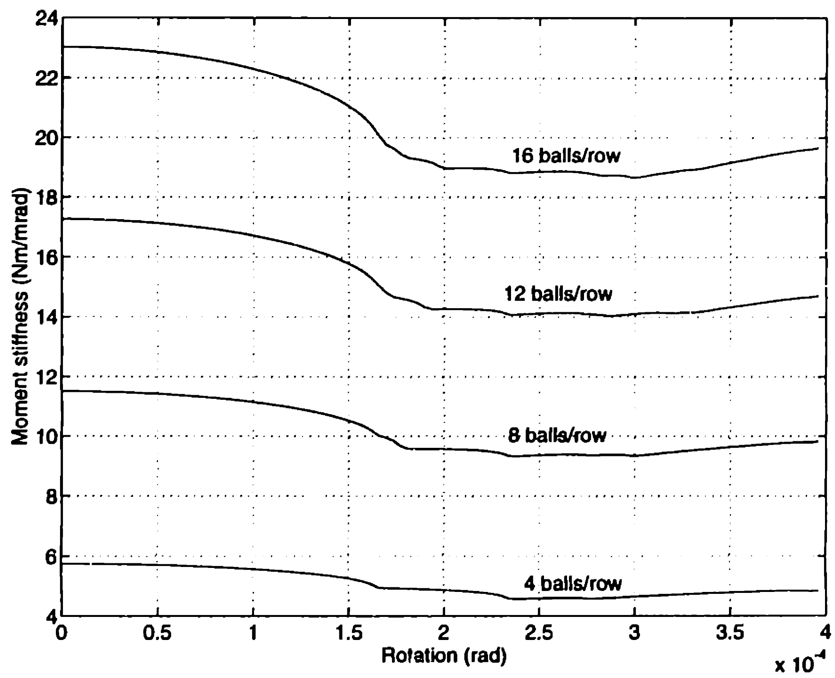

Figure 5-15: Moment stiffness of die set bushings as a function of number of balls per row and post rotation.

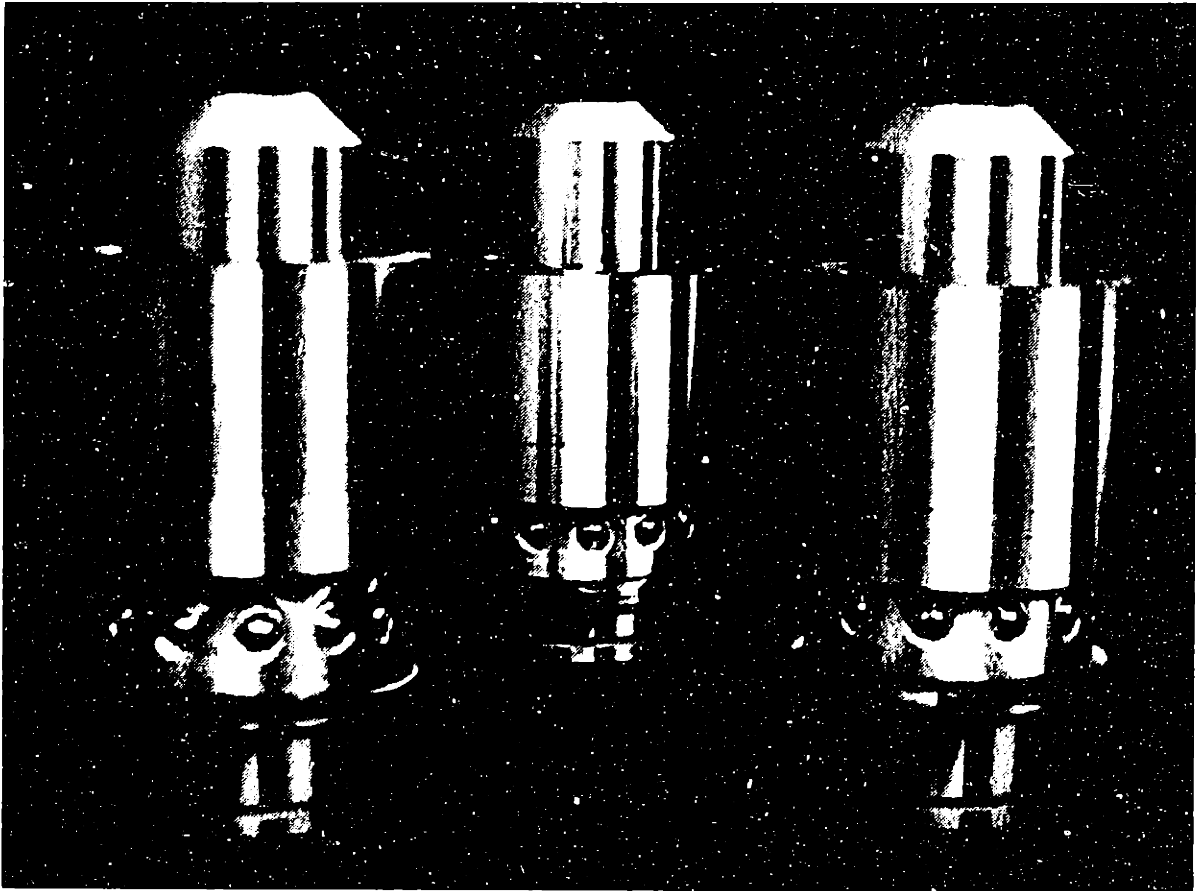

Figure 5-16: Die set bushings and cages, with crowned post for kinematic coupling.

repeatability is shown in Figure 5-19.

Dial indicators with 0.0001″ resolution were used to measure locational repeatability of the coupling. Capacitance probes were not used because of their limited dynamic range. The range was an issue, not because the coupling would exceed it, but because the probes would contact the face of the tooling plate during coupling engaging and disengaging. Therefore, the data presented in Figure 5-20 is limited to a $\pm 0.0001''$ resolution. The repeatability data for 500 cycles is shown in Figure 5-20. Since the measurement resolution was limited, positional deviation was difficult to assess. However, from the data, it is clear that the coupling repeats to within $\pm 0.0001 - 0.0002''$, or approximately $\pm 2.5 - 5\mu m$. Experimental data demonstrated positional repeatability consistent with manufacturers information.

Several compelling reasons for the use of a die-set kinematic coupling for circuit board artwork exposure exist. The coupling has superior repeatability performance to

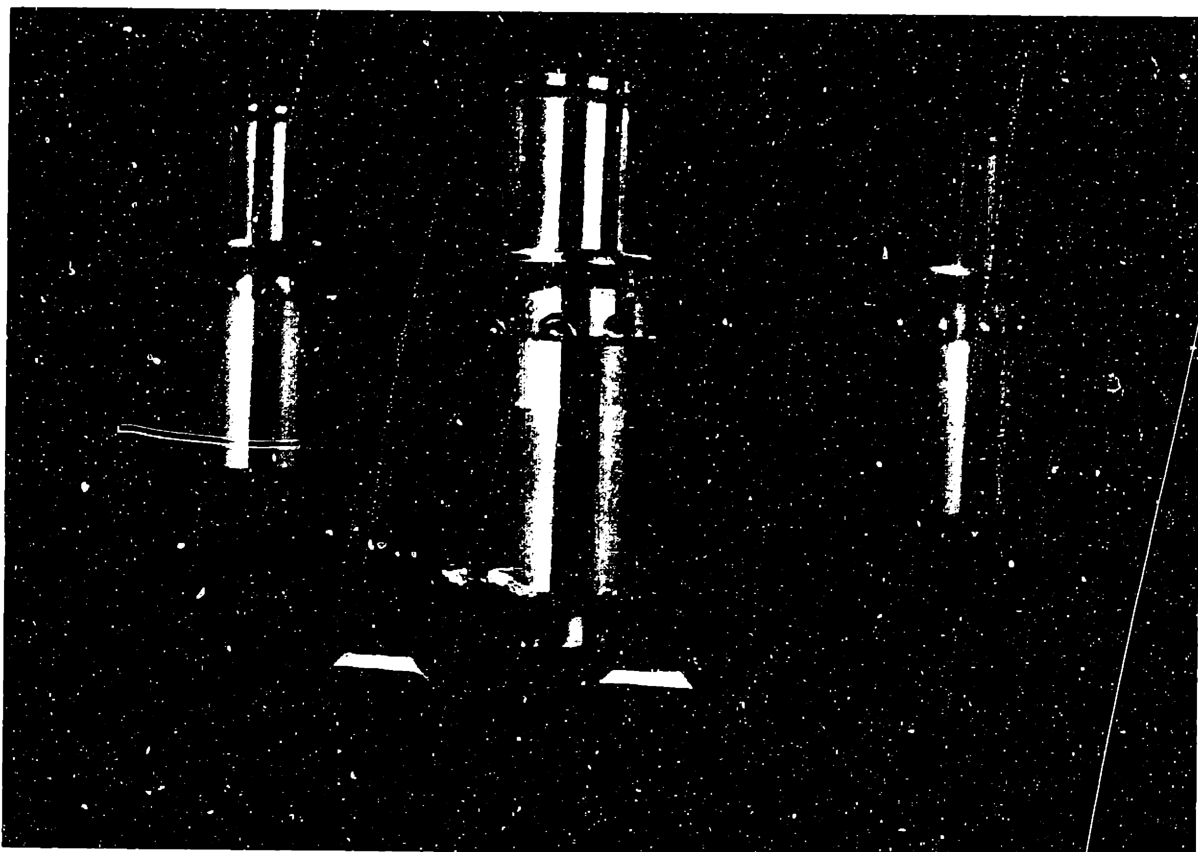

Figure 5-17: Set of three die set posts in vee grooves.

Figure 5-18: Kinematic die set post in vee groove.

the current ball and post method; repeatability performance improves with use because the contact points are self-burnishing; and most importantly, positional repeatability is unaffected by manufacturing tolerances.

5.3 Chapter Conclusions

In this chapter, methods for improving artwork registration through the use of kinematic couplings in artwork and in exposure frames were developed. For artwork tooling, the fixturing technique was bases on kinematic features that were punched into the film. To constrain three degrees of freedom, three points of contact were provided. The contact was achieved through use of a vee and a flat or by three edge slots. For demonstration, the vee and flat configuration was used. Although this configuration does not constitute a thermocentric design, as does the three inward slot pattern, superior film placement repeatability was still demonstrated. Placement repeatability is invariant to pin size and locational tolerances, hence manufacturing

Figure 5-19: Test table for measuring repeatability of kinematic die set coupling.

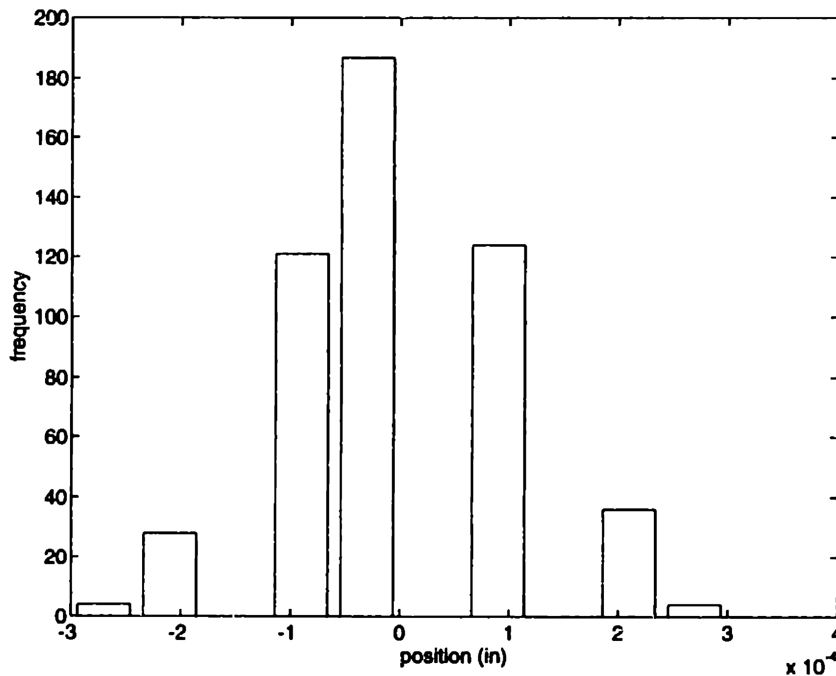

Figure 5-20: Repeatability results of kinematic die set coupling.

constraints may be relaxed. Furthermore, size of film tooling features may vary. The limiting factor in film registration is alignment to punches, which was addressed in Chapter 4. Film punching and fixturing repeatability was $3\sigma \approx 22\mu m$, as compared to the current state of the art, $3\sigma \approx 83\mu m$. Of the $22\mu m$ deviation of the proposed system, 98% is due to punch repeatability alone.

A frame to accommodate the kinematically tooled film was presented. This frame used a new type of coupling, which was a combination of a kinematic coupling and die-set bearings. The kinematic coupling located the frames relative to each other, while the bearings provided the necessary motion to accommodate various thickness boards. Preliminary data demonstrates frame repeatability to within approximately $\pm 3 - 5\mu m$. This deviation is well balanced with the film coupling repeatability of $3\mu m$. Efforts to improve punch repeatability are recommended. Immediate improvements include the use of a stripper plate or polymer replicated punch linings. These are outlined in Appendix A.

Table 5.4 summarizes front-to-back registration capability of the proposed frame

Measure	$3\sigma(\mu m)$
Artwork to Tooling	22
Tooling to frame	3
Frame to frame	3
Front-to-back	2 pieces of film
Total Front-to-back	31.7

Table 5.4: Front-to-back registration capability using moiré interferometric alignment, kinematic film tooling, and kinematic die-set frame coupling.

design and film alignment and fixturing system. Note that the dominant cause of registration error is punch repeatability. Actual deviation is approximately 20 times smaller than the current constraining deviation. Overall registration deviation of the proposed system, including punch and alignment error, is approximately 10 times smaller than the deviation of the existing system.

Having addressed the performance limitations of film alignment, tooling, and fixturing techniques, Chapter 6 presents the implications of the proposed methods to board metrics such as pad diameter and pitch, and wiring density.

Chapter 6

Conclusions

This thesis identified limitations of current manufacturing methods for circuit board production. Available techniques will not be able to satisfy density demands of forthcoming devices, such as μBGA, flip-chip, and other high-density components. Mechanical and chemical processes involved in the manufacture of circuit boards are approaching their limitations. For instance, developing, etching, and stripping cores with traces smaller than $50\mu m$ often results in a bare board. Mechanical processes such as core and panel fixturing contribute to registration errors among various layers and machine tools. This thesis specifically treated artwork and exposure frame alignment and fixturing. The methods developed demonstrated superior registration performance without significant equipment or process changes. Although, the techniques were applied to artwork for pattern exposure, some of the methods and their permutations are equally applicable to other processes, such as lamination and electrical test.

A tolerance study in Chapter 3, revealed that metrics such as pad diameter and pitch are most sensitive to inner-layer exposure processes. For this reason, alignment, tooling, and fixturing in inner-layer processing were specifically addressed. Furthermore, as inner-layer exposure is the first registration sensitive process, introduction of new technology to this area has been accepted by the industry. The proof o[illegible]iples at this stage will hopefully facilitate incorporation of the presented ideas into other areas of circuit board manufacture.

This thesis presented four enabling technologies for the production of fine pitch,

densely populated rigid multi-layer circuit boards. They are:

1. Film alignment based on moiré interferometry,
2. Diffraction pattern based film alignment,
3. Kinematic artwork tooling, and
4. Kinematic die-set exposure frame couplings.

Each method and design contributed significantly to the reduction of registration errors in circuit pattern exposure. Previous chapters described the specific contributions to registration at exposure process, but the implications of the new capabilities need addressing.

Since the front-to-back image registration of inner-layer cores may be reduced to approximately $30\mu m$ from $94\mu m$, the required inner-layer pad annular ring may be reduced accordingly. The pad diameter must account for lamination uncertainty and drill wander. Considering these additional sources of error, the minimum inner-layer pad diameter becomes,

$$\phi_{pad_{inner_{layer}}} > \phi_{via} + 2t_{ring} + 2(85\mu m) \tag{6.1}$$

Compare Equation 6.1 to the current criteria of,

$$\phi_{pad_{inner_{layer}}} > \phi_{via} + 2t_{ring} + 2(130\mu m) \tag{6.2}$$

For tangency, *i.e.* a specified annular ring of zero, and a pad diameter of $0.2mm$ (used as a benchmark), a reduction of pad diameter of 20% may be realized. This is not as dramatic an improvement as may be expected, given the performance improvement in inner-layer exposure. This is primarily due to the drilling operation, which has become the significant limiting factor in reducing pad diameters. Efforts toward drilling, and other via technologies, such as photo-defined and laser ablated vias, will have the next largest impact on PCB density improvements.

The diameter of outer-layer device pads, not directly over drilled vias, may be substantially reduced. The reduction of diameter is reflected here because drill errors are not contributing factors. Similarly, solder mask registration in only limited by artwork error in outer-layer pads and solder mask itself. Solder mask registration was used for establishing a minimum pitch, p_{min}, condition. For the proposed system, this becomes,

$$p_{min} = w_{web} + 2t_{oversize} + \phi_{pad} + 2(31\mu m) \tag{6.3}$$

By scaling the web thickness with pitch itself, say $w_{web} \approx 0.5p_{min}$, and a $t_{oversize}$ specification of zero (tangency), the minimum pitch becomes,

$$p_{min} \approx 4(31\mu m) \tag{6.4}$$

Again, compare to the current state of the art whereby, the minimum pitch would be $p_{min} \approx 4(105)$. The device pitch may be increased by a factor of three using the techniques described in previous chapters.

Similarly, photo-defined vias may be placed onto pads with annular ring specification 3 times smaller than current practice. A $0.1mm$ via, may be placed onto a $0.16mm$ pads, rather than the current practice of $0.25mm$ pads. Note that even current registration methods satisfy this requirement with approximately 50% yields. Actually, for 3σ yields, $0.35mm$ pads are required. The proposed methods decrease the photo-defined pad diameter by more than a factor of two.

Recall from Equation 2.5 that the connectivity density ρ_{line} is inversely proportional to the pad diameter. Equationeq:mymetric is repeated here,

$$\rho_{line} = \frac{1.125\sqrt{N_T}}{\phi_{pad}\zeta\zeta'} \tag{6.5}$$

where ζ and ζ' are scaling factors related to device pitch and pin pitch. By substitution of the improved pitch and pad diameter metrics, an estimate of wiring density may be obtained. Achievable pitches and diameters using the presented methods are designated by the subscript *new*. Pad pitch may be increased by a factor of three,

hence

$$\zeta'_{new} \approx 0.3\zeta' \quad (6.6)$$

Similarly, pad diameters may be reduced. For drilled vias, a conservative estimate of 20

$$\phi_{new} \approx 0.8\phi \quad (6.7)$$

By substitution into Equationeq:mymetric, the interconnect density, based upon these new approaches is written,

$$\rho_{line_{new}} \approx 4.2\rho_{line} \quad (6.8)$$

That is, line density may be increased over 400% per layer, assuming chemical processes may accommodate larger densities. The largest contributor to increased line density is the ability to increase pad pitches, due to alignment of outer-layer artwork and solder mask. The benefit of such an increase will be most significant in the placement of devices such as flip chips and μBGAs. Alternatively, device edge may remain the same, each device being able to accommodate three times as many I/Os. For area array BGAs, number of I/Os are proportional to the edge dimension squared. Using the described methods, area array BGAs with nine times the number of I/Os may be accommodated. Following limits described in Figure 2-3, new boundaries will be established. The developments in this thesis provide the means to cost effectively, mass-produce printed circuit boards which have otherwise been difficult to manufacture. Adoption of the presented methods will facilitate production of ultra-fine pitch, high density PCBs for the next generation of integrated circuits.

6.1 Future Work

The work described by this thesis begins to address the many areas where mechanical engineers specializing in precision machine design may contribute. Within each processing step, numerous opportunities existed for thorough investigation and design enhancements. Within the area of film alignment, measurement, tooling, and laminate exposure, the techniques presented here establish a particular approach to circuit

board manufacture. The notion of deterministic design applied to PCB manufacture is a new one, and it is apparent that improvements to board production equipment may be developed. Appendix A presents a few ideas conceived through the course of this research. Each one potentially spawning a few research endeavors.

Most notably, since film fixturing had been addressed, the next area for research would be in the creation of vias. It was shown in this thesis that once artwork registration has been enhanced, pad dimension and pitch are most sensitive to drilling operations. Within drilling, tool wander and panel fixturing are dominant causes of error. Panel fixturing may be improved using similar techniques to the proposed artwork tooling, as is presented in Appendix A. Drill wander is a function of drill compliance and glass weave of the panels. Because of material limitations in this instance of drilling, laser ablation and photo-defined vias are currently active areas of PCB research. In combination with research in lamination, collective efforts will produce boards able to support recently available and forthcoming integrated circuits. Registration of cores, panels, and artwork, however, should not be overlooked. High throughput and yields of dense PCBs are attainable by applying, in part, the deterministic design principles presented in this thesis.

Appendix A

Additional Concepts

The ideas outlined below certainly fall within the realm of "precise registration methods" as they are related to tooling and fixturing of various elements involved in PCB production. To maintain focus of the main chapters of this thesis, however, these concepts were omitted. Instead, I included them here, more for a matter of interest than anything else. There is a loose order to the presentation, but it is certainly not as formal as previous discussions. Each idea, I feel, is an interesting one, with the possibly of contributing to feature size reduction and density increases.

A.1 Pre-Expose Punching

To create tooling features in artwork, a precision punch is required to produce tooling features with respect to the artwork pattern. There are primarily two approaches to perform this task. One method would be to punch the films prior to exposing, in which case a plotter drum to accommodate kinematic tooling would be designed. Historically, films were tooled prior to exposing; however, it cannot be overemphasized, that this tooling was not kinematic, hence there was no benefit to pre-expose tooling, since the artwork punch could produce features which were more reliable. To obtain front-to-back registration which is limited by plotter accuracy and precision ($3.8\mu m, and 7.6\mu m$), pre-punching kinematic features can be used. Plotted work is printed with respect to tooling features, so that the location of the features is unim-

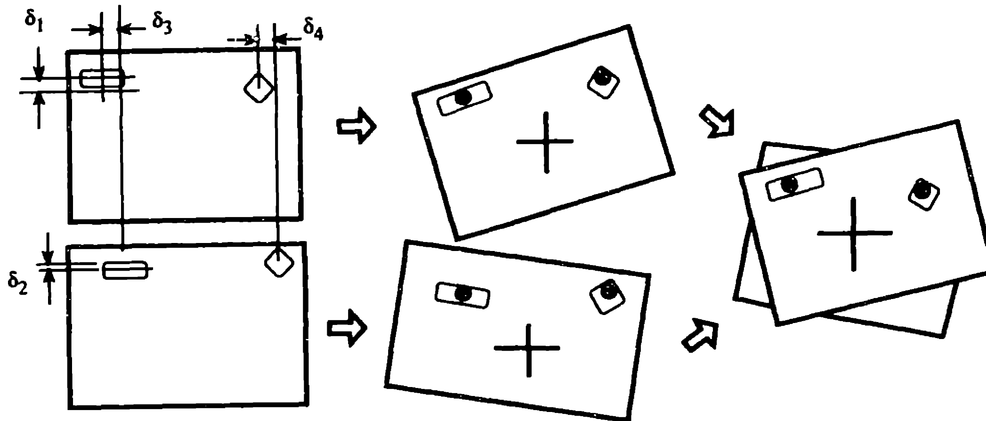

Figure A-1: Punch repeatability issues are avoided by pre-expose punching kinematic features since the pattern is exposed with respect to the fixture.

portant. Film rigid body rotations and translations due to sloppy punching, will not affect registration capabilities, as illustrated in Figure A-1.

Since features are kinematic, all artwork will register in subsequent machines (expose units), regardless of size and location variations in pins or holes. Since artwork is constrained deterministically, manufacturing tolerances have been decoupled from registration capability.

A.2 Post-Expose Punching

If pre-punching, which requires redesigning a plotter drum, presents practical hurdles, tooling features can be post-expose punched as usual. Contrary to the pre-punch method, registration capability would be limited by punch and film locational repeatability. Note that the artwork punch should be much more robust and operator independent to benefit from the extreme repeatability kinematic tooling provides. Again, once punched, the artwork will register from machine to machine, regardless of manufacturing tolerances. To enhance punching repeatability, prolong punch life, and minimize the chance of film breakage, stripper plates should be used. Furthermore, by kinematically coupling stripper and die blocks prior to manufacturing, the cut holes could be wire EDMed together and would therefore repeat to the concentric location during punching, as shown in Figure A-2. By making matched sets this way, the

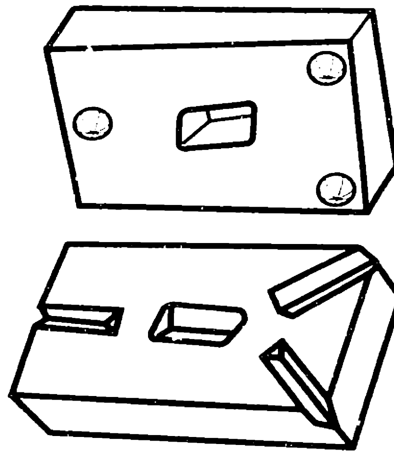

Figure A-2: Kinematically coupled punch and die sets can be manufactured as matching sets.

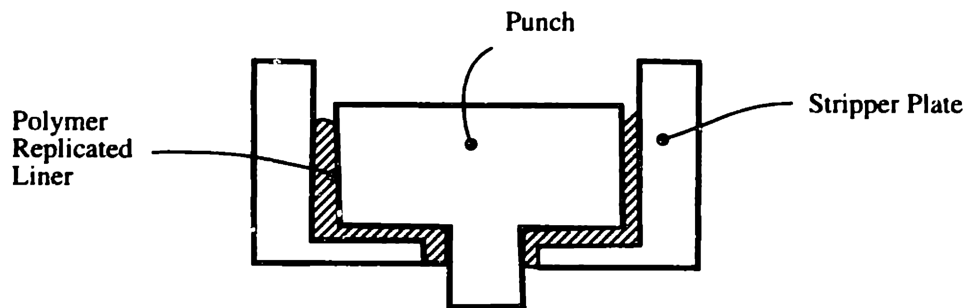

Figure A-3: Polymer replicated punch guides will increase repeatability performance of punches. Super Alloy^{TM} castable polymers from Philadelphia Resins are designed for this type of application.

punch die tolerances could be reduced, enhancing punch repeatability.

To further increase repeatability, the punch could be reproduced by polymer casting low friction structural material in the punch guide liners, as shown in Figure A-3.

A.3 Post-Etch Punch

A post-etch punch with kinematically coupled punch and die blocks is proposed. Further, an alignment technique based on moiré fringe method is proposed. Using these methods, the image to tooling uncertainty of $13\mu m$ is estimated, compared to the current $32\mu m$ approximate uncertainty of the current system.

As previously described, a significant source of punch error is the lack of an effect-

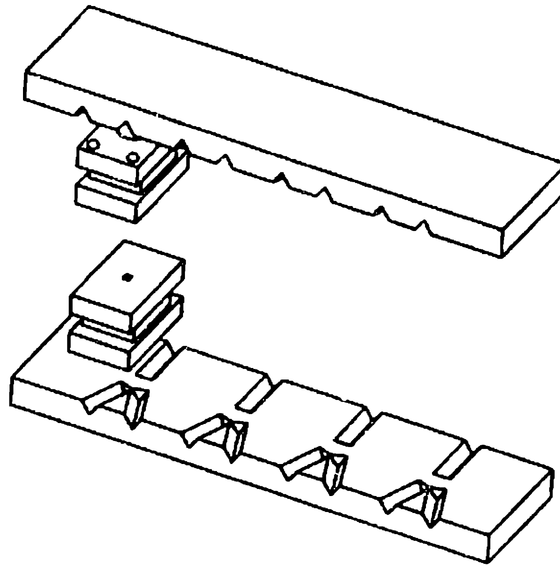

Figure A-4: Kinematically coupled punch and die blocks.

ive coupling element between the punch and die blocks. To overcome this limitation, the use of a six-point kinematic coupling is highly recommended, as illustrated in Figure A-4.

Design and optimization of coupling elements follows from the theory of point contact, whereby the optimum coupling radii may be calculated. Since the coupling is kinematic, and there is considerable flexibility on the geometry and materials which could be used, blocks could be designed with a positional repeatability within $1\mu m$, and rotational repeatability within $5mrad$. Currently, positional repeatability is $25\mu m(3\sigma)$.

Since positional repeatability of the punch/die coupling will be approximately one micron, blocks only need calibration once. Recentering punches after repeated use will be infrequent. Furthermore, because positional repeatability is assured, punch and die clearance may be reduced, minimizing core bending prior to shear failure, therefore producing features of more consistent size. Other improvements may include epoxy replicating the interior of the punch guide plate to maximize punch repeatability, as shown in Figure A-3.

An additional benefit of the coupling would be ease of format changeover. When the preloading mechanism is released, the blocks can easily be moved into another position. Again, since the coupling is kinematic, the blocks engage in unique positions. This eliminates operator variations in block setup.

To enhance the dynamic characteristics of the punch, the stage mechanism and its associated subassemblies should be redesigned to maximize system stiffness and damping. Triangulated, welded frame members with integral shear dampers could be used to satisfy this need. Furthermore, thermally isolating the critical elements from the drive electronics will reduce the possibility of thermally induced errors. This can be accomplished through the use of insulating barriers between punch subassemblies and electronics. Since the effects of machine dynamics is uncertain, an estimate on machine repeatability cannot be made.

While kinematic couplings significantly improve repeatability of punched features relative to each other, the alignment technique is still responsible for registration of tooling features with respect to the etched pattern. Alignment capabilities are limited by feature positions and optical servo-mechanism repeatability. Recall that feature-to-feature 3σ locational deviation is $7.6\mu m$ and that their sizes are normally distributed with a 3σ of $3.8\mu m$. Developing film introduces size variations due to over or underdeveloping, and etching the laminates also alters the size of the features. Note that the alignment algorithm locates the cores based on the centroid of an etched feature, in which case uniform size variations do not contribute to alignment error. Assuming that distortion will not occur during the etch process, the target centroid is independent of the absolute size.

By exposing and etching gratings into the core, $0.125mm$ lines and $0.125mm$ spacings, cores may be aligned to approximately $1\mu m$, using a moiré fringe technique as described in Chapter 4, and as illustrated in Figure A-5. For a detailed discussion of the technique, see Chapter 4 .

Stationary gratings within the punch placed against core gratings can center the laminates. Table A.1 shows the overall estimated performance compared to the current state of the art.

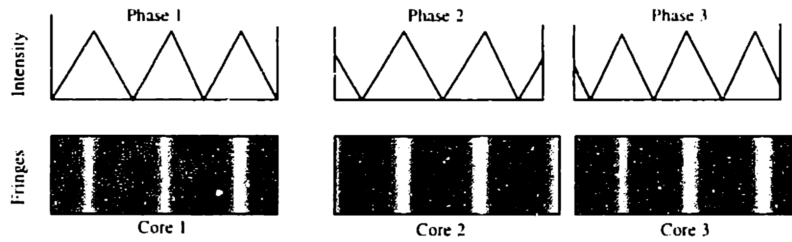

Figure A-5: Moiré fringe alignment of cores.

Measure	$3\sigma(\mu m)$ Proposed system	$3\sigma(\mu m)$ Current system
Punch repeatability	12	12
Alignment capability	1	17
Image to tooling uncertainty	12	21

Table A.1: Punch and alignment performance.

Tooling size variations for different laminate thicknesses may be reduced since punch to die clearance may be reduced; however, because this variation also depends on punch sharpness, a speculated improvement in size variations is not estimated.

It is further proposed that tooling pattern used for constraining artwork (Figure 5-3) be applied to cores, for constraining cores during lamination.

A.4 Lay-Up

To support the proposed kinematic tooling, press plates with constraining and preload pins are required. Recall that registration using the kinematic scheme is not a function of pin sizes or location, hence the stringent manufacturing requirements of the press plates may be relaxed. The "go/no-go" pin standards may be eliminated since pin variations have no impact on registration. Variation among press plates in no way affects registration performance. Another advantage of the technique is reduced hole wear, since the tooling features are not abraded against pins during lay-up. A conceptual press plate is shown in Figure 69.

The two constraining pins may be fit into position using a press (per prior recommendations); the exact location of the pin is not important. Pin profiles will be

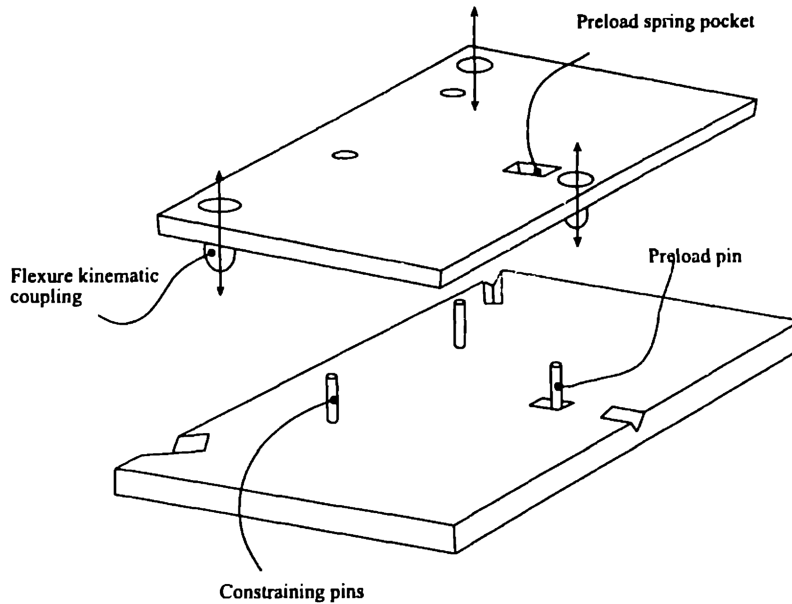

Figure A-6: Conceptual kinematic press plate.

discussed in the following lamination section. Cores are easily placed over the pins because features may be significantly larger than the pins. A top press plate is lowered onto the stack while the preload pin is fit through the preload holes and the force mechanism is engaged. A simple force mechanism consisting of a leaf spring, pocket milled into the top and bottom plates may be used to apply a uniform force across the thickness of the cores. To aid in the alignment of the cores during lay-up, the bottom plate may be inclined on an ultrasonic vibrating table. The vibrations facilitate sliding of the cores into position.

Because friction may be a limiting factoı on the repeatability of the kinematic couplings, the weight of the top plate should be supported by a constant force spring fixture until the preload mechanism is engaged. Furthermore, plate-to-plate repeatability is important to ensure pins are not tilted during assembly. The top-to-bottom plate stiffness could be achieved through the use of flexural kinematic couplings, described in Chapter 5. The couplings locate two plate planes, while allowing motion in the compressive degree-of-freedom. Large transverse stiffness of these couplings will ensure pins do not tilt, while lateral compliance of the coupling permits motion in the press direction. Flexural couplings may be used as the top plate supporting mechanism, then lightly preloaded against the cores after a preload pin is engaged.

A.5 Lamination

The dominant cause of layer-to-layer registration error is artwork alignment, and if the current core tooling remains the same, the estimated registration error is reduced to $31\mu m$ from $93\mu m$. Keeping the current tooling, but updating the post expose punch for kinematic punch and die blocks and moiré alignment will yield an estimated layer-to-layer registration error of $28\mu m$. Kinematic laminate tooling will further reduce the registration error to $23\mu m$.

The modulus of the laminates is an important design parameter, since the proposed kinematic coupling applies a transverse preload to maintain the three point contact, and will determine how the cores deflect under loading conditions. This is especially important above the glass transition temperature, where the stiffness is greatly reduced. The modulus will be lower bounded by that of the unclad modulus above glass transition, $2.75Gpa$. Since the contact areas, which maintain the largest stresses, are copper clad, the stiffness of the coupling is maintained; however, the affects of stresses throughout the laminates (albeit small) on registration, must be determined experimentally. The edge contact of the laminates must be maintained throughout the press cycle, even in the presence of thermal expansion. Notice that since the coupling is kinematic, thermal expansion never overconstraints the laminates, and rigid body translation and rotation of uniform expansion can be expressed in closed form. Because of modeling limitations, however, the only significant way to evaluate the performance of the kinematic coupling during lamination, will be through experimentation.

Interestingly, the flow of resin can be used as a method to produce kinematic features for subsequent processes. Epoxy replication is, in fact, a widely used technique in the machine tool industry, where, for example, precision surfaces for hydrostatic or aerostatic bearings are needed. For circuit board manufacture, the press cycle is conducted under vacuum for outgassing purposes, which is desirable from a replication point of view. To minimize the contact stresses of the pins against the flat punched features, pins can be ground with large radii as shown in Figure A-7.

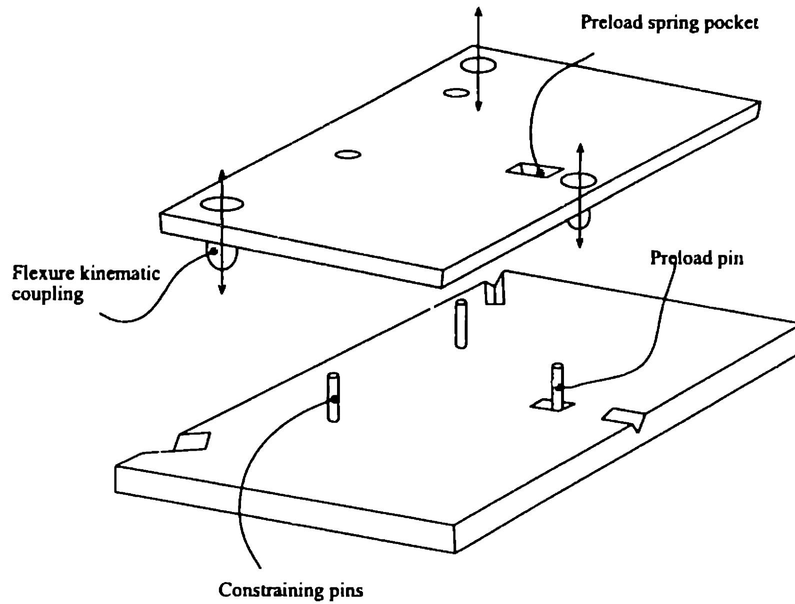

Figure A-7: Pins with large radii reduce contact stress from preload.

Three contact points constrain the cores. When the resin flows, the shaded area is filled and upon curing and pin removal, pin profiles have been replicated into the panels. The replicated shapes are gothic arches and serve as kinematic tooling features for round pins at subsequent processes, like drill or route, as shown in Figure A-8.

Ratios of the radii of replicated features to pin radii are important design parameters which can be optimized using contact theory to maximize coupling stiffness while minimizing contact stresses.

Assuming the preload stresses do not have an adverse effect upon registration, feature-to-feature registration among the layers is estimated in Table A.2.

Notice that the dominant cause of layer-to-layer registration error is artwork alignment, and that if the current core tooling remains the same, the estimated registration error is reduced to $31\mu m$ from $93\mu m$. Using current tooling methods, but updating the post expose punch for kinematic punch and die blocks and moiré alignment will yield an estimated layer-to-layer registration error of $28\mu m$.

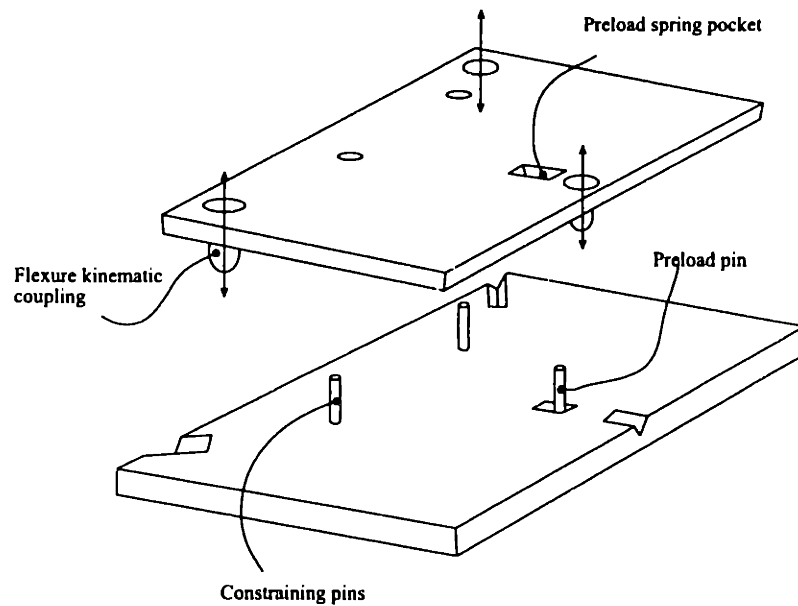

Figure A-8: Resin replicated tooling features remain kinematic for subsequent processes.

Measure	$3\sigma(\mu m)$ Proposed System	$3\sigma(\mu m)$ Current System
Environmental effects	8	8
Core alignment	5	16.8
Distribution of an ideal point	12	24
Top-to-bottom feature spread	5.4	58
Any two laminates factor of 1.4		
Total layer-to-layer registration	23	92.6

Table A.2: Estimated layer-to-layer registration performance using proposed laminate tooling.

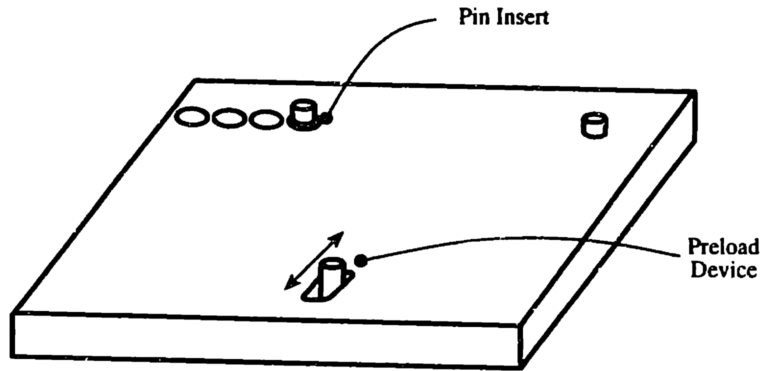

Figure A-9: Drill bed to accomodate resin replicated kinematic tooling features.

A.6 Drill

Proposed designs outlined here pertain only to fixturing and preloading the panels. Design work to improve the static and dynamic performance of the drill machine itself is beyond the scope of this investigation.

Since the incoming panels contain resin replicated gothic arch kinematic tooling features, as previously shown in Figure A-8, two round pins are required to provide three contact points for kinematic fixturing. A tooling plate to accommodate these tooled panels is shown in Figure A-9.

As in all cases of kinematic fixturing, a force source is required to maintain contact between the panels and pins. For this purpose, a solenoid actuated preload pin is shown, although any force source could be used. The applied preload is controlled, and since the system is statically determinant, the contact forces may be calculated explicitly. Hence the position and coupling stiffness can be calculated. Through the use of a planar kinematic coupling, the variability of the fixturing is reduced significantly, and registration errors caused by material movement or drill wander become more discernible.

Because fixturing is kinematic, the absolute location of the pins in the table is inconsequential. For instance, the upper right vee-groove acts as the origin of the panels, in which case the tooling beds may contain one hard-tooled pin in the upper right corner of each spindle's workspace. The second constraining pin, which constrains rotation, may be soft-tooled to accommodate various panel sizes. Errors in

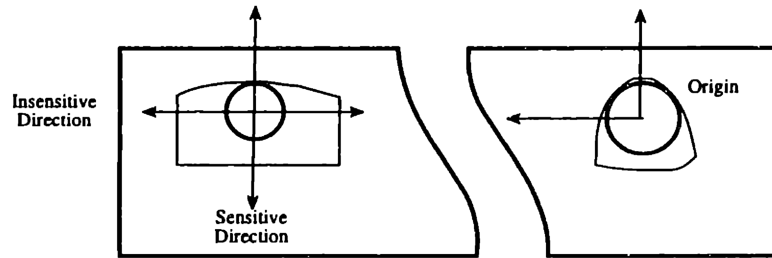

Figure A-10: Soft-tooled pin changes position along the insensitive coupling axis.

soft-tool position cause second order registration errors since the position of the pin is moved along an insensitive direction of the coupling, as illustrated in Figure A-10.

The position of the preload pin does not affect registration, and may be anywhere so long as the pin is in the vicinity of the preload tooling hole. Fixturing the panels has been reduced from soft tooling four pins to soft tooling one pin, whereby the drill bed can remain fixed, hence fixing the sensitive radial direction, while the spindle axis indexes along the insensitive direction to locate the pin. Again, because the kinematic features are significantly larger than the pins themselves, the position of the soft tooled pin is not important. Regardless of its position, the panels will locate into a unique position. If, however, an x-ray measurement is to be taken once and the coordinate transformation used by all drilling machines, clearly, the tooling must be accurate from machine to machine. Different pin positions on different machines would just relate to a different coordinate transformation since the kinematically located panels would be rotated as rigid bodies. Furthermore, since the panels will never be overconstrained, bending of the panels or damage to the tooling holes or pins is eliminated.

Considering the errors in drill head positioning, spindle run-out, layer-to-layer registration, and fixturing error, the overall hole to feature error (assuming a $0.2mm$ drilled via) is $80\mu m$, compared to $125\mu m$. The pad size required for a particular hole size is,

$$\phi_{pad} > \phi_{via} + 2t_{ring} + 2(80\mu m) \tag{A.1}$$

For example, for a $0.2mm$ diameter hole and a $0.025mm$ annular ring, the required pad diameter is $0.4mm$, as compared to the previous $0.5mm$ diameter pad. This represents a 20% decrease in the required diameter, or a 16% decrease in area. The

performance increase is not as dramatic as previous processes primarily because drill deflection for small vias is the dominant cause of error, which cannot be negated by clever fixturing techniques. Of the $80\mu m$ error, 89% is due to tool deflection. If, for instance, bit deflection can be halved, the hole to feature error will be $56\mu m$, in which case the area required is reduced by 50%.

For larger holes, too, where bit deflection is less an issue, registration error is small. Assuming that bit deflection is zero, the current state of the art maintains a $97\mu m$ error, while registration uncertainty of the proposed technique is $28\mu m$.

A.7 Outer-layer Image

Assuming tooling features have been protected from coating, the outer-layer image to solder mask image registration is limited to by the uncertainty in fixturing ($12\mu m$), the uncertainty in the outer-layer image relative to tooling holes ($13\mu m$), and the uncertainty in the artwork position ($5.4\mu m$). The total uncertainty in solder-mask image to outer-layer image is $18\mu m(3\sigma)$, compared to the uncertainty of the current method of $100\mu m$.

For a specified $0.1mm$ via and a $50\mu m$ annular ring, the minimum dot size is $0.236mm$, assuming protected tooling features. This is a 40% decrease in pad diameter, or a 65% decrease in the required area, as compared to the current methods. While currently, the desire to create $0.1mm$ vias over $0.25mm$ pads with a $50\mu m$ minimum annular ring will be satisfied at a rate of approximately 53%, the proposed methods will produce these features at a 4.2σ rate (essentially 100%), again assuming tooling features are protected from the coating process.

The methods pertaining to panel tooling are addressed here; for a discussion of the artwork tooling, see Chapter 5. The tantamount reason for using a kinematic system, is repeatability; however, in the instance of outer-layer expose, precision and accuracy is needed. Furthermore, if the resin replicated features cannot be used because of excessive movement during lamination, drilled features must be used. A planar kinematic coupling using round tooling is shown in Figure A-11.

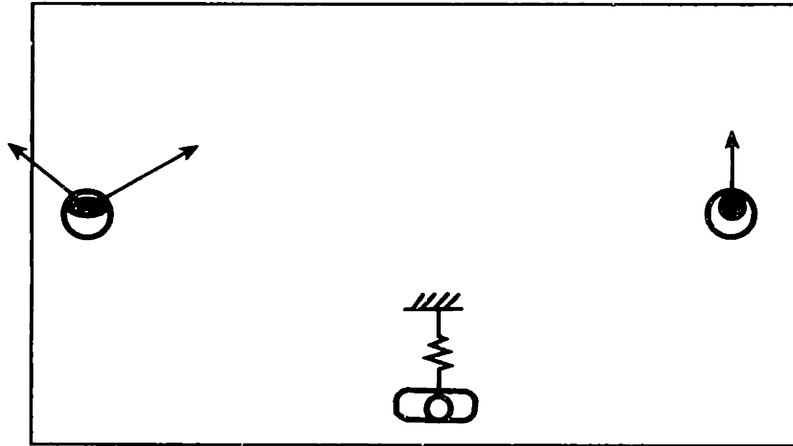

Figure A-11: Meta-stable kinematic coupling using drilled features.

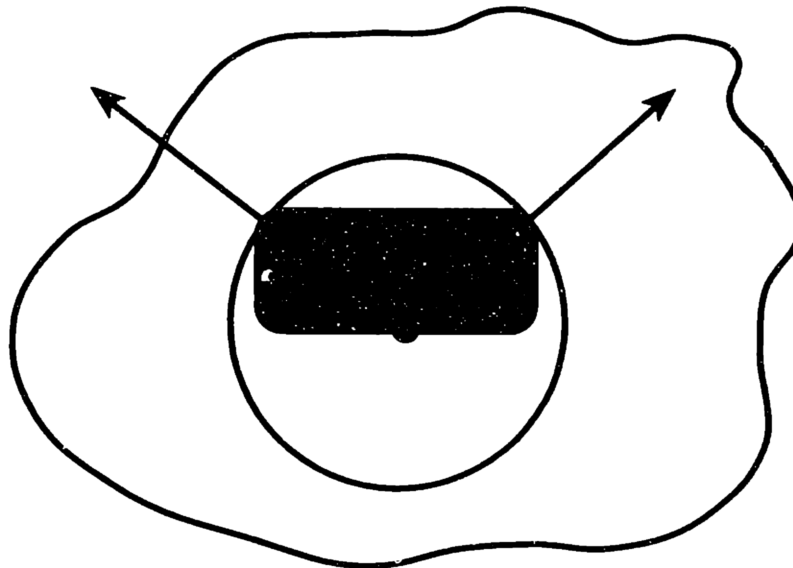

Figure A-12: Origin of panel coupling for outer-layer imaging.

Note that there are precisely three points of contact. The pin with two contact points may be ground, while the pin for the third contact point may be round. A preload mechanism to ensure contact is required, and is also shown in Figure A-11. The coupling will be as accurate to the artwork, as the drilled features are to the inner-layers, and as the pins are relative to the films. The origin of a kinematically located panel is at the intersection of the two contact forces, as shown in Figure A-12. Any errors in locating this pin relative to the artwork causes a direct translational error.

The position of the rotation constraining pin is sensitive in the direction indicated

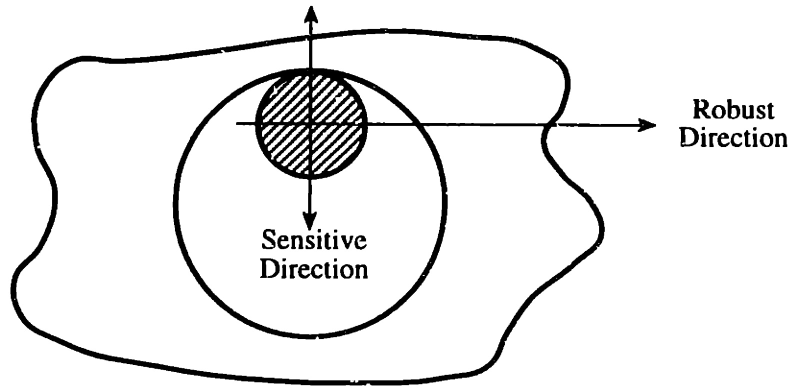

Figure A-13: Rotation constraining pin has only one sensitive direction.

in Figure A-13, but registration errors caused by positional errors along the insensitive direction involve higher order effects.

The degree to which this effect is higher order, is a function of the radius of the pin and hole, and pin positional error. The vertical displacement of the tooled hole may be calculated by considering a fixed panel, and a pin which can rotate along the edge of the hole. The dy displacement of the pin is the same as that of a free panel and fixed pin. The geometry is as shown in Figure A-14.

For small δx displacements, a small angle approximation can be used. Neglecting higher order terms associated with the $\sin(\theta)$ expansion, the relationship between the radii, δx, and δy is,

$$\delta y = \frac{\delta x^2}{2(r_{hole} + r_{pin})} \tag{A.2}$$

In the limit when the hole radius is infinite, pin location along the flat axis does not effect registration; that is, $\delta y = 0$.

Panel positioning using a kinematic coupling is more robust than that of the over-constrained system, due to a reduction of sensitive error motions, and panel and pin damage is reduced because there are no abrasive fits. Furthermore, bending of panels to fit onto pins is eliminated, since the system in not overconstrained. The coupling, however, is still required to be accurate to the films, and the holes accurate to the inner-layers, so the benefits of this method must be evaluated by experimentation. The frame is the same as that proposed in previous artwork sections, with the additional kinematic pins for the panels. Because of the accuracy issues, the performance

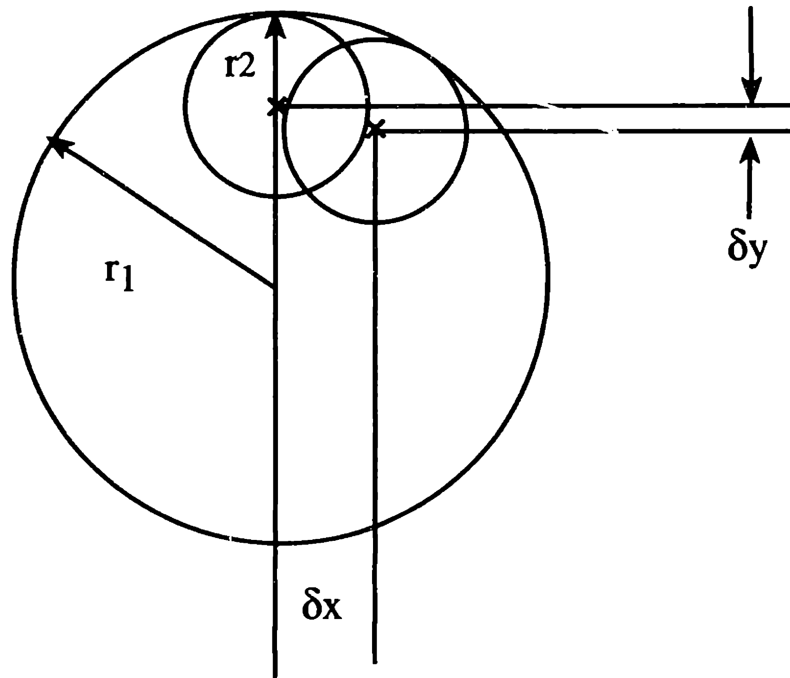

Figure A-14: Geometry of errors generated by pin placement error.

of the kinematic system as compared to the standard square pin technique should be determined experimentally.

A.8 Solder Mask and Photo-Defined Vias

Without going to the expense of creating new tooling features after curtain coating with liquid photo-resist, tooling holes must be protected for passive registration schemes. For example, clamps which seal tooling holes, as shown in Figure A-15, may be placed on the panels prior to coating and removed after. Clamps can be washed and reused. Similar in concept would be low profile rivet plugs which snap together and preload seal the perimeter of the tooling holes, as shown in Figure A-16. The rivet type plug is especially advantageous since it easily fits within the conveyor tracks, not disturbing the planarity of the panels. Holes at various locations for different panels are easily accommodated.

Assuming tooling features have been protected from coating, outer-layer image to solder mask image registration is limited by fixturing uncertainty ($12\mu m$), uncertainty

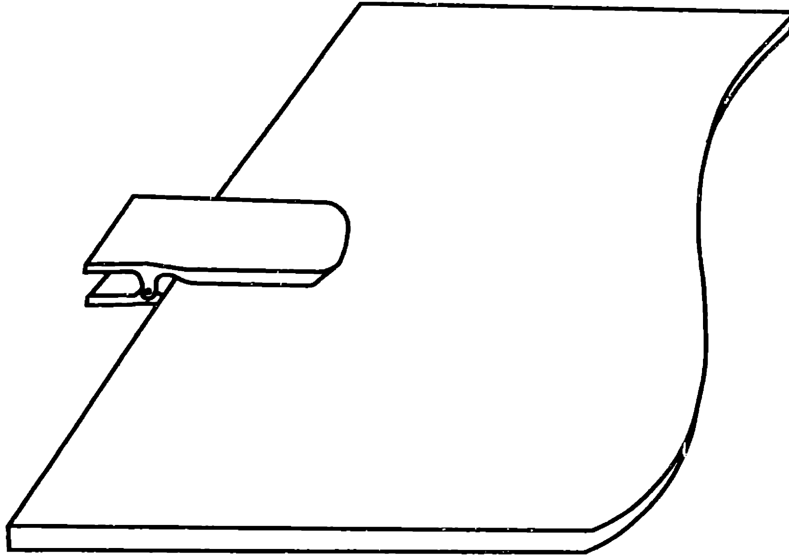

Figure A-15: Clamps may be used to protect tooling holes from curtain coating.

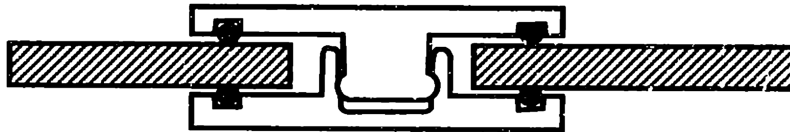

Figure A-16: Gasketing plugs may be used to protect tooling holes.

in outer-layer image relative to tooling holes ($13\mu m$), and uncertainty in the artwork position ($5.4\mu m$). The total uncertainty in solder-mask image to outer-layer image is $18\mu m(3\sigma)$, compared to the uncertainty of the current method of $100\mu m$. The smallest pad size may be determined by the Equation A.1, from which the minimum pad pitch may be calculated by specifying the amount solder mask should be oversized by and the minimum solder mask web. The pad pitch p is given by,

$$p > w_{web} + 2t_{oversize} + \phi_{pad} + 2(18\mu m) \tag{A.3}$$

Similarly, the size of an outer-layer dot for a specified photo-defined via is readily determined since the outer-layer pad to via artwork uncertainty is $18\mu m$,

$$\phi_{dot} = \phi_{via} + 2t_{ring} + 2(18\mu m) \tag{A.4}$$

For a specified $0.1mm$ via and a $50\mu m$ annular ring, the minimum dot size is

$0.236mm$, assuming passive fixturing techniques and protected tooling features. This is a 40% decrease in pad diameter, or a 65% decrease in the required area, compared to the current methods. While currently, the desire to create $0.1mm$ vias over $0.25mm$ pads with a $50\mu m$ minimum annular ring will be satisfied at a rate of approximately 53%, the proposed methods will produce these features at a 4.2σ rate (essentially 100%), again assuming tooling features are protected from the coating process.

Alternatively, an active registration system may be used, in which the films are kinematically located to the glass plates, and the panels are deterministically moved into position by actuating the positions of the two kinematic pins, based on a vision system. A panel is placed onto the phototool, and its position and orientation is measured. A coordinate transformation relating measured position to correct pin position is determined and applied to the actuators. Three actuators are required for x, y, and θ motion. The amount of travel required will depend on the amount of initial misregistration when placed onto the pins. Since most of the registration error will be due to coating material in the holes, motion of the pins in any one direction will be limited to approximately $0.5mm$. Once in position, panels are vacuum preloaded by the upper and lower glass plates. Because the actuators move the tooling pins relative to the glass plates, alignment mechanisms are located within frame subassemblies. It is conceivable that a frame with active pin alignment be retro-fittable to existing expose units. Issues involved with such a system include actuator travel, closed-loop servo stiffness, system bandwidth, and resolution. Further practical considerations are the ability to maintain a vacuum seal around the actuated pins, size limitations, and transmission stiffness. Candidates actuators include magnetostrictive or piezoelectric actuators, because of their high bandwidth, and positioning resolution. This system combines the advantages of a course kinematic tooling method, along with the positional accuracy of an active system. The design of this type of system poses a number of interesting design challenges, and it is uncertain if this system can outperform a passive system whereby the tooling features are protected from coating.

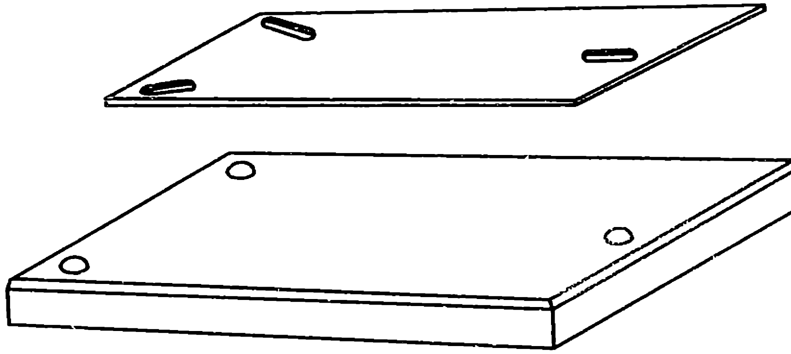

Figure A-17: Six point coupling used for fixturing fabricated boards to the test fixture.

A.9 Electrical Test

A test fixture in which the top and bottom are located with respect to each other through the use of a flexural kinematic coupling is proposed.

Board coupling using a planar kinematic coupling created at drill, similar to the coupling proposed for outer-layer expose, is also proposed. Estimated position uncertainty in probe to component pad is $23\mu m (3\sigma)$ as compared to $160\mu m$ of the current system. This allows the testing of devices with an 85% pitch decrease. This is beyond the limit of the piano wire probes, for all practical purposes. Most of the increased performance can be attributed to the reduction of artwork to tooling error.

Unlike previous processes which were either constraining thin, flexible elements (film and cores), or were constraining stacks of rigid bodies (panels for drill and route), electrical test is constrains a single rigid board. Because of this, there are primarily two choices for increasing fixturing repeatability. One choice would be use of a planar kinematic coupling with either routed or drilled tooling features. Errors introduced by routing are primarily from poor fixturing. These could be eliminated by creating the panel and board kinematic features immediately after lamination, using an x-ray vision system for image to feature accuracy, and by using a more robust routing machine. The planar kinematic coupling requires a transverse preload source, which may be as simple as a spring loaded pivot pin.

Another kinematic coupling which could be used is a six point contact type, where three slots routed into the boards, as shown in Figure A-17, couple to three balls.

Each ball and slot pair creates two points of contact. As noted above, the router performance determines the positional accuracy of the feature to artwork, which may preclude the use of kinematic tooling features in boards for fixturing during electrical test.

The preload for the six point coupling is provided by the lateral loading of the probe cards against the surface. Spherical elements of the coupling may be contained by monolithic or bolted type flexures.

Repeatability of the test probes is a strong function of hole to pin clearance, and should be reduced to increase performance. However, it is understood that this would cause difficulties during test fixture assembly. A compliant sheet in-between the acrylic layers could be used to preload the pins against an edge of a hole, increasing pin stiffness and repeatability. This would be a massively elastically averaged system, and as such the contact forces are unknown. However, transverse forces are negligible, and the elastic membrane is used as a method to obtain contact between the pins and their holes. Stiffness is not a significant concern. The membrane may be engaged once the system is brought into contact with the board, or may be engaged when the fixture is assembled.

Registration error of board tooling features to outer-layer components is approximately $13\mu m$ and board placement repeatability to the test fixture using the kinematic system is estimated as less than $1\mu m$. The total component pad position uncertainty relative to the nominal pin position is $13\mu m(3\sigma)$.

Pin position uncertainty using smaller drilled holes and a compliant preload membrane is primarily due to drill error, and is approximately $12\mu m$. Fixture position uncertainty is $15\mu m(3\sigma)$. Probe to component pad uncertainty is $23\mu m(3\sigma)$, compared to $160\mu m$ uncertainty of the existing system. Improvements are attributed to the decreased uncertainty in image position to tooling, decreased uncertainty in pin position from transverse preload, and the improved performance of the fixture-to-fixture repeatability through the use of flexural kinematic couplings.

For example, a pad would have to be at least $0.05mm$ wide to avoid a false alarm caused by probe to pad error. For 3σ certainty, this would correspond (approximately)

to a $0.1mm$ pitch device. This is an 33% reduction in the pitch of testable devices over the existing system. At this dimension, proper artwork scaling to account for material shrinkage is critical for test fixtures to be fabricated *a-priori*.

Bibliography

[1] D.J. Bone, H.A. Bachor, and R.J. Sanderman. Fringe pattern analysis using a 2-d fourier transform. *Applied Optics*, 25(10):1653–1660, 1986.

[2] D. Braunstein and H. Asada. Real-time estimation of solder paste properties for adaptive printing control. In *1994 International Mechanical Engineering Congress and Exposition, DSC 55-2*, pages 819–826. A.S.M.E., 1994.

[3] J. Choi et al. Wedge-plate shearing interferometers for collimation testing: use of a moire technique. *Applied Optics*, 34(19):3628–3638, 1995.

[4] T. DiStefano. The μbga as a chip size package. In *National Electronic Packaging and Production Conference Proceedings*, 1995.

[5] B.V. Dorrio et al. Fizeau phase-measuring interferometry using the moire effect. *Applied Optics*, 34(19):3639–3643, 1995.

[6] J. L. Doty. Projection moiré for remote contour analysis. *J. Opt. Soc. Am.*, 73:366–372, 1983.

[7] Eastman Kodak Company. *Kodak Data for Aerial Photography*, 1992.

[8] Stephen D. Fantone. Automated radius measurement apparatus, January 1994. United States Patent 5,280,336.

[9] J.W. Goodman. *Introduction to Fourier Optics*. McGraw-Hill, 1968.

[10] G. Hixon. Fixturing for tight tolerances. In *National Electronic Packaging and Production Conference Proceedings*, 1995.

[11] M. Idesawa, T. Yatagai, and T. Soma. Scanning moire method and automatic measurement of 3-d shapes. *Applied Optics*, 16(8):2152–2162, 1977.

[12] F.A. Jenkins and H.E. White. *Fundamentals of Optics.* McGraw-Hill, 1957.

[13] O. Kafri and I. Glatt. *The Physics of Moire Metrology.* Wiley-Interscience, 1990.

[14] R.S. Longhurst. *Geometrical and Physical Optics.* Longman Group, Ltd, 1973.

[15] G. Messner. Cost-density analysis of interconnections. *I.E.E.E. Transactions on Components, Hybrids, and Manufacturing Technology*, 10(2):143–151, 1987.

[16] G. Messner. *Electronic Packaging and Interconnectivity*, chapter 1. McGraw-Hill, 4 edition, 1996.

[17] Y. Morimoto et al. Carrier pattern analysis of moire interferometry using the fourier transform moire method. *Optical Engineering*, 33(8):2646–2653, 1994.

[18] Y. Morimoto and M. Fujisawa. Fringe pattern analysis by phase-shifting method using fourier transform. *Optical Engineering*, 33(11):3709–3714, 1994.

[19] T.W. Ng. Circular grating moire deflectometry analysis by zeroth and first radial fringe order angle measurement. *Optics Communications*, 129:334–346, 1996.

[20] O.V. Oppenheim et al. *Signals and Systems.* Prentice-Hall, 1983.

[21] O.V. Oppenheim and R.W. Schafer. *Discrete-Time Signal Processing.* Prentice-Hall, 1983.

[22] K. Patorski. *The Moiré Fringe Technique.* Elsevier, 1993.

[23] B. Paul. *Kinematics and Dynamics of Planar Machinery.* Prentice-Hall, 1979.

[24] J. C. Perrin and A. Thomas. Electronic processing of moire fringes: application to moire topography and comparison with photogrammetry. *Applied Optics*, 18(4):563–573, 1979.

[25] G.T. Reid, R.C. Rixon, and H.I. Messer. Absolute and comparitive measurements of three-dimensional shape by phase measuring moire topography. *Optics and Laser Technology*, 9:315–319, 1984.

[26] D.P. Seraphim. Chip-module-package interfaces. In *Proceedings Electronic Insulation Conference*, 1977.

[27] E.S. Simova and K.N. Stoev. Automated fourier transform fringe-pattern analysis in holographic moire. *Optical Engineering*, 32(9):2286–2294, 1986.

[28] H. Singh and J.S. Sirkis. Direct extraction of phase gradients from fourier-transform and phase-step fringe patterns. *Applied Optics*, 33(22):5016–5020, 1994.

[29] A. Slocum. Kinematic couplings for precision fixturing - part 1 - formulation of design parameters. *Precision Engineering*, 10(2):85–91, 1988.

[30] A. Slocum and A. Donmez. Kinematic couplings for precision fixturing - part 2 - experimental determination of repeatability and stiffness. *Precision Engineering*, 10(3):115–122, 1988.

[31] G. Taguchi. *System of Experimental Design.* Quality Resources, 1987.

[32] S.P. Timoshenko and J.N. Goodier. *Theory of Elasticity.* McGraw-Hill, 1987.

[33] J. Trent. Laminate technology update for multichip modules. In *National Electronic Packaging and Production Conference Proceedings*, 1996.

[34] J. J. Wasowski. Moiré surface contouring by addition method. In *Proceedings of the 6th International Conference on Experimental Stress Analysis*, pages 127–134, 1978.

[35] J. Yuan and N.H. Chao. Effect of lamination tooling on dimensional stability of multilayer circuit boards. In *National Electronic Packaging and Production Conference Proceedings*, 1994.